Dissertation zur Erlangung des Doktorgrades
der Fakultät für Chemie und Pharmazie
an der Ludwig-Maximilians-Universität München

Advancing molecular force measurements across talin

Pia Sabrina Ringer
aus Herrenberg, Deutschland

2017

Erklärung

Diese Dissertation wurde im Sinne von § 7 der Promotionsordnung vom 28. November 2011 von Herrn Prof. Dr. Reinhard Fässler betreut.

Eidesstattliche Versicherung

Diese Dissertation wurde eigenständig und ohne unerlaubte Hilfe erarbeitet.

München, 07.12.2017
Pia Sabrina Ringer

Dissertation eingereicht am 07.12.2017
Erstgutachter: Prof. Dr. Reinhard Fässler
Zweitgutachter: Prof. Dr. Martin Biel
Mündliche Prüfung am 29.01.2018

Contents

Summary

The ability of cells to sense and adapt to mechanical cues is indispensable for proper tissue development and function. Disruption of cells's mechanotransduction processes lead to diseases, like arteriosclerosis or tumor formation. Mechanical information is diversely transmitted by the cell depending on the mechanical signal and the subcellular structures responsible for the transmission. However, mechanical signals form the extracellular environment are sensed by integrin-dependent, multi-molecular complexes, called focal adhesions (FAs). The integrin family of adhesion receptors plays an essential role in those cell-matrix interactions by spanning the membrane and anchoring to the extracellular matrix (ECM). One key regulator of cell adhesion is the adaptor protein talin, which is able to activate integrins by binding with the N-terminal head domain to the cytoplasmic β-tails and at the same time mediates the link to the actin cytoskeleton via its elongated rod domain. Vertebrates express two very similar talin isoforms, the ubiquitously expressed talin-1, whereas the expression of talin-2 is mainly restricted to heart, skeletal muscle and brain. Even though the two isoforms share similar structures and binding partners, the reason for the diverse expression pattern remained unclear as well as isoform specific functions have been elusive. Several studies showed that integrins bear forces that reach values of a few tens of piconewtons (pNs) and it was hypothesized that talin tansduces those mechanical signals, however, quantitative evidence for force transmission across talin within living cells was still missing.

In order to unravel the mechanotransduction process across talin-1 and talin-2 (**Paper II**), I analyzed both isoforms on a talin double knockout background and could demonstrate that both talin-1 and talin-2 rescue cell spreading and localize to the same subcellular structures. Two single-molecule calibrated Förster resonance energy transfer (FRET)-based tension sensors, sensitive to force ranges of 6-8 pN and 9-11 pN, unraveled an isoform-specific force transduction across talin, which is regulated by actin and vinculin engagement. In addition, it was shown, that talin-2 recruits the stabilizing adapter protein vinculin more efficiently to its N-terminal rod domain, which allow cells

to reinforce FAs even on compliant substrates. By diverse expression of the two talin isoforms cells can modulate their ability of sensing substrate rigidity.

The question remained, how the different subdomains and interaction partners, that bind to the elongated talin rod, contribute to force transmission across this major adapter protein. In order to tackle this question and to elucidate the process of force propagation across talin's rod domain, I generated an additional talin-1 tension sensor, that allowed to distinguish force experienced by different subdomains (**Paper IV**). Using a novel tension sensor module with a near digital force response sensitive to 3-5 pN at position aa 447 and aa 1973 of the talin rod, it could be demonstrated that mechanical tension is not equally distributed. Instead, talin is subjected to a force gradient, with forces as high as 7 pN at the N-terminal rod domain and lower forces of around 3 pN generated by the very C-terminal actin binding site. This finding was furthermore confirmed by simultaneously evaluating the two talin tension sensors within one cell, using a newly developed multiplexing fluorescence-lifetime imaging microscopy (FLIM) method. Finally, the digital nature of the new sensor module enabled us to determine the fraction of stretched talin molecules per cell. Taken together, this study shows that force transduction across talin is regulated on multiple layers, first of all, talin molecules bear a range of forces, which is mostly modulated by vinculin and actomyosin contractility. In addition, cells tune the amount of mechanically engaged molecules within FAs.

During my work I acquired broad insights into the field of biosensors that allow force measurements across single molecules, especially FRET-based tension sensor probes. In **Paper I** we summarized the diverse techniques to measure molecular forces and suggested a strategy to carefully analyze the currently available FRET-based biosensors.

Additionally, in a second review article, the current knowledge about the mechano-chemical signaling hub of cell-ECM contact sites was outlined (**Paper III**). Here, I described the recent findings about the vertical and horizontal layered structure of FAs and their complex regulation. Furthermore, recent approaches in single molecule resolution micrsocopy, force spectroscopy methods, as well as molecular tension sensors were highlighted, which toghether with theoretical studies had a significant impact on the current understanding of how cells sense and adapt to the mechanical and chemical properties of the ECM.

Abbreviations

AFM	atomic force microscopy
ECM	extracellular matrix
FA	focal adhesion
FLIM	fluorescence-lifetime imaging microscopy
FRET	Förster resonance energy transfer
pN	piconewton
HP35	villin headpiece peptide
TSM	tension sensor module
FL	ferredoxin-like
TFM	traction force microscopy
D	donor
nm	nanometer
GFP	green fluorescent protein
VBS	vinculin binding site
RTK	receptor tyrosine kinase
MAPK	mitogen-activated protein kinase
GPCR	G-protein-coupled receptors
ATP	adenosine triphosphate
MLC	myosin light chain
FERM	four point one, ezrin, radixin, myosin
PTB	phosphotyrosine-binding
FAK	focal adhesion kinase
RIAM	Rap1-GTP interacting adapter molecule
PIPKIγ	Phosphatidylinositol phophate kinase type Iγ

TIAM	T-cell lymphoma invasion and metastasis 1
VBS	vinculin binding site
eq	equation

Publications

This thesis is based on the following publications, which are referred in the text by the following roman numeral letters (I-IV):

Paper I: Cost A.-L.*, **Ringer P.***, Chrostek-Grashoff A., Grashoff C., (2015). How to measure molecular forces in cells: A guide to evaluating genetically-encoded FRET-based tension sensors. *Cellular And Molecular Bioengineering*, 8(1), 96-105.
* equal contribution

Paper II: Austen K.*, **Ringer P.***, Mehlich A.*, Chrostek-Grashoff A., Kluger C., Klingner C. Sabass B., Zent R., Rief M., Grashoff C., (2015). Extracellular rigidity sensing by talin isoform-specific mechanical linkages. *Nature Cell Biology*, 17, 1597-1606.
* equal contribution

Paper III: Ringer P., Colo G., Fässler R., Grashoff C., (2017). Sensing the mechano-chemical properties of the extracellular matrix. *Matrix Biology*, 1336, 0945-053X.

Paper IV: Ringer P., Weißl A., Cost A.-L., Freikamp A., Sabass B., Mehlich A., Tramier M., Rief M., Grashoff C., (2017). Multiplexing molecular tension sensors reveals force gradient across talin-1. *Nature Methods*, 14, 1090-1096.

1 Introduction

1.1 Mechanobiology

1.1.1 Introduction into the field of mechanobiology

Essentially all organisms from bacteria to human are subjected to diverse mechanical forces from a wide variety of sources. For instance gravity is an ubiquitous force influencing the whole organism, whereas compressive loads act on cartilage and bones during walking. Additionally, tensile muscular forces act on bones via tendons, in order to move joints and allow locomotion. Another example are blood vessels, that need to sustain high pressure and shear stress exerted by the blood flow. Similarly, lung tissue is cyclically stretched during respiration and is exposed to mechanical forces from the blood flow and surface tension. The heart, in particular, is under constantly changing degrees of tension while pumping blood through the blood vessels, due to changes in blood volume and pressure. By now it is well established that tissue remodels in response of mechanical forces, such as bones that change in stiffness, density and shape upon alteration of mechanical loads [Mullender et al., 2004]. Furthermore, the morphology of blood vessels is modified by alterations of blood pressure and shear stress, leading to increasing thickness of the vessel wall [Osol, 1995]. Abnormal responses to mechanical stress lead to organ pathologies like osteoporosis, arterosclerosis or fibrosis [Grodzinsky et al., 2000; Lammerding et al., 2004; Ross, 1986].

It has been known for many years that the cells response to mechanical forces is related to tissue physiology as well as pathology, yet, the mechanism how cells sense mechanical loads and how the mechanical signal is translated into a biochemical signal remains obscure and needs further investigation. In 1998, Ingber [1998] describes the field of mechanobiology the following; ' Mechanobiology is an interdisciplinary study that is concerned with the cells' biological responses to mechanical loads and the mechanotransduction mechanism by which these loads are transduced into a cascade of

cellular and molecular events'. The comprehension of mechanotransduction processes will help to understand the physiological responses of various tissues to mechanical signals and to elucidate the pathogenesis of many diseases that are caused by the inability of cells to properly respond to mechanical cues.

1.1.2 Mechanical forces influence the cell's function

Mechanical cues – either extrinsic from the cell environment, or intrinsic form cellular structures – play a pivotal role in regulating cells function, like gene expression, protein synthesis, cell proliferation, differentiation or cell death. External mechanical stimuli experienced by cells include stretching, substrate rigidity and shear flow. As an example, tendon fibroblasts were shown to upregulate gene expression and protein synthesis of collagen type I upon uniaxial stretching [Yang et al., 2004]. Similarly, Kaspar et al. [2002] showed that cyclic stretching of human-derived osteoblast-like cells increase the cells' proliferation rate, intriguingly, showing a differential response with respect to the applied strain-rate. Furthermore, smooth muscle cells sense mechanical tension, like uniaxial stretching, and reorient uniformly relative to the stretch direction [Dartsch et al., 1986]. Another major mechanical cue is shear stress, which is experienced, for example, by endothelial cells in the vascular system. Changes in blood flow regulate the development of the blood vessel structure during embryogenesis [Resnick et al., 2003]. Furthermore, the integrity and permeability of the selective barrier built by vascular endothelial cells is altered by haemodynamic forces [White and Frangos, 2007].

1.1.2.1 Sensing the rigidity of the extracellular matrix

The stiffness and composition of the ECM is another mechanical stimulus the cell needs to sense and respond to. Tissue rigidity regulates tissue patterning and organ development, while altered tissue mechanics are associated with numerous diseases. Fibrosis, for instance, is characterized by altered mechanical properties of the fibrotic tissue, which is sensed by precursor cells that then become contractile myofibroblasts [Wells, 2013]. Other cell types, like macrophages and leukocytes, are also responsive to the increased matrix stiffness in fibrotic tissues, which leads to fibrosis-associated inflammation [Huynh et al., 2011; Patel et al., 2012]. Tissue stiffening can also drive the progression of certain tumors such as breast cancer [Paszek et al., 2005]. Furthermore, tissue elasticity conducts the differentiation of stem cells into either neurons on compliant

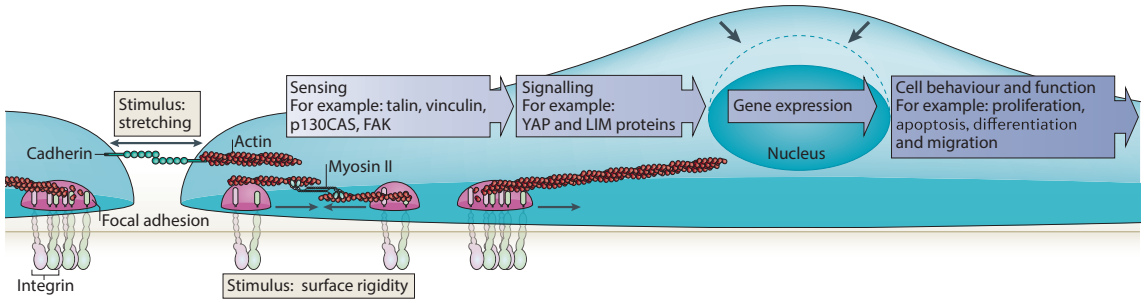

Figure 1.1: Mechanotransduction – converting mechanical cues into biochemical signals. Mechanical forces, externally applied or exerted by neighboring cells, like stretching, shear stress or substrate stiffness can be converted into chemical signals by cellular mechanotransduction processes. Receptors in different subcellular structures, like cell-cell contacts or cell-ECM adhesions, transmit those signals into the cell, where tension dependent phosphorylation or conformational changes of adapter proteins trigger signaling cascades that, for example, change gene expression pattern. Deformation of the nucleus (dashed line) can also lead to different gene expression profiles. Altogether, diverse mechanical signals alter the cell's behavior and function and can induce proliferation, apoptosis, differentiation or migration. Adapted from [Iskratsch et al., 2014].

substrate, resembling the brain, or osteoblasts on rigid substrate, mimicking bone [Engler et al., 2006]. Interestingly, however, many cell types respond differently to changes in matrix rigidity when cultured on flexible substrates. As an example, neurons can be cultured on soft surfaces, whereas astrocytes do not spread on compliant substrates and show a disorganized actin cytoskeleton [Georges et al., 2006]. Directional cell locomotion can be guided not only by chemical gradients, but also by the rigidity of the substrate, a process called durotaxis [Lo et al., 2000]. By exerting contractile forces on the surrounding matrix and then interpreting the substrate deformation, cells determine a preferred direction, which is crucial for processes like wound healing [Martin, 1997] and plays a role in tumor metastasis [Bernstein and Liotta, 1994]. Chemical, mechanical, as well as, topographical properties of the tissue microenvironment are also involved in the regulation of cell proliferation of several cell types [Chen et al., 1997]. This anchorage-dependent rigidity sensing is mediated by FAs, subcellular structures composed of ECM-binding integrin receptors, which are connected through adapter proteins to the intracellular actin cytoskeleton (subsection 1.2.1). Although it is known by now that individual integrin subtypes [Elosegui-Artola et al., 2014], as well as, several adapter molecules like focal adhesion kinase (FAK), vinculin and paxillin [Plotnikov

et al., 2012] hold a crucial role in this process, the exact mechanism of mechanosensation through FAs remained unknown.

1.1.3 Conversion of mechanical cues into biochemical signals

A range of cellular components mediate different aspects of mechanotransduction including stretch-activated ion-channels, the cytoskeleton, the plasma membrane, the nucleoskeleton and cell adhesion complexes. In addition, there are different modes of force sensation and transmission into biochemical signals, like force-induced conformational changes, which unravel crytpic binding or phosphorylation sites. Furthermore, mechanical cues can alter the enzymatic activity of proteins or lead to activation of proteolysis (Figure 1.1). Hereafter, the most important cellular components for the cell to sense mechanical forces are summarized and the major mechanotransduction processes are highlighted.

The first cellular compartment, able to convert mechanical into biochemical signals is the plasma membrane, which senses tension and in response orchestrates cytoskeletal remodeling and excocytosis of vesicles, in order to increase the membrane area during migration [Gauthier et al., 2011; Masters et al., 2013]. The mechanism how the membrane detects mechanical stress is not fully understood, however, one intensely-studied example of mechanotransduction is provided by the evolutionary conserved stretch-sensitive ion-channels [Maroto et al., 2005; Sukharev et al., 1999]. Stress-responsive ion channels are pore-forming subunits that open in response to the deformation of the membrane, like curvature or tension, and alter their conformation between a closed and an open state, which allows the movement of ions in and out of the cell, thereby converting mechanical stimuli into electrical signal [Sachs, 1992]. One famous type of ion channels transmits the mechanical signal of soundwaves and vibration in cochlear hair cells into electrochemical signals, which are then transmitted to the brain [Eberl et al., 2000]. However, they also play a role in the cardiovascular regulation, for example, in the transmission of blood flow induced shear stress in vascular endothelial cells into biochemical signals [Yin and Kuebler, 2009]. In 2010, a novel class of mechanosensitive ion channels, Piezo1 and Piezo2, were identified in mammals, with orthologs in numerous eukaryotes and plants [Coste et al., 2010]. Piezo channels are expressed in various tissues, contributing to a diverse set of physiological roles, like sensing light touch or proprioception and regulating the vascular blood flow [Wu et al., 2017].

Another important player in the transmission of force is the cytoskeleton with its elastic and flexible nature, that provides the mechanical properties required to withstand deformation and allows the cell to maintain its shape. Additionally, actin filaments themselves serve as tension sensors by modulating their susceptibility to cofilin-mediated severing upon force changes [Hayakawa et al., 2011]. Furthermore, the actin network plays a critical role in mechanotransduction by linking cellular components, like the nucleus to the force sensing apparatus. Here tension is transmitted via the LINC complex embedded in the nuclear envelope to the nucleoskeleton, which is build by laminins. Nesprin, is one of the force-sensing components in the LINC complex and mechanical load across Nesprin-1 leads to phosphorylation of emerin resulting in nuclear stiffening and induction of gene expression [Arsenovic et al., 2016]. One direct conversion of force into biochemical signal, is the mechanical deformation of the nucleus, which alters chromatin organization by changing accessibility of chromatin to transcriptional regulators, causing either transcriptional activation or repression [Fedorchak et al., 2014].

Moreover, force sensation and transmission of information takes plays at membrane receptors like the G-protein-coupled receptors (GPCR), which changes its conformation upon mechanical load [Gudi et al., 1996] and receptors involved in cell-cell contacts, like cadherin [Huveneers and de Rooij, 2013] and Notch [Wang and Ha, 2013]. Notch receptor is a typical example for force-induced proteolysis and release of a cleavage product, that directly functions downstream as a signal transducer [Shergill et al., 2012].

Finally, cell-ECM contacts are an important mechano-chemical signaling hub mediated by transmembrane proteins, called integrins, together with various adapter molecules, stretch-senstive receptor tyrosine kinases (RTKs) and mitogen-activated protein kinases (MAPKs) that localize to integrin clusters and reinforce a range of intracellular signaling cascades [Ullrich and Schlessinger, 1990], [Yamazaki et al., 1993]. Mechanical cues that are transduced from the ECM to the cytoskeleton are converted into biochemical signals by numerous adapter proteins [Wang and Ha, 2013], [Ringer et al., 2017]. The major linker protein talin, was shown to expose cryptic vinculin binding sites upon mechanical load, leading to enhanced vinculin recruitment [del Rio et al., 2009], which becomes phosphorylated and recruits further signaling proteins [Zhang et al., 2004]. Similarly, force induced extension of the adapter protein p130Cas promotes its phosphorylation by Src family kinases and in doing so activates downstream signaling [Sawada et al., 2006]. One example for increased catalytic activity upon mechanical stimulation is Src

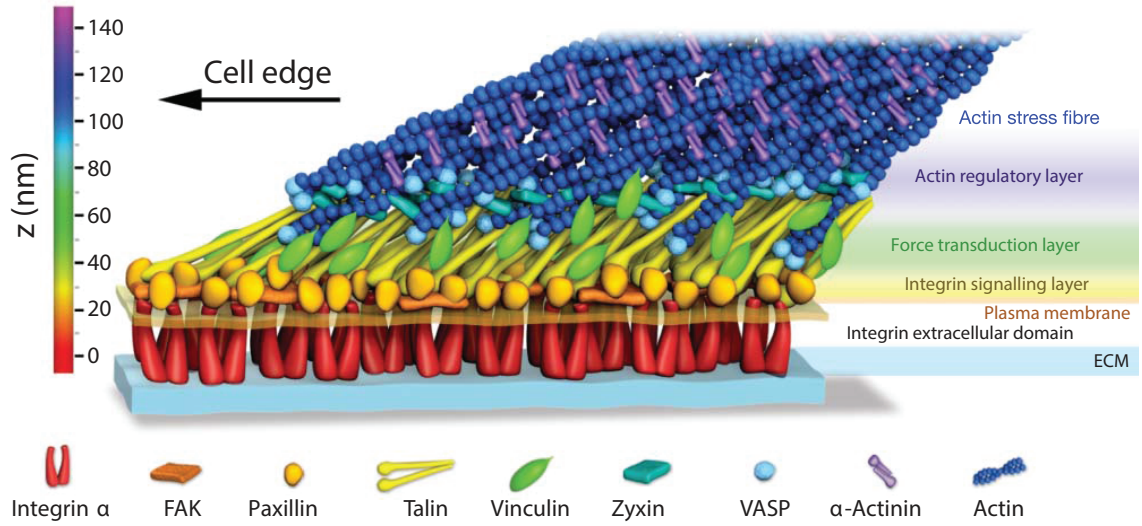

Figure 1.2: Architecture of integrin-based focal adhesions. Schematic model of the horizontal layering of cell-ECM contacts. Integrins form the outermost layer, attaching to the substrate and at the same time spanning the membrane and binding to adapter proteins in the signaling and force tansducing layer. The elongated adapter protein Talin is one of the key proteins in forming the nanoscale architecture of FAs, since it links integrins to the actin cytoskeleton, the most inner layer, thereby functions as a molecular ruler [Li et al., 2015]. Figure adapted from [Kanchanawong et al., 2010].

itself, which is thought to be modulated by a mechanical allosterism [Wang et al., 2005]. Furthermore, a whole class of adhesion-associated proteins, all belonging to the LIM protein family, are recruited to cell adhesion sites in response to high mechanical stress [Schiller et al., 2011].

1.2 Focal adhesions: Mechanical anchor to the ECM and signaling hub

Cell contacts to nearby cells and the underlying extracellular matrix (ECM) are essential for maintaining the integrity of multicellular organisms. Almost all mammalian cell types form adhesive structures to the ECM, which is crucial for morphogenesis, proliferation, differentiation and also cell migration [Wozniak et al., 2004]. These so called focal adhesions mechanically couple the ECM to the cell's actin cytoskeleton of the cell, thereby executing scaffolding and signaling roles.

1.2.1 Structure and components of cell-ECM adhesions

Focal adhesions are highly dynamic multimolecular complexes, comprising the membrane–spanning integrins, representing the key family of receptors that mediate the linkage of the ECM to the actin cytoskeleton [Zaidel-Bar and Geiger, 2010]. Several hundred proteins assemble to the sites of integrin clustering, building the cell's adhesome [Schiller et al., 2011]. Mechanical cues form the ECM can change the composition and size of the adhesion structure, inducing maturation of newly formed short-lived nascent adhesions into medium-sized focal complexes or mature FAs. The underlying 3-dimensional architecture of FAs can be divided in vertical and horizontal substructures [Ringer et al., 2017]. Kanchanawong et al. [2010] found the vertical layers to be divided in an outer layer, that consists of the integrin receptors that attach to the surrounding environment, an intermediate layer, comprising adapter and signaling proteins, consolidating all mechanical and chemical signals and an inner layer, that is represented by the actomyosin cytoskeleton (Figure 1.2). Horizontal segmentation, on the other hand, arises due to diverse types of cell-ECM adhesions, which are besides the most common FAs, elongated fibrillar adhesions, that are located to the center of the cell and comprise a different adhesome composition. Different integrin subtypes, for instance, localize to these different adhesion structures, where they perform distinct functions [Rossier et al., 2012]. Lately, a second horizontal layer, namely the FA belt, was found surrounding mature and centrally located FAs, which is characterized by localization of the Kank protein family and reduced force transmission [Sun et al., 2016].

1.2.2 Membrane-spanning integrin receptor family

In mammals, the integrin family of transmembrane receptors consists of 18 α and 8 β subunits, forming 24 heterodimers, which determines their ligand specificity and tissue distribution, as well as the intracellular adhesion complex formation and subsequent signaling. Knockout mice demonstrated the indispensable role of integrins including redundant and nonredundant functions, showing a wide variety of effects, ranging from embryonic lethality, developmental defects to perinatal death [Bouvard et al., 2013].

Integrins are characterized by a large ectodomain containing the ligand-binding region, a transmembrane helix and a generally short, 40-70 amino acids long, cytoplasmic tail, which mediates intracellular interactions (Figure 1.3) [Fu et al., 2012]. Depending on the integrin heterodimer, the globular extracellular domain build by the α and β

subunit can bind to diverse ECM proteins such as collagen, laminin, fibronectin and vitronectin [Plow et al., 2000]. Integrin receptors lack an enzymatic activity but instead recruit a range of signaling proteins. In addition, they provide a physical link between the ECM and the actin cytoskeleton thereby also permitting bidirectional mechanical signaling across the plasma membrane. ECM ligand binding can promote integrin activity and downstream signaling ("outside-in signaling"). On the other hand, binding of intracellular adapter proteins can also trigger the vast conformational change, from an closed "low affinity" state to an extended "high affinity" state ("inside-out signaling") (Figure 1.3) [Kim et al., 2003]. In addition to affinity modulations, multivalent ligands together with the cell's glycocalyx [Paszek et al., 2009] can cluster integrins, leading to avidity changes of integrin contacts [Carman and Springer, 2003]. Intriguingly, not only the ligand specificity varies between different integrin receptors, but atomic force microscopy (AFM) studies showed that some integrin subtypes, like integrin $\alpha 5\beta 1$, display a counterintuitive behavior, a so called 'catch bond', that is characterized by an increased ligand-bond lifetime upon increasing mechanical load in the range of 10-30 pN [Kong et al., 2009]. On the other hand, the integrin heterodimer $\alpha \mathrm{II}\beta 3$ shows a classical slip bond behavior when attached to its ligand fibrinogen, with reduced bond lifetime by increased tensile force [Litvinov et al., 2011].

1.2.3 Activation of integrins by talin and kindlin

The inside-out signaling pathway requires activating proteins that bind to the cytoplasmic tails of integrins. The access of binding partners to the integrin tail must be precisely tuned, which occurs mainly through competition among proteins for similar binding sites or post-translational modifications of the tail that changes the interactors affinities [Anthis et al., 2009; Gahmberg et al., 2009]. A functionally diverse set of intracellular proteins promotes the downstream signaling, with at least 40 direct interactors and many more indirect partners that have been reported by now [Geiger and Zaidel-Bar, 2012; Schiller et al., 2011]. However, there are two adapter proteins that stand out due to their distinguished role in activating integrin receptors, which are the four point one, ezrin, radixin, myosin (FERM) domain containing proteins, talin and the kindlin family of proteins. Most β-tails contain two NPXY motifs, which are the key regulatory sites for integrin activation. Talin binds the membrane proximal NPXY motif, whereas kindlins bind to the membrane distal binding site [Calderwood et al., 2013]. Talin

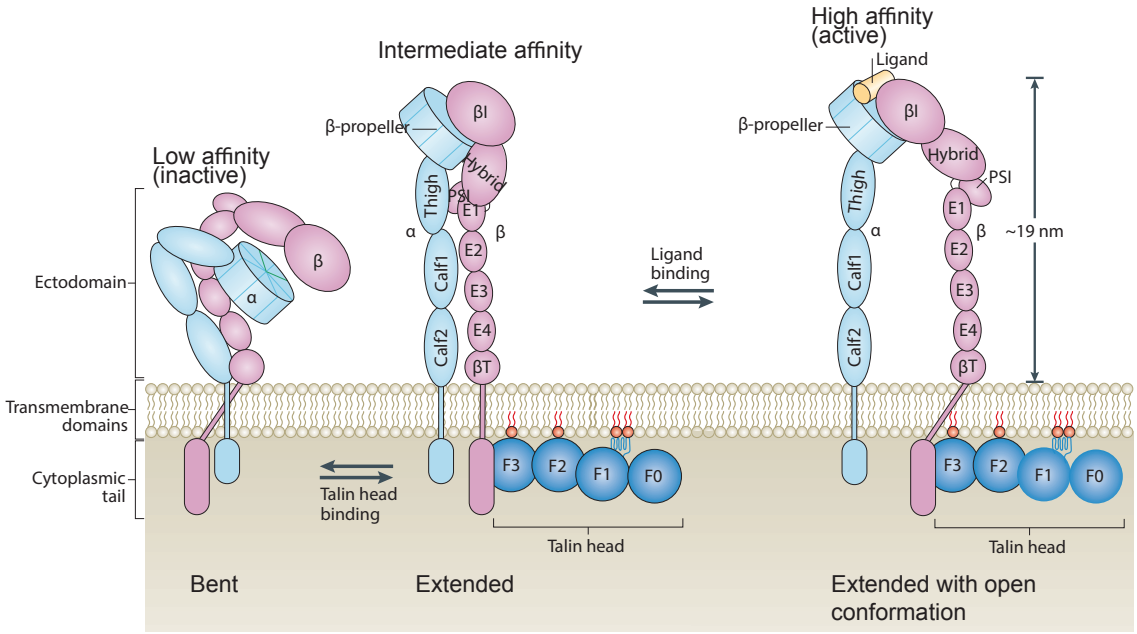

Figure 1.3: Integrin structure and activation. Integrins are non-covalently associated heterodimers formed by 18 α- and 8 β-subunits with diverse ligand specificity and tissue distribution, but a similar overall structure. Both subunits are composed of a short cytosolic tail, a transmembrane helix and a large ectodomain that is build by numerous modular units. Integrins exist in different states, they are inactive in the bend conformation, where the ligand binding site is oriented towards the membrane, however, upon binding of talin and kindlin (not shown) to the β tail, they switch to an extended ligand binding competent form. Furthermore, binding of adapter proteins to the cytosolic tails, disrupts their interaction and ligand binding leads to a conformational switch of a closed to an open headpiece. Adapted from [Calderwood et al., 2013].

binding to the β tail disrupts the association between the membrane-proximal parts of the α and β tails, thereby tilting the transmembrane helices, which triggers activation. *In vitro* studies from Ye et al. [2010] showed that talin binding is sufficient to trigger the extended conformation of integrins, however, *in vivo* the cooperative binding of talin in addition to kindlin binding to the distal binding motif is pivotal for integrin activation [Moser et al., 2008; Theodosiou et al., 2016]. Finally, integrin regulation occurs through competition between the aforementioned activating, but also inhibitory proteins, like filamin [Baldassarre et al., 2009] or ICAP1 [Liu et al., 2013], for the binding to the cytoplasmic tails of α and β subunits [Pouwels et al., 2012], which is further controlled

by phosphorylation of the binding motifs within the cytoplasmic integrin tails as well as the inhibitors and activators themselves [Li et al., 2015].

1.2.4 Actin cytoskeleton - architecture and mechanics

Focal adhesions transmit forces that are generated externally or by the actin network of the cell. This network consists of globular actin monomers assembling into double helical polymers, all arranged head to tail, which gives the filament a molecular polarity, that is key to actin filament assembly. Actin networks exert forces either by polymerization at the lamellipodium of the cell or by associated molecular motor proteins, like myosins [Chan et al., 2000; Small et al., 1978]. Actin advances at the lamellum by treadmilling, a process where polymerization occurs at the barbed end and depolyermization takes place at the pointed end of the filament, which pushes the membrane forward leading to cell protrusion [Pollard and Borisy, 2003]. Actin polymerization is regulated by vast amount of proteins, including profilin, providing ATP-bound actin subunits, Arp2/3, initiating nucleation and branching, formins and fascins, that promote elongation and crosslinking of filaments. Other actin modulators include cofilin, which severs actin cables. The tight regulation of the actin network is executed by many proteins, most notably, Rho GTPases, such as Rac, Rho and Cdc42, which links actin dynamics to adhesion signalling. It was shown by Galbraith et al. [2007] that actin polymerization at the protruding edge drives integrin clustering and positioning of nascent adhesions. Vice versa, integrins can promote actin assembly by recruiting Arp2/3 to adhesion sites via transient interactions with vinculin, FAK and Kindlin-2 [Böttcher et al., 2017; Chorev et al., 2014; Swaminathan et al., 2016]. Each actin filament generates a few piconewton [Abraham et al., 1999], however, membrane tension counterbalances this force, which induces an actin retrograde flow towards the cell center. Focal adhesions link the fast Arp2/3-dependent retrograde flow to the substratum, forming a so called "molecular clutch", creating traction and slowing down the retrograde flow (Figure 1.4) [Alexandrova et al., 2008; Pollard and Borisy, 2003].

In addition to the protrusive actin filament network, actin assembles into stress fibers, which are contractile bundles found in non-muscle cells. Filamentous actin is decorated with myosin II filaments, that use adenosine triphosphate (ATP) hydrolysis to power actin-myosin contraction [O'Connell et al., 2007]. Regulation of contractility occurs via phosophorylation of the myosin light chain (MLC) subunit, by numerous kinases,

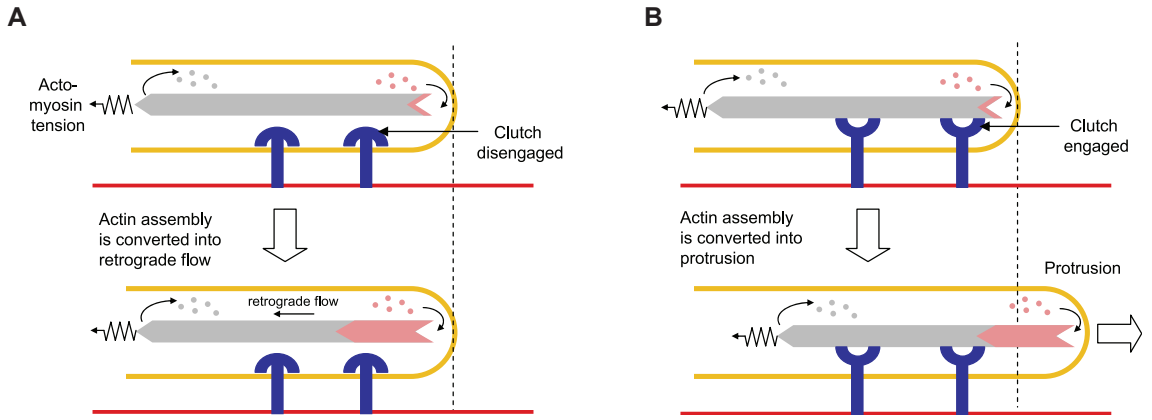

Figure 1.4: Adhesive structures build a "molecular clutch" between polymerizing actin and the substrate, which enables cell protrusion. (A) In case the "molecular clutch" is disengaged, tension generated by actin through actin-myosin contractions and actin treadmilling (shown in pink and grey) is counterbalanced by the membrane tension and results in actin retrograde flow. (B) Upon clutch engagement, forces are converted into traction which results in membrane protrusion and retraction of the cell rear [Le Clainche and Carlier, 2008].

including MLCK and Rho-regulated kinase ROCK [Amano et al., 1996; Totsukawa et al., 2004], as well as dephosphorylation by myosin phosphatase. Stress fibers are divided into distinct classes, comprising dorsal and ventral stress fibers, transverse arcs and perinuclear caps [Khatau et al., 2009; Tojkander et al., 2012]. Dorsal stress fibers are the exception and contain only little myosin, but attached to FAs, they transmit tension generated by other types of stress fibers to the ECM. Transverse arcs, on the other hand, are not linked to adhesion sites, but transmit contractile force to the connected dorsal fibers. The main contractile machinery are ventral stress fibers that are attached at both ends to FAs and enable the cell to constrict the rear and thereby migration [Chen, 1981].

1.3 Talin is the central adapter protein in FAs

1.3.1 Talin holds a crucial function in tissue physiologie and pathologie

In 1983, Burridge and Connell [1983] first identified talin in membrane ruffles and adhesion junctions formed between the cell and the ECM. Talin, which is conserved throughout metazoans and ubiquitously expressed in mammalian cells, was shown

to be one of the key proteins in focal adhesions, where it occupies diverse functions that are indispensable for cell adhesion, signaling and cell-ECM mechanotransduction [Calderwood et al., 2013]. Talin ablation in in worms [Cram et al., 2003], flies [Brown et al., 2002] and mice [Monkley et al., 2000] lead to phenotypes that are similar to deletion or mutation of integrins themselves, which confirms its essential role. RNA-interference induced down-regulation of talin in *Caenorhabditis elegans*, for instance, impaired distal tip cell migration leading to defects in gonad formation, whereas contractile muscle cells showed a disorganized actin cytoskeleton that resulted in complete paralysis [Cram et al., 2003]. *Drosophila melanogaster* embryos deficient in talin die during embryogenesis, displaying defects in germ band retraction and a muscle detachment phenotype [Brown et al., 2002].

Vertebrates, including mouse and human, have two talin genes, talin-1 and talin-2. Global deletion of talin-1 gene in mice is embryonic lethal due to defects in gastrulation; however, it is important to mention here, that talin-2 might have been still expressed in these embryos, which could have attenuated the phenotype [Monkley et al., 2000]. Talin is one of the key regulator of integrin activation and transient down-regulation of talin in numerous cell lines demonstrated a reduction of $\beta 1$ and $\beta 3$ affinity to their extracellular ligands [Tadokoro et al., 2003]. Similarly, conditional knockout of talin in mouse platelet precursors inhibited ligand induced αIIb$\beta 3$ integrin activation, platelet aggregation and thrombus formation [Nieswandt et al., 2007]. Another example for the importance of talin-mediated integrin activation was demonstrated in B lymphocytes, where talin is crucial for integrin-dependent homing of B cells to lymph nodes and bone marrow [Manevich-Mendelson et al., 2010]. Besides its role in integrin activation, talin is also an important adapter protein in FAs and mediates the linkage to the cells actin cytoskeleton. A study by Conti et al. [2008] showed the importance of this linkage, by a muscle-specific ablation of talin, which abrogates the integrity of myotendinous junctions, resulting in progressive myopathy in these mice. On a cellular level, Zhang et al. [2008] could show, that Talin depletion in fibroblasts dramatically sustained cell adhesion and spreading, disrupted downstream signaling pathways and also traction force generation was impaired in those cells. Finally, besides talins role in healthy cells, the dysregulation of talin can lead to diverse pathologies, such as hematologic disorders [Haining et al., 2016], as well as several cancer types, where talin was shown to be significantly up-regulated, resulting in increased adhesion, migration and invasion in these cells [Beaty et al., 2014; Kanamori et al., 2011; Sakamoto et al., 2010].

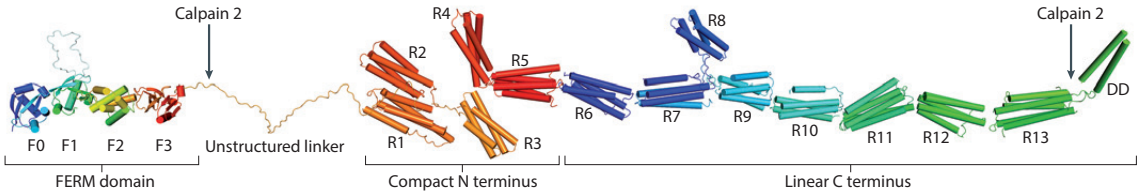

Figure 1.5: Structural model of talin. Crystal and NMR structures of individual domains of talin unraveled an elongated structure, with an atypical FERM domain consisting of four subunits, F0, F1, F2 and F3 [Elliott et al., 2010]. An unstructured linker region is connecting the head domain to the talin rod, which is comprised of thirteen subunits, R1-R13, followed by a C-terminal dimerization domain (DD) [Gingras et al., 2007b]. The rod domains are organized into four and five helical bundles, which are either connected at the same end of the subunit (R2-R4 and R8) forming the compact N-terminal rod region, or via their N- and C-termini building the elongated C-terminal part of the rod. Two calpain cleavage sites are indicated. Adapted from [Calderwood et al., 2013].

1.3.2 Domain structure of talin

Talin is a large protein of 270 kDa, with a N-terminal FERM domain forming the talin head and an elongated rod domain. The FERM domain of talin is atypically elongated rather than in a cloverleaf structure and is divided in four subunits, namely, F1, F2,+ F3 and the extra domain F0 (Figure 1.5) [Elliott et al., 2010; Goult et al., 2010]. Crystal structure analysis studies showed that the F3 domain is a phosphotyrosine-binding (PTB)-like fold [García-Alvarez et al., 2003]. Talin's head and rod domain are linked by a unstructured, flexible region, which contains phosphorylation and protease cleavage sites, including calpain II [Bate et al., 2012; Ratnikov et al., 2005]. The rod domain contains 62 α-helices, that are organized in 13 helical bundles, R1-R13, each consisting of four or five helices (Figure 1.5) [Goult et al., 2013a]. A second calpain cleavage site [Bate et al., 2012] is located between the rod domain R13 and the single helix at the very C-terminal end of the rod, which serves as dimerization domain and was shown to form antiparallel homodimers *in vitro* [Gingras et al., 2007a; Goult et al., 2013a].

1.3.3 Insights into talin binding partners

Talin mediates the major linkage between integrins and the actin cytoskeleton, however, in addition it serves as an adapter protein for many more FA resident proteins (Figure 1.6). The main integrin binding site (IBS1) is located in the F3 domain of talin's

FERM domain and is mediated by its PTB domain [García-Alvarez et al., 2003]. As already mentioned in section 1.2.2 the integrin receptor family is composed of numerous heterodimers, all of which bind to different extracellular ligands. Intriguingly, talin is able to activate most of them by binding to the NPxY motif in the cytoplasmic tails of integrin $\beta1$–$\beta3$, $\beta5$, $\beta7$ and most probably $\beta6$, whereas activation of $\alpha v\beta8$ and $\alpha6\beta4$ is likely to be talin-independent [Calderwood et al., 2003; Legate and Fässler, 2008]. The head domain of talin also directly interacts with phosphatidylinositol 4,5-bisphosphate (PIP2) containing membranes via the loop domain of F1, as well as F2 and F3 subdomains [Anthis et al., 2009]. Additionally, the head region binds actin via the F2-F3 domain, defined as actin binding site 1 (ABS1) [Lee et al., 2004]. The F0 domain of talin is the binding site for Rap1 [Goult et al., 2010], while F3 interacts with FAK, T-cell lymphoma invasion and metastasis 1 (TIAM), Phosphatidylinositol phophate kinase type Iγ (PIPKIγ) [Calderwood et al., 2013], as well as Rap1-GTP interacting adapter molecule (RIAM) [Yang et al., 2014].

Similarly, the talin rod domain contains several protein interaction sites. There are two further actin binding sites, one formed by R4-R8 (ABS2) [Hemmings et al., 1996] and a third one is formed by R13 together with the very C-terminal dimerization helix [Gingras et al., 2007a]. Moes et al. [2007] found a second integrin binding site (IBS2) in R11, although, a proof of function was only shown for drosophila wing adhesion sites by now [Klapholz et al., 2015]. Furthermore, the rod domain contains at least 11 vinculin binding sites (VBSs) that are distributed all over the elongated rod. VBSs consist of a single amphiphatic α-helix with hydrophobic residues on one site and are typically buried within the rod domains [Gingras et al., 2005]. These cryptic VBSs are thought to become accessible upon domain unfolding, which depends on hydrophopic interactions within the core of the rod domain and the force load applied to talin [del Rio et al., 2009]. Finally, in addition to its binding site in the head domain, RIAM also was shown to bind to several sites in the talin rod [Goult et al., 2013b]. Binding motifs were also identified for paxillin, DLC1, α-synemin and Kank [Bouchet et al., 2016; Sun et al., 2008; Zacharchenko et al., 2016].

1.3.4 Talin - recruitment and activation

Electron microscopy experiments together with cryo-electron microscopy studies suggest that cytosolic talin is in an autoinhibited global conformation, where the head domain

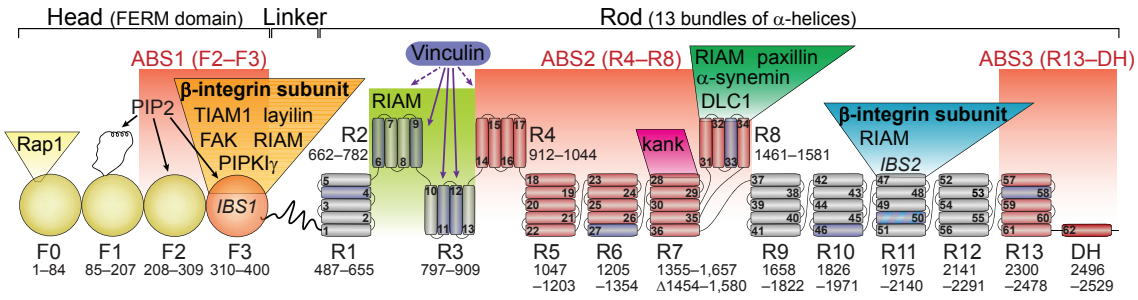

Figure 1.6: Domain organization and interaction sites of talin. Talin, a key adapter protein in adhesion complexes, holds numerous binding sites for structural as well as signaling proteins, as indicated. The major integrin binding site (IBS1) in the head region is shown in organge, the three actin binding sites are colored in red and α-helices that can be bound by vinculin are depicted in dark blue [Klapholz and Brown, 2017].

F3 is bound by R9 of the talin rod and is buried in the center of a donut-shaped dimer, which sterically prevents binding of IBS1 to integrin tails [Goksoy et al., 2008; Goult et al., 2013a; Winkler et al., 1997]. Several pathways of talin recruitment and activation at adhesion sites are described, which seem to be cell type specific [Stritt et al., 2015]; thus, further studies are needed to unravel how the diverse mechanisms are connected and regulated. One emerging pathway involves the small GTPase RAP1 and the effector protein RIAM. It is thought that talin translocates to the membrane in response to RAP1 activation by protein kinase C and binding to RIAM via its F3 domain, which then leads to talin unmasking [Lee et al., 2008; Stritt et al., 2015; Yang et al., 2014]. Another study by Goksoy et al. [2008] demonstrated that binding of the F3 domain to negatively charged phospholipids within the membrane, namely Phosphatidylinositol 4,5-bisphosphate (PIP2), provokes the conformational change in talin to its extended form [Goksoy et al., 2008]. Further known activators of talin are the heterotrimeric G protein Gα13, also binding to the F3 subunit [Schiemer et al., 2016] and Kank2, which binds to R7 in order to activate talin [Sun et al., 2016]. In mammalian cells, FAK was shown to be involved in talin recruitment to nascent adhesions [Lawson et al., 2012], yet, FAK depletion in drosophila does not impair adhesion formation [Grabbe et al., 2004].

Some interaction sites in talin are thought to be tightly regulated by conformation as already described for VBSs in subsection 1.3.3. The VBS in the R3 domain is likely to be the first site to bind vinculin, since it is destabilized by a unique cluster of threonine residues within the hydrophobic core [Goult et al., 2013b]. First, RIAM recruits talin

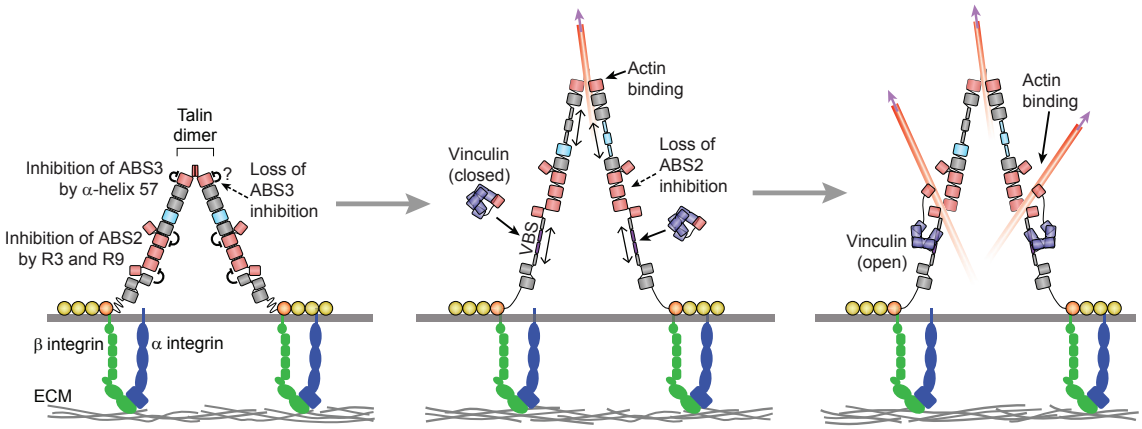

Figure 1.7: Talin binding sites are tightly regulated by steric inhibition. Talin activation requires RIAM dependent recruitment to the membrane, where PIP2 is responsible for the release of autoinhibition and binding of the head domain to β tails [Lee et al., 2008], [Goksoy et al., 2008]. In the initial state, both actin binding sites of talin are not accessible to actin due to steric hindrance through adjacent subdomains, which makes conformational rearrangements necessary. Upon actin binding to the C-terminal ABS3 in an unknown mechanism, the N-terminal rod domain R3 is the first helical bundle to unfold in a tension dependent manner, which releases RIAM (not shown) and at the same time enables binding of vinculin to the cyrptic vinculin binding site. Thus, the second actin binding site (ABS2) is not longer inhibited and actin can attach [Klapholz and Brown, 2017].

by binding to R2-R3 domains and in addition mediates VASP localization to nascent adhesions, which drives actin polymerization. Secondly, upon integrin activation by talin and additional binding of its ABS3 domain to f-actin rearward flow, vinculin displaces RIAM from R3 due to force-induced conformational changes [Goult et al., 2013b], which is further described in 1.4. Likewise, accessibility of both actin binding sites and also IBS2 are negatively regulated by adjacent subdomains, which is shown in figure 1.7. ABS3 consists of α-helices 58-62 which are shielded by α-helix 57 [Gingras et al., 2007b], whereas ABS2 is inhibited by the neighboring subunits R2-R3 and R9 [Atherton et al., 2015]. Similarly, IBS2 consists of α-helix 50, which is occupied in the native state by α-helix 51 [Klapholz et al., 2015]. At least for ABS2 it is known that tension-dependent vinculin binding to the N-terminal VBSs diminishes the repression [Atherton et al., 2015].

Talin function is regulated by localization and conformational changes, but also through competitor proteins (subsection 1.2.3) and by proteolysis-dependent turn over. The two calpain cleavage sites described in subsection 1.3.2, show diverse sensitivity for

calpain, but both promote FA turnover at the cell rear and thus cell migration [Bate et al., 2012].

1.3.5 Talin-2: isoform with almost unknown function

In vertebrates two talin genes are expressed, which encode similar proteins with 74% identity, called talin-1 and talin-2 [Monkley et al., 2001]. Although, talin-2 is the anchestral gene, with an increased gene size due to larger introns, both talin isoforms have a similar size on the protein level and the tertiary structure is characterized by the same subdomains. At the beginning of my study, the reason why vertebrates express two versions of talin was still unclear. While talin-1 was known to be ubiquitously expressed in mammals, talin-2 showed a distinct expression pattern with high levels in heart, skeletal muscle and brain, where it is is also the abundant isoform [Monkley et al., 2001]. Studies in cultured fibroblasts showed that talin-2 can compensate for the loss of talin-1, concerning adhesion and spreading of these cells [Zhang et al., 2008]. In contrast, on an organismal level, it was shown by knockout studies in mice that talin-1 depletion is embryonic lethal [Monkley et al., 2000] (subsection 1.3.1), whereas loss of talin-2 only results a mild form of muscular dystrophy [Conti et al., 2009]. These experiments showed that talin-1 can adopt most of the functions of talin-2, since it is ubiquitously expressed, but not in skeletal muscles, where talin isoforms occupy distinct, non-overlapping roles. On a cellular level, it was shown that talin-2 localizes to large FAs and fibrillar adhesions, while talin-1 is predominantly found in small FAs at the leading edge of the cell [Praekelt et al., 2012]. Recently, structural studies unraveled an increased affinity of talin-2's head domain for β-integrin tails compared to talin-1, particularly, talin-2 together with β1D, both expressed in striated muscles, form an unusually strong interaction [Anthis et al., 2010; Yuan et al., 2017]. Furthermore, Qi et al. [2016] demonstrated a unique role of talin-2 in cell invasion, which comprises the generation of traction forces, thereby driving invadopodium-mediated matrix degradation.

1.4 Talin a putative force sensitive protein

Forces applied to nascent focal adhesions induce strengthening of the integrin–cytoskeleton interaction [Choquet et al., 1997], which leads to focal complex stabilization. Studies determined forces pulling at single integrins to a range between 1 to 40 pN

[Blakely et al., 2014; Morimatsu et al., 2013; Wang and Ha, 2013]. Since talin is an essential linker protein [Priddle et al., 1998], its putative role in the early mechanosensory system was predicted using steered full atom molecular dynamics simulations by Lee et al. [2007] and Hytönen and Vogel [2008], proposing talin unfolding upon actomyosin contraction correlating with the recruitment of adapter proteins like vinculin.

First *in vitro* experiments using magnetic tweezer setups and purified N-terminal talin rod domains, R1-R3, showed a increased vinculin-talin interaction upon force load of around 12 pN [del Rio et al., 2009]. Yao et al. [2014] showed unfolding of R1-R3 in three distinct steps, the first domain (R3) already sensitive to very low forces of 5 pN. Upon mechanical stress, R1-R3 reveal VBSs and upon binding of vinculin talin is stabilized in its unfolded conformation [Yao et al., 2014].

While my study, additional reports substantiated these findings and revealed that talin undergoes myosin-dependent extension fluctuations *in vivo* using single-molecule super-resolution imaging in living cells [Margadant et al., 2011]. In a stretching phase talin elongates from its folded state of around 80 nanometer (nm) up to $\sim$ 350 nm. In order to reach such a significant length increase, several talin rod domains need to unfold when experiencing tensil forces. Extended *in vitro* experiments using a magnetic tweezer setup demonstrated, that all rod domains of talin are able to unfold upon force, however the more N-terminal rod domains unfold upon a few piconewton, whereas the more C-terminal ones, unfold upon highly increased tension loads of $\sim$ 20 pN [Yao et al., 2016].

The question still remained, if talin experiences tension, especially forces as high as 20 pN, in living cells and whether vinculin contributes to force transduction across talin by binding to the eleven VBSs. Moreover, this study aimed to answer the question of how mechanical tension across talin is regulated by other FA proteins, as well as, to elucidate if the two talin isoforms transduce mechanical information differently.

1.5 Techniques to measure cellular and molecular forces

Forces generated within entire tissues can be measured by methods like laser ablation, where the retraction of the ablated edges provide qualitative evidence of contractile forces generated by adjacent cells[Fernandez-Gonzalez and Zallen, 2013]. In addition,

several techniques to determine tension across proteins *in vitro* and inside living cells haven been developed over the past 20 years.

1.5.1 Cell-ECM traction

Contractile forces generated by single cells through actomyosin contraction to the ECM or adjacent cells are in the piconewton to nanonewton range and within a small length scale of nano- to micrometers, which makes traction measurements challenging. A variety of techniques exist to probe cellular traction, all of which make use of materials with defined mechanical properties and linear elastic behavior upon cellular deformation. For measuring cellular traction in 2D, microfabricated pliable pillars and traction force microscopy (TFM) are the most widely used techniques. Microfabricated platforms consist of hundreds of cantilevers decorated with substrate molecules to which cells can adhere. The resulting displacement of each individual cantilever can be tracked and the applied force can be calculated [Galbraith and Sheetz, 1997]. In contrast, TFM is based on a synthetic elastic polymer substrate with embedded small fluorescent beads, used as fiducial markers, which can be microscopically tracked in space and time, to determine the position in the stressed state upon cell adhesion and in the relaxed state after cell lysis [Plotnikov et al., 2014]. Using high-resolution TFM forces can be reliably mapped in submicrometer resolution [Plotnikov et al., 2014]. Further improvement of TFM enabled to characterize the 3D traction field of a cell by embedding them into hydrogel matrices [Legant et al., 2010]. Recently, probes have been developed that measure strain in molecular springs [Stabley et al., 2012] or DNA hairpin [Wang and Ha, 2013], which report traction forces at single adhesion sites. These probes, flanked by either a FRET pair or a fluorophore-quencher pair, are conjugated to the cell surface and strain can be microscopically measured [Stabley et al., 2012; Wang and Ha, 2013].

1.5.2 Probing the mechanical properties of proteins *in vitro*

Various methods have been established to scrutinize the mechanical responses of single molecules *in vitro*, like AFM [Puchner and Gaub, 2009], optical [Capitanio and Pavone, 2013] and magnetic tweezers [Kilinc and Lee, 2014]. These diverse experimental setups share a general principle that is to tether one end of the purified protein of interest to a functionalized cantiliver, a dielectric or paramagnetic bead, while the other end is fixed to a surface. By applying external force to the molecule and at the same time

recording the deflection of the cantiliver or the laser beam, force-extension traces give insights into the unfolding and refolding behavior of the protein and allow to pinpoint domains within the protein which unfold at specific force ranges [del Rio et al., 2009; Kong et al., 2009].

1.5.3 Förster resonance energy transfer

In order to measure tension across individual proteins within living cells, several biosensors have been developed over the past years, most of which are based on FRET as microscopically-traceable tension readout. FRET is a non-radiative energy transfer between a donor and an close-by acceptor molecule due to long-range intermolecular dipole-dipole coupling [Förster, 1965]. The FRET efficiency E, defined as the fraction of electronically exited donor (D) chormophores which transfers energy to the acceptor, is dependent on the distance r between the fluorophores and their characteristic Förster radius R_0 (equation (eq) 1.1) [Jares-Erijman and Jovin, 2003].

$$E = \frac{R_0^6}{R_0^6 + r^6} \tag{1.1}$$

The Förster radius R_0 is the distance between donor and acceptor at which the energy transfer is 50 % efficient, and is defined for each fluorophore by the quantum yield of the donor Q_D, the relative orientation between the two dipoles κ^2, the refractive index n and the overlap of the donor emission and acceptor absorption spectra, given by the integral J (eq. 1.2).

$$R_0^6 \sim \kappa^2 n^{-4} Q_D J \tag{1.2}$$

1.5.4 Microscopical methods for measuring FRET

FRET can be measured either with steady-state or time resolved methods. Steady-state methods are either intensity- or emission spectra based [Wallrabe and Periasamy, 2005], however, most frequently the donor is excited and the emission intensity of the donor (I_D) and the acceptor (I_A) is recorded and utilized to calculate the FRET ratio (eq. 1.3).

$$FRETratio = \frac{I_D}{I_A} \tag{1.3}$$

This intensity-based approach estimates a relative FRET ratio and does not yield in quantitative FRET efficiencies; in addition, the method is highly sensitive to experimental setting changes, like concentration of the fluorescent molecule or laser intensity [Wallrabe and Periasamy, 2005]. In contrast, time resolved methods, like FLIM directly measure the concentration-independent fluorescence decay of the donor molecule [Wallrabe and Periasamy, 2005]. The fluorescene lifetime is defined as the average time the molecule is in the excited state before emitting a photon. Two main approaches exist to measure fluorescence lifetime, namely, the time domain [Becker et al., 2004] and the frequency domain FLIM [Gratton et al., 2003]. Time-domain FLIM setups measure the exponential decay in intensity after the laser pulse from which the decay time is calculated. In frequency domain FLIM approaches the sample is excited with intensity-modulated light and by measuring the phase shift, the decay time can be calculated. In both approaches the recorded fluorescence lifetime can be used to calculate the FRET efficiency E from the donor lifetime in the presence (DA) or absence (D) of the acceptor (eq. 1.4).

$$E = 1 - \frac{\tau_D}{\tau_{DA}} \tag{1.4}$$

1.5.5 Genetically-encoded tension sensors: Unraveling molecular forces

In order to understand mechanotransduction on a molecular level, it is important to investigate force transmission across single molecules directly in living cells. *In vitro* studies showed that forces produced by a single cytoskeletal motor protein, like the f-actin binding protein myosin, or the microtubule-binding motors kinesin and dynein, are in the range of 3–4 pN and 5–7 pN, respectively [Finer et al., 1994; Gennerich et al., 2007; Svoboda et al., 1993]. Forces lower than 1–2 pN are difficult to detect since they disappear within thermal noise, whereas much higher forces are required to unfold a whole protein domain, for example the FNIII domain of fibronectin or the immunoglobulin domain of titin is denatured at forces as high as 80–300 pN [Oberhauser et al., 2002; Rief et al., 1997]. Altogether these studies indicate that the important mechanotransduction processes occur in the lower piconewton range, which can be displayed by the tension probes that have been developed over the past years. Several molecular designs exist that display intramolecular strain, all of which based on

genetically-encoded tension probes that are inserted into the protein of interest [Wang et al., 2011]. The general principle of most of the available tension sensor modules is based on a flexible, tension sensitive linker molecule, that elongates upon mechanical load which can be microscopically followed. The first published linker element was a stiff alpha-helix developed by Meng et al. [2008], followed by a the spider silk flagelliform peptide [Grashoff et al., 2010] and the spectrin repeat element [Meng and Sachs, 2010], the latter ones displaying forces in the range of 1-6 pN and 5-7 pN, respectively. The published tension sensitive linker peptides, not only display varying force-sensitivity ranges, but also show unique force-elongation profiles, such as the flagelliform element that linearly extends upon force load resembling the behavior of an elastic spring [Grashoff et al., 2010].

At the beginning of this study, the exact force range transduced by a protein of interest could not be resolved. Instead, rather rough estimations of average forces per cell had been be reported, owing to the gradual force response of the sensor modules and/or insufficient sensor calibration. Digital sensor modules with differing force sensitivities, that allow to pinpoint the force exerted on proteins and even to determine the fraction of mechanically engaged molecules within a subcellular structure, were still missing.

Most biosensors are based on FRET and make use of the distance dependency of the energy transfer between two fluorophores. Typically the modular design comprises two green fluorescent protein (GFP)-like fluorophores linked via an elastic tension sensitive module. Since the FRET efficiency is dependent on the inverse sixth power of the distance between donor and acceptor, mechanical tension extending the linker element leads to chromophore separation followed by a significant decrease in FRET.The average length of the tension sensitive linker is around 5-10 nm, which is approximately the Förster radius R_0 range of the currently available FRET fluorophore pairs.

Additionally, biosensors exist, in which mechanical tension across the linker element changes the orientation between the choromophores rather than the length [Meng and Sachs, 2012]. An alternative approach developed by Ichimura et al. [2012] utilizes an engineered strain-sensitive fluorophore and correlates molecular tension with fluorescence loss.

These diverse techniques already contributed to the understanding of intramolecular tension across diverse subcellular structures, for example a vinculin tension probe allowed the analysis of forces in cell-ECM contact sites [Grashoff et al., 2010]. A similar tension sensor module was used to investigate tension across cell-cell contacts

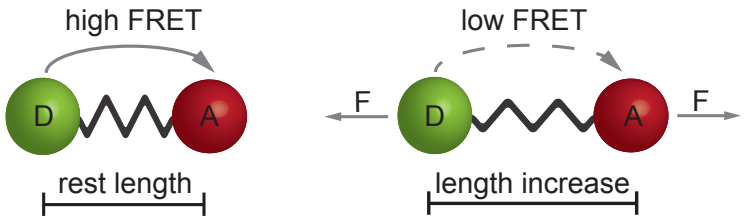

Figure 1.8: Distance-dependent FRET-based tension sensor module. Schematic representation of a genetically-encoded FRET-based tension sensor module, that is comprised of a donor fluorophore (D) and an acceptor fluorophore (A), connected by a tension sensitive linker molecule, that extends upon force load. FRET efficiency is highly distance dependent, resulting in an high energy transfer in the resting state, but reduced FRET efficiency upon mechanical stretch, which can be microscopically followed [Ringer et al., 2017].

via E-cadherin [Borghi et al., 2012], across the cytoskeleton using an α-actinin sensor [Meng and Sachs, 2010] as well as across the ECM component fibronectin [Smith et al., 2007].

In this study the aim was to apply the existing tension sensor published by Grashoff et al. [2010], as well as, newly developed, single-molecule calibrated tension sensitive probes with more like digital force-elongation behavior and diverse force sensitivity ranges to unravel force transduction across the FA protein talin.

2 Aim of Thesis

Talin is a key adapter protein in cell-extracellular matrix (ECM) contacts. By now it is well established that talin fulfills at least two substantial tasks, the first one is the activation of the focal adhesion (FA)-resident receptor family integrins in a process called "inside-out" signaling, whereas the second function is to establish the linkage between integrins, bound to the ECM, and the actin network within the cell. As an adapter protein talin serves as a signaling platform, recruiting numerous interaction partners to the adhesion complex. In addition, it was hypothesized that talin occupies a role in transmitting mechanical cues within FAs; however, by the time I started my PhD project direct evidence was lacking. Several *in vitro* studies demonstrated unfolding of talin's subdomains in response to force, yet, whether talin was exposed to these forces in living cells was unclear. Additionally, the exact force range that talin bears and the fraction of mechanically engaged molecules was highly debated. Finally, the reason for vertebrates to express two talin isoforms and especially the role of talin-2 in cellular mechanotransduction remained elusive. In the past years, several approaches were established in order to investigate force transmission in living cells, most of them on the basis of genetically-encoded elastic linker peptides that act as piconewton (pN) force sensors when flanked by a fluorophore pair undergoing efficient Förster resonance energy transfer (FRET). However, most of the published sensor modules were either poorly calibrated or gradually elongate upon force load, which does not allow the exact determination of force per molecule.

To allow the comparative analysis of talin-1 and talin-2 mechanotransduction in living cells, my **first aim** was to generate and evaluate talin-2 tension sensor constructs, based on newly developed tension sensor modules. Furthermore, I investigated the isoform-specific force transmission and its regulation by other FA proteins. In addition, I aimed to elucidate the mechanism of rigidity sensing upon differential expression of talin-1 and talin-2.

My **second aim** was to improve our understanding of force propagation across the elongated rod domain of talin-1. By generating a new talin tension sensor, I aimed to unravel the contribution of different subdomains of the talin rod to force generation. Additionally, I established a method which allowed for the first time the simultaneous analysis of two different tension sensors within one cell. Using a novel tension sensor module, sensitive to the lower piconewton range with near-digital force response, I determined the fraction of mechanically engaged talin-1 molecules within FAs.

Finally, I wrote, together with a student fellow, a review article, in which I summarized and discussed recent developments of biosensors that allow molecular force measurements, with an emphasis on the systematic evaluation of FRET-based tension sensor experiments. In a second review article I recapitulated the current knowledge of cell-ECM adhesions and their way to sense the complex nature of the ECM. Furthermore, the impact of newly established experimental as well as theoretical approaches that assist to complement the image of mechano-chemical coupling at FAs was highlighted.

3 Short summary of manuscripts

3.1 Paper I – How to measure molecular forces in cells: A guide to evaluating genetically-encoded FRET-based tension sensors.

Cost A.-L.*, Ringer P.*, Chrostek-Grashoff A., Grashoff C. (* equal contribution)

Cells are exposed to a broad variety of forces, like shear stress, contraction or compression and have to sense and adapt to them. A variety of subcellular structures known to mediate these different aspects of mechanotransduction are the plasma membrane, the cytoskeleton, the nuclear envelope, mechanosensitive ion-channels and cell adhesion complexes. Techniques like traction force microscopy as well as force spectroscopy methods such as atomic force microscopy (AFM), optical and magnetic tweezers brought a major breakthrough for understanding those forces on a cellular and even on a molecular level. To complete these *in vitro* studies on force transduction, molecular tension sensors were developed to quantify lower piconewton (pN) forces across proteins *in vivo* and several designs of such biosensors exist that allow determining forces at the cell surface and within the cell. In this study, we review recent advances in the development of biosensors, especially the currently available Förster resonance energy transfer (FRET)-based tension sensors and propose a strategy to systematically evaluate them. A number of approaches have been developed to measure molecular tension, which are based beside FRET upon photo-quenching, loss of fluorescence and change of fluorophore emission properties. All of these techniques depend on an extendable molecule that undergoes a length increase upon application of mechanical force. However, FRET-based tension sensors are most frequently used and depend on a process of nonradiative energy transfer between two fluorophores, which is highly

dependent on the separation distance of the chromophores. Beside the fluorophores Förster radius, FRET is sensitive to the relative orientation of the fluorophores, the donor quantum yield and the overlap of the donor emission and the acceptor absorption spectra. Therefore we highlight in this review the need of an in depth characterization of the tension sensor modules, for example by single-molecule calibration and by performing several controls to ensure that the effect of FRET differences is tension dependent and not caused by other confounding factors. Additionally, effects of the tension sensor module integration into the protein of interest need to be carefully evaluated. Approaches to determine FRET in cells are either intensity-based or depend on the determination of the fluorophore lifetime, which gives either qualitative or quantitative results, respectively. However, in both cases a proper data analysis is critical, which is greatly facilitated by an automated data analysis software. In summery, we review how molecular tension sensors should, ideally, be evaluated. Only then, molecular tension sensors are a powerful tool to elucidate cellular mechanotransduction processes.

3.2 Paper II – Extracellular rigidity sensing by talin isoform-specific mechanical linkages.

Austen K.*, Ringer P.*, Mehlich A.*, Chrostek-Grashoff A., Kluger C., Klingner C. Sabass B., Zent R., Rief M., Grashoff C. (* equal contribution)

Cells sense the stiffness of their extracellular environment, which is crucial for normal organ development and function, whereas deregulation of rigidity sensation is connected to numerous diseases, like tumor formation and cardiovascular disorders. To distinguish between different matrix rigidities, cells probe their surrounding by anchoring to the extracellular matrix (ECM) via focal adhesions (FAs). The main anchor of FAs are integrin receptors that span the membrane and bind to the ECM. At the same time integrin tails can be bound by cytosolic adapter proteins that are thought to transmit mechanical cues to the actin cytoskeleton and in addition translate it into a biochemical signals. One of the major adapter proteins, which is additionally known for its important role as integrin activator, is talin. Talin directly binds integrins with its head domain and at the same time connects to the actin cytoskeleton via its elongated rod domain. It was proposed by *in vitro* studies that talin transmits mechanical information, however, direct and quantitative evidence for force transmission across talin was still missing.
In this study, we engineered two genetically-encoded Förster resonance energy transfer (FRET)-based biosensors based on the ultrafast-folding villin headpiece peptide (HP35) flanked by the YPet/mCherry fluorophore pair, called HP35-tension sensor module (TSM). Single-molecule calibration of the HP35-TSM and a mutated stable variant (stHP35-TSM), using an optical tweezer setup, revealed transitions between the unfolding and folding conformation in response to mechanical force of 7 piconewton (pN) and 10 pN, respectively. To examine forces across talin in cells, we genetically inserted the TSM into the unstructured linker region between the head and the rod domain. Expression of the talin tension sensor in talin double knockout cells revealed proper localization, as well as rescue of the sever cell adhesion defect of talin-deficient cells and normal FA turnover rates, indicating normal function of the protein. Performing fluorescence-lifetime imaging microscopy (FLIM) and ratiometric FRET experiments, we were able to show that talin bears forces of 7 pN on average and that a subset of molecules transmits even forces higher than 10 pN. Force transmission across talin is dependent on its

association with mechanically engaged vinculin and f-actin. Furthermore, our studies revealed that talins' mechanical engagement with the actin cytoskeleton is dispensable for integrin activation, but crucial for FA reinforcement and hence extracellular rigidity sensing.

Mammals express two talin genes, which encode similar proteins with 74 % identity, the ubiquitous expressed talin-1 and the more restrictively expressed talin-2. Intriguingly, our studies revealed that talin mechanics are isoform-specific. Specifically, talin-2 bears higher forces than talin-1 and additionally, more talin-2 molecules are engaged within FAs. The observed tension increase in cells expressing talin-2 is due to differences in vinculin recruitment to the N-terminal rod domains R1-R3 of talin-2, which stabilizes FAs in these cells even on compliant substrate. By regulating the expression of talin-1 and talin-2, cells can modulate their extracellular rigidity sensing. Altogether, our experiments unraveled a new mechanism that couples cell adhesion with mechanosensing, in which talin mediates an essential linkage, that is crucial for cells to detect tissue stiffness.

3.3 Paper III – Sensing the mechano-chemical properties of the extracellular matrix

Ringer P., Colo G., Fässler R., Grashoff C.

Many developmental and also pathological processes depend on the ability of cells to sense and respond to their mechanical and chemical environment. Cells need to detect chemical compositions and mechanical cues from the extracellular matrix (ECM), which are transmitted by complex multi-molecular structures called focal adhesions (FAs). In this review, we summarized recent findings about the intricate nature of FAs and their way of integrating mechanotransduction and chemical signaling. Furthermore, we discussed how the combination of experimental and theoretical approaches can be used to unravel the mechanisms behind the coupling of mechanical and chemical cues during cell adhesion. The architecture of FAs can be divided in horizontal and vertical substructures, which are individually regulated. FAs are composed of three main vertical layers, with an outer layer in which diverse integrin receptor subtypes anchor to a wide range of ECM proteins, an intermediate layer where most of the chemical and mechanical signals are processed and finally an inner layer, that is characterized by the force generating actin cytoskeleton. Horizontal segmentation of FAs depends mainly on the segregation of different integrin subtypes and the discrimination between a FA core and a belt region, the latter characterized by accumulation of Kank proteins and reduced force transmission. The concept emerged that FAs act similar to an elastic spring, which extends and reinforces when tension is applied and the ECM is sufficiently rigid, but remains small when forces are low. To understand these complex subcelluar signaling hubs in more detail, a number of recently developed techniques were utilized. For example, force spectroscopy methods revealed the force load across proteins in the diverse FA layers, whereas improved mass-spectrometry methods shed light on the composition of FAs, and the improvements in high-resolution microscopy techniques unraveled the nanostructure and the molecular dynamics of FAs. In addition, theoretical approaches integrated experimental findings to predict FA behavior leading to a new conceptual understanding of cell-ECM adhesion and the mechanism of sensing mechano-chemical properties of the surrounding environment.

3.4 Paper IV – Multiplexing molecular tension sensors reveals force gradient across talin-1

Ringer P., Weißl A., Cost A.-L., Freikamp A., Sabass B., Mehlich A., Tramier M., Rief M., Grashoff C.

Cells experience a wide range of forces externally applied or produced by motor proteins inside the cell. Forces are transferred by scaffold proteins via the actin cytoskeleton and modulate all kind of biological processes. Förster resonance energy transfer (FRET)-based tension sensors were developed to report on piconewton scale forces across proteins *in vivo*. However, until now, forces in the lower piconewton range were difficult to resolve and methods to analyze several tension sensors simultaneously were not available.

In this study, we report the development and single-molecule calibration of a genetically-encoded FRET-based biosensor comprising a ferredoxin-like (FL) fold as force sensitive linker peptide, which displays forces in an almost digital fashion with high sensitivity for forces between 3-5 piconewton (pN). The calibration of the FL linker flanked by two fluorophores, namely YPet and mCherry (FL-tension sensor module (TSM)) was performed using a dual-trap optical tweezer setup, which showed a switch-like unfolding at forces higher than 3 pN and a quick refolding to the original conformation when forces were reduced.

The focal adhesion (FA) protein talin is one of the major scaffold proteins, connecting the actin cytoskeleton to the extracellular matrix via integrins and is known to bear forces; yet, the contribution of the different subdomains to the force transmission was missing. By inserting the FL-TSM and a 7 pN sensitive TSM at two positions within the elongated protein and performing fluorescence-lifetime imaging microscopy (FLIM) and ratiometric FRET, we were able to show that there is a tension gradient across talin. An average mechanical tension of more than 7 pN was determined at the N-terminal position of the talin rod, whereas forces of only 3 pN are transmitted by a subset of talin molecules at the lower C-terminal region. This tension gradient is modulated by the adapter protein vinculin and the rigidity of the extracellular environment. Intriguingly, forces generated by the very C-terminal actin binding domain are especially sensitive to myosin-II activity and FA size.

In addition, we established a method that allows simultaneous evaluation of two tension sensor constructs within the same cell and therefore under identical conditions, utilizing a single excitation wavelength and dual-color FLIM. For that matter, I generated orthogonal FRET pairs both of which can be excited at 440 nm; however, the first donor emits to a dark quencher and the second donor fluorophore has a long stoke shift, therefore a far red acceptor could be used and FRET spectra can be spectrally separated. The application of this technique using the two talin tension sensors and coexpression of the constructs within one cell substantiated the evidence for an intramolecular force gradient across talin. Finally, taking advantage of the digital nature of the FL-TSM, we introduced a data analysis procedure that allows calculating the fraction of mechanically engaged molecules per cell form FL-TSM bulk measurements. By fitting the FLIM data with a bi-exponential fit, we were able to show that 70% of talin molecules are mechanically engaged at the more N-terminal part of the talin rod domain, while only 40% of talin molecules are exposed to tension at the C-terminal rod domain.
Together, these findings imply that cells modulate the amount of force per talin molecule and in addition adjust the number of mechanically engaged molecules at its different subdomains. Both regulation modes are sensitive to vinculin and actin engagement, and myosin-II activity. Furthermore, the study shows that tension is not equally distributed across talin, and the regulation of force transmission across talin is more complex than previously thought. The methods described in this study should be valuable for further studies on talin force transduction and adaptable to similar research questions.

Bibliography

Abraham, V. C., Krishnamurthi, V., Taylor, D. L., and Lanni, F. (1999). The actin-based nanomachine at the leading edge of migrating cells. *Biophysical Journal*, 77(3):1721 – 1732.

Alexandrova, A. Y., Arnold, K., Schaub, S., Vasiliev, J. M., Meister, J.-J., Bershadsky, A. D., and Verkhovsky, A. B. (2008). Comparative dynamics of retrograde actin flow and focal adhesions: Formation of nascent adhesions triggers transition from fast to slow flow. *PLOS ONE*, 3(9):1–9.

Amano, M., Ito, M., Kimura, K., Fukata, Y., Chihara, K., Nakano, T., Matsuura, Y., and Kaibuchi, K. (1996). Phosphorylation and activation of myosin by rho-associated kinase (rho-kinase). *Journal of Biological Chemistry*, 271(34):20246–20249.

Anthis, N. J., Haling, J. R., Oxley, C. L., Memo, M., Wegener, K. L., Lim, C. J., Ginsberg, M. H., and Campbell, I. D. (2009). β integrin tyrosine phosphorylation is a conserved mechanism for regulating talin-induced integrin activation. *Journal of Biological Chemistry*, 284(52):36700–36710.

Anthis, N. J., Wegener, K. L., Critchley, D. R., and Campbell, I. D. (2010). Structural diversity in integrin/talin interactions. *Structure*, 18(12):1654 – 1666.

Arsenovic, P. T., Ramachandran, I., Bathula, K., Zhu, R., Narang, J. D., Noll, N. A., Lemmon, C. A., Gundersen, G. G., and Conway, D. E. (2016). Nesprin-2g, a component of the nuclear linc complex, is subject to myosin-dependent tension. *Biophysical Journal*, 110(1):34 – 43.

Atherton, P., Stutchbury, B., Wang, D.-Y., Jethwa, D., Tsang, R., Meiler-Rodriguez, E., Wang, P., Bate, N., Zent, R., Barsukov, I. L., Goult, B. T., Critchley, D. R., and Ballestrem, C. (2015). Vinculin controls talin engagement with the actomyosin machinery. *Nature Communication*, 6:10038.

Baldassarre, M., Razinia, Z., Burande, C. F., Lamsoul, I., Lutz, P. G., and Calderwood, D. A. (2009). Filamins regulate cell spreading and initiation of cell migration. *PLOS ONE*, 4(11):1–16.

Bate, N., Gingras, A. R., Bachir, A., Horwitz, R., Ye, F., Patel, B., Goult, B. T., and Critchley, D. R. (2012). Talin contains a c-terminal calpain2 cleavage site important in focal adhesion dynamics. *PLOS ONE*, 7(4):1–11.

Beaty, B. T., Wang, Y., Bravo-Cordero, J. J., Sharma, V. P., Miskolci, V., Hodgson, L., and Condeelis, J. (2014). Talin regulates moesin–nhe-1 recruitment to invadopodia and promotes mammary tumor metastasis. *The Journal of Cell Biology*, 205(5):737–751.

Becker, W., Bergmann, A., Hink, M., König, K., Benndorf, K., and Biskup, C. (2004). Fluorescence lifetime imaging by time-correlated single-photon counting. *Microscopy Research and Technique*, 63(1):58–66.

Bernstein, L. R. and Liotta, L. A. (1994). Molecular mediators of interactions with extracellular matrix components in metastasis and angiogenesis. *Current opinion in oncology*, 6(1):106 – 113.

Blakely, B. L., Dumelin, C. E., Trappmann, B., McGregor, L. M., Choi, C. K., Anthony, P. C., Duesterberg, V. K., Baker, B. M., Block, S. M., Liu, D. R., and Chen, C. S. (2014). A dna-based molecular probe for optically reporting cellular traction forces. *Nature Methods*, 11:1229–1232.

Borghi, N., Sorokina, M., Shcherbakova, O. G., Weis, W. I., Pruitt, B. L., Nelson, W. J., and Dunn, A. R. (2012). E-cadherin is under constitutive actomyosin-generated tension that is increased at cell–cell contacts upon externally applied stretch. *Proceedings of the National Academy of Sciences*, 109(31):12568–12573.

Böttcher, R. T., Veelders, M., Rombaut, P., Faix, J., Theodosiou, M., Stradal, T. E., Rottner, K., Zent, R., Herzog, F., and Fässler, R. (2017). Kindlin-2 recruits paxillin and arp2/3 to promote membrane protrusions during initial cell spreading. *The Journal of Cell Biology*.

Bouchet, B. P., Gough, R. E., Ammon, Y.-C., van de Willige, D., Post, H., Jacquemet, G., Altelaar, A. M., Heck, A. J., Goult, B. T., and Akhmanova, A. (2016). Talin-kank1 interaction controls the recruitment of cortical microtubule stabilizing complexes to focal adhesions. *eLife*, 5:e18124.

Bouvard, D., Pouwels, J., De Franceschi, N., and Ivaska, J. (2013). Integrin inactivators: balancing cellular functions in vitro and in vivo. *Molecular Cell Biology*, 14(7):430 – 442.

Brown, N. H., Gregory, S. L., Rickoll, W. L., Fessler, L. I., Prout, M., White, R. A., and Fristrom, J. W. (2002). Talin is essential for integrin function in drosophila. *Developmental Cell*, 3(4):569 – 579.

Burridge, K. and Connell, L. (1983). A new protein of adhesion plaques and ruffling membranes. *The Journal of Cell Biology*, 97(2):359–367.

Calderwood, D. A., Campbell, I. D., and Critchley, D. R. (2013). Talins and kindlins: partners in integrin-mediated adhesion. *Nature Cell Biology*, 14(8):503–517.

Calderwood, D. A., Fujioka, Y., de Pereda, J. M., García-Alvarez, B., Nakamoto, T., Margolis, B., McGlade, C. J., Liddington, R. C., and Ginsberg, M. H. (2003). Integrin β cytoplasmic domain interactions with phosphotyrosine-binding domains: A structural prototype for diversity in integrin signaling. *PNAS*, 100(5):2272–2277.

Capitanio, M. and Pavone, F. S. (2013). Interrogating biology with force: Single molecule high-resolution measurements with optical tweezers. *Biophysical Journal*, 105(6):1293 – 1303.

Carman, C. V. and Springer, T. A. (2003). Integrin avidity regulation: are changes in affinity and conformation underemphasized? *Current Opinion in Cell Biology*, 15(5):547 – 556.

Chan, A. Y., Bailly, M., Zebda, N., Segall, J. E., and Condeelis, J. S. (2000). Role of cofilin in epidermal growth factor–stimulated actin polymerization and lamellipod protrusion. *Journal of Cell Biology*, 112(148):531 – 542.

Chen, C. S., Mrksich, M., Huang, S., Whitesides, G. M., and Ingber, D. E. (1997). Geometric control of cell life and death. *Science*, 276(5317):1425–1428.

Chen, W. T. (1981). Mechanism of retraction of the trailing edge during fibroblast movement. *The Journal of Cell Biology*, 90(1):187–200.

Choquet, D., Felsenfeld, D. P., and Sheetz, M. P. (1997). Extracellular matrix rigidity causes strengthening of integrin–cytoskeleton linkages. *Cell*, 88(1):39 – 48.

Chorev, D. S., Moscovitz, O., Geiger, B., and Sharon, M. (2014). Regulation of focal adhesion formation by a vinculin-arp2/3 hybrid complex. *Nature Communications*, 5:3758.

Conti, F. J., Felder, A., Monkley, S., Schwander, M., Wood, M. R., Lieber, R., Critchley, D., and Müller, U. (2008). Progressive myopathy and defects in the maintenance of myotendinous junctions in mice that lack talin 1 in skeletal muscle. *Development*, 135(11):2043–2053.

Conti, F. J., Monkley, S. J., Wood, M. R., Critchley, D. R., and Müller, U. (2009). Talin 1 and 2 are required for myoblast fusion, sarcomere assembly and the maintenance of myotendinous junctions. *Development*, 136(21):3597–3606.

Coste, B., Mathur, J., Schmidt, M., Earley, T. J., Ranade, S., Petrus, M. J., Dubin, A. E., and Patapoutian, A. (2010). Piezo1 and piezo2 are essential components of distinct mechanically activated cation channels. *Science*, 330(6000):55–60.

Cram, E. J., Clark, S. G., and Schwarzbauer, J. E. (2003). Talin loss-of-function uncovers roles in cell contractility and migration in c. elegans. *Journal of Cell Science*, 116(19):3871–3878.

Dartsch, P., Hämmerle, H., and Bety, E. (1986). Orientation of cultured arterial smooth muscle cells growing on cyclically stretched substrates. *Cells Tissues Organs*, 125:108 – 113.

del Rio, A., Perez-Jimenez, R., Liu, R., Roca-Cusachs, P., Fernandez, J. M., and Sheetz, M. P. (2009). Stretching single talin rod molecules activates vinculin binding. *Science*, 323(5914):638–641.

Eberl, D. F., Hardy, R. W., and Kernan, M. J. (2000). Genetically similar transduction mechanisms for touch and hearing in drosophila. *Journal of Neuroscience*, 20(16):5981–5988.

Elliott, P. R., Goult, B. T., Kopp, P. M., Bate, N., Grossmann, J. G., Roberts, G. C., Critchley, D. R., and Barsukov, I. L. (2010). The structure of the talin head reveals a novel extended conformation of the ferm domain. *Structure*, 18(10):1289 – 1299.

Elosegui-Artola, A., Bazellières, E., Allen, M. D., Andreu, I., Oria, R., Sunyer, R., Gomm, J. J., Marshall, J. F., Jones, J. L., Trepat, X., and Roca-Cusachs, P. (2014). Rigidity sensing and adaptation through regulation of integrin types. *Nature Materials*, 13(6):631–637.

Engler, A. J., Sen, S., Sweeney, H. L., and Discher, D. E. (2006). Matrix elasticity directs stem cell lineage specification. *Cell*, 126(4):677 – 689.

Fedorchak, G. R., Kaminski, A., and Lammerding, J. (2014). Cellular mechanosensing: Getting to the nucleus of it all. *Progress in Biophysics and Molecular Biology*, 115(2–3):76 – 92. Novel Technologies as Drivers of Progress in Cardiac Biophysics.

Fernandez-Gonzalez, R. and Zallen, J. A. (2013). Wounded cells drive rapid epidermal repair in the early drosophila embryo. pages 3227–3237.

Finer, J. T., Simmons, R. M., and Spudich, J. A. (1994). Single myosin molecule mechanics: piconewton forces and nanometre steps. *Nature*, 368:113 – 119.

Förster, T. (1965). Delocalization excitation and excitation transfer. *Modern Quantum Chemistry*, 3:93 – 137.

Fu, G., Wang, W., and Luo, B.-H. (2012). *Overview: Structural Biology of Integrins*, pages 81–99. Humana Press, Totowa, NJ.

Gahmberg, C. G., Fagerholm, S. C., Nurmi, S. M., Chavakis, T., Marchesan, S., and Grönholm, M. (2009). Regulation of integrin activity and signalling. *Biochimica et Biophysica Acta (BBA) - General Subjects*, 1790(6):431 – 444. Recent Advances in Biochemistry, Biophysics and Molecular Biology.

Galbraith, C. G. and Sheetz, M. P. (1997). A micromachined device provides a new bend on fibroblast traction forces. *Proceedings of the National Academy of Sciences*, 94(17):9114–9118.

Galbraith, C. G., Yamada, K. M., and Galbraith, J. A. (2007). Polymerizing actin fibers position integrins primed to probe for adhesion sites. *Science*, 315(5814):992–995.

García-Alvarez, B., de Pereda, d. M., Calderwood, D. A., Ulmer, T. S., Critchley, D., D., C. I., Ginsberg, M. H., and Liddington, R. C. (2003). Structural determinants of integrin recognition by talin. *Molecular Cell*, 11(1):49 – 58.

Gauthier, N. C., Fardin, M. A., Roca-Cusachs, P., and Sheetz, M. P. (2011). Temporary increase in plasma membrane tension coordinates the activation of exocytosis and contraction during cell spreading. *Proceedings of the National Academy of Sciences*, 108(35):14467–14472.

Geiger, T. and Zaidel-Bar, R. (2012). Opening the floodgates: proteomics and the integrin adhesome. *Current Opinion in Cell Biology*, 24(5):562 – 568. Cell-to-cell contact and extracellular matrix.

Gennerich, A., Carter, A. P., Reck-Peterson, S. L., and Vale, R. D. (2007). Force-induced bidirectional stepping of cytoplasmic dynein. *Cell*, 131(5):952–965.

Georges, P. C., Miller, W. J., Meaney, D. F., Sawyer, E. S., and Janmey, P. A. (2006). Matrices with compliance comparable to that of brain tissue select neuronal over glial growth in mixed cortical cultures. *Biophysical Journal*, 90(8):3012 – 3018.

Gingras, A. R., Bate, N., Goult, B. T., Hazelwood, L., Canestrelli, I., Grossmann, J. G., Liu, H., Putz, N. S. M., Roberts, G. C. K., Volkmann, N., Hanein, D., Barsukov, I. L., and Critchley, D. R. (2007a). The structure of the c-terminal actin-binding domain of talin. *The EMBO Journal*, 27(2):458–469.

Gingras, A. R., Bate, N., Goult, B. T., Hazelwood, L., Canestrelli, I., Grossmann, J. G., Liu, H., Putz, N. S. M., Roberts, G. C. K., Volkmann, N., Hanein, D., Barsukov, I. L., and

Critchley, D. R. (2007b). The structure of the c-terminal actin-binding domain of talin. *The EMBO Journal*, 27(2):458–469.

Gingras, A. R., Ziegler, W. H., Frank, R., Barsukov, I. L., Roberts, G. C. K., Critchley, D. R., and Emsley, J. (2005). Mapping and consensus sequence identification for multiple vinculin binding sites within the talin rod. *Journal of Biological Chemistry*, 280(44):37217–37224.

Goksoy, E., Ma, Y.-Q., Wang, X., Kong, X., Perera, D., Plow, E. F., and Qin, J. (2008). Structural basis for the autoinhibition of talin in regulating integrin activation. *Molecular Cell*, 31(1):124–133.

Goult, B. T., Bouaouina, M., Elliott, P. R., Bate, N., Patel, B., Gingras, A. R., Grossmann, J. G., Roberts, G. C. K., Calderwood, D. A., Critchley, D. R., and Barsukov, I. L. (2010). Structure of a double ubiquitin-like domain in the talin head: a role in integrin activation. *The EMBO Journal*, 29(6):1069–1080.

Goult, B. T., Xu, X.-P., Gingras, A. R., Swift, M., Patel, B., Bate, N., Kopp, P. M., Barsukov, I. L., Critchley, D. R., Volkmann, N., and Hanein, D. (2013a). Structural studies on full-length talin1 reveal a compact auto-inhibited dimer: Implications for talin activation. *Journal of Structural Biology*, 184(1):21 – 32. Hybrid Methods in Macromolecular Structure.

Goult, B. T., Zacharchenko, T., Bate, N., Tsang, R., Hey, F., Gingras, A. R., Elliott, P. R., Roberts, G. C. K., Ballestrem, C., Critchley, D. R., and Barsukov, I. L. (2013b). Riam and vinculin binding to talin are mutually exclusive and regulate adhesion assembly and turnover. *Journal of Biological Chemistry*, 288(12):8238–8249.

Grabbe, C., Zervas, C. G., Hunter, T., Brown, N. H., and Palmer, R. H. (2004). Focal adhesion kinase is not required for integrin function or viability in drosophila. *Development*, 131(23):5795–5805.

Grashoff, C., Hoffman, B. D., Brenner, M. D., Zhou, R., Parsons, M., Yang, M. T., McLean, M. A., Sligar, S. G., Chen, C. S., Ha, T., and Schwartz, M. A. (2010). Measuring mechanical tension across vinculin reveals regulation of focal adhesion dynamics. *Nature*, 466:263 – 266.

Gratton, E., Breusegem, S., Sutin, J. D. B., Ruan, Q., and Barry, N. P. (2003). Fluorescence lifetime imaging for the two-photon microscope: time-domain and frequency-domain methods. *Journal of Biomedical Optics*, 8:8 – 8 – 10.

Grodzinsky, A. J., Levenston, M. E., Jin, M., and Frank, E. H. (2000). Cartilage tissue remodeling in response to mechanical forces. *Annual Review of Biomedical Engineering*, 2(1):691–713. PMID: 11701528.

Gudi, S. R., Clark, C. B., and Frangos, J. A. (1996). Fluid flow rapidly activates g proteins in human endothelial cells. *Circulation Research*, 79(4):834–839.

Haining, A. W. M., Lieberthal, T. J., and del Río Hernández, A. (2016). Talin: a mechanosensitive molecule in health and disease. *The FASEB Journal*, 30(6):2073–2085.

Hayakawa, K., Tatsumi, H., and Sokabe, M. (2011). Actin filaments function as a tension sensor by tension-dependent binding of cofilin to the filament. *Journal of Cell Biology*, 195:721–727.

Hemmings, L., Rees, D., Ohanian, V., Bolton, S., Gilmore, A., Patel, B., Priddle, H., Trevithick, J., Hynes, R., and Critchley, D. (1996). Talin contains three actin-binding sites each of which is adjacent to a vinculin-binding site. *Journal of Cell Science*, 109(11):2715–2726.

Huveneers, S. and de Rooij, J. (2013). Mechanosensitive systems at the cadherin–f-actin interface. *Journal of Cell Science*, 126(2):403–413.

Huynh, J., Nishimura, N., Rana, K., Peloquin, J. M., Califano, J. P., Montague, C. R., King, M. R., Schaffer, C. B., and Reinhart-King, C. A. (2011). Age-related intimal stiffening enhances endothelial permeability and leukocyte transmigration. *Science translational medicine*, 3(112).

Hytönen, V. P. and Vogel, V. (2008). How force might activate talin's vinculin binding sites: Smd reveals a structural mechanism. *PLOS Computational Biology*, 4(2):1–15.

Ichimura, T., Fujita, H., Yoshizawa, K., and Watanabe, T. M. (2012). Engineering strain-sensitive yellow fluorescent protein. *Chem. Commun.*, 48:7871–7873.

Ingber, D. E. (1998). Cellular basis of mechanotransduction. *The biological bulletin*, 194.

Iskratsch, T., Wolfenson, H., and Sheetz, M. P. (2014). Appreciating force and shape [mdash] the rise of mechanotransduction in cell biology. *Nature Reviews Molecular Cell Biology*, 15(12):825–833.

Jares-Erijman, E. A. and Jovin, T. M. (2003). Fret imaging. *Nat. Biotech.*, 21:1387 – 1395.

Kanamori, H., Kawakami, T., Effendi, K., Yamazaki, K., Mori, T., Ebinuma, H., Masugi, Y., Du, W., Nagasaka, K., Ogiwara, A., Kyono, Y., Tanabe, M., Saito, H., Hibi, T., and Sakamoto, M. (2011). Identification by differential tissue proteome analysis of talin-1 as a novel molecular marker of progression of hepatocellular carcinoma. *Oncology*, 80(5–6):406–415.

Kanchanawong, P., Shtengel, G., Pasapera, A. M., Ramko, E. B., Davidson, M. W., Hess, H. F., and Waterman, C. M. (2010). Nanoscale architecture of integrin-based cell adhesions. *Nature*, 468:580 – 584.

Kaspar, D., Seidl, W., Neidlinger-Wilke, C., Beck, A., Claes, L., and Ignatius, A. (2002). Proliferation of human-derived osteoblast-like cells depends on the cycle number and frequency of uniaxial strain. *Journal of Biomechanics*, 35(7):873 – 880.

Khatau, S. B., Hale, C. M., Stewart-Hutchinson, P. J., Patel, M. S., Stewart, C. L., Searson, P. C., Hodzic, D., and Wirtz, D. (2009). A perinuclear actin cap regulates nuclear shape. *Proceedings of the National Academy of Sciences*, 106(45):19017–19022.

Kilinc, D. and Lee, G. U. (2014). Advances in magnetic tweezers for single molecule and cell biophysics. *Integr. Biol.*, 6:27–34.

Kim, M., Carman, C. V., and Springer, T. A. (2003). Bidirectional transmembrane signaling by cytoplasmic domain separation in integrins. *Science*, 301(5640):1720–1725.

Klapholz, B. and Brown, N. H. (2017). Talin – the master of integrin adhesions. *Journal of Cell Science*, 130(15):2435–2446.

Klapholz, B., Herbert, S. L., Wellmann, J., Johnson, R., Parsons, M., and Brown, N. H. (2015). Alternative mechanisms for talin to mediate integrin function. *Current Biology*, 25(7):847 – 857.

Kong, F., García, A. J., Mould, A. P., Humphries, M. J., and Zhu, C. (2009). Demonstration of catch bonds between an integrin and its ligand. *The Journal of Cell Biology*, 185(7):1275–1284.

Lammerding, J., Kamm, R. D., and Lee, R. T. (2004). Mechanotransduction in cardiac myocytes. *Annals of the New York Academy of Sciences*, 1015(1):53–70.

Lawson, C., Lim, S.-T., Uryu, S., Chen, X. L., Calderwood, D. A., and Schlaepfer, D. D. (2012). Fak promotes recruitment of talin to nascent adhesions to control cell motility. *The Journal of Cell Biology*, 196(2):223–232.

Le Clainche, C. and Carlier, M.-F. (2008). Regulation of actin assembly associated with protrusion and adhesion in cell migration. *Physiological Reviews*, 88(2):489–513.

Lee, H.-S., Bellin, R. M., Walker, D. L., Patel, B., Powers, P., Liu, H., Garcia-Alvarez, B., de Pereda, J. M., Liddington, R. C., Volkmann, N., Hanein, D., Critchley, D. R., and

Robson, R. M. (2004). Characterization of an actin-binding site within the talin ferm domain. *Journal of Molecular Biology*, 343(3):771 – 784.

Lee, H.-S., Lim, C. J., Puzon-McLaughlin, W., Shattil, S. J., and Ginsberg, M. H. (2008). Riam activates integrins by linking talin to ras gtpase membrane-targeting sequences. *Journal of Biological Chemistry*, 284(8):5119–5127.

Lee, S. E., Kamm, R. D., and Mofrad, M. R. (2007). Force-induced activation of talin and its possible role in focal adhesion mechanotransduction. *Journal of Biomechanics*, 40(9):2096 – 2106.

Legant, W. R., Miller, J. S., Blakely, B. L., Cohen, D. M., Genin, G. M., and Chen, C. S. (2010). Measurement of mechanical tractions exerted by cells within three-dimensional matrices. *Nature Methods*, 7(12):969 – 971.

Legate, K. R. and Fässler, R. (2008). Mechanisms that regulate adaptor binding to β-integrin cytoplasmic tails. *Journal of Cell Science*, 122(2):187–198.

Li, L., Lu, Y., Stemmer, P. M., and Chen, F. (2015). Filamin a phosphorylation by akt promotes cell migration in response to arsenic. *Oncotarget*, 6:12009–12019.

Litvinov, R. I., Barsegov, V., Schissler, A. J., Fisher, A. R., Bennett, J. S., Weisel, J. W., and Shuman, H. (2011). Dissociation of bimolecular αiibβ3-fibrinogen complex under a constant tensile force. *Biophysical Journal*, 100(1):165 – 173.

Liu, W., Draheim, K. M., Zhang, R., Calderwood, D. A., and Boggon, T. J. (2013). Mechanism for krit1 release of icap1-mediated suppression of integrin activation. *Molecular Cell*, 49(4):719 – 729.

Lo, C. M., Wang, H. B., Dembo, M., and Wang, Y. L. (2000). Cell movement is guided by the rigidity of the substrate. *Biophysical Journal*, 79:144 – 152.

Manevich-Mendelson, E., Grabovsky, V., Feigelson, S. W., Cinamon, G., Gore, Y., Goverse, G., Monkley, S. J., Margalit, R., Melamed, D., Mebius, R. E., Critchley, D. R., Shachar, I., and Alon, R. (2010). Talin1 is required for integrin-dependent b lymphocyte homing to lymph nodes and the bone marrow but not for follicular b-cell maturation in the spleen. *Blood*, 116(26):5907–5918.

Margadant, F., Chew, L. L., Hu, X., Yu, H., Bate, N., Zhang, X., and Sheetz, M. (2011). Mechanotransduction in vivo by repeated talin stretch-relaxation events depends upon vinculin. *PLOS Biology*, 9(12):1–13.

Maroto, R., Raso, A., Wood, T. G., Kurosky, A., Martinac, B., and Hamill, O. P. (2005). Trpc1 forms the stretch-activated cation channel in vertebrate cells. *Nature Cell Biology*, 7:179–185.

Martin, P. (1997). Wound healing–aiming for perfect skin regeneration. *Science*, 276(5309):75–81.

Masters, T. A., Pontes, B., Viasnoff, V., Li, Y., and Gauthier, N. C. (2013). Plasma membrane tension orchestrates membrane trafficking, cytoskeletal remodeling, and biochemical signaling during phagocytosis. *Proceedings of the National Academy of Sciences*, 110(29):11875–11880.

Meng, F. and Sachs, F. (2010). Visualizing dynamic cytoplasmic forces with a compliance-matched fret sensor. *Journal of Cell Science*, 124(2):261–269.

Meng, F. and Sachs, F. (2012). Orientation-based fret sensor for real-time imaging of cellular forces. *Journal of Cell Science*, 125(3):743–750.

Meng, F., Suchyna, T. M., and Sachs, F. (2008). A fluorescence energy transfer-based mechanical stress sensor for specific proteins in situ. *FEBS Journal*, 275(12):3072–3087.

Moes, M., Rodius, S., Coleman, S. J., Monkley, S. J., Goormaghtigh, E., Tremuth, L., Kox, C., van der Holst, P. P. G., Critchley, D. R., and Kieffer, N. (2007). The integrin binding site 2 (ibs2) in the talin rod domain is essential for linking integrin β subunits to the cytoskeleton. *Journal of Biological Chemistry*, 282(23):17280–17288.

Monkley, S. J., Pritchard, C. A., and Critchley, D. R. (2001). Analysis of the mammalian talin2 gene {TLN2}. *Biochemical and Biophysical Research Communications*, 286(5):880 – 885.

Monkley, S. J., Zhou, X.-H., Kinston, S. J., Giblett, S. M., Hemmings, L., Priddle, H., Brown, J. E., Pritchard, C. A., Critchley, D. R., and Fässler, R. (2000). Disruption of the talin gene arrests mouse development at the gastrulation stage. *Developmental Dynamics*, 219(4):560–574.

Morimatsu, M., Mekhdjian, A. H., Adhikari, A. S., and Dunn, A. R. (2013). Molecular tension sensors report forces generated by single integrin molecules in living cells. *Nano Letters*, 13(9):3985–3989.

Moser, M., Nieswandt, B., Ussar, S., Pozgajova, M., and Fassler, R. (2008). Kindlin-3 is essential for integrin activation and platelet aggregation. *Nature Medicine*, 14(3):325–330.

Mullender, M., El Haj, A. J., Yang, Y., van Duin, M. A., Burger, E. H., and Klein-Nulend, J. (2004). Mechanotransduction of bone cellsin vitro: Mechanobiology of bone tissue. *Medical and Biological Engineering and Computing*, 42(1):14–21.

Nieswandt, B., Moser, M., Pleines, I., Varga-Szabo, D., Monkley, S., Critchley, D., and Fässler, R. (2007). Loss of talin1 in platelets abrogates integrin activation, platelet aggregation, and thrombus formation in vitro and in vivo. *Journal of Experimental Medicine*, 204(13):3113–3118.

Oberhauser, A. F., Badilla-Fernandez, C., Carrion-Vazquez, M., and Fernandez, J. M. (2002). The mechanical hierarchies of fibronectin observed with single-molecule afm. *Journal of Molecular Biology*, 319(2):433 – 447.

O'Connell, C. B., Tyska, M. J., and Mooseker, M. S. (2007). Myosin at work: Motor adaptations for a variety of cellular functions. *Biochimica et Biophysica Acta (BBA) - Molecular Cell Research*, 1773(5):615 – 630. Integrated approaches to cytoskeleton research.

Osol, G. (1995). Mechanotransduction by vascular smooth muscle. *Journal of vascular research*, 32:275–292.

Paszek, M. J., Boettiger, D., Weaver, V. M., and Hammer, D. A. (2009). Integrin clustering is driven by mechanical resistance from the glycocalyx and the substrate. *PLOS Computational Biology*, 5(12):1–16.

Paszek, M. J., Zahir, N., Johnson, K. R., Lakins, J. N., Rozenberg, G. I., Gefen, A., Reinhart-King, C. A., Margulies, S. S., Dembo, M., Boettiger, D., Hammer, D. A., and Weaver, V. M. (2005). Tensional homeostasis and the malignant phenotype. *Cancer Cell*, 8(3):241 – 254.

Patel, N. R., Bole, M., Chen, C., Hardin, C. C., Kho, A. T., Mih, J., Deng, L., Butler, J., Tschumperlin, D., Fredberg, J. J., Krishnan, R., and Koziel, H. (2012). Cell elasticity determines macrophage function. *PLOS ONE*, 7(9):1–10.

Plotnikov, S. V., Pasapera, A. M., Sabass, B., and Waterman, C. M. (2012). Force fluctuations within focal adhesions mediate ecm-rigidity sensing to guide directed cell migration. *Cell*, 151(7).

Plotnikov, S. V., Sabass, B., Schwarz, U. S., and Waterman, C. M. (2014). High-resolution traction force microscopy. *Methods in Cell Biology*, 123:367 – 394. Quantitative Imaging in Cell Biology.

Plow, E. F., Haas, T. A., Zhang, L., Loftus, J., and Smith, J. W. (2000). Ligand binding to integrins. *Journal of Biological Chemistry*, 275(29):21785–21788.

Pollard, T. D. and Borisy, G. G. (2003). Cellular motility driven by assembly and disassembly of actin filaments. *Cell*, 112(4):453 – 465.

Pouwels, J., Nevo, J., Pellinen, T., Ylänne, J., and Ivaska, J. (2012). Negative regulators of integrin activity. *Journal of Cell Science*, 125(14):3271–3280.

Praekelt, U., Kopp, P. M., Rehm, K., Linder, S., Bate, N., Patel, B., Debrand, E., Manso, A. M., Ross, R. S., Conti, F., Zhang, M.-Z., Harris, R. C., Zent, R., Critchley, D. R., and Monkley, S. J. (2012). New isoform-specific monoclonal antibodies reveal different sub-cellular localisations for talin1 and talin2. *European Journal of Cell Biology*, 91(3):180 – 191.

Priddle, H., Hemmings, L., Monkley, S., Woods, A., Patel, B., Sutton, D., Dunn, G. A., Zicha, D., and Critchley, D. R. (1998). Disruption of the talin gene compromises focal adhesion assembly in undifferentiated but not differentiated embryonic stem cells. *The Journal of Cell Biology*, 142(4):1121–1133.

Puchner, E. M. and Gaub, H. E. (2009). Force and function: probing proteins with afm-based force spectroscopy. *Current Opinion in Structural Biology*, 19(5):605 – 614. Carbohydradtes and glycoconjugates / Biophysical methods.

Qi, L., Jafari, N., Li, X., Chen, Z., Li, L., Hytönen, V. P., Goult, B. T., Zhan, C.-G., and Huang, C. (2016). Talin2-mediated traction force drives matrix degradation and cell invasion. *Journal of Cell Science*, 129(19):3661–3674.

Ratnikov, B., Ptak, C., Han, J., Shabanowitz, J., Hunt, D. F., and Ginsberg, M. H. (2005). Talin phosphorylation sites mapped by mass spectrometry. *Journal of Cell Science*, 118(21):4921–4923.

Resnick, N., Yahav, H., Shay-Salit, A., Shushy, M., Schubert, S., Zilberman, L. C. M., and Wofovitz, E. (2003). Fluid shear stress and the vascular endothelium: for better and for worse. *Progress in Biophysics and Molecular Biology*, 81(3):177 – 199.

Rief, M., Gautel, M., Oesterhelt, F., Fernandez, J. M., and Gaub, H. E. (1997). Reversible unfolding of individual titin immunoglobulin domains by afm. *Science*, 276(5315):1109–1112.

Ringer, P., Colo, G., Fässler, R., and Grashoff, C. (2017). Sensing the mechano-chemical properties of the extracellular matrix. *Matrix Biology*.

Ross, R. (1986). The pathogenesis of atherosclerosis — an update. *New England Journal of Medicine*, 314(8):488–500. PMID: 3511384.

Rossier, O., Octeau, V., Sibarita, J.-B., Leduc, C., Tessier, B., Nair, D., Gatterdam, V., AU Destaing, O., Albigès-Rizo, C., Tampé, R., Cognet, L., Choquet, D., Lounis, B., and Giannone, G. (2012). Integrins β1 and β3 exhibit distinct dynamic nanoscale organizations inside focal adhesions. *Nature Cell Biology*, 14(10):1057–1067.

Sachs, F. (1992). Stretch-sensitive ion channels: an update. *Soc. Gen. Physiol. Ser.*, 47:241–60.

Sakamoto, S., McCann, R. O., Dhir, R., and Kyprianou, N. (2010). Talin1 promotes tumor invasion and metastasis via focal adhesion signaling and anoikis resistance. *Cancer Research*, 70(5):1885–1895.

Sawada, Y., Tamada, M., Dubin-Thaler, B. J., Cherniavskaya, O., Sakai, R., Tanaka, S., and Sheetz, M. P. (2006). Force sensing by mechanical extension of the src family kinase substrate p130cas. *Cell*, 127(5):1015 – 1026.

Schiemer, J., Bohm, A., Lin, L., Merrill-Skoloff, G., Flaumenhaft, R., Huang, J.-S., Le Breton, G. C., and Chishti, A. H. (2016). Gα13 switch region 2 relieves talin autoinhibition to activate αiiβ3 integrin. *Journal of Biological Chemistry*, 291(52):26598–26612.

Schiller, H. B., Friedel, C. C., Boulegue, C., and Fässler, R. (2011). Quantitative proteomics of the integrin adhesome show a myosin ii-dependent recruitment of lim domain proteins. *EMBO reports*, 12(3):259–266.

Shergill, B., Meloty-Kapella, L., Musse, A. A., Weinmaster, G., and Botvinick, E. (2012). Optical tweezers studies on notch: Single-molecule interaction strength is independent of ligand endocytosis. *Developmental Cell*, 22(6):1313 – 1320.

Small, J. V., Isenberg, G., and Celis, J. E. (1978). Polarity of actin at the leading edge of cultured cells. *Nature*, 272(5654):638 – 639.

Smith, M. L., Gourdon, D., Little, W. C., Kubow, K. E., Eguiluz, R. A., Luna-Morris, S., and Vogel, V. (2007). Force-induced unfolding of fibronectin in the extracellular matrix of living cells. *PLOS Biology*, 5(10):1–12.

Stabley, D. R., Jurchenko, C., Marshall, S. S., and Salaita, K. S. (2012). Visualizing mechanical tension across membrane receptors with a fluorescent sensor. *Nature Methods*, 9(1):64 – 67.

Stritt, S., Wolf, K., Lorenz, V., Vögtle, T., Gupta, S., Bösl, M. R., and Nieswandt, B. (2015). Rap1-gtp–interacting adaptor molecule (riam) is dispensable for platelet integrin activation and function in mice. *Blood*, 125(2):219–222.

Sukharev, S. I., Sigurdson, W. J., Kung, C., and Sachs, F. (1999). Energetic and spatial parameters for gating of the bacterial large conductance mechanosensitive channel, mscl. *The Journal of General Physiology*, 113(4):525–540.

Sun, N., Critchley, D. R., Paulin, D., Li, Z., and Robson, R. M. (2008). Identification of a repeated domain within mammalian α-synemin that interacts directly with talin. *Experimental Cell Research*, 314(8):1839 – 1849.

Sun, Z., Tseng, H.-Y., Tan, S., Senger, F., Kurzawa, L., Dedden, D., Mizuno, N., Wasik, A. A., Thery, M., Dunn, A. R., and Fassler, R. (2016). Kank2 activates talin, reduces force transduction across integrins and induces central adhesion formation. *Nature Cell Biology*, 18(9):941–953.

Svoboda, K., Schmidt, C. F., Schnapp, B. J., and Block, S. M. (1993). Direct observation of kinesin stepping by optical trapping interferometry. *Nature*, 365(6448):721–727.

Swaminathan, V., Fischer, R. S., and Waterman, C. M. (2016). The fak–arp2/3 interaction promotes leading edge advance and haptosensing by coupling nascent adhesions to lamellipodia actin. *Molecular Biology of the Cell*, 27(7):1085 – 1100.

Tadokoro, S., Shattil, S. J., Eto, K., Tai, V., Liddington, R. C., de Pereda, J. M., Ginsberg, M. H., and Calderwood, D. A. (2003). Talin binding to integrin ß tails: A final common step in integrin activation. *Science*, 302(5642):103–106.

Theodosiou, M., Widmaier, M., Böttcher, R. T., Rognoni, E., Veelders, M., Bharadwaj, M., Lambacher, A., Austen, K., Müller, D. J., Zent, R., and Fässler, R. (2016). Kindlin-2 cooperates with talin to activate integrins and induces cell spreading by directly binding paxillin. *eLife*, 5:e10130.

Tojkander, S., Gateva, G., and Lappalainen, P. (2012). Actin stress fibers – assembly, dynamics and biological roles. *Journal of Cell Science*, 125(8):1855–1864.

Totsukawa, G., Wu, Y., Sasaki, Y., Hartshorne, D. J., Yamakita, Y., Yamashiro, S., and Matsumura, F. (2004). Distinct roles of mlck and rock in the regulation of membrane protrusions and focal adhesion dynamics during cell migration of fibroblasts. *The Journal of Cell Biology*, 164(3):427–439.

Ullrich, A. and Schlessinger, J. (1990). Signal transduction by receptors with tyrosine kinase activity. *Cell*, 61(2):203 – 212.

Wallrabe, H. and Periasamy, A. (2005). Imaging protein molecules using fret and flim microscopy. *Current Opinion in Biotechnology*, 16(1):19 – 27. Analytical biotechnology.

Wang, X. and Ha, T. (2013). Defining single molecular forces required to activate integrin and notch signaling. *Science*, 340(6135):991 – 994.

Wang, Y., Botvinick, E. L., Zhao, Y., Berns, M. W., Usami, S., Tsien, R. Y., and Chien, S. (2005). Visualizing the mechanical activation of src. *Nature*, 434(7036):1040 – 1045.

Wang, Y., Meng, F., and Sachs, F. (2011). Genetically encoded force sensors for measuring mechanical forces in proteins. *Communicative Integrative Biology*, 4(4):385 – 390.

Wells, R. G. (2013). Tissue mechanics and fibrosis. *Biochimica et Biophysica Acta (BBA) - Molecular Basis of Disease*, 1832(7):884 – 890. Fibrosis: Translation of basic research to human disease.

White, C. R. and Frangos, J. A. (2007). The shear stress of it all: the cell membrane and mechanochemical transduction. *Philosophical Transactions of the Royal Society B: Biological Sciences*, 362:1459 – 1467.

Winkler, J., Lünsdorf, H., and Jockusch, B. M. (1997). Energy-filtered electron microscopy reveals that talin is a highly flexible protein composed of a series of globular domains. *European Journal of Biochemistry*, 243(1-2):430–436.

Wozniak, M. A., Modzelewska, K., Kwong, L., and Keely, P. J. (2004). Focal adhesion regulation of cell behavior. *Biochimica et Biophysica Acta (BBA) - Molecular Cell Research*, 1692(2):103 – 119. Cell Adhesion and Signalling.

Wu, J., Lewis, A. H., and Grandl, J. (2017). Touch, tension, and transduction – the function and regulation of piezo ion channels. *Trends in Biochemical Sciences*, 42(1):57 – 71.

Yamazaki, T., Tobe, K., Hoh, E., Maemura, K., Kaida, T., Komuro, I., Tamemoto, H., Kadowaki, T., Nagai, R., and Yazaki, Y. (1993). Mechanical loading activates mitogen-activated protein kinase and s6 peptide kinase in cultured rat cardiac myocytes. *Journal of Biological Chemistry*, 268(16):12069–12076.

Yang, G., Crawford, R. C., and Wang, J. H.-C. (2004). Proliferation and collagen production of human patellar tendon fibroblasts in response to cyclic uniaxial stretching in serum-free conditions. *Journal of Biomechanics*, 37(10):1543 – 1550.

Yang, J., Zhu, L., Zhang, H., Hirbawi, J., Fukuda, K., Dwivedi, P., Liu, J., Byzova, T., Plow, E. F., Wu, J., and Qin, J. (2014). Conformational activation of talin by riam triggers integrin-mediated cell adhesion. *Nature Communication*, 5(3):5880.

Yao, M., Goult, B. T., Chen, H., Cong, P., Toseland, C. P., Guo, Y., Cong, P., Sheetz, M. P., and Yan, J. (2014). Mechanical activation of vinculin binding to talin locks talin in an unfolded conformation. *Nature*, 4.

Yao, M., Goult, B. T., Klapholz, B., Hu, X., Toseland, C. P., Guo, Y., Cong, P., Sheetz, M. P., and Yan, J. (2016). The mechanical response of talin. *Nature Communication*, 7.

Ye, F., Hu, G., Taylor, D., Ratnikov, B., Bobkov, A. A., McLean, M. A., Sligar, S. G., Taylor, K. A., and Ginsberg, M. H. (2010). Recreation of the terminal events in physiological integrin activation. *The Journal of Cell Biology*, 188(1):157–173.

Yin, J. and Kuebler, W. M. (2009). Mechanotransduction by trp channels: General concepts and specific role in the vasculature. *Cell Biochemistry and Biophysics*, 56(1):1.

Yuan, Y., Li, L., Zhu, Y., Qi, L., Azizi, L., Hytönen, V. P., Zhan, C.-G., and Huang, C. (2017). The molecular basis of talin2's high affinity toward β1-integrin. *Nature*, 7:41989.

Zacharchenko, T., Qian, X., Goult, B. T., Jethwa, D., Almeida, T. B., Ballestrem, C., Critchley, D. R., Lowy, D. R., and Barsukov, I. L. (2016). Ld motif recognition by talin: Structure of the talin-dlc1 complex. *Cell Press*, 24(7):1130–1141.

Zaidel-Bar, R. and Geiger, B. (2010). The switchable integrin adhesome. *Journal of Cell Science*, 123(9):1385–1388.

Zhang, X., Jiang, G., Cai, Y., Monkley, S. J., Critchley, D. R., and Sheetz, M. P. (2008). Talin depletion reveals independence of initial cell spreading from integrin activation and traction. *Nature Cell Biology*, 10(9):1062–1068.

Zhang, Z., Izaguirre, G., Lin, S.-Y., Lee, H. Y., Schaefer, E., and Haimovich, B. (2004). The phosphorylation of vinculin on tyrosine residues 100 and 1065, mediated by src kinases, affects cell spreading. *Molecular Biology of the Cell*, 15(9):4234–4247.

Acknowledgments

First of all, I want to thank Dr. Carsten Grashoff for his support and the supervision over the last three years, but also for the freedom he gave me to develop my own ideas.

I further want to thank Prof. Reinhard Fässler for taking on the task of being my "Dokorvater" and especially for the critical input on my PhD project and for providing all the materials and the great infrastructure in his department.

Without the input of all my former and current lab members, this work would not be the same. I especially appreciated all the serious, but also the nonsense and funny discussions we had in the lab. My special thanks goes to Christoph, Anna-Lena and Carleen for establishing and maintaining all the analysis programs. I also want to thank Christian for all the help and support with our analysis programs, wedding cakes and finally for debugging of my latex files.

Furthermore, I want to thank Prof. Dr. Marc Tramier for giving me the opportunity to work in his lab and learn new methods, as well as, all the other collaborators, that contributed to this work.

Zu guter Letzt, aber für mich persönlich am wichtigsten, möchte ich meiner Familie und Julian danken, dass sie immer für mich da waren und sich immer "Alles" angehört haben. Vorallem meinen Eltern bin ich sehr dankbar, da sie immer an mich geglaubt (meistens mehr als ich selber) und mich in jeder Situation immer unterstützt haben.

Curriculum Vitae

Pia Ringer
Ganghoferstr.78
81373 Munich
✉ *pringer@gmx.de*

Personal data

Name	Pia Sabrina Ringer
Date of birth	24.02.1989, in Herrenberg
Nationality	German

Education

since June 2014	**PhD student**, *in the group of Dr. C. Grashoff (Molecular Mechanotransduction)*, Max Planck Institute of Biochemistry (MPIB), Martinsried.
October 2013 – June 2014	**Diplomarbeit**, *in the group of Dr. C. Grashoff*, MPIB, Martinsried.
2008 – June 2014	**Diplom in Biochemistry**, *with major subject Biochemistry and minor subjects Cell Biochemistry and Organic Chemistry*, final grade: 1.3 (excellent), Eberhard Karls University, Tübingen.
October 2011 – January 2012	**Research laboratory course - Chromosome Organizaton and Dynamics**, *Group of Dr. S. Gruber*, MPIB (now University of Lusanne, Switzerland).
April 2012 – June 2012	**Research laboratory course - Chemical biology of nucleic acids**, *Group of Dr. T. Stafforst* , Eberhard Karls University, Tübingen.
October 2010	**Vordiplom**, *final grade: 1.5*, Eberhard Karls University, Tübingen.
1999 – 2008	**Abitur(high school degree)**, *final grade: 1.3*, Andreae-Gymnasium, Herrenberg.

Peer-Reviewed Publications and Awards

Scientific report	*Advanced molecular force microscopy reveals force gradient across talin-1. **Pia Ringer**, A. Weißl, A.-L. Cost, A. Freikamp, B. Sabass, A. Mehlich, M. Tramier, M. Rief, C. Grashoff, (2017). Nature Methods.*
	*Extraccellular rigidity sensing by talin isoform-specific mechanical linkages. **Pia Ringer** , K. Austen, A. Mehlich, A. Chrostek-Grashoff, C. Kluger, C. Kligner, B. Sabass, R. Zent, M. Rief, C. Grashoff, (2015).Nature Cell Biology, 17, 1597-1606.*

Review article *Sensing the mechano-chemical properties of the extracellular matrix.* ***Pia Ringer***, *G. Colo, R. Fässler, C. Grashoff, (2017). Matrix Biology, 1336, No 11;4C.*

How to measure molecular forces in cells: A guide to evaluating genetically-encoded FRET-based tension sensors. ***Pia Ringer*** *, A.-L. Cost, A. Chrostek-Grashoff, C. Grashoff, (2015). Cellular and Molecular Bioengineering, 8(1):96-105*

Award *Paper Award of Cellular and Molecular Bioengineering.*

Conferences

October 2016 **Sonderforschungsbereich (SFB) confernece: Forces in Biomolecular Systems**, *Venice*, Italy.
Poster presentation

June 2016 **Gordon Research Conference: Signaling by Adhesion Receptors**, *Boston*, USA.
Poster presentation

March 2016 **International Meeting of German Society for Cell Biology**, *Munich*, Germany.

Languages

German Mother tongue

English fluent (oral and written English)

French Intermediate level

Appendix

The appendix includes reprints of the papers **I** to **IV**. The supplementary materials for each paper can be found on the enclosed CD.

Cellular and Molecular Bioengineering, Vol. 8, No. 1, March 2015 *(© 2014)* pp. 96–105
DOI: 10.1007/s12195-014-0368-1

How to Measure Molecular Forces in Cells: A Guide to Evaluating Genetically-Encoded FRET-Based Tension Sensors

ANNA-LENA COST, PIA RINGER, ANNA CHROSTEK-GRASHOFF, and CARSTEN GRASHOFF

Group of Molecular Mechanotransduction, Max Planck Institute of Biochemistry, Am Klopferspitz 18, Martinsried 82152, Germany

(Received 1 August 2014; accepted 21 November 2014; published online 2 December 2014)

Associate Editor Roger D Kamm oversaw the review of this article.

Abstract—The ability of cells to sense and respond to mechanical forces is central to a wide range of biological processes and plays an important role in numerous pathologies. The molecular mechanisms underlying cellular mechanotransduction, however, have remained largely elusive because suitable methods to investigate subcellular force propagation were missing. Here, we review recent advances in the development of biosensors that allow molecular force measurements. We describe the underlying principle of currently available techniques and propose a strategy to systematically evaluate new Förster resonance energy transfer (FRET)-based biosensors.

Keywords—Mechanobiology, Förster resonance energy transfer, Biosensors, Mechanotransduction, Fluorescence lifetime imaging microscopy.

INTRODUCTION

Cells are exposed to a wide range of mechanical forces. Endothelial cells, for instance, are subject to high shear stress in arteries but low forces in veinous or lymphatic vessels,[14] cardiomyocytes bear the rhythmic contractions of the heart,[27] keratinocytes are stimulated by shear or tension in the skin,[57] and chondrocytes sense forces from cartilage compression.[51] Interestingly, cells respond to such mechanical stimuli—that may vary over orders of magnitude—with astonishing specificity suggesting that cell type-specific mechanisms exist, which convey fine-tuned mechanoresponses. Indeed, a range of subcellular structures mediating different aspects of mechanotransduction has been identified including mechanosensitive ion-channels,[16] the plasma membrane,[18] the cytoskeleton,[26] the nucleus,[24] and cell-adhesion complexes.[21] Techniques such as traction force microscopy[67] have greatly contributed to our understanding of force transduction across these subcellular structures.[3] Yet, how forces propagate on the molecular level is still largely unknown.

Address correspondence to Carsten Grashoff, Group of Molecular Mechanotransduction, Max Planck Institute of Biochemistry, Am Klopferspitz 18, Martinsried 82152, Germany. Electronic mail: cgrasho@biochem.mpg.de

Anna-Lena Cost and Pia Ringer have contributed equally to this study.

MOLECULAR FORCE TRANSDUCTION OCCURS IN THE PICONEWTON RANGE

A major breakthrough for our understanding of molecular force transduction has been the development of highly sensitive atomic force microscopy (AFM)[55] as well as optical[8] and magnetic[32] tweezer systems, which allow researchers to scrutinize mechanical responses of single molecules *in vitro*.[81] Such experiments revealed that forces produced by microtubule-binding motor proteins, such as kinesins or dyneins, are in the range of 5–7 piconewton (pN) per molecule[22,70] (Fig. 1), highly similar to forces generated by growing microtubules (3–4 pN)[19] or f-actin–binding myosin motors (3–4 pN).[20]

The notion that mechanotransduction—the translation of mechanical information into a biochemical response—may occur at similar forces was supported by the observation that conformational changes in the adhesion protein talin can be induced by mechanical tension as low as 2 pN.[15,77] Likewise, cleavage of the von Willebrand factor is facilitated by force-induced protein unfolding at 5 pN[80] and collagen proteolysis is increased 100-fold upon application of 10 pN force.[1] Interestingly, some receptor-ligand pairs form adhesive interactions, called catch bonds, which strengthen under pN forces.[72] The linkage between P-selectin and monomeric P-selectin glycoprotein ligand-1, for instance, is characterized by catch bond behavior below 11 pN,[42,71] and $\alpha 5\beta 1$ integrin shows enhanced binding to fibronectin

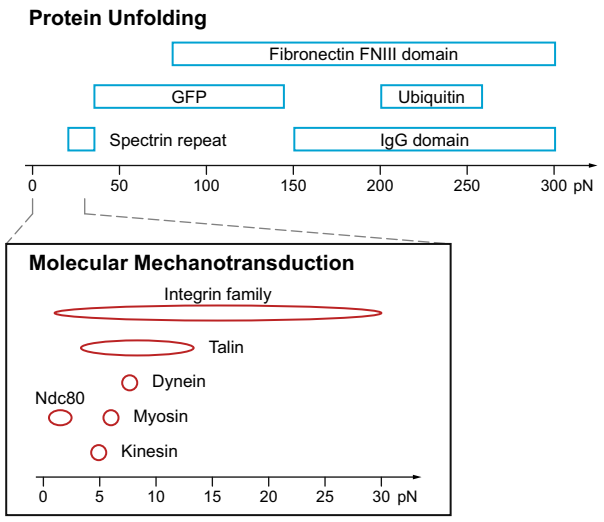

FIGURE 1. Mechanotransduction occurs in the low pN range. Motor proteins such as dynein,[22] myosin[25] or kinesin,[70] cell adhesion molecules like talin[15] or some integrins receptors[31,33,41,47] as well as the kinetochore protein Ndc80[54] are sensitive to forces below 30 pN. Even though single protein domains like spectrin repeats unfold in the similar force range,[38,60] most proteins require higher forces for unfolding. GFP, for example, starts to unfold at 35 pN[17] and even higher forces (80–300 pN) are necessary to unfold fibronectin's FN type III domain,[50,59] ubiquitin,[11] or the IgG domain.[58] It should be noted that some of the force ranges are still controversial and that this figure only summarizes the currently published results.

type III repeats at 10–30 pN.[33] As the unfolding of whole protein domains usually requires higher forces—the green fluorescent protein (GFP) starts to unfold at about 35 pN[17] and immunoglobulin (Ig) or fibronectin type III domains unfold at 80–300 pN[50,58,59]—it appears that important aspects of mechanotransduction do indeed occur in the low pN range (Fig. 1). But how can such low forces be measured in cells?

CURRENT APPROACHES FOR MEASURING MOLECULAR TENSION

A number of approaches to measure molecular tension across cell-surface or intracellular molecules have been developed; they are based upon Förster resonance energy transfer (FRET), photo-quenching, loss of fluorescence or changes in fluorophore emission properties. For a better understanding how to design new biosensors, we will briefly introduce FRET and how it can be measured in cells, before we provide a short overview of the different techniques and their applications (see also Tables 1, 2; Fig. 2).

A Brief Introduction to Förster Resonance Energy Transfer (FRET)

FRET is a process in which energy is transferred nonradiatively from an electronically excited donor (D) chromophore to a nearby acceptor (A). The FRET efficiency E, defined as the proportion of donor molecules that transfer excitation energy to the acceptor, is highly dependent on the D–A separation distance r and characterized by the Förster distance R_0.

$$E = \frac{R_0^6}{R_0^6 + r^6} \tag{1}$$

R_0 embodies the relative orientation of donor and acceptor dipoles κ^2, the refractive index n, the donor quantum yield Q_D, and the overlap integral of donor emission and acceptor absorption spectra J.

$$R_0^6 \sim \kappa^2 n^{-4} Q_D J \tag{2}$$

The spectral overlap integral in turn depends on the acceptor extinction coefficient ε_A according to

$$J(\lambda) = \int \varepsilon_A(\lambda)\lambda^4 F_D(\lambda)\mathrm{d}\lambda \tag{3}$$

where F_D is the donor emission spectrum and λ the wavelength. Thus, FRET is highly distance-dependent but can be strongly affected by the D–A orientation as well. It is worth noting that the orientation factor κ^2 is often assumed to be constant throughout the experiment, which may not always be a valid assumption.[36] In fact, the relative orientation of donor and acceptor transition dipoles has been utilized in orientation-dependent FRET biosensors[44] (Fig. 2b). The equations above also show that properties of FRET-based biosensors can be adjusted to some degree by employing different donor and acceptor fluorophores with varying quantum yields and extinction coefficients.[63,64] For a more detailed overview of FRET we refer to excellent literature.[30,36]

FRET Measurements in Cells

To fully harness the power of FRET-based biosensors, suitable microscopy techniques and data analysis algorithms are critical. For this purpose, a number of approaches to determine FRET in cells are available.[40,75] One of the most frequently used methods is based on intensity measurements, in which the donor fluorophore is excited and the emission intensities of donor and acceptor fluorophore are used to calculate a FRET ratio. This estimate of relative FRET is useful for biosensors that are characterized by fixed donor/acceptor stoichiometry and can be measured with any appropriately equipped wide-field or confocal microscope. However, these intensity-based measurements do not readily yield quantitative information on FRET efficiencies, are sensitive to the experimental settings (e.g. excitation intensity or biosensor expression level) and require careful image data analysis to account for spectral bleed-through, cross-excitation or photobleaching.[75] Alternatively, fluorescence lifetime

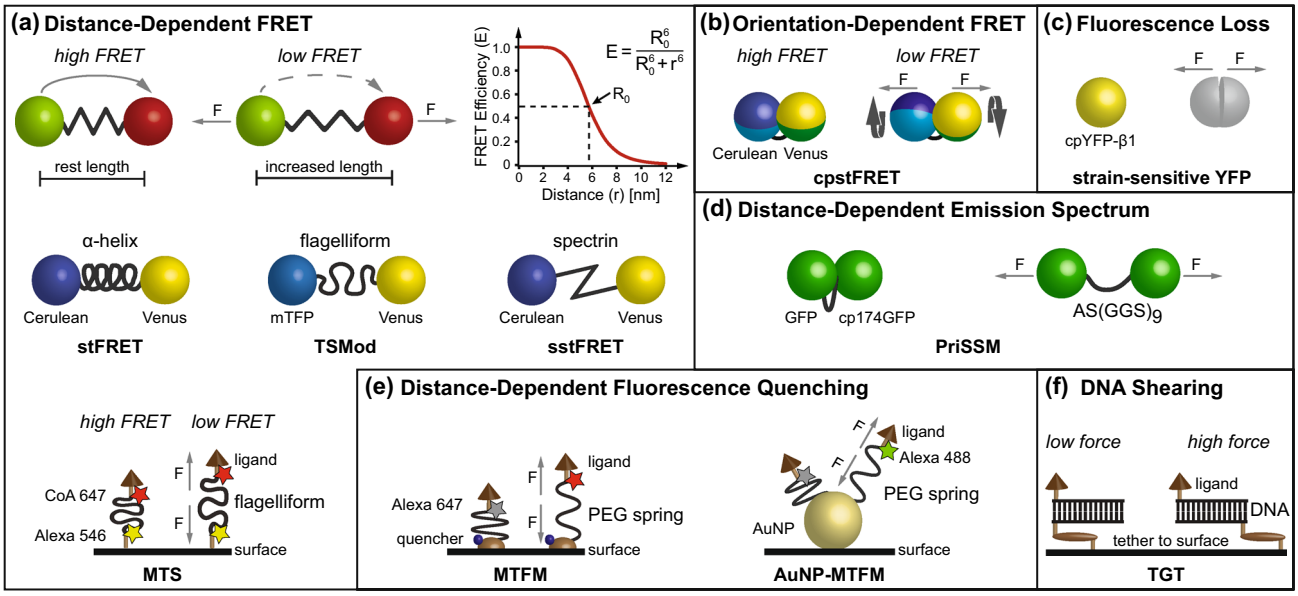

FIGURE 2. Overview of existing tension sensing techniques. (a) Distance-dependent FRET-based tension sensor modules use elastic linker elements that extend in response to force (*F*). Sufficient length increase of the linker under force is critical as the FRET efficiency (*E*) is highly dependent on the chromophore separation distance (*r*). Currently available FRET pairs are characterized by Förster distances (R_0) of 5–6 nm; as an example, the FRET vs. distance correlation for R_0 = 5.8 nm is shown. Employed linkers include an α-helix in strain-sensitive FRET (stFRET),[46] $(GPGGA)_8$ repeats in the flagelliform tension sensor module (TSMod)[23] as well as in the molecular tension sensor (MTS),[47] and a spectrin repeat in spectrin stFRET (sstFRET).[43] (b) Force across the circularly permuted (cp) stFRET (cpstFRET) sensor rotates the fluorophores thereby reducing FRET efficiency.[44] (c) Force across a strain-sensitive cpYFP causes fluorescence loss.[28] (d) In the proximity imaging-based strain sensor module (PriSSM), the emission spectrum changes in response to force-dependent distance increase between green fluorescent protein (GFP) and cp174GFP.[29] (e) Some tension sensors used to measure extracellular forces are based on a polyethylene glycol (PEG)-spring. In the molecular tension–based fluorescence microscopy (MTFM) approach, organic dye fluorescence rises as the distance to a synthetic quencher[66] or a gold nanoparticle (AuNP)[41] increases in response to stretch. (f) The tension gauge tether (TGT) method uses double-stranded DNA fragments, which separate at defined forces *via* unzipping (low force) or shearing (high force).[76]

imaging microscopy (FLIM)[48,68,69] can be used to calculate FRET efficiencies from the donor lifetime (τ) in the presence (DA) or absence (D) of the acceptor.

$$E = 1 - \frac{\tau_{DA}}{\tau_D} \tag{4}$$

The FLIM approach is insensitive to fluorophore concentration and experimental settings but nevertheless requires rigorous controls and careful data analysis.[75] Other imaging methods include acceptor photobleaching[73] or anisotropy measurements,[40] each with its own advantages and disadvantages. In general, life-cell FRET experiments are complicated by cellular auto-fluorescence, undesired photobleaching and the fact that fluorophore properties depend on environmental factors such as pH, ion concentration or temperature.[52,61] Thus, an in-depth understanding of the limitations inherent to the different FRET analysis methods is essential.[30,53,69,78]

Genetically-Encoded Tension Sensor Modules for Measuring Intracellular Molecular Forces

Most of the existing tension sensor modules are based upon the initial observation that elastic molecules such as single-stranded DNA (ssDNA) can act as pN force sensors when inserted between two fluorescent dyes undergoing efficient FRET.[65] Since the FRET efficiency inversely correlates with the D–A distance (Eq. 1), forces that extend the linker and thereby increase chromophore separation strongly reduce FRET (Fig. 2a). Therefore, the selection of an appropriate elastic element is critical and the following requirements have to be satisfied. First, the linker has to be short because currently available FRET pairs are characterized by a Förster distance $R_0 \approx$ 5–6 nm, at which the FRET efficiency is most sensitive to changes in fluorophore separation distance (Fig. 2a).[53,69] Second, the increase in linker length has to be sufficiently large so that applied tension translates into measurable FRET efficiency differences. Finally, data interpretation is greatly facilitated if the linker follows a simple folding/unfolding pathway and quickly returns to its original conformation when forces subside.

Following these principles, a number of FRET-based tension-sensitive modules have been developed (Table 1; Fig. 2). The linker elements range from a comparably stiff α-helix[46] and spectrin repeat[43] to the elastic spider silk flagelliform peptide[23] (Fig. 2a). An alternative approach was recently tested, in which the

TABLE 1. Genetically-encoded tension sensors.

Name	Sensing element	Sensor sensitivity	Molecular size	Original publication	Application by original group	Independent application
PriSSM	$AS(GGS)_9$	pN range	~55 kDa	Iwai *et al.*[29]		
stFRET	α-helix	pN range	~56 kDa[a]	Meng *et al.*[46]	Meng *et al.*[45]	
TSMod	Flagelliform $(GPGGA)_8$	1–6 pN; by single-molecule spectroscopy	~56 kDa	Grashoff *et al.*[23]	Conway *et al.*[12] Kuriyama *et al.*[35] Leerberg *et al.*[39]	Borghi *et al.*[5] Chang *et al.*[9] Cai *et al.*[6] Krieg *et al.*[34]
sstFRET	Spectrin repeat[b]	5–7 pN; by DNA springs	~65 kDa	Meng and Sachs[43]	Rahimzadeh *et al.*[56] Verma *et al.*[74]	
cpYFP[c]	Chromophore	pN range	~29 kDa	Ichimura *et al.*[28]		
cpstFRET		5–7 pN; by DNA springs	~54 kDa	Meng and Sachs[44]		

[a] The original publication indicates a size of ~70 kDa; based on the used amino acid sequence, however, a size of ~56 kDa is expected.
[b] Other groups have reported spectrin repeat unfolding at ~20 pN[38] and 25–35 pN[60].
[c] This sensor has not been used in cells.

TABLE 2. Synthetic tension sensors.

Name	Sensing element	Sensor sensitivity	Sensor calibration	Principle	Original publication	Application by original group
MTFM	PEG_n^a	0–20 pN[a]	Theoretical; WLC model[c]	QSF 21-quenching	Stabley *et al.*[66]	Jurchencko *et al.*[31]
AuNP-MTFM	PEG_n^a	0–25 pN[a]	Theoretical; WLC model[c]	AuNP-quenching	Liu *et al.*[41]	
MTS	Flagelliform $(GPGGA)_8$	1–6 pN	Grashoff *et al.*[23]	FRET	Morimatsu *et al.*[47]	
TGT	dsDNA tether	12–56 pN	Single molecule AFM	Fluorescence loss[b]	Wang and Ha[76]	

[a] Force sensitivity can be tuned by adjusting the PEG polymer length.
[b] The TGT response is non-reversible.
[c] Worm-like chain model.

force-sensitive element does not change its length but rather conformation (Fig. 2b).[44] In addition to the FRET-based approaches, a circularly permuted (cp) YFP has been generated that loses fluorescence under force[28] (Fig. 2c). Similarly, proximity imaging (PRIM) has been used to correlate molecular strain with changes in the emission spectrum of an engineered GFP-dimer[29] (Fig. 2d). Whether all these techniques will be useful for further applications in cells, however, remains to be determined.

Synthetic Tension Sensing Techniques for Measuring Forces at the Cell Surface

Measuring mechanical forces at the cell surface does not require genetic encoding of the tension sensing element but can be performed using mechanically well-described polymers. In addition, organic dyes can be employed which are more photostable than most genetically encoded fluorophores and rarely affect the functionality of the labeled molecules. Together with the versatile surface chemistry technologies that are available, these tools have enabled the development of highly sensitive methods to determine extracellular molecular forces (Table 2). For example, the molecular tension–based fluorescence microscopy (MTFM) approach uses polyethylene glycol (PEG) as a force-sensitive tether molecule to measure mechanical tension across growth factor[66] and cell adhesion receptors[31,41] (Fig. 2e). Similarly, functionalization of the flagelliform peptide[23] with organic dyes and arginine–glycine–glutamine (RGD)-ligands allows the estimation of force across single integrin receptors[47] (Fig. 2a). An addition to these synthetic sensors is the tension gauge tether (TGT) approach, where immobilized double-stranded DNA (dsDNA) is functionalized with cell surface receptor ligands so that force above a well-defined threshold can be easily detected[76] (Fig. 2f).

Applications of FRET-Based Molecular Tension Sensors

The genetic tension sensor modules described above have been applied to a range of proteins (Fig. 2; Table 1) in different cell types and even whole organisms such as *C. elegans*[34] or *D. melanogaster*.[6] The targeted molecules include actin-binding proteins such as α-actinin,[43–46,74] filamin,[45,46] and spectrin[34,43,46] as well as cell adhesion molecules like cadherin,[5,6,12] PECAM-1,[12] and vinculin.[23] These measurements confirmed the long held assumption that many cytoskeletal proteins bear pN forces and are an ideal starting point for a more detailed analysis. The use of a vinculin tension sensor, for instance, revealed an average force of about 2.5 pN across vinculin. More interestingly, however, the vinculin transduced tension strongly depends on the cell adhesion state, with highest tension occurring in assembling focal adhesions but low forces in disassembling complexes[23]; this indicates that vinculin stabilizes cell adhesions under mechanical force. In another study, a β-spectrin tension sensor revealed constitutive tension of about 1.5 pN across this cytoskeletal adaptor protein. Interestingly, genetic manipulations decreasing β-spectrin pre-stress correlate with impaired touch sensation suggesting that cytoskeletal pre-tension is critical for efficient mechanosensation in neurons.[34] These examples illustrate that the true power of FRET-based tension sensors lies not only in the force measurement itself but also in the possibility to unravel molecular mechanisms that are currently inaccessible to other techniques.

A GUIDE TO EVALUATING GENETICALLY-ENCODED FRET-BASED TENSION SENSORS

A detailed understanding of a tension sensor's biophysical properties is crucial. In which force range is the tension sensor module applicable? How does the linker unfold in response to force, and how large is the dynamic FRET range? These kind of questions need to be answered before meaningful experiments can be performed. Furthermore, effects of tension sensor module integration into the protein of interest (POI) need to be carefully evaluated and the FRET experiments must be properly controlled. While every novel genetically-encoded biosensor will require its specific evaluation strategy, we propose here a series of experimental controls which, in our opinion, are indispensable for any FRET-based tension sensor characterization.

Tension Sensor Design: Which Forces are to be Measured?

Before the experiment, a number of obvious (but not trivial) questions should be addressed. Which molecule should be targeted, what are the expected mechanical forces and do tension sensor modules that are sensitive to these forces exist? It is important to note that molecular tension sensors are unsuitable to measure forces across subcellular structures in general (in fact, this is precisely what they do *not* do), but specifically report tension across the POI. Our previously published vinculin tension sensor, for instance, can be efficiently used to determine vinculin tension but is unsuitable to measure focal adhesion forces in general.[23] So, it is also worth asking: Are we interested in forces across distinct proteins or across whole subcellular structures?

Once a target protein has been identified, it is necessary to carefully evaluate whether the tension sensor module can be inserted into the POI without significantly affecting its function. We find that structural information is often helpful to identify possible insertion sites, which are preferably unstructured and flexible. In case of the vinculin tension sensor, for example, the chosen integration site is located in a flexible linker region between two well-defined structural domains and vinculin function is preserved after tension sensor module integration.[10,23] If little structure information is available for the POI, we recommend testing several integrations in parallel.

Characterizing the Tension Sensor Module: What is the Sensor's Force Sensitivity?

As discussed above, proteins are subject to a range of pN forces. As the main purpose of a tension sensor is the quantification of these forces, a careful evaluation of the probe's force sensitivity is required. For elastic elements such as PEG, ssDNA or unstructured polypeptides like $(GGS)_n$, which are well-described by established polymer models, a theoretical calibration may be sufficient.[65,66] However, experimental calibration is inevitable when more complex linker elements are employed. For such measurements, we strongly recommend the use of single-molecule techniques that allow well-controlled and repeated stretching of sensor peptides over a wide range of forces.[81] Such a single-molecule calibration has been successfully used to determine the force sensitivity of the flagelliform peptide,[23] but can also be employed to investigate the force response of a complete tension sensor module including donor and acceptor fluorophores (Fig. 3b) (unpublished observation, *C. Grashoff* and *M. Rief*). A tension sensor module calibration using optical tweezers typically involves purification of the protein from bacteria or eukaryotic cells, followed by its functionalization and linkage to DNA handles, which are then attached to micro-beads. Application of pN forces by an optical trap allows a detailed analysis of tension

sensor module unfolding under force and, importantly, refolding when tension is reduced.

Biosensor Characterization I: Are the Fluorophores Functional After Integration into the POI?

Next to the *in vitro* calibration of the tension sensor module, its functionality after integration into the POI needs to be validated. Steric constraints, for instance, could impair fluorophore folding. Furthermore, forces of about 35 pN[17] are sufficient to partially unfold GFP-like proteins, which might influence fluorescence.[61] Therefore, we recommend comparing the properties of individual donor (D) and acceptor (A) fluorophores terminally fused to the target protein (X) (Fig. 3a, X-D_C or X-A_C) with fluorophores that have been integrated into the POI (Fig. 3a, X-D_I, X-A_I). Alternatively, integrated tension sensor modules harboring one non-fluorescent mutant fluorophore (Fig. 3a, X-mTS_I(D), X-mTS_I(A)) may be used for a comparison. Fluorescence lifetime as well as absorption or emission spectra are useful parameters to determine whether properties of internally placed fluorophores are affected (Fig. 3c).

Biosensor Characterization II: Is the POI Functional After Tension Sensor Module Integration?

A critical step in the development of a genetically-encoded biosensor is the insertion of the tension sensor module into the POI; quite obviously, this involves the risk of altering the target protein's function. Therefore, a detailed evaluation of the biosensor is critical and requires the generation of genetic control constructs (Fig. 3a), for which protocols have been described before.[2] To evaluate the biosensor's biological functionality, these constructs should be expressed in cells depleted of the endogenous protein, which has several advantages (Fig. 3d). First, overexpression artifacts can be avoided by adjusting biosensor expression to physiological levels. Second, it can be easily tested whether the biosensor is able to functionally replace the endogenous protein. The β-spectrin tension sensor, for example, rescues the paralysis phenotype of spectrin mutant *C. elegans* to wild type behavior[34] and an E-cadherin tension sensor was shown to rescue the migration defect in E-cadherin–depleted border cells in *D. melanogaster*.[6] Finally, force measurements are likely to be more accurate as the total amount of force distributes only across biosensor molecules.

A typical evaluation experiment includes the reconstitution of knockout (or knockdown) cells with the tension sensor construct (Fig. 3a, X-TS_I) and the N- or C-terminally tagged POI (Fig. 3a, X-D_C or X-A_C). This is followed by confirmation of proper subcellular localization using fluorescence microscopy methods as well as the evaluation of expression levels by western blotting. Depending on the POI, functionality may be further tested by fluorescence recovery after photobleaching (FRAP) analysis, where the subcellular dynamics of X-TS_I and X-D_C can be easily compared (Fig. 3d).

Controlling the FRET Experiment: Are Effects of Intermolecular FRET or conformation changes significant?

As described above, FRET experiments are complex because energy transfer does not only depend on the chromophore separation distance and orientation but also on the biophysical properties of the individual fluorophores (Eqs. 2 and 3).[53] Therefore, FRET-based tension sensor experiments need to be carefully controlled.

To ensure that differences in FRET are caused by mechanical tension across the biosensor and are not a result of changes in the microenvironment (such as pH, temperature, etc.), we emphasize the need to use a zero-force control, which can be easily generated by fusing the tension sensor module to either end of the POI (Fig. 3a, X-TS_0). This control should show identical subcellular localization as the biosensor (X-TS_I) but should not display changes in FRET as no significant tension can be applied across the module. The second possibly confounding factor in a tension sensor FRET experiment is energy transfer between adjacent molecules (so-called intermolecular FRET) that can significantly contribute to the overall FRET in compact subcellular structures such as focal adhesions or cell–cell contacts. Intermolecular FRET can be easily estimated using a pair of control constructs in which either the individual fluorophores[23] (Fig. 3a, X-D_I, X-A_I) or tension sensor modules with one non-fluorescent mutant fluorophore[12] (Fig. 3a, X-mTS_I(D), X-mTS_I(A)) are integrated into the POI. Co-expression of such constructs in one cell and subsequent FRET measurement in the relevant subcellular structure allow calculation of intermolecular FRET. Furthermore, potential effects of protein conformation changes on FRET need to be considered. As this strongly depends on the molecule of interest, however, these control experiments are not generalizable. Nevertheless, conformation controls should be included to ensure that changes in FRET are reflective of differences in mechanical tension and not κ^2 artifacts. Finally, the notion that FRET changes actually reflect changes in tension may be reinforced by experiments in which external forces are rapidly applied using mechanical stretch[5] or fluid shear flow.[12]

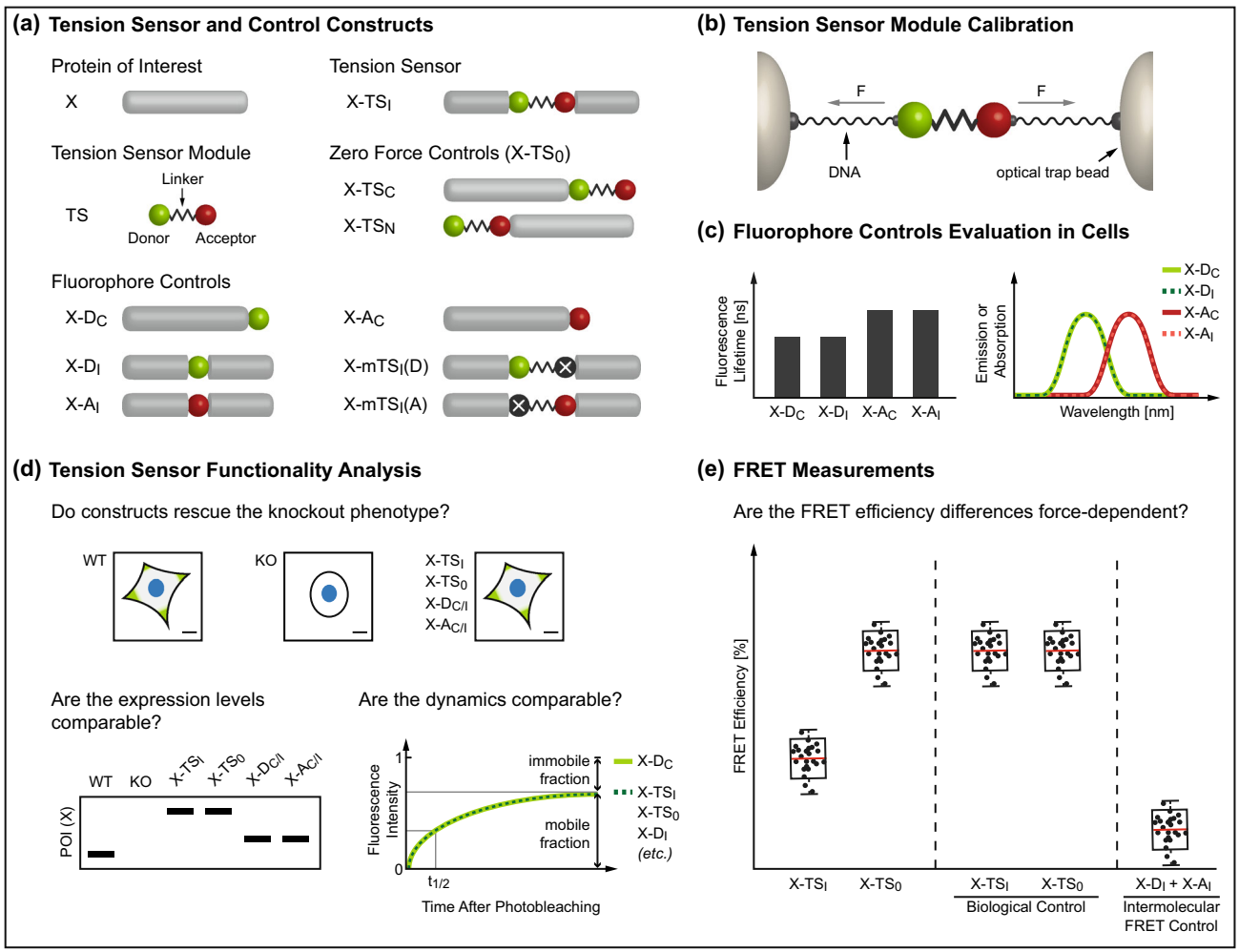

FIGURE 3. Recommended control constructs and experimental strategies for FRET-based tension sensor evaluation. (a) The tension sensor (X-TS$_I$) consists of the tension sensor module (TS) internally integrated into the protein of interest (POI) (X). As a zero-force control (X-TS$_0$), the TS can be fused C- (X-TS$_C$) or N-terminally (X-TS$_N$) to the POI. To evaluate functionality of the targeted protein as well as the fluorophores, N- or C-terminal (X-D$_C$, X-A$_C$) fusions and internal (X-D$_I$, X-A$_I$) integrations of donor (D) and acceptor (A) fluorophores are recommended. Additionally, tension sensor constructs with non-fluorescent mutant donor (X-mTS$_I$(A)) or acceptor fluorophore (X-mTS$_I$(D)) can be used. (b) Single-molecule force spectroscopy techniques can be used to calibrate new tension sensor modules. The protein is attached to micro-beads *via* dsDNA handles and an optical tweezer applies pN forces. (c) Fluorescence lifetimes or emission spectra of donor (X-D$_C$ vs. X-D$_I$ or X-mTS$_I$(D)) and acceptor (X-A$_C$ vs. X-A$_I$ or X-mTS$_I$(A)) fluorophores can be compared to test whether fluorophore properties are preserved after insertion into the target protein. (d) Functionality of the tension sensor can be efficiently analyzed by comparing knockout (KO) cell lines reconstituted with the either the tension sensor or control constructs. Ideally, reconstituted cells resemble the parental wild type (WT) cells. Subcellular localization can be checked by fluorescence microscopy; physiological expression levels should be confirmed by western blotting. Subcellular dynamics may be evaluated through fluorescence recovery after photobleaching (FRAP) experiments, which allow the analysis of mobile and immobile fractions. (e) Calculation of FRET efficiencies is recommended to quantify FRET measurements. In addition to genetic controls, where X-TS$_I$ is compared to X-TS$_0$, biological controls should be included. For instance, chemical inhibitor treatments can be used to prevent force generation across the POI, which should lead to a substantial increase in FRET efficiency of X-TS$_I$. Intermolecular FRET can be determined using co-expressed X-D$_I$ and X-A$_I$ or X-mTS$_I$(D) and X-mTS$_I$(A).

Data Analysis and Interpretation: What Do the FRET Efficiency Differences Mean?

At the end, proper data analysis is critical. We highly recommend the use of quantitative techniques such as fluorescence lifetime imaging microscopy (FLIM) allowing the calculation of FRET efficiencies instead of FRET ratios (Fig. 3e). Moreover, automated data analysis software to determine transfer rates in subcellular compartments greatly facilitates data interpretation. The evaluation experiments described above should be followed by additional controls that will depend on the individual context (such as

inhibition of intracellular contractility or application of external forces). Together, this experimental strategy will allow a straightforward evaluation of new tension-sensitive biosensors. We wish to emphasize that insufficiently characterized tension sensors should not be utilized by the scientific community as their application all too often results in misleading interpretations and confusion.

OUTLOOK

While the development of molecular tension sensors has already made significant contributions to a deeper understanding of force transduction, further improvements will be necessary to further elucidate molecular mechanisms. For instance, more calibrated tension sensor modules are required to evaluate distinct force ranges. Also, probes with increased dynamic range, quantum yield and photostability would be useful to perform intracellular single-molecule measurements that unravel the heterogeneity and dynamics of molecular processes. In this context, the development of orthogonal labeling techniques using genetically encoded proteins,[13] peptides, and non-natural amino acids[37] is promising, as they allow site-specific labeling of intracellular proteins with organic dyes. Another approach that seems worth pursuing is genomic integration of biosensors into the locus of the target proteins by the recently developed CRISPR/Cas9 technique.[62] This strategy should ensure physiological expression levels of a biosensor and avoid the time-consuming generation of knockout (or knockdown) cell lines. Finally, other approaches to determine forces in cells could be combined with FRET-based tension sensors. These may include optical tweezers methods that can be applied to individual molecules within cells,[49] the specific functionalization of micro-droplets, which were recently used to determine mechanical forces on the cellular level in embryonic tissue,[7] or traction force microscopy techniques allowing the simultaneous measurement of traction forces and molecular forces in cell adhesions. In fact, while this manuscript was under revision, two new, synthetic tension sensor techniques that use hairpin-DNA as force sensitive linkers and fluorescence quenching as read-out were published,[4,79] which allow molecular traction force microscopy.

In summary, properly characterized molecular tension sensors provide a powerful tool to gain insight into cellular mechanotransduction. Further improvements that will allow experiments at single-molecule resolution within cells, the application of tension sensors to a wider range of proteins, and the combination of biosensors with other quantitative techniques may pave the way to a better understanding of how cells sense and respond to their mechanical environment.

ACKNOWLEDGMENTS

The authors thank Andrea Freikamp for help with the figures. C. Grashoff is supported by the German Research Council (DFG) through the Emmy Noether program grant (EN GR3399-2-1), the Collaborative Research Center SFB63 (B9), and a Paul Gerson Unna Research Group of the Max Planck Society (MPG).

CONFLICT OF INTEREST

A.-L. Cost, P. Ringer, A. Chrostek-Grashoff, and C. Grashoff declare that they have no conflicts of interest.

ETHICAL STANDARDS

No human or animal studies were carried out by the authors for this article.

OPEN ACCESS

REFERENCES

[1]Adhikari, A. S., J. Chai, and A. R. Dunn. Mechanical load induces a 100-fold increase in the rate of collagen proteolysis by MMP-1. *J. Am. Chem. Soc*. 133:1686–1689, 2011.
[2]Austen, K., C. Kluger, A. Freikamp, A. Chrostek-Grashoff, and C. Grashoff. Generation and analysis of biosensors to measure mechanical forces within cells. In: Cell-Cell Interactions, edited by T. A. Baudino. New York: Humana Press, 2013, pp. 169–184.
[3]Bao, G., and S. Suresh. Cell and molecular mechanics of biological materials. *Nat. Mater*. 2:715–725, 2003.
[4]Blakely, B. L., C. E. Dumelin, B. Trappmann, L. M. McGregor, C. K. Choi, P. C. Anthony, V. K. Duesterberg, B. M. Baker, S. M. Block, D. R. Liu, and C. S. Chen. A DNA-based molecular probe for optically reporting cellular traction forces. *Nat. Methods* 11:1229–1232, 2014.
[5]Borghi, N., M. Sorokina, O. G. Shcherbakova, W. I. Weis, B. L. Pruitt, W. J. Nelson, and A. R. Dunn. E-cadherin is under constitutive actomyosin-generated tension that is increased at cell–cell contacts upon externally applied stretch. *Proc. Natl. Acad. Sci. USA* 109:12568–12573, 2012.
[6]Cai, D., S.-C. Chen, M. Prasad, L. He, X. Wang, V. Choesmel-Cadamuro, J. K. Sawyer, G. Danuser, and D. J.

Montell. Mechanical feedback through E-cadherin promotes direction sensing during collective cell migration. *Cell* 157:1146–1159, 2014.
[7]Campàs, O., T. Mammoto, S. Hasso, R. A. Sperling, D. O'Connell, A. G. Bischof, R. Maas, D. A. Weitz, L. Mahadevan, and D. E. Ingber. Quantifying cell-generated mechanical forces within living embryonic tissues. *Nat. Methods* 11:183–189, 2014.
[8]Capitanio, M., and F. S. Pavone. Interrogating biology with force: single molecule high-resolution measurements with optical tweezers. *Biophys. J.* 105:1293–1303, 2013.
[9]Chang, C.-W., and S. Kumar. Vinculin tension distributions of individual stress fibers within cell-matrix adhesions. *J. Cell Sci.* 126:3021–3030, 2013.
[10]Chen, H., D. M. Cohen, D. M. Choudhury, N. Kioka, and S. W. Craig. Spatial distribution and functional significance of activated vinculin in living cells. *J. Cell Biol.* 169:459–470, 2005.
[11]Chyan, C.-L., F.-C. Lin, H. Peng, J.-M. Yuan, C.-H. Chang, S.-H. Lin, and G. Yang. Reversible mechanical unfolding of single ubiquitin molecules. *Biophys. J.* 87:3995–4006, 2004.
[12]Conway, D. E., M. T. Breckenridge, E. Hinde, E. Gratton, C. S. Chen, and M. A. Schwartz. Fluid shear stress on endothelial cells modulates mechanical tension across VE-cadherin and PECAM-1. *Curr. Biol.* 23:1024–1030, 2013.
[13]Crivat, G., and J. W. Taraska. Imaging proteins inside cells with fluorescent tags. *Trends Biotechnol.* 30:8–16, 2012.
[14]Davies, P. F. Flow-mediated endothelial mechanotransduction. *Physiol. Rev.* 75:519–560, 1995.
[15]del Rio, A., R. Perez-Jimenez, R. Liu, P. Roca-Cusachs, J. M. Fernandez, and M. P. Sheetz. Stretching single talin rod molecules activates vinculin binding. *Science* 323:638–641, 2009.
[16]Delmas, P., and B. Coste. Mechano-gated ion channels in sensory systems. *Cell* 155:278–284, 2013.
[17]Dietz, H., and M. Rief. Exploring the energy landscape of GFP by single-molecule mechanical experiments. *Proc. Natl. Acad. Sci. USA* 101:16192–16197, 2004.
[18]Diz-Muñoz, A., D. A. Fletcher, and O. D. Weiner. Use the force: membrane tension as an organizer of cell shape and motility. *Trends Cell Biol.* 23:47–53, 2013.
[19]Dogterom, M., and B. Yurke. Measurement of the force-velocity relation for growing microtubules. *Science* 278:856–860, 1997.
[20]Finer, J. T., R. M. Simmons, and J. A. Spudich. Single myosin molecule mechanics: piconewton forces and nanometre steps. *Nature* 368:113–119, 1994.
[21]Geiger, B., J. P. Spatz, and A. D. Bershadsky. Environmental sensing through focal adhesions. *Nat. Rev. Mol. Cell Biol.* 10:21–33, 2009.
[22]Gennerich, A., A. P. Carter, S. L. Reck-Peterson, and R. D. Vale. Force-induced bidirectional stepping of cytoplasmic dynein. *Cell* 131:952–965, 2007.
[23]Grashoff, C., B. D. Hoffman, M. D. Brenner, R. Zhou, M. Parsons, M. T. Yang, M. A. McLean, S. G. Sligar, C. S. Chen, T. Ha, and M. A. Schwartz. Measuring mechanical tension across vinculin reveals regulation of focal adhesion dynamics. *Nature* 466:263–266, 2010.
[24]Guilluy, C., L. D. Osborne, L. Van Landeghem, L. Sharek, R. Superfine, R. Garcia-Mata, and K. Burridge. Isolated nuclei adapt to force and reveal a mechanotransduction pathway in the nucleus. *Nat. Cell Biol.* 16:376–381, 2014.
[25]Guo, B., and W. H. Guilford. Mechanics of actomyosin bonds in different nucleotide states are tuned to muscle contraction. *Proc. Natl. Acad. Sci. USA* 103:9844–9849, 2006.
[26]Hayakawa, K., H. Tatsumi, and M. Sokabe. Actin filaments function as a tension sensor by tension-dependent binding of cofilin to the filament. *J. Cell Biol.* 195:721–727, 2011.
[27]Hersch, N., B. Wolters, G. Dreissen, R. Springer, N. Kirchgeßner, R. Merkel, and B. Hoffmann. The constant beat: cardiomyocytes adapt their forces by equal contraction upon environmental stiffening. *Biol. Open* 2:351–361, 2013.
[28]Ichimura, T., H. Fujita, K. Yoshizawa, and T. M. Watanabe. Engineering strain-sensitive yellow fluorescent protein. *Chem. Commun.* 48:7871–7873, 2012.
[29]Iwai, S., and T. Q. P. Uyeda. Visualizing myosin-actin interaction with a genetically-encoded fluorescent strain sensor. *Proc. Natl. Acad. Sci. USA* 105:16882–16887, 2008.
[30]Jares-Erijman, E. A., and T. M. Jovin. FRET imaging. *Nat. Biotechnol.* 21:1387–1395, 2003.
[31]Jurchenko, C., Y. Chang, Y. Narui, Y. Zhang, and K. S. Salaita. Integrin-generated forces lead to streptavidin-biotin unbinding in cellular adhesions. *Biophys. J.* 106:1436–1446, 2014.
[32]Kilinc, D., and G. U. Lee. Advances in magnetic tweezers for single molecule and cell biophysics. *Integr. Biol.* 6:27–34, 2014.
[33]Kong, F., A. J. García, A. P. Mould, M. J. Humphries, and C. Zhu. Demonstration of catch bonds between an integrin and its ligand. *J. Cell Biol.* 185:1275–1284, 2009.
[34]Krieg, M., A. R. Dunn, and M. B. Goodman. Mechanical control of the sense of touch by β-spectrin. *Nat. Cell Biol.* 16:224–233, 2014.
[35]Kuriyama, S., E. Theveneau, A. Benedetto, M. Parsons, M. Tanaka, G. Charras, A. Kabla, and R. Mayor. *In vivo* collective cell migration requires an LPAR2-dependent increase in tissue fluidity. *J. Cell Biol.* 206:113–127, 2014.
[36]Lakowicz, J. R. Principles of Fluorescence Spectroscopy. New York: Springer, p. 954, 2006.
[37]Lang, K., and J. W. Chin. Cellular incorporation of unnatural amino acids and bioorthogonal labeling of proteins. *Chem. Rev.* 114:4764–4806, 2014.
[38]Law, R., G. Liao, S. Harper, G. Yang, D. W. Speicher, and D. E. Discher. Pathway shifts and thermal softening in temperature-coupled forced unfolding of spectrin domains. *Biophys. J.* 85:3286–3293, 2003.
[39]Leerberg, J. M., G. A. Gomez, S. Verma, E. J. Moussa, S. K. Wu, R. Priya, B. D. Hoffman, C. Grashoff, M. A. Schwartz, and A. S. Yap. Tension-sensitive actin assembly supports contractility at the epithelial zonula adherens. *Curr. Biol.* 24:1–11, 2014.
[40]Lidke, D. S., P. Nagy, B. G. Barisas, R. Heintzmann, J. N. Post, K. A. Lidke, A. H. A. Clayton, D. J. Arndt-Jovin, and T. M. Jovin. Imaging molecular interactions in cells by dynamic and static fluorescence aniosotropy (rFLIM and emFRET). *Biochem. Soc. Trans.* 31:1020–1027, 2003.
[41]Liu, Y., K. Yehl, Y. Narui, and K. Salaita. Tension sensing nanoparticles for mechano-imaging at the living/nonliving interface. *J. Am. Chem. Soc.* 135:5320–5323, 2013.
[42]Marshall, B. T., M. Long, J. W. Piper, T. Yago, R. P. McEver, and C. Zhu. Direct observation of catch bonds involving cell-adhesion molecules. *Nature* 423:190–193, 2003.
[43]Meng, F., and F. Sachs. Visualizing dynamic cytoplasmic forces with a compliance-matched FRET sensor. *J. Cell Sci.* 124:261–269, 2011.
[44]Meng, F., and F. Sachs. Orientation-based FRET sensor for real-time imaging of cellular forces. *J. Cell Sci.* 125:743–750, 2012.

[45]Meng, F., T. M. Suchyna, E. Lazakovitch, R. M. Gronostajski, and F. Sachs. Real time FRET based detection of mechanical stress in cytoskeletal and extracellular matrix proteins. *Cell. Mol. Bioeng*. 4:148–159, 2011.
[46]Meng, F., T. M. Suchyna, and F. Sachs. A fluorescence energy transfer-based mechanical stress sensor for specific proteins *in situ*. *FEBS J*. 275:3072–3087, 2008.
[47]Morimatsu, M., A. H. Mekhdjian, A. S. Adhikari, and A. R. Dunn. Molecular tension sensors report forces generated by single integrin molecules in living cells. *Nano Lett*. 13:3985–3989, 2013.
[48]Morton, P. E., and M. Parsons. Measuring FRET using time-resolved FLIM. In: Cell Migration, edited by C. M. Wells, and M. Parsons. New York: Humana Press, 2011, pp. 403–413.
[49]Norregaard, K., L. Jauffred, K. Berg-Sørensen, and L. B. Oddershede. Optical manipulation of single molecules in the living cell. *Phys. Chem. Chem. Phys*. 16:12614–12624, 2014.
[50]Oberhauser, A. F., C. Badilla-Fernandez, M. Carrion-Vazquez, and J. M. Fernandez. The mechanical hierarchies of fibronectin observed with single-molecule AFM. *J. Mol. Biol*. 319:433–447, 2002.
[51]O'Conor, C. J., H. A. Leddy, H. C. Benefield, W. B. Liedtke, and F. Guilak. TRPV4-mediated mechanotransduction regulates the metabolic response of chondrocytes to dynamic loading. *Proc. Natl. Acad. Sci. USA* 111:1316–1321, 2014.
[52]Padilla-Parra, S., N. Audugé, H. Lalucque, J.-C. Mevel, M. Coppey-Moisan, and M. Tramier. Quantitative comparison of different fluorescent protein couples for fast FRET-FLIM acquisition. *Biophys. J*. 97:2368–2376, 2009.
[53]Piston, D. W., and G.-J. Kremers. Fluorescent protein FRET: the good, the bad and the ugly. *Trends Biochem. Sci*. 32:407–414, 2007.
[54]Powers, A. F., A. D. Franck, D. R. Gestaut, J. Cooper, B. Gracyzk, R. R. Wei, L. Wordeman, T. N. Davis, and C. L. Asbury. The Ndc80 kinetochore complex forms load-bearing attachments to dynamic microtubule tips via biased diffusion. *Cell* 136:865–875, 2009.
[55]Puchner, E. M., and H. E. Gaub. Force and function: probing proteins with AFM-based force spectroscopy. *Curr. Opin. Struct. Biol*. 19:605–614, 2009.
[56]Rahimzadeh, J., F. Meng, F. Sachs, J. Wang, D. Verma, and S. Z. Hua. Real-time observation of flow-induced cytoskeletal stress in living cells. *Am. J. Physiol. Cell Physiol*. 301:C646–C652, 2011.
[57]Reichelt, J. Mechanotransduction of keratinocytes in culture and in the epidermis. *Eur. J. Cell Biol*. 86:807–816, 2007.
[58]Rief, M., M. Gautel, F. Oesterhelt, J. M. Fernandez, and H. E. Gaub. Reversible unfolding of individual titin immunoglobulin domains by AFM. *Science* 276:1109–1112, 1997.
[59]Rief, M., M. Gautel, A. Schemmel, and H. E. Gaub. The mechanical stability of immunoglobulin and fibronectin III domains in the muscle protein titin measured by atomic force microscopy. *Biophys. J*. 75:3008–3014, 1998.
[60]Rief, M., J. Pascual, M. Saraste, and H. E. Gaub. Single molecule force spectroscopy of spectrin repeats: low unfolding forces in helix bundles. *J. Mol. Biol*. 286:553–561, 1999.
[61]Saeger, J., V. P. Hytönen, E. Klotzsch, and V. Vogel. GFP's mechanical intermediate states. *PLoS One* 7:e46962, 2012.
[62]Sander, J. D., and J. K. Joung. CRISPR-Cas systems for editing, regulating and targeting genomes. *Nat. Biotechnol*. 32:347–355, 2014.
[63]Shaner, N. C., P. A. Steinbach, and R. Y. Tsien. A guide to choosing fluorescent proteins. *Nat. Methods* 2:905–909, 2005.
[64]Shcherbo, D., E. Souslova, J. Goedhart, T. Chepurnykh, A. Gaintzeva, I. Shemiakina, T. Gadella, S. Lukyanov, and D. Chudakov. Practical and reliable FRET/FLIM pair of fluorescent proteins. *BMC Biotechnol*. 9:24, 2009.
[65]Shroff, H., B. M. Reinhard, M. Siu, H. Agarwal, A. Spakowitz, and J. Liphardt. Biocompatible force sensor with optical readout and dimensions of 6 nm^3. *Nano Lett*. 5:1509–1514, 2005.
[66]Stabley, D. R., C. Jurchenko, S. S. Marshall, and K. S. Salaita. Visualizing mechanical tension across membrane receptors with a fluorescent sensor. *Nat. Methods* 9:64–67, 2012.
[67]Style, R. W., R. Boltyanskiy, G. K. German, C. Hyland, C. W. MacMinn, A. F. Mertz, L. A. Wilen, Y. Xu, and E. R. Dufresne. Traction force microscopy in physics and biology. *Soft Matter* 10:4047–4055, 2014.
[68]Suhling, K., P. M. W. French, and D. Phillips. Time-resolved fluorescence microscopy. *Photochem. Photobiol. Sci*. 4:13–22, 2005.
[69]Sun, Y., C. Rombola, V. Jyothikumar, and A. Periasamy. Förster resonance energy transfer microscopy and spectroscopy for localizing protein–protein interactions in living cells. *Cytometry Part A* 83:780–793, 2013.
[70]Svoboda, K., C. F. Schmidt, B. J. Schnapp, and S. M. Block. Direct observation of kinesin stepping by optical trapping interferometry. *Nature* 365:721–727, 1993.
[71]Thomas, W. Catch bonds in adhesion. *Annu. Rev. Biomed. Eng*. 10:39–57, 2008.
[72]Thomas, W. E., V. Vogel, and E. Sokurenko. Biophysics of catch bonds. *Annu. Rev. Biophys*. 37:399–416, 2008.
[73]Van Munster, E. B., G. J. Kremers, M. J. W. Adjobo-Hermans, and T. W. J. Gadella, Jr. Fluorescence resonance energy transfer (FRET) measurement by gradual acceptor photobleaching. *J. Microsc*. 218:253–262, 2005.
[74]Verma, D., N. Ye, F. Meng, F. Sachs, J. Rahimzadeh, and S. Z. Hua. Interplay between cytoskeletal stresses and cell adaptation under chronic flow. *PLoS One* 7:e44167, 2012.
[75]Wallrabe, H., and A. Periasamy. Imaging protein molecules using FRET and FLIM microscopy. *Curr. Opin. Biotechnol*. 16:19–27, 2005.
[76]Wang, X., and T. Ha. Defining single molecular forces required to activate integrin and notch signaling. *Science* 340:991–994, 2013.
[77]Yao, M., B. T. Goult, H. Chen, P. Cong, M. P. Sheetz, and J. Yan. Mechanical activation of vinculin binding to talin locks talin in an unfolded conformation. *Sci. Rep*. 4:4610, 2014.
[78]Zeug, A., A. Woehler, E. Neher, and E. G. Ponimaskin. Quantitative intensity-based FRET approaches—a comparative snapshot. *Biophys. J*. 103:1821–1827, 2012.
[79]Zhang, Y., C. Ge, C. Zhu, and K. Salaita. DNA-based digital tension probes reveal integrin forces during early cell adhesion. *Nat. Commun*. 5, 2014.
[80]Zhang, X., K. Halvorsen, C. Z. Zhang, W. P. Wong, and T. A. Springer. Mechanoenzymatic cleavage of the ultralarge vascular protein von Willebrand factor. *Science* 324:1330–1334, 2009.
[81]Žoldák, G., and M. Rief. Force as a single molecule probe of multidimensional protein energy landscapes. *Curr. Opin. Struct. Biol*. 23:48–57, 2013.

TECHNICAL REPORT

nature cell biology

Extracellular rigidity sensing by talin isoform-specific mechanical linkages

Katharina Austen[1,6], Pia Ringer[1,6], Alexander Mehlich[2,6], Anna Chrostek-Grashoff[1], Carleen Kluger[1], Christoph Klingner[1], Benedikt Sabass[3], Roy Zent[4], Matthias Rief[2,5] and Carsten Grashoff[1,7]

The ability of cells to adhere and sense differences in tissue stiffness is crucial for organ development and function. The central mechanisms by which adherent cells detect extracellular matrix compliance, however, are still unknown. Using two single-molecule-calibrated biosensors that allow the analysis of a previously inaccessible but physiologically highly relevant force regime in cells, we demonstrate that the integrin activator talin establishes mechanical linkages following cell adhesion, which are indispensable for cells to probe tissue stiffness. Talin linkages are exposed to a range of piconewton forces and bear, on average, 7–10 pN during cell adhesion depending on their association with F-actin and vinculin. Disruption of talin's mechanical engagement does not impair integrin activation and initial cell adhesion but prevents focal adhesion reinforcement and thus extracellular rigidity sensing. Intriguingly, talin mechanics are isoform specific so that expression of either talin-1 or talin-2 modulates extracellular rigidity sensing.

Tissue rigidity is an epigenetic factor that governs tissue patterning and organ development[1–3], while altered tissue mechanics is associated with numerous disease states including cardiovascular disorders, spinal cord injury or tumour formation[4,5]. To distinguish differences in tissue stiffness, cells constantly probe the mechanical properties of their environment by anchoring and pulling on the surrounding extracellular matrix[6–8] (ECM). This anchorage-dependent rigidity sensing is mediated by focal adhesions (FAs), subcellular structures in which ECM-binding integrin receptors are connected through adaptor proteins with the intracellular actin cytoskeleton[9,10]. Although the important role of individual integrin subunits and distinct FA molecules such as focal adhesion kinase (FAK), paxillin or vinculin has been appreciated[7,11,12], the central mechanism that couples cell adhesion with mechanosensing remained unknown.

Among the implicated regulators of FA mechanosensing are talins, primarily known for their essential role during integrin activation[13]. Talins directly bind and thereby activate integrin receptors with an amino-terminal head domain and are thought to transduce mechanical information by simultaneously connecting to the actin cytoskeleton with their carboxy-terminal rod domain[14–16]. Owing to the lack of suitable techniques to measure subcellular talin forces, however, quantitative evidence for mechanical tension across talin in cells was missing. We therefore embarked on the development of biosensors to examine the piconewton mechanics of talin linkages in living cells.

RESULTS

Single-molecule calibration of two genetically encoded tension sensors

We have previously generated a probe (called TSMod), in which an elastic peptide is flanked by two fluorophores allowing the measurement of molecular forces of 1–6 pN using Förster resonance energy transfer[12,17–19] (FRET). Yet individual myosin motors can generate single piconewton forces[20] and forces across distinct integrin receptors were recently shown to be significantly higher[21,22]. This suggests that the proteins that directly connect adhesion receptors with actomyosin networks such as talin may experience higher mechanical forces as well. We therefore engineered two tension sensors using the 35 amino acid-long villin headpiece peptide (HP35) as a force-sensitive element flanked by an YPet/mCherry pair of fluorophores (Fig. 1a). HP35 is an ultrafast-folding peptide that undergoes an equilibrium unfolding/folding transition in response to mechanical forces of about 7 pN, whereas a stable HP35 mutant (HP35st) undergoes this transition at about 10 pN (refs 23,24). To test whether HP35 unfolding/folding dynamics are affected by the presence of N- and C-terminally fused fluorophores, we performed

[1]Max Planck Institute of Biochemistry, Group of Molecular Mechanotransduction, Martinsried D-82152, Germany. [2]Technical University of Munich, Physics Department E22, Garching D-85748, Germany. [3]Princeton University, Department of Mechanical & Aerospace Engineering, Princeton, New Jersey 08544, USA. [4]Vanderbilt University, Division of Nephrology, Department of Medicine, Nashville, Tennessee 37232, USA. [5]Munich Centre for Integrated Protein Science, Munich D-81377, Germany. [6]These authors contributed equally to this work.
[7]Correspondence should be addressed to C.G. (e-mail: cgrasho@biochem.mpg.de)

Received 28 April 2015; accepted 8 October 2015; published online 2 November 2015; DOI: 10.1038/ncb3268

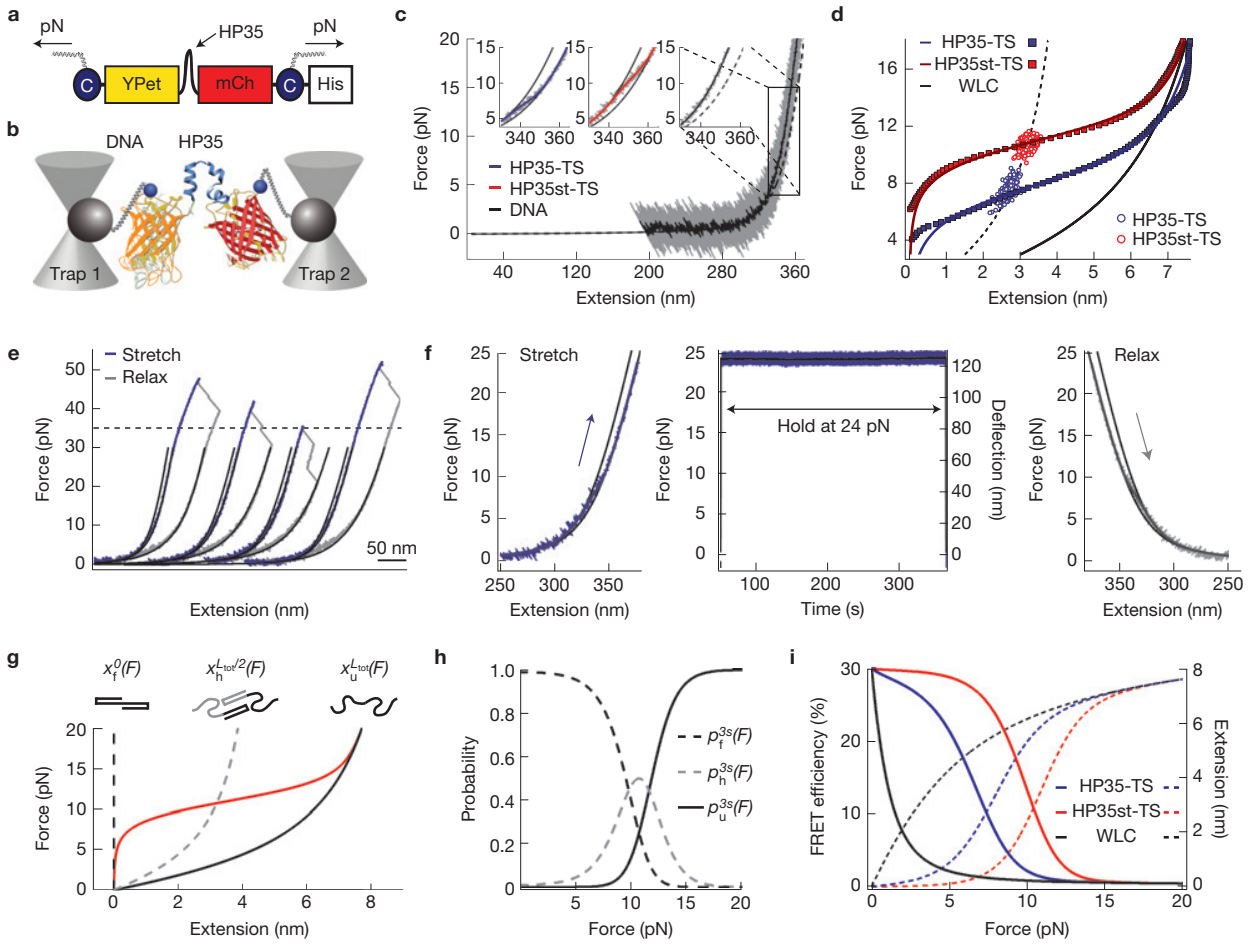

Figure 1 Biosensor calibration using single-molecule force spectroscopy. (**a**) HP35-TS comprises two fluorophores, YPet and mCherry (mCh), which are linked by the villin headpiece peptide (HP35). Mechanical force across this biosensor leads to HP35 unfolding, increase in fluorophore separation distance and reduced FRET. For single-molecule calibration, DNA handles were attached using cysteines (C), a His-tag was used for purification. (**b**) Schematic illustration of the dual-trap optical tweezer set-up used for calibration. (**c**) 200 kHz resolution force–extension trace (grey) fitted with an extensible worm-like chain model (black). Inset: zoom into representative force–extension traces of individual HP35(st)-TS molecules as compared to DNA; the fit to HP35-TS data is shown in blue, HP35st-TS in red and DNA in black. (**d**) Average force–extension traces of individual HP35-TS (blue) and HP35st-TS (red) molecules. Experimental data are shown as filled squares; solid lines are fits to the data; open circles represent transition midpoint forces (HP35-TS: $n = 344$ single pulls pooled from 15 independent repeats, that is, different molecules; HP35st-TS: $n = 338$ single pulls pooled from 10 independent repeats). (**e**) Force–extension traces of four representative HP35-TS molecules showing fluorophore unfolding at high (≥35 pN) forces following stretching (pulling velocity: 500 nm s^{-1}); traces were horizontally shifted for better representation. (**f**) After stretching to 24 pN, HP35-TS was exposed to high force for more than five min before relaxation; no indications of fluorophore unfolding were observed. (**g**) Average force–extension fit for HP35st-TS using a three-state model. The dashed black line represents the folded state, the grey dashed line the half-folded/half-unfolded state with contour length $L_{tot}/2$, and the black solid line the completely unfolded state with contour length L_{tot}; the red line indicates the average protein extension $\langle x_P \rangle$. (**h**) Probability plot for the folded, half-folded/half-unfolded and unfolded state. (**i**) Modelled FRET–force (solid lines) and extension–force (dashed lines) correlations of HP35(st)-TS.

single-molecule calibrations using a custom-built optical tweezer set-up (Fig. 1b and Supplementary Note and Methods). As expected, the average equilibrium transition mid-forces were at 7.4 pN (HP35-TS) and 10.6 pN (HP35st-TS), and both sensors quickly recovered their original conformation when forces were released (Fig. 1c,d and Supplementary Fig. 1a–e). Importantly, unfolding of fluorophores was not observed below 35 pN (pulling velocity: 500 nm s^{-1}; Fig. 1e) and also did not occur when constructs were subjected to a constant force of 24 pN for more than five minutes (Fig. 1f). The force–extension data of HP35-TS and HP35st-TS were well fitted by a three-state model assuming HP35(st) to be either in a folded, half-folded/half-unfolded or unfolded state (Fig. 1g and Supplementary Note and Supplementary Fig. 1c,f–h). The resulting probabilities for HP35(st) to be in any of these conformations at a given force were used to calculate the biosensors' force–FRET responses revealing highest sensitivity between 6–8 pN and 9–11 pN, respectively. (Fig. 1i). Thus, HP35-TS and HP35st-TS are efficiently folding, rapidly responding and reversibly switching tension sensors with response thresholds at about 7 pN and 10 pN.

Talin tension sensor evaluation

To examine talin forces in cells, we genetically inserted HP35-TS into the unstructured linker region connecting the head and rod domains of mouse talin-1 (Tln1TS; ref. 13). In parallel, we

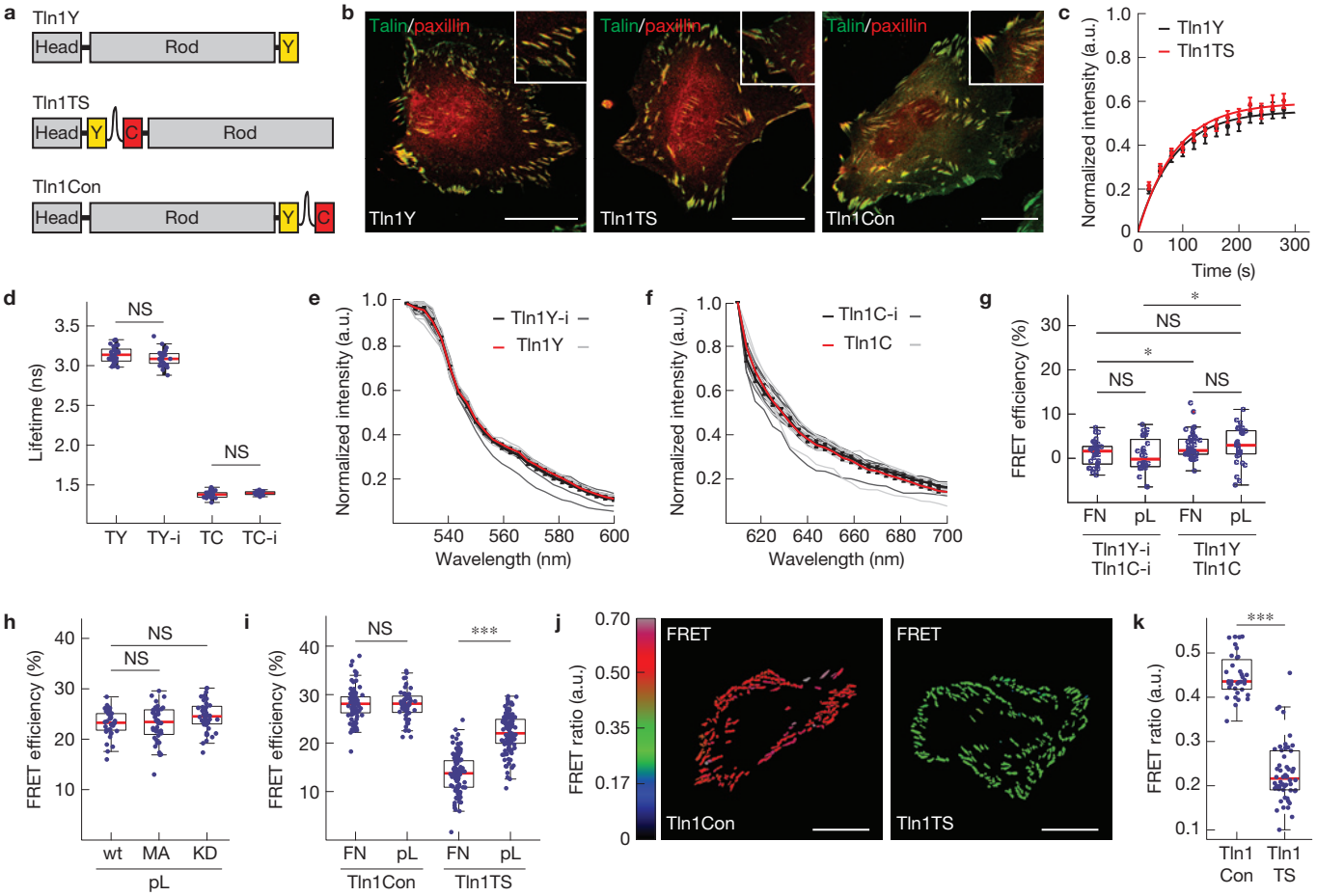

Figure 2 Generation and evaluation of the talin-1 tension sensor. (**a**) Schematic illustrations of C-terminally YPet-tagged talin-1 (Tln1Y), the talin-1–HP35 tension sensor (Tln1TS) and the talin-1 zero force control (Tln1Con). (**b**) Representative images from 4 independent experiments showing *Tln1*$^{-/-}$*Tln2*$^{-/-}$ cells expressing Tln1Y, Tln1TS or Tln1Con. Talin constructs are shown in green and paxillin in red; scale bars, 20 μm. (**c**) FRAP analyses demonstrating normal FA turnover rates of Tln1Y (black) and Tln1TS (red). Error bars indicate s.e.m.; $n=21$ and 24 cells respectively for Tln1Y and Tln1TS, pooled from 5 independent experiments. (**d**) Live-cell fluorescence lifetimes of internally and C-terminally tagged talin-1 constructs expressed in *Tln1*$^{-/-}$*Tln2*$^{-/-}$ cells ($n=29$, 28, 30, 23 cells respectively from left to right, 3 independent experiments). (**e**) Live-cell emission spectra of FA-localized Tln1Y-i (single measurements, dark grey lines; mean, black line) and Tln1Y (single measurements, light grey lines; mean, red line). Error bars indicate s.e.m.; $n=10$ and 10 cells, 3 independent experiments. (**f**) Live-cell emission spectra of FA-localized Tln1C-i (single measurements, dark grey lines; mean, black line) and Tln1C (single measurements, light grey lines; mean, red line). Error bars indicate s.e.m.; $n=10$ (Tln1C-i) and 10 (Tln1C) cells, 3 independent experiments. (**g**) Intermolecular FRET analysis in *Tln1*$^{-/-}$*Tln2*$^{-/-}$ cells co-expressing Tln1C-i/Tln1Y-i or Tln1C/Tln1Y on FN- or pL-coated glass coverslips ($n=35$, 28, 44, 36 cells respectively from left to right; 3 independent experiments). (**h**) No FRET efficiency differences in cells expressing Tln1TS (wt), Tln1TS-M319A (MA) and Tln1TS-K324D (KD) when seeded on pL-coated glass coverslips ($n=39$, 40, 42 cells respectively from left to right; 3 independent experiments). (**i**) Live-cell FLIM analysis demonstrating decreased FRET efficiency in Tln1TS cells when seeded on FN-coated surfaces indicating tension across talin-1 ($n=35$, 56, 102, 115 cells respectively from left to right; 5 independent experiments). (**j**) Representative ratiometric FA FRET images of non-motile Tln1Con and Tln1TS cells confirming reduced FRET in Tln1TS cells; scale bars, 20 μm (3 independent experiments). (**k**) Mean ratiometric FA FRET in Tln1Con and Tln1TS cells ($n=32$ and 47 cells respectively for Tln1Con and Tln1TS; 3 independent experiments). (**d**,**g**,**h**,**i**, Kolmogorov–Smirnov test, ***, $P<0.001$; *, $P<0.05$; not significant (NS), $P>0.05$.) Box plots indicate the median (red line) as well as 25th and 75th percentiles; whiskers reach out to 2.7 standard deviations (σ). Statistic source data are available in Supplementary Table 1.

generated a C-terminally YPet-tagged control to test for talin function (Tln1Y), a C-terminally HP35-TS-tagged talin-1 to determine force-independent effects (Tln1Con; Fig. 2a), and intermolecular FRET controls in which the individual fluorophores were inserted into talin-1 (Tln1Y-i, Tln1C-i) or C-terminally attached (Tln1Y, Tln1C). Stable expression of these constructs in cells lacking talin-1 and talin-2 (*Tln1*$^{-/-}$*Tln2*$^{-/-}$) revealed proper subcellular localization as well as rescue of the severe cell adhesion and FAK activation defects of talin-deficient cells[25] (Fig. 2b and Supplementary Fig. 2a,b). Furthermore, fluorescence recovery after photobleaching (FRAP) experiments demonstrated normal FA turnover rates of Tln1TS as compared with Tln1Y (Fig. 2c), together indicating that insertion of HP35-TS does not impair talin function. Next, we confirmed that the fluorescence lifetimes and the emission spectra of donor and acceptor fluorophores were unaffected by the insertion into talin-1 (Fig. 2d–f), and we quantified effects of intermolecular FRET

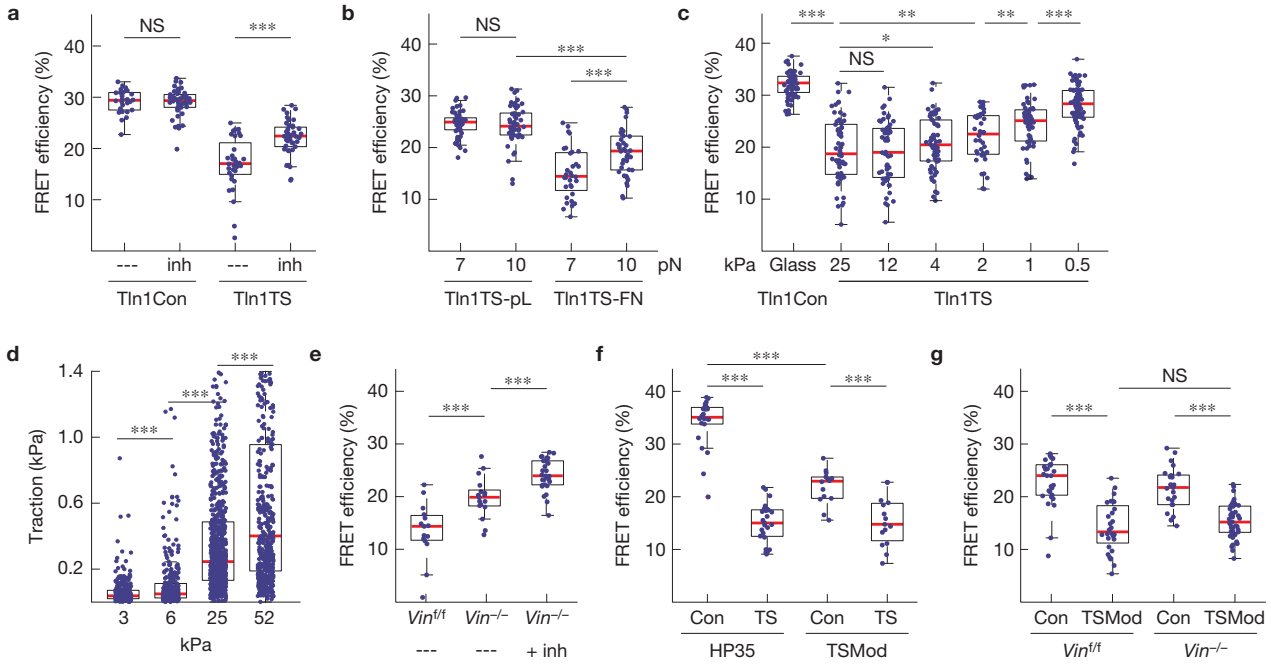

Figure 3 Talin-1 mediates a constitutive mechanical linkage in FAs that is modulated by F-actin and vinculin association. (**a**) Treatment of cells with 10 μM Y-27632 (inh) induces an increase in average FRET efficiency specifically in Tln1TS cells ($n = 26$, 42, 32 and 42 respectively from left to right; pooled from 3 independent experiments). (**b**) Comparing HP35-TS (7 pN) with HP35st-TS (10 pN)-based talin sensors in cells on FN- or pL-coated surfaces suggests that most talin-1 linkages experience force of more than 7 pN, some even more than 10 pN ($n = 52$, 53, 32 and 40 cells respectively from left to right; 4 independent experiments). (**c**) FRET efficiencies in Tln1Con cells seeded on FN-coated glass coverslips ($n = 68$) and in Tln1TS cells seeded on FN-coated 25 kPa ($n = 61$), 12 kPa ($n = 58$), 4 kPa ($n = 64$), 2 kPa ($n = 40$), 1 kPa ($n = 58$) and 0.5 kPa ($n = 81$) matrices; n represents the number of cells that were pooled from 5 independent experiments. (**d**) Rigidity-dependent traction force increase of Tln1Y cells seeded on FN-coated polyacrylamide gels with elastic moduli of 3.2 kPa ($n = 20$), 6.3 kPa ($n = 16$), 24.7 kPa ($n = 30$) and 52 kPa ($n = 15$); n represents the number of cells that were pooled from 3 independent experiments. Single data points represent traction forces from displacement of every hundredth bead. (**e**) Depletion of vinculin leads to an increase in FRET whereas treatment of Tln1TS-expressing $Vin^{-/-}$ cells with 10 μM Y-27632 further increases transfer rates indicating that loss of vinculin leads to a reduction but not entire loss of talin tension ($n = 15$, 17 and 29 cells respectively from left to right, pooled from 7 independent experiments). (**f**) The HP35-based sensor monitors talin-1 tension more efficiently than a biosensor using TSMod ($n = 22$, 25, 14 and 15 cells respectively from left to right, 5 independent experiments). (**g**) TSMod does not properly resolve vinculin-dependent differences in talin-1 tension ($n = 29$, 28, 25 and 41 cells respectively from left to right, 3 independent experiments). (**a**–**c** and **e**–**g**, Kolmogorov–Smirnov test; **d**, Wilcoxon–Mann–Whitney test. ***, $P < 0.001$; **, $P < 0.01$; *, $P < 0.05$; not significant (NS), $P > 0.05$.) Box plots indicate the median (red line) as well as 25th and 75th percentiles; whiskers reach out to 2.7 standard deviations (σ). Statistic source data are available in Supplementary Table 1.

(Fig. 2g), talin conformation (Fig. 2h), fluorescence intensity and temperature (Supplementary Fig. 2c,d) but found these confounding factors to be negligible in our experiments (see Methods for more detailed information). However, live-cell FRET analysis by time-correlated single-photon counting fluorescence lifetime microscopy or ratiometric imaging revealed an integrin-dependent reduction of energy transfer rates in Tln1TS cells indicating mechanical tension across talin-1 (Fig. 2i–k).

Talin-1 bears piconewton forces during cell adhesion

Next, we treated integrin-engaged Tln1TS and control cells with the Rock inhibitor Y-27632 to confirm that talin forces are actomyosin dependent. As expected, inhibitor treatment increased FRET efficiencies in Tln1TS cells but did not alter energy transfers in controls (Fig. 3a). Moreover, FRET efficiencies were specifically increased in integrin-engaged cells when the 9–11 pN-sensitive talin sensor (HP35st-TS) was used. Intriguingly, FRET was still lower than under control conditions indicating that a population of talin-1 molecules was subject to forces larger than 10 pN (Fig. 3b). To test whether talin establishes mechanical linkages also in softer environments, we analysed cells on matrices characterized by elastic moduli of 0.5–25 kPa. Tension across talin-1 was rather constant over a wide range of substrate rigidities and only gradually decreased on very soft substrates (Fig. 3c), although cells exhibited the expected rigidity-dependent reduction in traction forces as described before[11] (Fig. 3d). Thus, talin-1 mediates constitutive mechanical linkages, a significant subset of which experience forces of more than 7 pN and some even more than 10 pN.

High talin tension depends on association with mechanically engaged vinculin

Vinculin is an adaptor protein thought to regulate force transmission in FAs (refs 12,26,27). As the talin rod domain comprises 11 vinculin-binding sites[13] (VBS), we examined talin tension by transiently expressing Tln1TS in vinculin-expressing ($Vin^{f/f}$) or vinculin-deficient ($Vin^{-/-}$) cells. These experiments suggested that talin-1 tension was decreased in the absence of vinculin, whereas tension was restored by stable re-expression of full-length vinculin (V-wt) but not by a

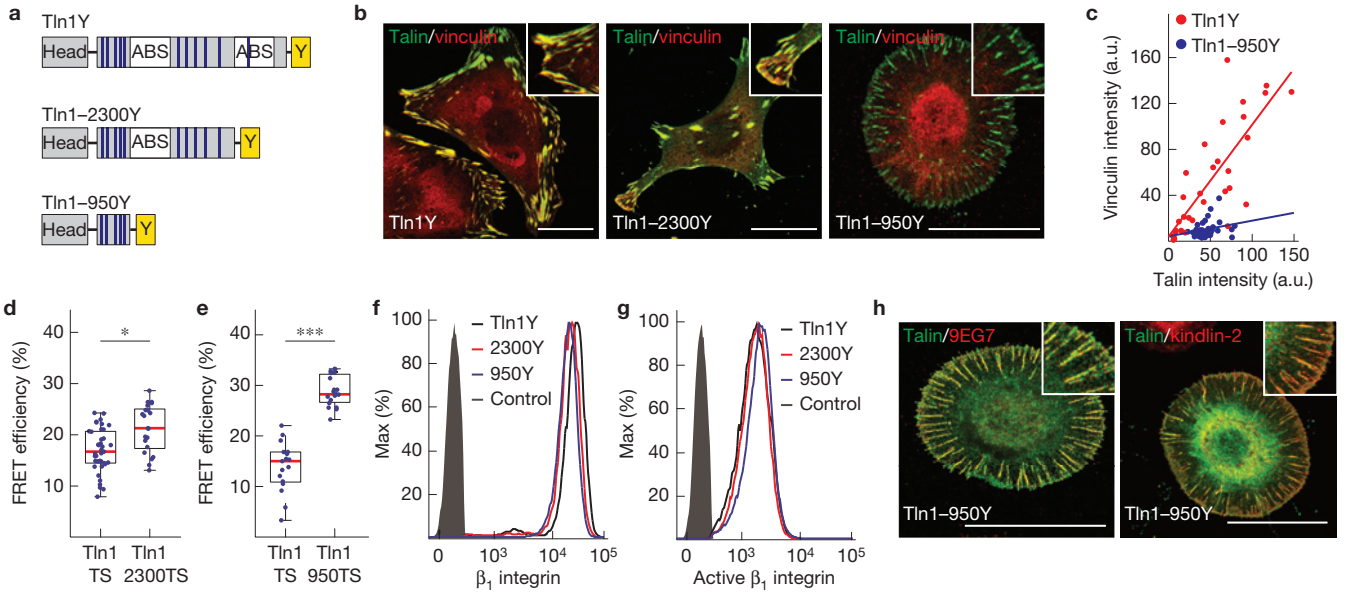

Figure 4 The talin-rod cytoskeletal engagement is essential for vinculin recruitment and talin tension but indispensable for integrin activation. (**a**) Schematic illustration of Tln1Y, Tln1–2300Y and Tln1–950Y constructs; blue lines indicate VBS, white rectangles ABS, yellow rectangles the C-terminal YPet-tag. (**b**) Representative images from 3 independent experiments showing *Tln1*$^{-/-}$*Tln2*$^{-/-}$ cells stably expressing Tln1Y, Tln1–2300Y and Tln1–950Y cells (green) stained with vinculin (red); scale bars, 20 μm. (**c**) Talin-1/vinculin FA co-localization analysis demonstrating the lack of vinculin recruitment to talin-positive adhesion sites in Tln1–950Y cells ($n = 32$ (Tln1Y) and 33 (Tln1–950Y) FAs, pooled from 3 independent experiments). Pearson correlation coefficient (talin versus vinculin intensity): Tln1Y = 0.8060, Tln1–950Y = 0.2424. (**d**) Moderate reduction in talin-1 tension following deletion of the dimerization domain and C-terminal ABS (Tln1–2300) ($n = 39$ (Tln1TS) and 21 (Tln1–2300TS) cells, 4 independent experiments). (**e**) Loss of talin-1 tension in Tln1–950 cells ($n = 17$ (Tln1TS) and 19 (Tln1–950TS), 4 independent experiments). (**f**,**g**) Representative FACS histograms of 4 independent experiments showing cells expressing Tln1Y (black), Tln1–2300Y (red) and Tln1–950Y (blue) labelled for β_1 integrin (**f**) or active β_1 integrin (9EG7) (**g**); the negative control is shown in grey. Tln1–950Y cells exhibit normal integrin expression and activation. (**h**) Representative images from 3 independent experiments showing *Tln1*$^{-/-}$*Tln2*$^{-/-}$ cells reconstituted with Tln1–950Y (green) and labelled for active β_1 integrin or kindlin-2 (red). The recruitment of kindlin-2 in Tln1–950Y cells is consistent with normal integrin activation and cell adhesion; scale bars, 20 μm. (**d**,**e**, Kolmogorov–Smirnov test. ***, $P < 0.001$; *, $P < 0.05$.) Box plots indicate the median (red line) as well as 25th and 75th percentiles; whiskers reach out to 2.7 standard deviations (σ). Statistic source data are available in Supplementary Table 1.

vinculin truncation mutant (V-mut) unable to transduce mechanical forces[12,27,28] (Supplementary Fig. 2e). To confirm these results, we generated *Vin*$^{f/f}$ and *Vin*$^{-/-}$ cells stably expressing Tln1TS and again observed higher FRET efficiencies in vinculin-deficient cells that could be further increased by Y-27632 treatment indicating that forces across talin-1 were reduced but not entirely lost in the absence of vinculin (Fig. 3e). To investigate this in more detail, we generated a talin tension sensor using a YPet/mCherry version of our previously published 1–6 pN-sensitive probe[12] (TSMod) and first analysed it in *Tln1*$^{-/-}$*Tln2*$^{-/-}$ cells. Consistent with our Tln1TS measurements, this construct also indicated tension across talin-1, even though FRET efficiency differences were smaller owing to the rather narrow dynamic range of TSMod (Fig. 3f). In contrast to the HP35 probes, however, TSMod-based sensors indicated very similar FRET values in *Vin*$^{f/f}$ and *Vin*$^{-/-}$ cells demonstrating that talin-1 is still subject to low forces of 1–6 pN in the absence of vinculin (Fig. 3g). Together, these results provide direct evidence that mechanical tension across talin-1 is determined by its association with F-actin and vinculin. While talin's F-actin engagement is sufficient to establish mechanically resilient linkages that bear low piconewton forces, vinculin binding seems to promote higher tension states. The results also underline the significance of the HP35 sensors that detect higher piconewton forces that cannot be resolved by TSMod.

The mechanical engagement of the talin rod domain is dispensable for integrin activation but critical for vinculin recruitment to domains R1–R3

To elucidate whether vinculin recruitment to talin-1 depends on talin tension as proposed earlier[15,29,30], we generated mutants in which the C-terminal actin-binding sites (ABS) and VBS of talin-1 were deleted to varying degrees and stably expressed them in *Tln1*$^{-/-}$*Tln2*$^{-/-}$ cells (Fig. 4a). Removing talin's dimerization domain as well as the entire C-terminal ABS (Tln1–2300) resulted in less efficient cell spreading and impaired formation of peripheral actin bundles but only slightly reduced forces across talin-1 and hardly influenced vinculin's FA recruitment (Fig. 4b,d and Supplementary Fig. 3a). In contrast, deletion of the second ABS and six additional VBS (Tln1–950) strongly impaired cell spreading and stress fibre formation (Fig. 4b). Tln1–950 cells exhibited normal surface levels of activated β_1 integrin and readily adhered to ECM substrates forming integrin-, talin- and kindlin-2-positive adhesion sites (Fig. 4f–h). However, talin tension and vinculin recruitment were abolished even though Tln1–950 still harboured five VBS in the talin rod domains R1–R3 and vinculin was present at normal levels in the cytoplasm (Fig. 4b,c,e and Supplementary Fig. 3b,c). Together, the data indicate that vinculin association with talin-1's N-terminal VBS requires preceding cytoskeletal engagement. This observation is consistent with a previously suspected positive

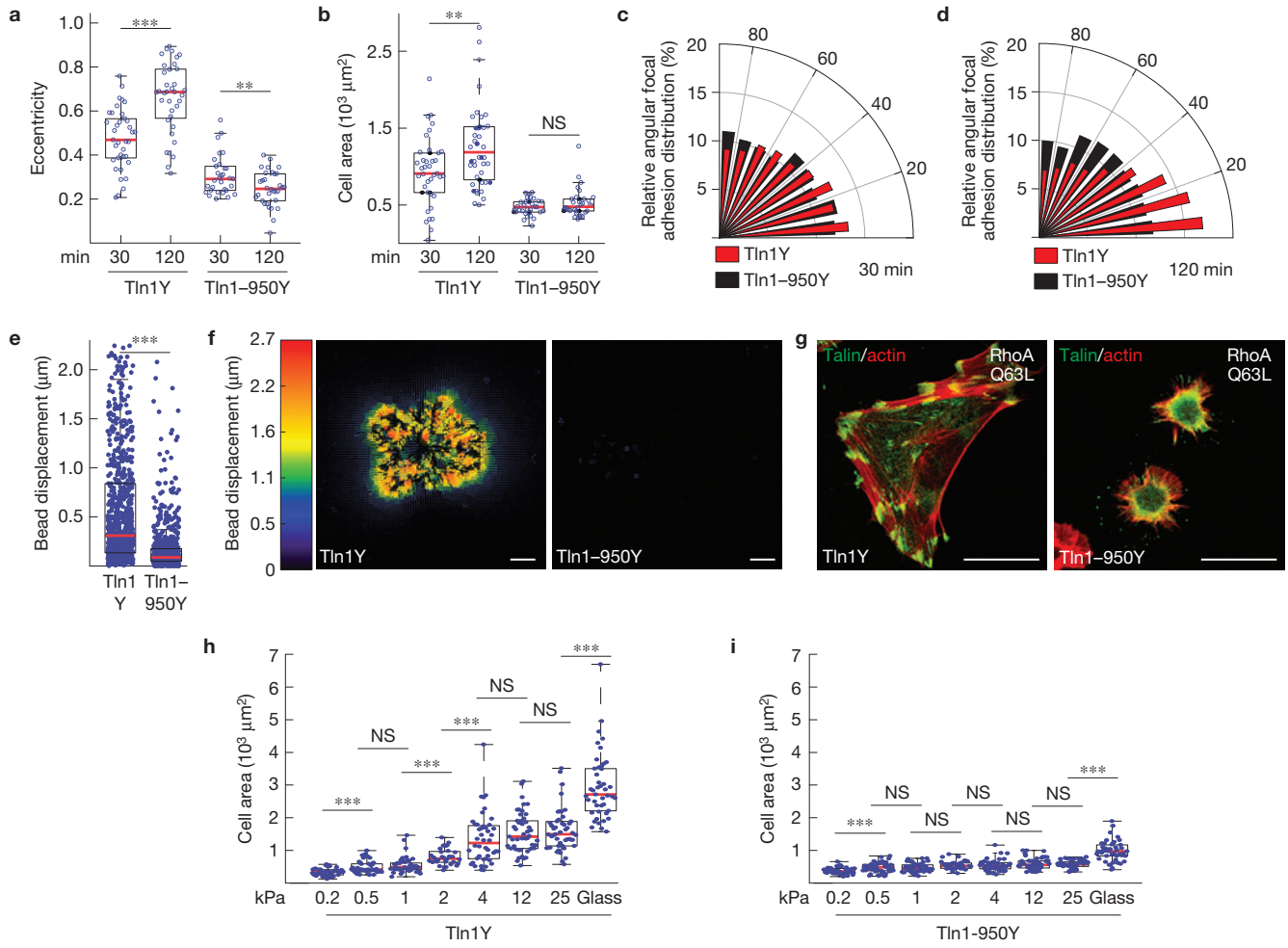

Figure 5 Cytoskeletal engagement of the talin-1 rod domain is indispensable for cell spreading, polarization, traction force generation and extracellular rigidity sensing. (**a**,**b**) Cellular eccentricity (**a**) and cell area (**b**) of Tln1Y and Tln1–950Y cells after 30 min or 120 min of spreading on FN-coated glass coverslips; Tln1–950Y cells are unable to polarize and spread (in **a** and **b** $n=37$, 36, 31 and 32 cells respectively from left to right, pooled from 3 independent experiments). (**c**,**d**) Relative angular FA distribution in Tln1Y cells (red) and Tln1–950Y cells (black) after 30 min (**c**) and 120 min (**d**) of spreading on FN-coated glass coverslips indicating lack of polarization in Tln1–950Y cells (in **c** and **d** $n=37$ (Tln1Y 30 min), 36 (Tln1–950Y 30 min), 31 (Tln1Y 120 min) and 32 (Tln1–950Y 120 min) cells, 3 independent experiments). (**e**) Bead displacements observed under Tln1Y ($n=21$) and Tln1–950Y ($n=22$) cells cultured on 2 kPa polyacrylamide gels; data were pooled from 4 independent experiments. Tln1–950Y cells are characterized by significantly lower traction forces indicated by very small bead displacements. (**f**) Representative displacement images (4 independent experiments, corresponding quantification shown in **e**) of Tln1Y and Tln1–950Y cells indicating the virtual absence of traction forces in Tln1–950Y cells; scale bars, 10 μm. (**g**) Representative images from 3 independent experiments showing Tln1Y and Tln1–950Y cells (green) expressing active RhoAQ63L, stained for F-actin (red); Tln1–950Y cells fail to reinforce their FAs; scale bars, 20 μm. (**h**,**i**) Cell area of Tln1Y (**h**) and Tln1–950Y (**i**) cells after overnight culture on glass or FN-coated polyacrylamide gels with the indicated elastic moduli ranging from 0.2–25 kPa; Tln1Y ($n=45$, 45, 45, 32, 44, 47, 47 and 45 cells respectively from left to right, 3 independent experiments), Tln1–950Y ($n=47$, 49, 47, 32, 47, 46, 46 and 45 cells respectively from left to right, 3 independent experiments). Note that Tln1–950Y cells fail to distinguish rigidity differences. (**a**,**b**,**h**,**i**, two-sided *t*-test; **e**, Wilcoxon–Mann–Whitney test. ***, $P<0.001$; **, $P<0.01$; *, $P<0.05$; not significant (NS), $P>0.05$). Box plots indicate the median (red line) as well as 25th and 75th percentiles; whiskers reach out to 2.7 standard deviations (σ). Statistic source data are available in Supplementary Table 1.

feedback regulation of FA strengthening, where F-actin-dependent vinculin engagement promotes talin tension leading to further vinculin recruitment at R1–R3 and cell adhesion reinforcement[15,29–31].

Talin linkages are essential for extracellular rigidity sensing

Throughout the experiments, we noticed that cell spreading and polarization, FA enlargement, and the generation of traction forces—all processes that require mechanical stabilization of FAs—were strongly impaired in Tln1–950 cells (Fig. 5a–f). Moreover, Tln1–950 cells failed to strengthen their FAs in response to increased intracellular contractile forces after expression of active RhoA (RhoA Q63L) (Fig. 5g). We therefore tested whether extracellular rigidity sensing, which seems to require FA strengthening[9], is affected in cells lacking mechanically engaged talin-1. Indeed, Tln1–950 cells seemed incapable of sensing and/or responding to different ECM rigidities whereas Tln1Y control cells reacted with the expected rigidity-dependent increase in cell area (Fig. 5h,i). Thus, the mechanical engagement of the talin rod domain with the actin cytoskeleton is indispensable for cell adhesion reinforcement and hence extracellular rigidity sensing.

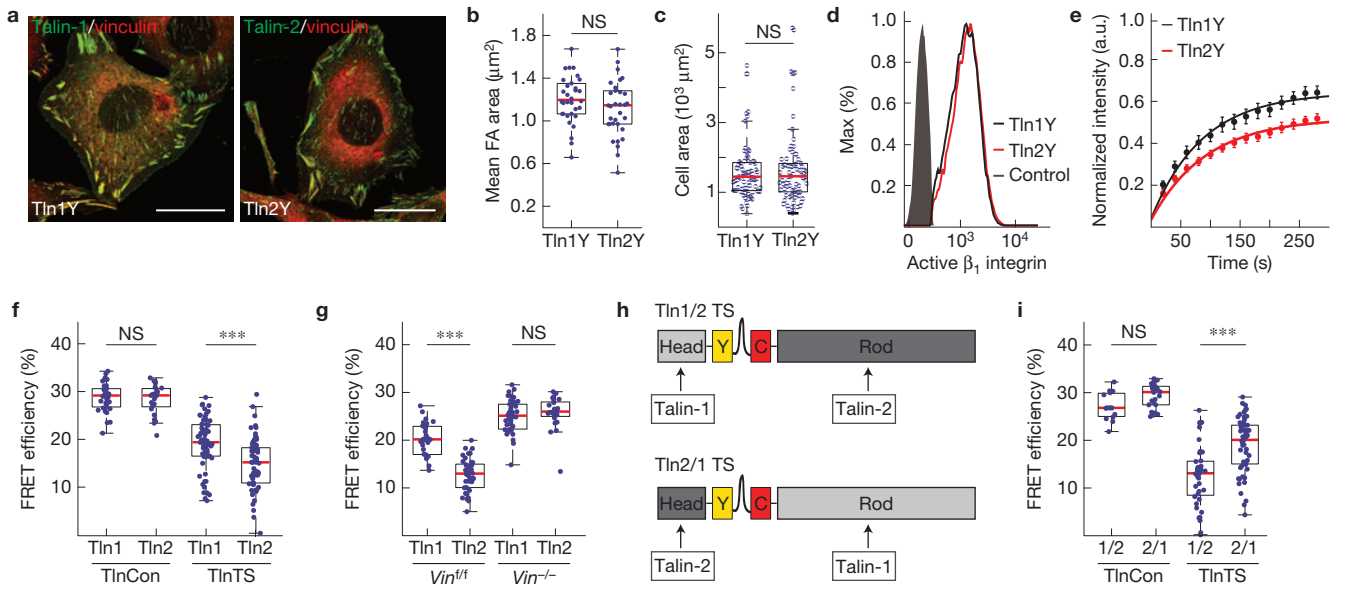

Figure 6 Talin-1 and talin-2 both rescue cell spreading and integrin activation but they transduce mechanical forces differently. (**a**) Representative images (3 independent experiments) of *Tln1*$^{-/-}$*Tln2*$^{-/-}$ cells reconstituted with Tln1Y or Tln2Y (green) and labelled for vinculin (red). Cell lines are indistinguishable when cultured on plastic or glass coverslips; scale bars, 20 μm. (**b**,**c**) Mean FA area ($n = 30$ (Tln1Y) and 34 (Tln2Y) cells; pooled from 4 independent experiments) (**b**) and mean cell area ($n = 77$ (Tln1Y) and 77 (Tln2Y) cells; 4 independent experiments) (**c**) determined from Tln1Y and Tln2Y cells seeded on FN-coated glass coverslips. (**d**) Representative FACS histogram of cells expressing Tln1Y (black) or Tln2Y (red) labelled for active β_1 integrin; the negative control is shown in grey (4 independent experiments). (**e**) Normalized fluorescence recovery rates of Tln1Y (black, $n = 18$ cells) and Tln2Y cells (red, $n = 17$ cells) as determined by live-cell FRAP experiments. Cells were pooled from 3 independent experiments; error bars indicate s.e.m. (**f**) FRET efficiencies in Tln1Con, Tln2Con, Tln1TS and Tln2TS cells ($n = 35$, 25, 63 and 63 cells respectively from left to right, 3 independent experiments) indicating increased tension across talin-2. (**g**) Isoform-specific tension differences are abolished in vinculin-deficient cells ($n = 28$, 41, 42 and 24 cells respectively from left to right; 3 independent experiments). (**h**) Schematic illustrations of chimaeric talin-1-head/talin-2-rod (Tln1/2-TS) and talin-2-head/talin-1-rod (Tln2/1-TS) tension sensor constructs. (**i**) FRET analysis of chimaeric talin constructs demonstrating that the isoform-specific tension increase is talin rod dependent ($n = 15$, 24, 43 and 58 cells respectively from left to right; 7 independent experiments). (**b**,**c** two-sided *t*-test; **f**,**g**,**i**, Kolmogorov–Smirnov test. ***, $P < 0.001$; not significant (NS), $P > 0.05$). Box plots indicate the median (red line) as well as 25th and 75th percentiles; whiskers reach out to 2.7 standard deviations (σ). Statistic source data are available in Supplementary Table 1.

Integrin force transduction is talin isoform specific

Mammals express two very similar talin isoforms, the ubiquitous talin-1 and the more restrictively expressed talin-2. It is unclear why certain tissues require the expression of a second talin isoform, as both proteins efficiently activate integrins and connect to the cytoskeleton[13,32]. We therefore wanted to test whether mechanical forces may be differentially transduced by talin-1 and talin-2 and generated a whole set of human talin-1 and talin-2 expression constructs to stably reconstitute *Tln1*$^{-/-}$*Tln2*$^{-/-}$ cells. Although individual expression of the talin isoforms rescued the cell spreading, integrin activation, and FAK phosphorylation phenotype of talin-deficient cells equally (Fig. 6a–d and Supplementary Fig. 4a–c), more talin-2 was immobilized in FAs (Fig. 6e and Supplementary Fig. 4d) and an increased number of talin-2 molecules were exposed to tension in integrin-engaged cells (Fig. 6f and Supplementary Fig. 4e–g). Elevated talin-2 tension levels were also observed in *Vin*$^{f/f}$ but not in *Vin*$^{-/-}$ cells, emphasizing the important role of the talin–vinculin interaction for generating high talin forces (Fig. 6g). To confirm that differences in isoform-specific talin tension were mediated exclusively by the talin rod domain, we engineered chimaeric talin constructs, in which the C-terminal domains of talin-1 and talin-2 were exchanged (Fig. 6h). Stable expression of these constructs rescued the cell adhesion and cell spreading defect of talin-deficient cells, and FLIM experiments demonstrated that the tension increase was indeed entirely mediated by the rod domain of talin-2 (Fig. 6i). Next, we generated a talin-2 truncation mutant lacking all C-terminal ABS but retaining the five VBS residing in R1–R3 (Tln2–950) analogous to the talin-1 construct described above. Remarkably, Tln2–950 FAs were vinculin-positive, exposed to mechanical tension and able to induce, albeit not completely rescue, cell spreading (Fig. 7a–d). Together, these results show that the two human talin isoforms bear mechanical forces differently; they also suggest that the F-actin-dependent vinculin recruitment to talin's N-terminal rod domain, specifically to domains R1–R3, is talin-1 specific.

Isoform-specific effects are mediated by the talin rod domains R1–R3

As our data indicated that initial vinculin recruitment to talin-2 is independent of preceding force generation through F-actin association, we tested whether FA strengthening and cell spreading on low-rigidity substrates, where actomyosin contractility is naturally reduced, is talin isoform dependent. Indeed, talin-2 cells spread more efficiently than talin-1 cells on 1–2 kPa matrices but behaved like talin-1-expressing cells on very soft (0.2–0.5 kPa) and more rigid (4–25 kPa) substrates (Fig. 7e). To test whether the observed isoform-specific effects are mediated by the talin rod domains R1–R3,

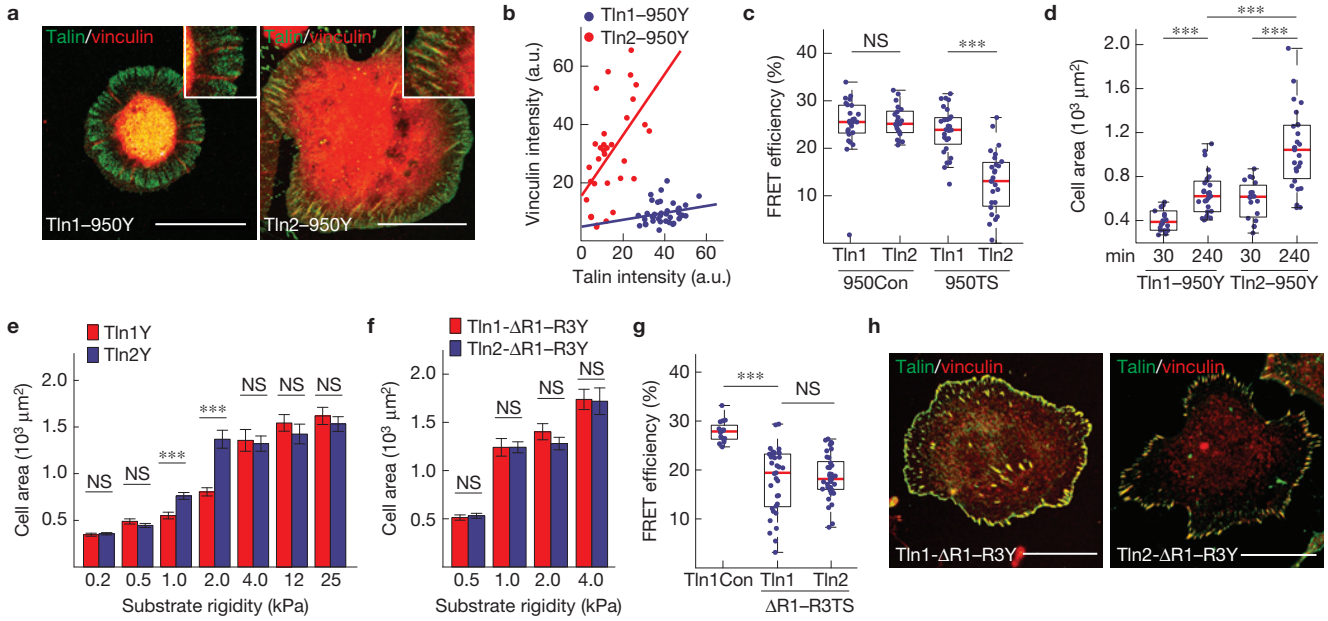

Figure 7 Talin isoform-specific differences are mediated by domains R1–R3. (**a**) Representative images from 3 independent experiments showing that vinculin (red) co-localizes with Tln2–950Y but not with Tln1–950Y adhesion sites; scale bars, 20 µm. (**b**) Quantification of talin/vinculin co-localization in adhesion sites of cells expressing Tln1–950Y ($n=32$ adhesions) and Tln2–950Y ($n=38$ adhesions); n values represent pooled adhesions from 3 independent experiments. Pearson correlation coefficient (talin versus vinculin intensity): Tln1–950Y = 0.2214, Tln2–950Y = 0.5323. (**c**) Deletion of C-terminal ABS abolishes tension across talin-1 but not across talin-2 ($n=24$, 21, 28 and 25 cells respectively from left to right; 5 independent experiments). (**d**) Cell area of Tln1–950Y and Tln2–950Y cells after 30 min and 240 min spreading on FN-coated glass coverslips ($n=18$, 27, 19 and 27 cells respectively from left to right; 3 independent experiments). (**e**) Cell area quantification of Tln1Y and Tln2Y cells seeded on FN-coated substrates of indicated stiffness; Tln2Y cells respond differently on 1 kPa and 2 kPa matrices ($n=47$, 49, 45, 46, 45, 48, 32, 30, 44, 47, 48, 48, 46 and 46 cells respectively from left to right; 3 independent experiments; data are means ± s.e.m.). (**f**) No differences in cell spreading of Tln1-ΔR1R3Y ($n=50$ (0.5 kPa), 50 (1 kPa), 53 (2 kPa) and 47 (4 kPa) cells) and Tln2-ΔR1R3Y cells ($n=52$ (0.5 kPa), 47 (1 kPa), 47 (2 kPa) and 47 (4 kPa) cells). Cells were pooled from 3 independent experiments; data are means ± s.e.m. (**g**) FRET analysis of talin-deficient cells expressing Tln1-ΔR1R3TS and Tln2-ΔR1R3TS constructs seeded on FN-coated glass coverslips ($n=16$, 33 and 37 cells respectively from left to right; 3 independent experiments). (**h**) Representative images from 3 independent experiments showing Tln1-ΔR1R3Y and Tln2-ΔR1R3Y cells on FN-coated glass coverslips stained for vinculin; the talin signal is labelled in green, the vinculin signal is shown in red; scale bars, 20 µm. (**c**,**g**, Kolmogorov–Smirnov test; **d**–**f**, two-sided t-test. ***, $P<0.001$; not significant (NS), $P>0.05$). Box plots indicate the median (red line) as well as 25th and 75th percentiles; whiskers reach out to 2.7 standard deviations (σ). Statistic source data are available in Supplementary Table 1.

we generated talin-1 and talin-2 expression constructs in which these domains were deleted (Tln1-ΔR1–R3). Indeed, *Tln1*$^{-/-}$ *Tln2*$^{-/-}$ cells expressing talin-1 or talin-2 ΔR1–R3 deletion constructs did not exhibit differences in cell spreading on 1–2 kPa substrates and differences in talin tension were abolished (Fig. 7f,g). As vinculin was still efficiently recruited by the remaining VBS (Fig. 7h), we conclude that the observed talin isoform-specific effects are mediated by talin's N-terminal rod domains R1–R3.

DISCUSSION

The ability of cells to efficiently sense their mechanical environment is critical for many developmental, homeostatic and pathological processes[1–6]. Yet the underlying molecular mechanisms have been difficult to elucidate because suitable methods to study force propagation across individual molecules in cells were missing. We therefore developed a biosensor that allows molecular force measurements at 1–6 pN and the technique has been widely used to determine forces across various proteins in living cells and even whole organisms[12,17,18,33–37]. An obvious limitation of the method, however, has been its inability to resolve forces higher than 6 pN. In this work, we describe the generation, single-molecule calibration and application of two biosensors that enable efficient measurements at 6–8 pN and 9–11 pN. The probes are characterized by sharp and very fast force responses, they are reversible, benefit from an improved dynamic range and do not unravel until forces of about 35 pN are reached (Fig. 1).

Application of these biosensors revealed that the integrin activator talin establishes mechanical linkages during cell adhesion that are indeed subject to forces larger than 7 pN; furthermore, a small but significant fraction of talin molecules experiences forces of more than 10 pN. On the other hand, talin tension dropped to relatively low levels in the absence of vinculin binding and disappeared on talin's disengagement from the actin cytoskeleton (Figs 2 and 3). Thus, talin bears a range of forces depending on the degree of its mechanical engagement and it should be worthwhile investigating how talin tension correlates with FA dynamics for instance during cell migration. Interestingly, the formation of force-bearing talin linkages occurred over a wide range of substrate rigidities and seemed inherently linked to the formation of enlarged FAs. Consistent with this observation, cells expressing a truncated talin mutant lacking all C-terminal F-actin-binding sites (Tln1–950) were unable to form large FAs; they failed to generate significant cellular traction forces and did not sense extracellular rigidity differences even

though integrin activation was unaffected (Figs 4 and 5). Thus, in addition to its crucial role as an integrin activator, talin is an indispensable mediator of integrin mechanosensing. This dual role distinguishes talin from kindlins, which are also critical for integrin activation but do not seem to mediate a direct connection to the actin cytoskeleton[38].

Intriguingly, integrin-dependent mechanosensing is talin isoform specific (Fig. 6). Although our data are consistent with the previously proposed tension-dependent vinculin recruitment to talin-1's N-terminal rod domain[15,29–31], this mechanism does not seem to exist for talin-2. Instead, vinculin recruitment occurs even in the absence of C-terminal F-actin binding, which coincides with increased talin-2 FA immobilization and elevated average tension levels. As a consequence, talin-2-expressing cells spread more efficiently on 1–2 kPa surfaces than their talin-1 counterparts and it is interesting to note that talin-2 is expressed highest in brain tissue, which is characterized by similar rigidities[32,39]. In our experiments, the observed mechanical differences can be ascribed to talin's R1–R3 domains (Fig. 7), which seemingly contrasts a previous study that attributed isoform-specific differences to distinct integrin–talin head-domain affinities[40]. It has to be noted, however, that the *Tln1*$^{-/-}$*Tln2*$^{-/-}$ cells used here do not express integrin β_1D, a muscle-specific integrin isoform for which especially high affinities to talin-2 have been reported[40]. Thus, a study using muscle-specific cell types or genetically modified cell lines expressing distinct integrin receptor subtypes is needed.

Collectively, our experiments reveal that talins mediate a mechanical linkage that is essential for coupling cell adhesion with integrin mechanosensing and is thus required for cells to detect tissue stiffness. It seems that differential expression of talin isoforms provides a means by which cells adjust to different ECM rigidities and the fact that integrins and at least one talin isoform are abundantly expressed in all cell types indicates that the observed mechanical linkages are relevant in many tissues. As tissue rigidity changes during development or with the onset of numerous disease states[1–4,6], it will be important to investigate the role of the individual talin isoforms during these processes in more detail. The biosensors described in this study will allow the isoform-specific analysis of talin force transduction in many cell types and should be useful for such studies. Furthermore, they will be valuable to investigate effects of other talin interaction partners, such as RIAM or FAK, on molecular force propagation in FAs. Finally, application of the HP35 probes to other force-transducing proteins should allow the detailed analysis of many different mechanobiological processes that are subject to higher single piconewton forces in cells and whole organisms. □

METHODS

Methods and any associated references are available in the online version of the paper.

Note: Supplementary Information is available in the online version of the paper

ACKNOWLEDGEMENTS

C.G. is supported by the German Research Council (DFG, GR3399/2-1 and GR3399/5-1), the Collaborative Research Centre SFB863 (B9) and a Paul Gerson Unna Research Group of the Max Planck Förderstiftung. A.M. is supported by the Nanosystems Initiative Munich (NIM); M.R. is supported by the German Research Council through the Collaborative Research Centre SFB863 (A2). R.Z. is supported by R01-DK083187, R01-DK075594, R01-DK069221 and VA Merit Award 1I01BX002196. B.S. acknowledges financial support from the DAAD. The authors thank R. Fässler for continuous support and helpful discussions; F. Schnorrer for critically reading the manuscript; A. Lambacher and the MPIB core facility for technical support; G. Zoldak for helpful discussion, A. Sechi for sharing data analysis software and D. Critchley (University of Leicester, UK) for providing talin-2 cDNA.

AUTHOR CONTRIBUTIONS

C.G. and K.A. initiated the project, generated cell lines, performed cellular and biochemical experiments and analysed data; P.R. generated cell lines, performed cellular experiments, wrote data analysis software and analysed data. A.M. and M.R. performed the single-molecule calibration and theoretical modelling. A.C.-G. created talin expression constructs, C.Kluger generated vinculin expression constructs and cell lines, C.Kluger and C.Klingner wrote data analysis software. K.A., C.Kluger and B.S. performed traction force microscopy experiments and analyses. R.Z. provided genetically modified talin cells. C.G. wrote the manuscript with the input from all authors. K.A., P.R. and A.M. contributed equally.

COMPETING FINANCIAL INTERESTS

The authors declare no competing financial interests.

Published online at http://dx.doi.org/10.1038/ncb3268
Reprints and permissions information is available online at www.nature.com/reprints

1. Heisenberg, C. P. & Bellaiche, Y. Forces in tissue morphogenesis and patterning. *Cell* **153,** 948–962 (2013).
2. Wozniak, M. A. & Chen, C. S. Mechanotransduction in development: a growing role for contractility. *Nat. Rev. Mol. Cell Biol.* **10,** 34–43 (2009).
3. Franze, K., Janmey, P. A. & Guck, J. Mechanics in neuronal development and repair. *Annu. Rev. Biomed. Eng.* **15,** 227–251 (2013).
4. Ingber, D. E. Mechanobiology and diseases of mechanotransduction. *Ann. Med.* **35,** 564–577 (2003).
5. Lu, P., Takai, K., Weaver, V. M. & Werb, Z. Extracellular matrix degradation and remodeling in development and disease. *Cold Spring Harb. Perspect. Biol.* **3,** http://dx.doi.org/10.1101/cshperspect.a005058 (2011).
6. Discher, D. E., Janmey, P. & Wang, Y. L. Tissue cells feel and respond to the stiffness of their substrate. *Science* **310,** 1139–1143 (2005).
7. Plotnikov, S. V., Pasapera, A. M., Sabass, B. & Waterman, C. M. Force fluctuations within focal adhesions mediate ECM-rigidity sensing to guide directed cell migration. *Cell* **151,** 1513–1527 (2012).
8. Schoen, I., Pruitt, B. L. & Vogel, V. The Yin-Yang of rigidity sensing: how forces and mechanical properties regulate the cellular response to materials. *Annu. Rev. Mater. Res.* **43,** 589–618 (2013).
9. Geiger, B., Spatz, J. P. & Bershadsky, A. D. Environmental sensing through focal adhesions. *Nat. Rev. Mol. Cell Biol.* **10,** 21–33 (2009).
10. Hoffman, B. D., Grashoff, C. & Schwartz, M. A. Dynamic molecular processes mediate cellular mechanotransduction. *Nature* **475,** 316–323 (2011).
11. Elosegui-Artola, A. *et al.* Rigidity sensing and adaptation through regulation of integrin types. *Nat. Mater.* **13,** 631–637 (2014).
12. Grashoff, C. *et al.* Measuring mechanical tension across vinculin reveals regulation of focal adhesion dynamics. *Nature* **466,** 263–266 (2010).
13. Critchley, D. R. Biochemical and structural properties of the integrin-associated cytoskeletal protein talin. *Annu. Rev. Biophys.* **38,** 235–254 (2009).
14. Kanchanawong, P. *et al.* Nanoscale architecture of integrin-based cell adhesions. *Nature* **468,** 580–584 (2010).
15. del Rio, A. *et al.* Stretching single talin rod molecules activates vinculin binding. *Science* **323,** 638–641 (2009).
16. Liu, J. *et al.* Talin determines the nanoscale architecture of focal adhesions. *Proc. Natl Acad. Sci. USA* **112,** E4864–E4873 (2015).
17. Austen, K., Kluger, C., Freikamp, A., Chrostek-Grashoff, A. & Grashoff, C. Generation and analysis of biosensors to measure mechanical forces within cells. *Methods Mol. Biol.* **1066,** 169–184 (2013).
18. Cost, A. L., Ringer, P., Chrostek-Grashoff, A. & Grashoff, C. How to measure molecular forces in cells: a guide to evaluating genetically-encoded FRET-based tension sensors. *Cell. Mol. Bioeng.* **8,** 96–105 (2015).
19. Guo, J., Sachs, F. & Meng, F. Fluorescence-based force/tension sensors: a novel tool to visualize mechanical forces in structural proteins in live cells. *Antioxid. Redox. Signal.* **20,** 986–999 (2014).
20. Finer, J. T., Simmons, R. M. & Spudich, J. A. Single myosin molecule mechanics: piconewton forces and nanometre steps. *Nature* **368,** 113–119 (1994).
21. Wang, X. & Ha, T. Defining single molecular forces required to activate integrin and notch signaling. *Science* **340,** 991–994 (2013).
22. Blakely, B. L. *et al.* A DNA-based molecular probe for optically reporting cellular traction forces. *Nat. Methods* **11,** 1229–1232 (2014).
23. Duan, Y. & Kollman, P. A. Pathways to a protein folding intermediate observed in a 1-microsecond simulation in aqueous solution. *Science* **282,** 740–744 (1998).
24. Zoldak, G., Stigler, J., Pelz, B., Li, H. & Rief, M. Ultrafast folding kinetics and cooperativity of villin headpiece in single-molecule force spectroscopy. *Proc. Natl Acad. Sci. USA* **110,** 18156–18161 (2013).

25. Zhang, X. *et al.* Talin depletion reveals independence of initial cell spreading from integrin activation and traction. *Nat. Cell Biol.* **10,** 1062–1068 (2008).
26. Carisey, A. *et al.* Vinculin regulates the recruitment and release of core focal adhesion proteins in a force-dependent manner. *Curr. Biol.* **23,** 271–281 (2013).
27. Dumbauld, D. W. *et al.* How vinculin regulates force transmission. *Proc. Natl Acad. Sci. USA* **110,** 9788–9793 (2013).
28. Humphries, J. D. *et al.* Vinculin controls focal adhesion formation by direct interactions with talin and actin. *J. Cell Biol.* **179,** 1043–1057 (2007).
29. Hytonen, V. P. & Vogel, V. How force might activate talin's vinculin binding sites: SMD reveals a structural mechanism. *PLoS Comput. Biol.* **4,** e24 (2008).
30. Yao, M. *et al.* Mechanical activation of vinculin binding to talin locks talin in an unfolded conformation. *Sci. Rep.* **4,** 4610 (2014).
31. Ciobanasu, C., Faivre, B. & Le Clainche, C. Actomyosin-dependent formation of the mechanosensitive talin-vinculin complex reinforces actin anchoring. *Nat. Commun.* **5,** 3095 (2014).
32. Praekelt, U. *et al.* New isoform-specific monoclonal antibodies reveal different sub-cellular localisations for talin1 and talin2. *Eur. J. Cell Biol.* **91,** 180–191 (2012).
33. Borghi, N. *et al.* E-cadherin is under constitutive actomyosin-generated tension that is increased at cell–cell contacts upon externally applied stretch. *Proc. Natl Acad. Sci. USA* **109,** 12568–12573 (2012).
34. Krieg, M., Dunn, A. R. & Goodman, M. B. Mechanical control of the sense of touch by β-spectrin. *Nat. Cell Biol.* **16,** 224–233 (2014).
35. Paszek, M. J. *et al.* The cancer glycocalyx mechanically primes integrin-mediated growth and survival. *Nature* **511,** 319–325 (2014).
36. Cai, D. *et al.* Mechanical feedback through E-cadherin promotes direction sensing during collective cell migration. *Cell* **157,** 1146–1159 (2014).
37. Conway, D. E. *et al.* Fluid shear stress on endothelial cells modulates mechanical tension across VE-cadherin and PECAM-1. *Curr. Biol.* **23,** 1024–1030 (2013).
38. Moser, M., Legate, K. R., Zent, R. & Fassler, R. The tail of integrins, talin, and kindlins. *Science* **324,** 895–899 (2009).
39. Miller, K., Chinzei, K., Orssengo, G. & Bednarz, P. Mechanical properties of brain tissue *in-vivo*: experiment and computer simulation. *J. Biomech.* **33,** 1369–1376 (2000).
40. Anthis, N. J., Wegener, K. L., Critchley, D. R. & Campbell, I. D. Structural diversity in integrin/talin interactions. *Structure* **18,** 1654–1666 (2010).

METHODS

Antibodies and reagents. The following antibodies were used: anti-paxillin (clone 349; BD Transduction Laboratories, 610051; immunofluorescence (IF) 1:400), anti-talin-1 (C45F1; Cell Signaling, 4021; western blotting (WB) 1:1,000), anti-talin-1/2 (8d4; Sigma, T3287; WB 1:2,000), anti-talin-2 (68E7; Abcam, ab105458; WB 1:2,000), anti-vinculin (hVIN-1; Sigma, V9131; WB 1:4,000 and IF 1:200), anti-tubulin (DM1A; Sigma, T9026; WB 1:3,000), anti-FAK (Millipore, 06-543; WB 1:2,000 and IF 1:200), anti-pY397-FAK (Life Technologies, 44-624; WB 1:1,000), anti-kindlin2 (Millipore, MAB2617; IF 1:400), anti-GFP (Abcam, ab290; WB 1:2,000), anti-β_1 integrin (Chemicon, MAB1997; FACS 1:400 and IF 1:200), anti-β_1 integrin (9EG7; PharMingen, 550531; FACS 1:200 and IF 1:200), anti-mouse IgG–horseradish peroxidase (HRP) conjugate (Bio-Rad, 170-6516; WB 1:15,000), anti-rabbit IgG–HRP conjugate (Bio-Rad, 170-6515; WB 1:15,000), anti-mouse IgG–Alexa Fluor-405 (Life Technologies, A31553; IF 1:400), anti-mouse IgG–Alexa Fluor-647 (Life Technologies, A31571; IF 1:400), anti-rat IgG–Alexa Fluor-647 (Life Technologies, A21247; IF 1:400). The following reagents were used: Alexa Fluor-568 phalloidin (Life Technologies, A12380; IF 1:400), Alexa Fluor-647 phalloidin (Life Technologies, A22287; IF 1:400), poly-L-lysine (Sigma, P4707), puromycin (Sigma, P8833), Y-27632 (Sigma, Y0503), fibronectin (Calbiochem, 341631). Micro-patterned substrates (CYTOO) and Softview Easy Coat 0.2, 0.5, 1.0, 2.0, 4.0, 12 and 25 kPa soft substrate dishes (Matrigen Life Technologies) were used.

Generation of HP35-TS cDNA expression constructs. HP35-TS cDNA constructs were generated according to our published protocols[17]. In brief, restriction sites were added to YPet (amino acids (aa) 1–228) (5′Xho/3′BamHI) and mCherry (5′BamHI/3′NotI) cDNA by polymerase chain reaction (PCR) and PCR products were combined in a pBluescript SK(+) vector. The sequence encoding for the HP35 linker peptide (LSDEDFKAVFGMTRSAFANLPLWKQQNLKKEKGLF) was inserted between fluorophores using annealed oligonucleotides with 5′BglII/3′BamHI overhangs (forward primer: 5′-aat tca gat ctC TCT CCG ATG AGG ACT TCA AAG CTG TGT TTG GCA TGA CCA GGA GCG CAT TTG CCA ACC TTC CTC TGT GGA AAC AGC AAC ACC TGA AGA AGG AAA AGG GAC TGT TCg-3′; reverse primer: 5′-gat ccG AAC AGT CCC TTT TCC TTC TTC AGG TGT TGC TGT TTC CAC AGA GGA AGG TTG GCA AAT GCG CTC CTG GTC ATG CCA AAC ACA GCT TTG AAG TCC TCA TCG GAG AGa gat ctg-3′). The TS module containing the stable HP35st linker peptide (LSDEDFKAVFGMTRSAFANLPLWKQQALMKEKGLF) was created using the QuikChange II Site-Directed Mutagenesis kit (Agilent Technologies). For expression in cells, HP35(st)-TS cDNA was transferred into the pLPCX plasmid (Clontech) containing a modified multiple cloning site (pLPCXmod). To modify HP35(st)-TS for single-molecule calibration (smHP35-TS and smHP35st-TS), terminal cysteine residues to allow attachment of DNA oligonucleotides and a histidine-tag for protein purification were added by PCR; the cDNA was then transferred into pLPCXmod. The correct sequence of all constructs was confirmed by DNA sequencing (Eurofins Genomics).

Protein expression and purification. For protein expression, smHP35-TS or smHP35st-TS was transiently transfected into HEK293 cells by $CaPO_4$-precipitation as described before[17]. After 48 h, cells were detached, re-suspended in hypotonic lysis buffer, incubated for 20 min on ice and then homogenized with a Dounce homogenizer. Lysates were cleared by centrifugation and subjected to metal ion affinity chromatography (His-Trap, GE Healthcare), followed by ion-exchange chromatography (Sephadex, GE Healthcare). Purified samples were then concentrated to about 20 μM by membrane ultrafiltration (Vivaspin, GE Healthcare) and subjected to the protein–oligonucleotide binding reaction described below.

Assembling protein–DNA chimaeras. To attach DNA handles to smHP35-TS or smHP35st-TS, cysteine-based chemistry was used according to previously published protocols[41,42]. In brief, 34 base pair-long, lyophilized maleimide-modified single-stranded (ss) DNA oligonucleotides were dissolved in phosphate buffered saline (PBS, pH 6.7) and incubated overnight at 4 °C with the purified protein; the protein was kept in PBS supplemented with 0.2 mM Tris-2-carboxyethylphosphine (TCEP) to avoid oligomerization through disulphide bonds. By-products, namely unreacted oligonucleotides, unreacted protein and protein with only one attached DNA handle, were removed using metal ion affinity chromatography (His-Trap, GE Healthcare) in combination with size-exclusion chromatography (Superdex 200, GE Healthcare). Finally, double-stranded (ds) DNA (λ-DNA, NEB) handles, carrying a biotin modification or a digoxigenin modification at one end and a ss-overhang at the other, were hybridized to complementary ssDNA oligonucleotides at either end of the protein resulting in a contour length of 185 nm for each handle.

Optical tweezers set-up, sample preparation and measurement procedure. To calibrate the new HP35(st)-TS biosensors, we performed single-molecule force spectroscopy measurements using a custom-built, dual-trap optical tweezers set-up with back-focal plane detection as described previously[43]; for improved temporal resolution, quadrant photodiodes were used as position-sensitive devices (QP154-Q-HVSD, Pacific Silicon Sensor). Data on the beads' positions with respect to their trap centres as well as the distance between the two traps were sampled at 200 kHz and filtered at the Nyquist frequency. Each trap's signal was corrected for cross-talk; trap stiffnesses calculated from corrected power spectra were determined to be about 0.37 pN nm^{-1}; the error of the trap stiffness calibration is approximately 10%. To prepare the sample, streptavidin-coated 1 μm-sized silica beads (Bangs Laboratories) were incubated with protein–DNA chimaeras in PBS (pH 7.4). Next, functionalized anti-digoxigenin silica beads were added; glucose oxidase and catalase were used as an oxygen scavenger system (26 U ml^{-1} glucose oxidase, 1,700 U ml^{-1} catalase, and 0.6% (w/v) glucose)[41,42]. To obtain the dumbbell-like configuration schematically shown in Fig. 1b, one anti-digoxigenin and one streptavidin-functionalized bead were trapped, each in one of the two laser foci of the dual trap. By moving the laser beam of one steerable laser focus, both beads were brought in close proximity until a single tether was successfully formed. Subsequently, repeated stretch-and-relax cycles were performed at constant velocities of 10–500 nm s^{-1}. Each cycle yielded typical force–extension traces where protein unfolding and refolding could be observed. Keeping the traps at constant distance allowed us to record time traces of protein fluctuations at constant force bias; maximal forces of about 50 pN were reached. A step-by-step protocol describing the biosensor calibration can be found at Nature Protocol Exchange[44].

HP35-TS and HP35st-TS force–extension relation. To generate force–extension calibration curves (Fig. 1i, dashed lines), we converted our force–distance measurements and complete fits to the data into corresponding force–extension curves (Supplementary Note). The gain in extension caused by the dsDNA handles was subtracted using the parameters supplied by the extensible worm-like chain fit (eWLC-fit; see Supplementary Note) so that the remaining force–extension relation is characteristic for HP35(st)-TS and the thermal motion of the system. By averaging multiple smoothed force–extension traces of one single molecule, sub-nanometre resolution was obtained (Fig. 1d, squares).

Evaluating the mechanical stability of genetically encoded fluorophores. Fluorophore stability is critical to any FRET-based force sensor as unfolding of donor or acceptor fluorophore would prohibit quantitative measurements. We therefore set up experiments to specifically examine HP35-TS fluorophore stability under force. As expected, fluorophore unfolding occurred only if at least 35 pN were reached/exceeded during pulling measurements (pulling velocity: 500 nm s^{-1}; Fig. 1e). To examine fluorophore stability under constant force, we exposed HP35-TS to 24 pN for more than 5 min but also did not observe any fluorophore unfolding (Fig. 1f). We also note that the observed average contour length of 363 nm was actually less than the expected theoretical 370 nm for both handles (Supplementary Note) indicating that both fluorophores are properly folded in HP35-TS. Altogether, these experiments suggest that the employed fluorophores in HP35-TS are insensitive to the mechanical forces the biosensors are supposed to measure.

Generation of talin expression constructs. Talin-1 expression constructs are based on murine talin-1 cDNA (accession number: X56123). To generate C-terminal fusion constructs (Tln1Y, Tln1C and Tln1Con), restriction sites (5′EcoRI/3′NotI) along with 5′ Kozak-sequence (ACC ATG) were added and the 3′ stop codon was removed by PCR. In parallel, restriction sites (5′NotI/3′ClaI) and stop codon were added to YPet, mCherry or HP35-TS cDNA by PCR and these fragments were combined with talin cDNA using NotI/ClaI restriction sites. For transient or stable expression in cells, constructs were cloned into pLPCXmod. To insert individual fluorophores (Tln1Y-i, Tln1C-i) or tension sensors into talin-1, we generated a short linker encoding for 5′SalI/3′NotI restriction sites after the codon corresponding to aa 447 in murine talin-1 cDNA by overlap extension PCR; cDNAs of the individual fluorophores or the HP35-TS were inserted using 5′XhoI/3′NotI restriction sites. Point mutations (M319A, K324D) were introduced into talin-1 cDNA using the QuikChange II Site-Directed Mutagenesis kit (Agilent Technologies); deletion mutants (Tln1–2300 and Tln1–950) were generated by PCR amplification of the respective cDNA fragments. As we had access only to human talin-2 cDNA, we generated expression constructs based on human talin-1 (BC042923) and human talin-2 (NM015059) to allow a direct comparison of both isoforms. On the basis of aa homology, HP35-TS(st) was inserted into talin-2 after the codon corresponding to aa 450. In the chimaeric talin-1/2 constructs, the talin-1 head domain (aa 1–447) was fused to the talin-2 rod domain (aa 451–2,542); in the talin-2/1 construct, the talin-2 head domain (aa 1–450) was fused to the talin-1 rod domain (aa 448–2,541). To delete domains R1–R3, sequences corresponding to aa 482–911 for talin-1 and aa 485–914 for talin-2 were removed.

DOI: 10.1038/ncb3268

Generation of vinculin and RhoA cDNA expression constructs. To generate vinculin expression constructs, human full-length vinculin cDNA was isolated from an ImaGene cDNA library (BG284191) and 5′ApaI/3′XbaI restriction sites as well as a Kozak sequence were added by PCR; also the vinculin truncation mutant (encoding for aa 1–883) was amplified by PCR. A TagBFP-fluorophore was added C-terminally to each construct using 5′XhoI/3′NotI (vinculin truncation mutant) or 5′XbaI/3′NotI (full-length vinculin) restriction sites, and the final cDNAs were transferred into a pLPCXmod by 5′ApaI/3′NotI. The active RhoA expression construct was based on a previously described EGFP-tagged RhoQ63L cDNA (ref. 45). To allow fluorescence analysis in the presence of YPet-tagged talin-1 constructs, the N-terminal EGFP was exchanged for TagBFP using 5′HindIII/3′EcoRI restriction sites.

Generation of talin- and vinculin-deficient cell lines and stable protein re-expression. To generate cells in which both talin-1 and talin-2 are genetically inactivated, talin-2 knockout mice (*Tln2*$^{-/-}$; ref. 46) were intercrossed with mice in which the talin-1 gene is flanked with loxP sites (*Tln1*$^{f/f}$; ref. 47). Mice with the *Tln1*$^{f/f}$*Tln2*$^{-/-}$ genotype were used to isolate fibroblastoid cells from kidneys of a three-week-old mouse and cells were subsequently immortalized with the SV40 large T antigen. Talin-1 was abrogated by adenoviral transduction of Cre recombinase and clonal cell lines were isolated. To generate vinculin-deficient cells, SV40 large T immortalized fibroblasts, in which the vinculin gene is flanked with loxP sites (*Vin*$^{f/f}$), were transduced with Cre recombinase and clonal cell lines were isolated (*Vin*$^{-/-}$). Vinculin cDNA constructs were transiently transduced using Lipofectamine 2000 (Invitrogen) and talin double knockout cells (*Tln1*$^{-/-}$*Tln2*$^{-/-}$) were stably transduced by the phoenix cell transfection system as described earlier[17]. After infection, cells were puromycin-selected and stable protein expression was confirmed by western blotting using standard protocols. When necessary, cells were sorted by fluorescence-activated cell sorting (FACS) using a FACSAria cell sorter IIu (BD Biosciences) to isolate cells with comparable expression levels. Cell lines were freshly generated for this work and thus are not listed in the database of commonly misidentified cell lines maintained by ICLAC and NCBI Biosample; the cell lines have not been authenticated.

Cell culture conditions and immunostaining protocol. Cell lines were cultured in high-glucose DMEM-GlutaMAX medium (Life Technologies) supplemented with 10% fetal bovine serum (FBS, Life Technologies) and 1% penicillin/streptomycin (P/S, Life Technologies; growth medium). For live-cell imaging, DMEM without phenol red containing 4.5 mg ml^{-1} glucose, 25 mM HEPES, 2 mM glutamine (Life Technologies) was used and supplemented with 10% FBS and 1% P/S (imaging medium). For cell staining, cells were seeded on FN-coated (10 µg ml^{-1}) glass slides (Menzel, no. 1.5) and allowed to spread overnight, if not indicated otherwise. Cells were fixed in 4% paraformaldehyde (PFA) for 10 min at room temperature and immunostainings were performed as described before[17]. Samples were mounted in Prolong Gold (Life Technologies) and stored at 4 °C. Images were acquired using a LSM780 confocal scanning microscope equipped with a 100× oil objective (Plan-APOCHROMAT, NA = 1.46). For image acquisition of cells on soft substrates, a Leica TCS SP5 X confocal microscope equipped with a 40× long-distance water objective (APO 40×/1.10 W CORR C S2) was used.

Fluorescence-activated cell sorting (FACS). Integrin surface expression was determined by FACS using a BD FACS Canto II instrument (BD Biosciences). Cell stainings with anti-integrin antibodies were performed in 5% BSA solution containing 1 mM $MgCl_2$, 1 mM $CaCl_2$ and 0.02% NaN_3. To control for unspecific antibody labelling, cells lacking β_1, β_2, β_3 and β_7 integrin subunits were used[48]. Surface expression of integrins was quantified by geometric mean fluorescence intensity using FlowJo software (Tree Star).

Fluorescence recovery after photobleaching (FRAP) experiment and analysis. To allow FRAP analysis of cells with comparable FA sizes and states, cells were seeded on FN-coated micro-patterned substrates (CYTOO); under these conditions, cells adapt highly similar morphologies and develop very regular FAs of comparable size, shape and intensity. For each experiment, Tln1Y, Tln2Y and Tln1TS cells were seeded on Y-shaped micro-patterned substrates for at least 4 h and were analysed at 37 °C and 5% CO_2 on a Leica SP8 confocal laser scanning microscope equipped with a 63× water objective (HCX PL APO, NA = 1.2). Cells of comparable intensity were excited at 514 nm with a laser power of 5% to record two pre-bleach images within an interval of 10 s. Selected FAs were then photobleached using a laser power of 100% for 1 s and post-bleach images were acquired every 20 s for 260–280 s; the fluorescence intensity was recorded between 530–570 nm. Next, fluorescence intensity data were imported into ImageJ and analysed using the ImageJ plugin 'FRAP profiler'. Only data with comparable initial mean intensities and sufficient initial photobleaching were processed in MATLAB (Mathworks). To determine fluorescence recovery, we assumed a reaction-dominated model as described before[49,50] and fitted the data according to equation (1). Only data sets with a fitting quality of $R^2 = 0.98$ were considered for further analysis.

$$f(t) = A(1 - e^{-k_{off}^{t}}) \quad (1)$$

where t is time, k_{off} is the rate constant and A is the mobile fraction. The recovery half-time $\tau_{1/2}$ was calculated according to equation (2).

$$\tau_{1/2} = \frac{\ln(2)}{k_{off}} \quad (2)$$

Time-correlated single-photon counting fluorescence lifetime microscopy (TCSPC-FLIM). TCSPC-FLIM experiments were performed using a confocal microscope (Leica TCS SP5 X) equipped with a pulsed white light laser (WLL, 80 MHz repetition rate, NKT Photonics), a FLIM X16 TCSPC detector (LaVision Biotec) and a 63× water objective (HCX PL APO CS, NA = 1.2); a band-pass filter 545/30 (AHF Analysentechnik) was used to block photons emitted by the acceptor fluorophore. Images were acquired with a scanning velocity of 400 Hz, a spatial resolution of 512 × 512 pixels and resulting image field coverage of 123.02 × 123.02 µm^2. The detection covered a time window of 12.24 ns after the excitation pulse with a temporal resolution of 0.08 ns. For each experimental condition 15–20 cells were recorded and each experiment was repeated at least 3–5 times. Data analysis was conducted by a custom-written MATLAB program calculating the FRET efficiency E according to equation (3), where τ_D is the mean donor lifetime and τ_{DA} is the lifetime of the donor in the presence of an acceptor fluorophore. For more detailed information see our previously published protocols[17].

$$E = 1 - \frac{\tau_{DA}}{\tau_D} \quad (3)$$

Measurement of fluorophore emission spectra in FAs of living cells. To examine whether the photo-physical properties of the donor or acceptor fluorophore are affected by their insertion into talin, *Tln1*$^{-/-}$*Tln2*$^{-/-}$ cells were reconstituted with constructs in which the individual fluorophores had been inserted into talin-1 (Tln1Y-i, Tln1C-i) or were C-terminally attached (Tln1Y, Tln1C). Cells were seeded on FN-coated coverslips and the emission spectra of integrated or C-terminally tagged fluorophores from FAs of living cells were measured. The emission spectra of YPet (excitation: 508 nm; detection: 525–605 nm; 10 nm detection band width) and mCherry (excitation 587 nm; detection: 610–710 nm; 20 nm detection band width) were recorded using a confocal microscope equipped with an acousto-optical beamsplitter (Leica TCS SP5 X) and a pulsed white light laser (WLL, 80 MHz repetition rate, NKT Photonics). Only FA-specific signal was processed in the subsequent data analysis.

FRET control experiment I—effects of intermolecular FRET. To test for effects of intermolecular FRET (that is, energy transfer between adjacent molecules), *Tln1*$^{-/-}$*Tln2*$^{-/-}$ cells were co-transfected with constructs in which the individual fluorophores were inserted into talin-1 or C-terminally attached. These cells were then seeded on FN- or pL-coated glass slides and FRET efficiencies were determined using TCSPC-FLIM. We did not observe differences when pL and FN conditions were compared indicating that effects of intermolecular FRET in these experiments are negligible. However, a slight increase of intermolecular FRET in C-terminally tagged talin controls was detectable, presumably due to talin dimerization that is mediated at talin's C terminus (Fig. 2g); this may explain the slightly increased FRET efficiency values determined in Tln1Con cells as compared with Tln1TS cells on pL (for example, Fig. 2i).

FRET control experiment II—effects of talin's inter-domain association. To examine whether Tln1TS FRET is affected by the inter-domain association between the talin head and the talin rod domains[51], we inserted point mutations (K324D and M319A) into Tln1TS that were previously described to abolish the intramolecular interaction[51,52]. As talin is expected to predominantly exist in an auto-inhibited conformation in the cytoplasm[53], we reasoned that the high FRET efficiencies observed in cells on pL should be significantly reduced by these activating point mutations if FRET of the biosensor was sensitive to conformational changes. However, FRET efficiencies of Tln1TS-M319A, Tln1TS-K324D and Tln1TS were indistinguishable when cells were seeded on pL (Fig. 2h). This indicates that effects of the inter-domain association on Tln1TS FRET are negligible.

FRET control experiment III—evaluating effects of fluorescence intensity and temperature. To examine whether the observed FRET effects are fluorescence intensity dependent, FRET efficiencies were plotted over mean fluorescence intensities and the Pearson's correlation coefficient (PCC) was determined (Supplementary Fig. 2c); however, no correlation was observed. As HP35 unfolding shows a small but significant temperature dependency (see Supplementary Note and Supplementary Fig. 1i) we also tested how moderate changes in temperature affect FRET measurements. Thus, FRET ratio measurements of Tln1Con or Tln1TS cells

were performed at 30 °C (the temperature at which the single-molecule calibration was performed) and 37 °C (the temperature used during FRET ratio measurements; Supplementary Fig. 2d).

Isolating FA-specific signals for FLIM and ratiometric FRET analysis. To isolate the FA-specific signals from FLIM data sets, images were imported into MATLAB and regions of interest (ROIs) were manually set to exclude cytoplasmic background and signals from adjacent cells. A three-level multi-Otsu thresholding algorithm was applied and the highest intensities were defined as FA signal. After conversion into a binary image, these FA masks were used to calculate the mean FA FRET efficiency per cell. To isolate FA signals for morphological analysis and ratiometric FRET measurements, fluorescence images were imported to MATLAB followed by manual ROI selection to analyse individual cells. Cytosolic background was subtracted from the donor image by convolving the image (Gaussian structure element; width: 25, height: 2) and applying a top-hat filtering step (disk structure element; radius: 7 pixel) as described before[54]. Obtained individual FA masks were then used to calculate FA mean intensity of donor and acceptor signal. For mean acceptor values 1.7 times larger than manually determined average background signal, individual FA ratiometric FRET values were calculated by mean intensity acceptor/donor division. Step-by-step protocols describing the live-cell FLIM and FRET experiments can be found at Nature Protocol Exchange[44].

Morphological FA analysis and FA co-localization analysis. For cell size and polarization analysis, cells were allowed to spread on FN-coated glass coverslips or on FN-coated Softview Easy Coat dishes (Matrigen Life Technologies). At the indicated time points, cells were fixed and stained. Images of phalloidin-stained cells were then used to determine the cell area and the cell's major principal axis. Using Otsu thresholding as a cutoff criterion, binarized cellular shape masks were created and mask orientation was calculated to define the reference major principal axis. Subsequently, individual FA masks were analysed with respect to their eccentricity and area. The FA orientation with respect to cell major principal axis was used to evaluate cell polarization. To quantify subcellular co-localization of vinculin with talin, cells were fixed and immunostained for vinculin as described above. Intensity line plots across at least 25 FAs were defined in ImageJ and evaluated in MATLAB. To find the local maximum of individual FAs, a Gaussian fit was applied in the talin channel. Intensity values for both channels at the fitted maximum ±2 pixels were averaged to minimize local errors.

Traction force microscopy. Traction force microscopy was performed using an SP8 confocal laser scanning microscope equipped with a 63× glycerol objective (HC PL APO, NA = 1.3). Fluorescent beads of 0.2 µm diameter (FluoSpheres (625/645), Life Technologies) were incorporated into polyacrylamide gels with defined elastic properties that were produced according to established protocols[55]. Young's moduli of the substrates were calculated from acrylamide/bis-acrylamide concentrations as previously described[56] and obtained moduli were checked by measuring the indentation profile of a coloured bead that was placed on the gel surface as described in ref. 57; the analysis of traction force microscopy data was performed as described before[58].

Sources of noise and data interpretation. Live-cell FRET experiments are inherently noisy because the energy transfer rate between the donor and acceptor fluorophore does not depend only on the fluorophore separation distance but also on other factors[18,59] including temperature, pH or ion concentration. Furthermore, targeting a biosensor to a specific subcellular location can further complicate the experiment as effects through intermolecular FRET or molecular crowding may become more prominent. In addition, the biosensor expression level and the used cell type, in particular potentially high expression levels of the endogenous protein, need to be taken into account. Finally, chromatic aberrations, laser fluctuations, the Poisson statistics of photon arrival at the detector or other technical limitations contribute to the noise in FRET measurements. It is also important to note that in contrast to the single-molecule calibration experiments described in Fig. 1, the live-cell FRET experiments presented in Figs 2–4 and Figs 6 and 7 are based on bulk measurements, in which the signal from hundreds of FAs containing many molecules is averaged to calculate a mean FRET efficiency per cell. As a consequence, only an average force per molecule can be calculated.

Statistical analyses. Error bars represent the standard error of the mean (s.e.m.) if not indicated otherwise; to confirm that data are normally distributed, the Lilliefors test was used. Statistical significance is given by a P value calculated from a two-sample Kolmogorov–Smirnov test using the default significance level of $\alpha = 0.05$. Additional testing was performed with a two-sided t-test as indicated. The following nomenclature was used in all figures: ***, $P < 0.001$; **, $P < 0.01$; *, $P < 0.05$; not significant (NS), $P > 0.05$. Box plots were generated using the MATLAB function box plot() or the origin Lab software indicating the median as well as 25th and 75th percentiles; whiskers reach out to 2.7 standard deviations (σ). Statistic source data are available in Supplementary Table 1.

Computational codes. Mechanical fits were performed using previously published custom-written code[24,42]; analysis software code runs on: IGOR Pro 6.31, 64-bit. Software for FA FRAP and TCSPC-FLIM analyses was generated specifically for the project and can be used in MATLAB. The data analysis algorithm for ratiometric FRET analyses is based on a previously published Focal Adhesion Tracking algorithm[54]. All software is available on request.

41. Cecconi, C., Shank, E. A., Dahlquist, F. W., Marqusee, S. & Bustamante, C. Protein-DNA chimeras for single molecule mechanical folding studies with the optical tweezers. *Eur. Biophys. J.* **37,** 729–738 (2008).
42. Stigler, J., Ziegler, F., Gieseke, A., Gebhardt, J. C. & Rief, M. The complex folding network of single calmodulin molecules. *Science* **334,** 512–516 (2011).
43. von Hansen, Y., Mehlich, A., Pelz, B., Rief, M. & Netz, R. R. Auto- and cross-power spectral analysis of dual trap optical tweezer experiments using Bayesian inference. *Rev. Sci. Instrum.* **83,** 095116 (2012).
44. Mehlich, A., Austen, K., Ringer, P., Rief, M. & Grashoff, C. Evaluation of molecular tension sensors using single-molecule force spectroscopy and live cell FRET imaging. *Protoc. Exch.* http://dx.doi.org/10.1038/protex.2015.095 (2015).
45. Subauste, M. C. *et al.* Rho family proteins modulate rapid apoptosis induced by cytotoxic T lymphocytes and Fas. *J. Biol. Chem.* **275,** 9725–9733 (2000).
46. Conti, F. J., Monkley, S. J., Wood, M. R., Critchley, D. R. & Muller, U. Talin 1 and 2 are required for myoblast fusion, sarcomere assembly and the maintenance of myotendinous junctions. *Development* **136,** 3597–3606 (2009).
47. Monkley, S. J. *et al.* Disruption of the talin gene arrests mouse development at the gastrulation stage. *Dev. Dyn.* **219,** 560–574 (2000).
48. Schiller, H. B. *et al.* β_1- and αv-class integrins cooperate to regulate myosin II during rigidity sensing of fibronectin-based microenvironments. *Nat. Cell Biol.* **15,** 625–636 (2013).
49. Sprague, B. L. & McNally, J. G. FRAP analysis of binding: proper and fitting. *Trends Cell Biol.* **15,** 84–91 (2005).
50. Carisey, A., Stroud, M., Tsang, R. & Ballestrem, C. Fluorescence recovery after photobleaching. *Methods Mol. Biol.* **769,** 387–402 (2011).
51. Goult, B. T. *et al.* The structure of an interdomain complex that regulates talin activity. *J. Biol. Chem.* **284,** 15097–15106 (2009).
52. Goksoy, E. *et al.* Structural basis for the autoinhibition of talin in regulating integrin activation. *Mol. Cell* **31,** 124–133 (2008).
53. Goult, B. T. *et al.* Structural studies on full-length talin1 reveal a compact auto-inhibited dimer: implications for talin activation. *J. Struct. Biol.* **184,** 21–32 (2013).
54. Wurflinger, T., Gamper, I., Aach, T. & Sechi, A. S. Automated segmentation and tracking for large-scale analysis of focal adhesion dynamics. *J. Microsc.* **241,** 37–53 (2011).
55. Yeung, T. *et al.* Effects of substrate stiffness on cell morphology, cytoskeletal structure, and adhesion. *Cell Motil. Cytoskeleton* **60,** 24–34 (2005).
56. Boudou, T., Ohayon, J., Picart, C., Pettigrew, R. I. & Tracqui, P. Nonlinear elastic properties of polyacrylamide gels: implications for quantification of cellular forces. *Biorheology* **46,** 191–205 (2009).
57. Lembong, J., Sabass, B., Sun, B., Rogers, M. E. & Stone, H. A. Mechanics regulates ATP-stimulated collective calcium response in fibroblast cells. *J. R. Soc. Interface* **12,** 20150140 (2015).
58. Sabass, B., Gardel, M. L., Waterman, C. M. & Schwarz, U. S. High resolution traction force microscopy based on experimental and computational advances. *Biophys. J.* **94,** 207–220 (2008).
59. Jares-Erijman, E. A. & Jovin, T. M. FRET imaging. *Nat. Biotechnol.* **21,** 1387–1395 (2003).

Sensing the mechano-chemical properties of the extracellular matrix

Pia Ringer[a], **Georgina Colo**[b], **Reinhard Fässler**[b] **and Carsten Grashoff**[a]

a - Group of Molecular Mechanotransduction, *Max Planck Institute of Biochemistry, Martinsried D-82152, Germany*
b - Department of Molecular Medicine, *Max Planck Institute of Biochemistry, Martinsried D-82152, Germany*

Correspondence to Carsten Grashoff: *cgrasho@biochem.mpg.de*
http://dx.doi.org/10.1016/j.matbio.2017.03.004

Abstract

The ability of cells to adhere and sense their mechano-chemical environment is key to many developmental, postnatal homeostatic and pathological processes; however, the underlying molecular mechanisms are still poorly understood. Here, we summarize recent progress that indicates how cell adhesion, mechanotransduction and chemical signaling are coordinated in cells, and we discuss how the combination of novel experimental approaches with theoretical studies is currently utilized to unravel the molecular mechanisms governing mechano-chemical coupling during cell adhesion.

Introduction

Many biological processes depend on the ability of cells to sense and respond to the chemical as well as mechanical cues of the extracellular matrix (ECM). The differentiation of stem cells, for instance, is sensitive to matrix composition and rigidity [1,2]. Cell migration, which is important to a wide range of homeostatic processes, is modulated by ECM rigidity gradients in a process termed durotaxis [3]. The proliferation rates of many cell types are strongly influenced by the extent of their spread area which, in turn, depends on the chemical, mechanical and topographical properties of the extracellular environment [4]. The increased mechanical stress in fibrotic tissues is felt by resident cells that transdifferentiate into highly contractile myofibroblasts [5], and the mechanical properties of healing scars, for example in skin or heart muscle, determine tissue function after injury [6,7]. Moreover, increased ECM stiffness drives the progression of certain tumors such as breast cancer [8], and the inability of cells to properly sense their mechanical environment has been associated with a range of pathologies including muscular dystrophies or kidney malfunction [9,10].

The mechanisms by which cells detect and process mechanical information depend on the nature of the mechanical signal and the subcellular structures transmitting it. Mechanosensitive ion-channels, for instance, detect changes in plasma membrane tension [11,12], whereas cadherin-based adherens junctions transduce intercellular stresses [13]. By contrast, the chemical composition and mechanical properties of the ECM are sensed by integrin-associated, multi-molecular complexes called focal adhesions (FAs), and a conceptual understanding of FA function has been developed [14,15]. However, given the complex nature of the ECM [16], it appears increasingly important to consider the molecular complexity of FAs as well [17–22]. To aid this process, we here discuss the inner life of these enigmatic subcellular adhesion structures in more detail.

The architecture of focal adhesions

FAs display a complex, 3-dimensional organization with vertically and horizontally arranged substructures (Fig. 1). The vertical layers consist of an outer FA layer

Please cite this article as: P. Ringer, et al., Sensing the mechano-chemical properties of the extracellular matrix, Matrix Biol (2017), http://dx.doi.org/10.1016/j.matbio.2017.03.004

in which integrin receptors associate with the ECM, an intermediate layer where chemical and mechanical signals are processed, and an inner layer that is dominated by the actomyosin cytoskeleton (Fig. 1A). The horizontal layering facilitates the compartmentalization into distinct integrin subtype-dependent regions with different mechano-chemical characteristics (Fig. 1B, C). One fascinating challenge of today's cell adhesion research is to elucidate how the organization and dynamics of these individual FA layers are regulated.

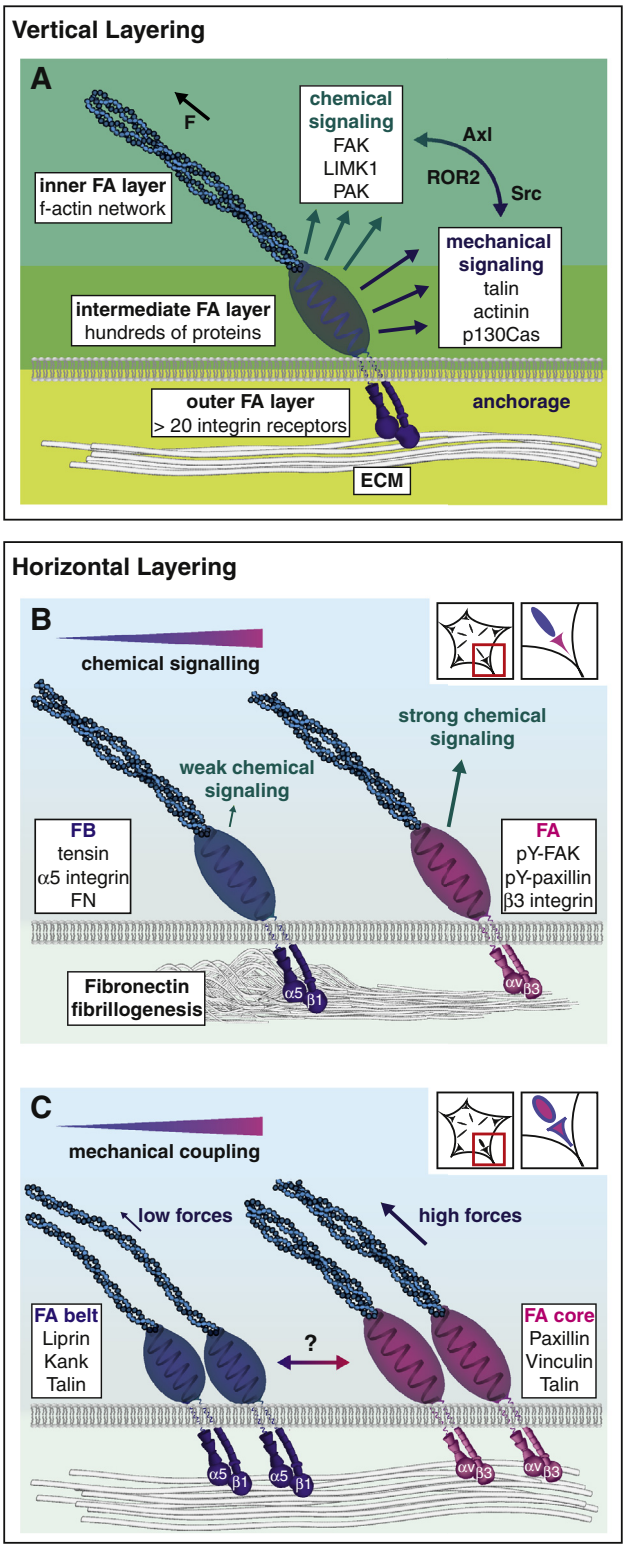

The outer FA layer – ECM-specific anchorage by integrin receptors

The outer FA layer contains the integrin receptors. Integrins are heterodimeric transmembrane proteins that physically connect cells to a wide range of ECM proteins including fibronectin (FN), vitronectin, collagens and laminins but also to other cell surface receptors like VCAM and ICAM [23]. Mammals can express 18 α- and 8 β-integrin subunits to form 24 functionally distinct receptors, and it is clear that many, if not all, integrin subtypes have specific, non-redundant properties [23–25]. As a result, the integrin expression signature determines how FAs assemble, chemical signals are processed and mechanical information is propagated. Cells adhering to collagen type I by integrin α2β1, for instance, induce a very different signaling response as compared to cells binding collagen type IV with

Fig. 1. A vertical (A) and a horizontal (B, C) layering characterize the architecture of FAs. (A) Vertical layering. The outer FA layer, in which integrin receptors bind to extracellular ligands, provides anchorage to the ECM; depending on the expressed integrin receptor subtypes, distinct mechano-chemical signaling networks are activated. The intermediate FA layer comprises hundreds of proteins that respond to mechanical stimuli (e.g. talin, actinin or p130Cas) or mediate chemical signaling (e.g. FAK, LIMK1 or PAK). The crosstalk between FA's mechanical and chemical signaling is, at least to some extent, mediated by tyrosine kinase such as ROR2, Axl and Src. The inner FA layer merges into the actomyosin network, but also acts as a mechanosensitive module during cell adhesion. (B). Horizontal layering – fibrillar adhesions (FBs). The formation of FBs occurs on pliable FN-rich matrices and coincides with FN fibrillogenesis. While αvβ3 integrin receptors and tyrosine-phosphorylated (pY) proteins reside in the FA core, FBs are enriched in α5β1 integrin and tensin. Since FBs display very low levels of tyrosine-phosphorylated proteins as compared to FAs, their chemical signaling is likely to be different. (C). Horizontal layering – the FA belt. This type of horizontal layering is characterized by an accumulation of Kank family of proteins around mature FAs. As Kank proteins blunt integrin force transduction by partially uncoupling talin from f-actin, integrin receptors in the FA belt connect less efficiently to the actomyosin cytoskeleton. In addition, Kank associates with Liprins leading to the formation of cortical microtubule stabilization complexes (not illustrated) that regulate FA turnover. Why Kank proteins are excluded from the FA core remains to be investigated.

Please cite this article as: P. Ringer, et al., Sensing the mechano-chemical properties of the extracellular matrix, Matrix Biol (2017), http://dx.doi.org/10.1016/j.matbio.2017.03.004

α1β1 integrin [26,27]. Even similar integrins like the FN-receptors α5β1 and αvβ3 induce adhesion structures with different molecular composition and signaling characteristics [28]. In addition, most cells express various integrin receptor subtypes that may synergize, for example to amplify myosin-dependent signal transduction cascades [28].

Integrin-receptor specificity becomes even more apparent when applying mechanical loads to distinct ECM–receptor linkages. While collagen-bound α2β1 integrins appear to withstand mechanical forces of more than 100 piconewton (pN) [29], FN–α5β1 bonds are likely to break at around 30–50 pN [30], whereas αvβ3 integrins are thought to rupture at even lower forces [31,32]. Interestingly, α5β1 integrin receptors display a so-called 'catch-slip bond' behavior characterized by a transient increase in the FN-bond lifetime between 10–30 pN (Fig. 2C). How many integrin receptors display this rather unusual behavior (i.e. tighter ECM–integrin binding under force) remains to be investigated, but it appears that such catch bond properties are specific to distinct ECM–integrin interactions. Experiments on the fibrinogen–αIIβ3 linkage, for instance, revealed reduced bond lifetimes when pulling forces were increased from 5–50 pN, which is characteristic for a classical slip bond linkage [33].

Together, the available data suggest that the integrin receptor subtypes present in the outer FA layer critically determine how chemical signals and mechanical forces are processed during cell adhesion. Even though morphologically similar, FAs of different cell types may be functionally very dissimilar depending on the set of expressed integrin receptors.

The intermediate FA layer – coupling mechanical and chemical signaling

Integrins, with the exception of the hemidesmosomal β4 integrin [34], are characterized by short

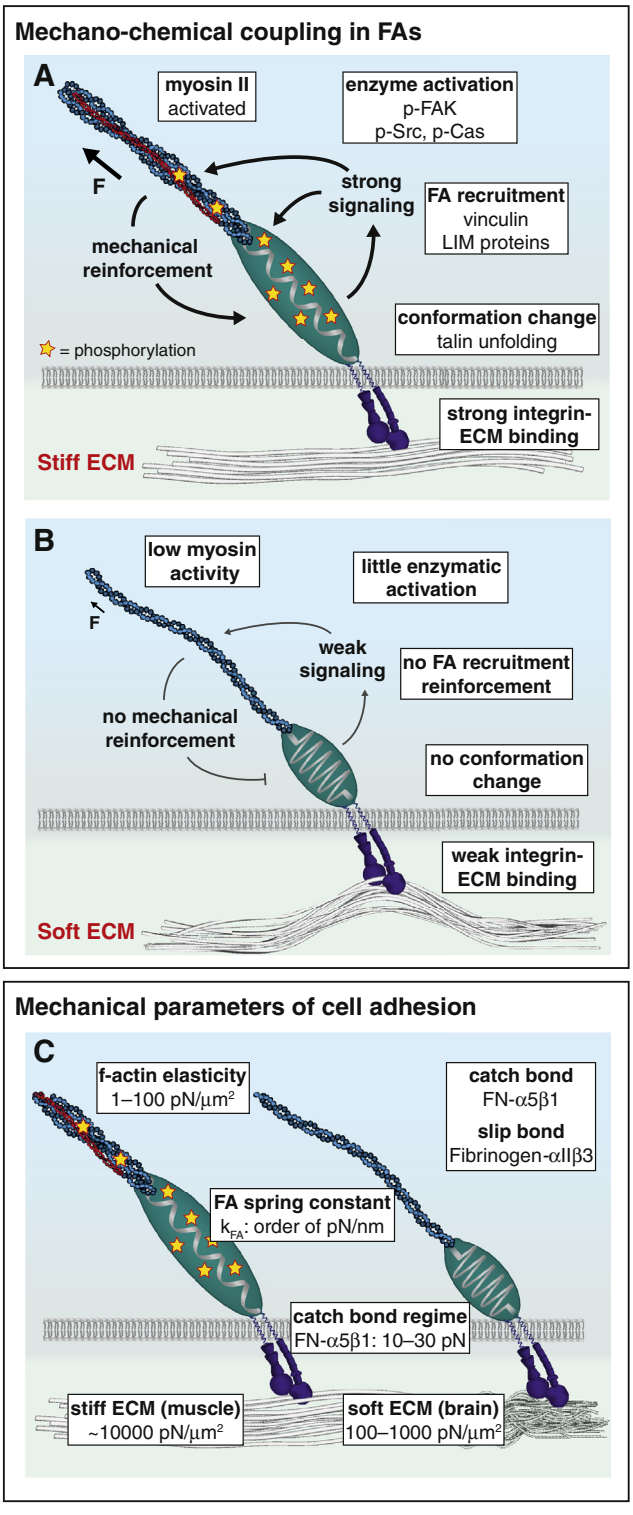

Fig. 2. FAs couple chemical and mechanical signaling. (A) Stiff ECM. Cells adhering to rigid matrices enforce their FAs under load through mechano-chemical feedback mechanisms. For instance, high mechanical tension across integrin receptors leads to partial talin unfolding and subsequent vinculin recruitment; also LIM domain proteins are recruited to FAs in response to mechanical tension but the underlying mechanisms are still unclear [17]. Mechanical force may also activate FA-resident kinases that amplify chemical signaling in FAs through protein phosphorylation [49]. Modulation of RhoGTPase signaling pathways leads to increased actomyosin contractility and stress fiber formation. (B) FAs in cells on soft matrices may not experience high enough stresses to activate force-sensitive proteins that, as a result, remain insensitive to chemical signals. (C). Typical mechanical parameters of cell-matrix adhesions. The elastic modules of the extracellular matrix typically ranges from hundreds–thousands of pN/μm ; the actomyosin network is comparably soft [120]. Typically, FA spring constants are modelled in the order of tens of pN/nm [121]. Force of 10–30 pN increase the lifetime of the α5β1–FN linkage [30], whereas the fibrinogen–αvβ3 bond displays slip bond characteristics [33].

Please cite this article as: P. Ringer, et al., Sensing the mechano-chemical properties of the extracellular matrix, Matrix Biol (2017), http://dx.doi.org/10.1016/j.matbio.2017.03.004

cytoplasmic tails of 13–70 amino acids that have neither enzymatic activity nor binding sites to directly associate with the actomyosin cytoskeleton [35]. Instead, intracellular proteins assemble at the cytoplasmic tails leading to integrin clustering and the formation of the second FA layer, where most of the chemical and mechanical signals are integrated.

Crucial for the formation of the intermediate FA layer are the integrin regulators talin and kindlin both of which are required for inducing and then maintaining the active, ligand-binding competent state of integrins [36]. Talin comprises three f-actin and eleven vinculin-binding sites and mediates one of the first mechanical connections to the actomyosin network [37]. Interestingly, a similar f-actin binding function of kindlin-2 has been recently proposed [38], but it remains to be tested whether kindlin can bear mechanical forces during cell adhesion. Other important integrin interactors are the f-actin binding proteins filamin, α-actinin and tensin, the adaptor protein paxillin and focal adhesion kinase (FAK) [39], but also integrin inactivators like ICAP1 [40] or the recently described pan-integrin inactivator SHARPIN [24,41]. These integrin-binding proteins engage further cytoplasmic molecules such as the ternary ILK-PINCH-Parvin (IPP) complex, actin-binding proteins like vinculin [42], as well as protein kinases, phosphatases, and other protein modifying enzymes to form the adhesome comprising hundreds of distinct proteins [17,18]. How these individual FA components associate in space and time to transduce mechanical and chemical information in the dynamic context of a living cell has remained poorly understood.

Yet, it is believed that chemical and mechanical signals synergize to enforce distinct signal transduction pathways (Fig. 2). Tension across the integrin activator talin, for example, leads to the exposure of cryptic vinculin binding sites and enhanced recruitment of vinculin [43,44] that then becomes phosphorylated [45,46]. Likewise, mechanical tension across the adaptor protein p130Cas promotes phosphorylation of specific tyrosine residues by Src family kinases [47]. Since many proteins are recruited to FAs in a force-dependent manner – numerous LIM-domain containing proteins localize to FAs only when cell adhesion forces are high [17,18,48] – it is likely that other proteins are regulated in a similar fashion. Furthermore, the catalytic activities of certain FA components are thought to be modulated by a mechanical allosterism; the enzymatic activity of Src, for instance, rapidly increases upon mechanical stimulation [49]. As other tyrosine kinases like Axl and ROR2 are critical for FA-mediated ECM rigidity sensing [50,51], it is clear that this class of enzymes plays a key role in FAs' mechano-chemical regulation. In addition, many growth factors induce pathways that modulate FA-resident tyrosine kinases such as FAK [52]; therefore, these enzymes are also key to the integration of FA- and growth factor-dependent signaling cascades during cell adhesion.

The inner FA layer – force generation and mechanosensing

The actomyosin network dominates the inner FA layer that does not only generate mechanical forces but also senses mechanical and chemical stimuli. For instance, the stability of the actin–myosin bond is sensitive to applied mechanical loads [53,54], and the probability of f-actin to be severed by cofilin decreases when the filaments experiences mechanical tension [55]. In addition, growth factor receptor pathways modulate the actin cytoskeleton through controlling Rho-like GTPases [56] as well as non-muscle myosin II activity [57], and certain GTPase-activating proteins seem to bind f-actin directly [58]. Thus, the actomyosin network acts as a mechanosensitive force generator in FAs [59].

The function of this innermost FA layer is dominated by the inherently dynamic nature of the actomyosin network, which is regulated in a spatially and temporally highly sensitive fashion [60]. While FAs in the lamellipodium of cells are exposed to a fast Arp2/3-dependent retrograde flow of actin filaments, more centrally located adhesions connect to stress fibers that can be classified, according to their morphology and myosin content, into distinct elements such as dorsal and ventral stress fibers, transverse arcs and the perinuclear cap [61]. Moreover, cells can express different actin- and myosin-isoforms as well as a myriad of f-actin associated proteins, all of which affect actomyosin assembly and activity to very different extents [61–63]. Therefore, the organization and functional role of the inner FA layer is cell-type dependent and sensitive to the FA's subcellular location.

The horizontal layering of FAs

In addition to the vertical layering, FAs frequently undergo a horizontal segmentation (Fig. 1B). The FN-binding integrin receptors α5β1 and αvβ3, for instance, segregate into distinct FA-substructures when adhering to pliable FN-rich surfaces. Under these conditions, α5β1 integrins translocate from FAs into elongated fibrillar adhesions (FBs), while αvβ3 integrin remains associated with the FA core [64,65]. In addition to the assembly of FN and the associated α5β1 integrin receptor, FBs accumulate the actin-crosslinking protein tensin, which binds to the same NPxY motif in β-integrins like talin. Since NPxY phosphorylation impairs talin binding but does not affect the tensin–integrin interaction, this modification may act as a molecular switch that regulates the horizontal compartmentalization of αvβ3–talin

Please cite this article as: P. Ringer, et al., Sensing the mechano-chemical properties of the extracellular matrix, Matrix Biol (2017), http://dx.doi.org/10.1016/j.matbio.2017.03.004

and α5β1–tensin enriched adhesion domains [66]. Both compartments are likely to have very different biochemical properties, as FBs are devoid of tyrosine-phosphorylated proteins such as pY397-FAK indicating rather weak or at least very different signaling activity [50]. In addition, FAs and FBs have different mechanical characteristics. Matured FBs are rather insensitive to myosin inhibition, whereas FA maintenance as well as FB formation strictly depend on actomyosin contractility [65]. Interestingly, the composition of FBs depends on whether cells are cultured in 2D or 3D environments [67], and it has been recognized that distinct cell types express different tensin isoforms (tensin-1, -2 and -3) displaying various degrees of FB enrichment [68]. Thus, FB formation and the physiological role of the FB–type of horizontal layering remains somewhat enigmatic and needs further investigation.

Another form of horizontal layering has been identified in a morphologically distinct structure, called the FA belt (Fig. 1C), which is characterized by the evolutionary conserved Kank proteins. Kank assembles in the immediate vicinity of FAs through talin-binding thereby promoting the active conformation of talin and thus integrin activation [69,70]. In parallel, Kank impairs talin's ability to associate with f-actin and to transduce mechanical forces. As a result, adhesions surrounded by a FA-belt display reduced force transmission leading to FA sliding and slower cell migration [69]. Intriguingly, Kank proteins also associate with cortical microtubule stabilization complexes (CMSC) through liprins that recruit microtubule plus-end tracking proteins like CLASPs [71]. Since microtubule targeting coincides with FAs turnover [72,73], this Kank-dependent type of horizontal layering is likely to play an important role in regulating FA stability through microtubule plus-end capture. Why Kank proteins bind to talin exclusively at the β1-rich FA border and not in the FA core is unclear.

As the glycocalxy of cells facilitates the lateral organization of integrin receptors during cell adhesion [74,75], it will be interesting to test whether the different types of horizontal layering within FAs are also glycocalyx-dependent.

Towards a conceptual understanding of FA function

Our current understanding of FA function is strongly influenced by the observation that cell adhesions can strengthen under mechanical loads [76,77]. Indeed, many cell types form large FAs on rigid substrates when cellular traction forces are high, while they display small FAs on soft matrices [77,78]. Similarly, inhibition of myosin activity usually reduces FA size, whereas the induction of intracellular contractility (e.g. by activating RhoA) stimulates FA growth. Consistent with these experiments, certain integrin receptors enforce their binding to extracellular ligands in response to mechanical tension [30,79], and force-induced unfolding of molecules such as talin can increase the recruitment of other FA proteins like vinculin [43]. Together, these experiments have led to the concept that FAs act very much like elastic springs that enlarge and become enforced when mechanical tension increases, but remain small and short-lived when forces are low. In this model, the spring constant assigned to a FA determines the adhesion growth rate under force, which occurs only when the ECM is sufficiently rigid (Fig. 2); on substrates that are significantly softer than the FA spring, adhesions do not enlarge because the ECM deforms and the spring does not stretch [80,81].

While this model correctly describes a large body of experimentation and provides an excellent framework for further theoretical approaches [81–83], some data indicate that the molecular regulation of FAs is far more complex. First and most importantly, FAs do not always grow under force. In fact, the opposite – FA disassembly under mechanical load – frequently occurs during cell migration and is necessary for cells to move forward [84]. Second, small and short-lived FAs termed 'nascent adhesions' (NAs) at the lamellipodium of cells generate comparably high traction forces [85], while large, centrally-located FAs often exert only low stresses [69,86]. Third, the cellular response to distinct matrix rigidities is integrin receptor subtype-dependent [28] and can be extracellularly (e.g. by addition of hyaluronic acid) [87] or intracellularly (by affecting protein tyrosine kinase signaling) modulated [50]. Finally, FAs display a heterogeneous substructure [88,89] and traction forces are often unevenly distributed below individual adhesion sites [21,86]. Thus, further experimentation and theoretical modelling is needed to comprehend FA function in cells.

Experimental approaches to investigate FA function

A number of recently developed technologies including mass-spectrometry methods and high-resolution microscopy techniques have revolutionized cell adhesion research. FAs' molecular composition is analyzed with a depth and the individual components become visualized with a resolution that is mind-blowing and was considered unrealistic just a few years ago. In addition, a set of genetically modified cell lines to investigate molecular mechanisms has become available and Crispr-Cas9 approaches will likely complement this toolbox. In the following, we will discuss how some of

Please cite this article as: P. Ringer, et al., Sensing the mechano-chemical properties of the extracellular matrix, Matrix Biol (2017), http://dx.doi.org/10.1016/j.matbio.2017.03.004

these techniques may be utilized to evaluate the composition and function of the distinct FA layers.

Probing the outer FA layer – how do distinct integrins propagate mechanical forces?

One of the open questions regarding the outer FA layer is how different integrin receptor subtypes govern FA function. The establishment of integrin-deficient cell lines, in which distinct receptor subtypes can be re-expressed and individually investigated, have been useful to study different FN-binding integrin receptors such as α5β1 and αvβ3 [28]. An exciting alternative is the use of engineered surfaces to which only distinct FN-binding integrin receptor subtypes can bind [90,91]; yet it seems important to extend these systems so that also other integrin receptors subtypes can be studied [92].

Similarly, it will be important to elucidate how distinct ECM–integrin interactions respond to applied mechanical forces, for example by atomic force microscopy (AFM) methods that revealed catch-bond behavior in FN–$\alpha_5\beta_1$ integrin linkages [30,79]. Unfortunately, a comparison with other integrin receptor types has been difficult because different experimental setups or loading rates – the speed at which mechanical forces are applied – were used [30,31,93]. It should be also noted that ECM–integrin linkages might be sensitive to the history of force application such as the FN–α5β1 bond, which is strengthened by repeated applications of mechanical forces [79]. Whether such a force-strengthening mechanism is a general feature of ECM–integrin linkages or specific to the FN–α5β1 integrin bond will be important to determine. Direct evidence that the observed mechanical responses occur in the crowded environment of a living cell may be obtained by methods allowing force measurements across individual integrin-ligand bonds during cell adhesion [94–96].

Finally, super-resolution experiments have become indispensable to study the nanostructure of FAs (Fig. 3) and the molecular dynamics of distinct integrin receptors in living cells. Single-protein tracking photo-activated localization microscopy was used to investigate the movement of individual integrin receptors molecules within and outside of FAs [97]. These experiments revealed a rather static behavior for β3 integrin receptors, while β1 integrins appeared more mobile during cell adhesion. Extending such experiments to other integrin subunits should provide valuable insights into the integrin-subtype specific properties of FAs.

Investigating the intermediate FA layer – how are mechano-chemical signals transduced?

The development of efficient mass spectrometry protocols has dramatically improved our understanding of the intermediate FA layer. Hundreds of proteins, many of which with yet unknown function, have been identified to associate with FAs [17–19], and the development of high-throughput proteomics platforms should further facilitate testing how chemical signals are transduced within FAs in a force-dependent fashion [98]. An exciting perspective is that the integration of various such data sets should provide important indications on the relevance and patho-physiological function of newly identified FA-associated molecules [99,100]. However, establishing consistent protocols that permit meta-analyses will be key to those bioinformatics approaches.

In parallel, various microscopy methods are currently being utilized to study FA structure and 3D organization with nanoscale resolution [20,22,101]. Molecular mechanics can be analyzed by FRET-based tension sensors [44,102–104] that

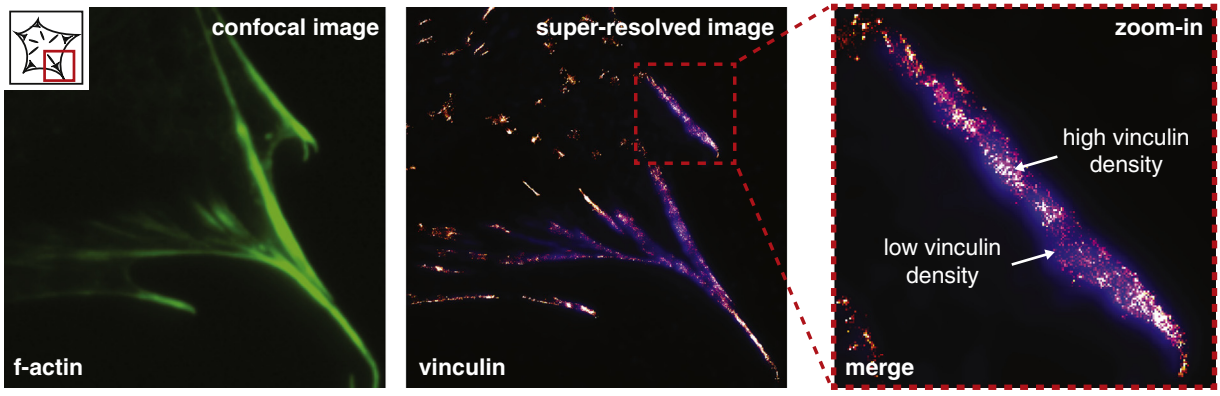

Fig. 3. FA nano-scale organization. Super-resolution microscopy reveals that proteins display an uneven distribution in FAs. The mechanisms governing this complex spatio-temporal organization are still unclear. Here, we show a fibroblast adhering to a FN-coated glass coverslip stained for f-actin; visualization of an expressed vinculin construct by stochastic optical reconstruction microscopy reveals areas of high and low protein density.

Please cite this article as: P. Ringer, et al., Sensing the mechano-chemical properties of the extracellular matrix, Matrix Biol (2017), http://dx.doi.org/10.1016/j.matbio.2017.03.004

provided first insights into vinculin- and talin-dependent processes of FA force transduction [44,105,106]. Together, these microscopy approaches revealed that FAs assemble in a much more dynamic and heterogeneous fashion than previously appreciated, and understanding how the observed FA substructures are spatio-temporally organized will be crucial. This is likely to require the further development of existing imaging techniques, for example to resolve intracellular force transduction processes with single-molecule resolution in cells.

Analyzing FAs' inner layer – quantifying acto-myosin forces in cells

The use of optical or magnetic tweezer techniques has been especially useful to study the mechanics of individual actin fibers and the actin-myosin linkage in vitro [53–55]. As distinct actin modulators and myosin isoforms regulate actomyosin function locally in cells [63,107], it will become increasingly important to complement these studies with live cell experiments. Potentially useful methods include correlational fluorescence speckle microscopy to determine acto-myosin kinetics in cells [108,109] and stochastic optical reconstruction microscopy as well as cryo-electron tomography to visualize and study distinct actin networks in situ [110,111]. Visualizing the mechanics of actomyosin networks in living cells, however, has remained challenging. A FRET-based actin tension sensor was described [112], but its rather diffuse intracellular localization may complicate the extraction of mechanical parameters with sufficient spatio-temporal resolution.

Theoretical approaches to study FA function

Many attempts to describe FA behavior theoretically are essentially captured by the original idea of Mitchison and Kirschner [113], which describe FAs as mechanical clutches that engage with the actin retrograde flow in an ECM stiffness-dependent fashion.

A stochastic simulation that considered ECM stiffness, load-and-fail-behavior of FA clutches and a force-velocity relationship of the actomyosin cytoskeleton predicted that cells tune their sensitivity towards distinct ECM rigidities by two distinguishable mechanisms. For stiff substrates, the model predicted a 'frictional slippage' state in which individual FA springs quickly increase tension and then break before other clutches can be mechanically engaged leading to high retrograde flow rates with low traction forces. On soft substrates, the model assumed a 'load-and-fail' regime where FA springs disengage less frequently resulting in slower retrograde flow velocity, maximal traction forces but frequent failure of all clutches leading to traction force fluctuations [83]. Interestingly, these predictions are consistent with the behavior of neural growth cones, and force fluctuations have been observed in migrating fibroblasts [114]. However, many cell types are known to react differently to distinct ECM rigidities. Neurons, for instance, are easily cultured on soft substrates whereas astrocytes do not spread on compliant surfaces and likely exert very little traction forces under these conditions [115]. Furthermore, distinct cell lines display maximal migration speeds on substrates with different rigidities [116]. Thus, an updated version of the stochastic simulation suggested a second frictional slippage regime on soft substrates where FA clutches failed spontaneously before mechanical loads could build up [116]. This model made the intuitive prediction that cells adjust to different extracellular compliances by modulating the 'clutch' (outer and intermediate FA layer) and 'motor' parameters (inner FA layer).

An independent study predicted and experimentally observed myoepithelial cells adapting to distinct matrix rigidities by regulating their integrin expression profile and thus modulating integrin-ECM binding/unbinding rates [117]. Another model included tension-dependent reinforcement of the FA clutch (through vinculin recruitment to partially unfolded talin molecules) and successfully predicted the frequently observed behavior of cells to increase traction forces monotonically when ECM stiffness is elevated [118]. In the future, it will be fascinating to test how well these models predict the behavior of other FA subtypes. The recent identification of the Kank family of proteins, which bind and activate talin but reduce force transduction in centrally located FAs, suggests are more complex scenario in mature adhesion structures [69]. Then again, the description of NAs, in which talin binds RIAM rather than vinculin [119], may require a different set of parameters.

Outlook

Given the highly complex nature of cell-ECM adhesions that are dependent on the mechano-chemical nature of the extracellular substrate, the integrin expression profile and the composition of the intracellular FA layers, it seems unlikely that, for the time being, one unifying theoretical model will describe the versatile behavior of FAs. Instead, the fascinatingly complex biology of FAs will likely require a set of theoretical descriptions, which consider the molecular complexity of the horizontal and vertical FA layers in more detail. The development of new technologies and their application to physiologically relevant studies should allow the identification of those parameters worth implementing.

Please cite this article as: P. Ringer, et al., Sensing the mechano-chemical properties of the extracellular matrix, Matrix Biol (2017), http://dx.doi.org/10.1016/j.matbio.2017.03.004

Acknowledgement

R.F. is funded by the European Research Council (Grant Agreement no. 322652) and the Max Planck Society. C.G. is supported by the Max Planck Foundation. R.F. and C.G. acknowledge support by the German Research Council through the Research Consortium SFB 863 (Projects B03 and B09).

Received 21 January 2017;
Received in revised form 29 March 2017;
Accepted 30 March 2017
Available online xxxx

Keywords:
Extracellular matrix;
Focal adhesion;
Integrin;
Mechanotransduction

Abbreviations used:
AFM, atomic force microscopy; CMSC, cortical microtubule stabilization complex; ECM, extracellular matrix; FA, focal adhesion; FB, fibrillar adhesion; FN, fibronectin; FRET, Förster resonance energy transfer; NA, nascent adhesions.

References

[1] A.J. Engler, S. Sen, H.L. Sweeney, D.E. Discher, Matrix elasticity directs stem cell lineage specification, Cell 126 (4) (2006) 677-89.
[2] Y. Hayashi, M.K. Furue, T. Okamoto, K. Ohnuma, Y. Myoishi, Y. Fukuhara, T. Abe, J.D. Sato, R. Hata, M. Asashima, Integrins regulate mouse embryonic stem cell self-renewal, Stem Cells 25 (12) (2007) 3005-15.
[3] C.M. Lo, H.B. Wang, M. Dembo, Y.L. Wang, Cell movement is guided by the rigidity of the substrate, Biophys. J. 79 (1) (2000) 144–152.
[4] C.S. Chen, M. Mrksich, S. Huang, G.M. Whitesides, D.E. Ingber, Geometric control of cell life and death, Science 276 (5317) (1997) 1425–1428.
[5] R.G. Wells, Tissue mechanics and fibrosis, Biochim. Biophys. Acta 1832 (7) (2013) 884-90.
[6] J.W. Holmes, T.K. Borg, J.W. Covell, Structure and mechanics of healing myocardial infarcts, Annu. Rev. Biomed. Eng. 7 (2005) 223-53.
[7] D.T. Corr, D.A. Hart, Biomechanics of scar tissue and uninjured skin, Adv. Wound Care (New Rochelle) 2 (2) (2013) 37–43.
[8] M.J. Paszek, N. Zahir, K.R. Johnson, J.N. Lakins, G.I. Rozenberg, A. Gefen, C.A. Reinhart-King, S.S. Margulies, M. Dembo, D. Boettiger, D.A. Hammer, V.M. Weaver, Tensional homeostasis and the malignant phenotype, Cancer Cell 8 (3) (2005) 241-54.
[9] D.E. Jaalouk, J. Lammerding, Mechanotransduction gone awry, Nat. Rev. Mol. Cell Biol. 10 (1) (2009) 63–73.
[10] D.E. Ingber, Mechanobiology and diseases of mechanotransduction, Ann. Med. 35 (8) (2003) 564-77.
[11] J. Arnadottir, M. Chalfie, Eukaryotic mechanosensitive channels, Annu. Rev. Biophys. 39 (2010) 111-37.
[12] A. Anishkin, S.H. Loukin, J. Teng, C. Kung, Feeling the hidden mechanical forces in lipid bilayer is an original sense, Proc. Natl. Acad. Sci. U. S. A. 111 (22) (2014) 7898-905.
[13] D.E. Leckband, J. de Rooij, Cadherin adhesion and mechanotransduction, Annu. Rev. Cell Dev. Biol. 30 (2014) 291–315.
[14] L.B. Case, C.M. Waterman, Integration of actin dynamics and cell adhesion by a three-dimensional, mechanosensitive molecular clutch, Nat. Cell Biol. 17 (8) (2015) 955-63.
[15] B. Geiger, J.P. Spatz, A.D. Bershadsky, Environmental sensing through focal adhesions, Nat. Rev. Mol. Cell Biol. 10 (1) (2009) 21–33.
[16] R.O. Hynes, The extracellular matrix: not just pretty fibrils, Science 326 (5957) (2009) 1216–1219.
[17] H.B. Schiller, C.C. Friedel, C. Boulegue, R. Fassler, Quantitative proteomics of the integrin adhesome show a myosin II-dependent recruitment of LIM domain proteins, EMBO Rep. 12 (3) (2011) 259-66.
[18] J.C. Kuo, X. Han, C.T. Hsiao, J.R. Yates 3rd, C.M. Waterman, Analysis of the myosin-II-responsive focal adhesion proteome reveals a role for beta-Pix in negative regulation of focal adhesion maturation, Nat. Cell Biol. 13 (4) (2011) 383-93.
[19] J. Robertson, G. Jacquemet, A. Byron, M.C. Jones, S. Warwood, J.N. Selley, D. Knight, J.D. Humphries, M.J. Humphries, Defining the phospho-adhesome through the phosphoproteomic analysis of integrin signalling, Nat. Commun. 6 (2015) 6265.
[20] P. Kanchanawong, G. Shtengel, A.M. Pasapera, E.B. Ramko, M.W. Davidson, H.F. Hess, C.M. Waterman, Nanoscale architecture of integrin-based cell adhesions, Nature 468 (7323) (2010) 580-4.
[21] S.V. Plotnikov, B. Sabass, U.S. Schwarz, C.M. Waterman, High-resolution traction force microscopy, Methods Cell Biol. 123 (2014) 367-94.
[22] J. Liu, Y. Wang, W.I. Goh, H. Goh, M.A. Baird, S. Ruehland, S. Teo, N. Bate, D.R. Critchley, M.W. Davidson, P. Kanchanawong, Talin determines the nanoscale architecture of focal adhesions, Proc. Natl. Acad. Sci. U. S. A. 112 (35) (2015) E4864-73.
[23] R.O. Hynes, Integrins: bidirectional, allosteric signaling machines, Cell 110 (6) (2002) 673-87.
[24] D. Bouvard, J. Pouwels, N. De Franceschi, J. Ivaska, Integrin inactivators: balancing cellular functions in vitro and in vivo, Nat. Rev. Mol. Cell Biol. 14 (7) (2013) 430-42.
[25] E.F. Plow, T.K. Haas, L. Zhang, J. Loftus, J.W. Smith, Ligand binding to integrins, J. Biol. Chem. 275 (29) (2000) 21785–21788.
[26] J. Ivaska, H. Reunanen, J. Westermarck, L. Koivisto, V.M. Kahari, J. Heino, Integrin alpha2beta1 mediates isoform-specific activation of p38 and upregulation of collagen gene transcription by a mechanism involving the alpha2 cytoplasmic tail, J. Cell Biol. 147 (2) (1999) 401-16.
[27] C.M. Borza, Y. Su, X. Chen, L. Yu, S. Mont, S. Chetyrkin, P. Voziyan, B.G. Hudson, P.C. Billings, H. Jo, J.S. Bennett, W.F. Degrado, B. Eckes, R. Zent, A. Pozzi, Inhibition of integrin alpha2beta1 ameliorates glomerular injury, J. Am. Soc. Nephrol. 23 (6) (2012) 1027-38.
[28] H.B. Schiller, M.R. Hermann, J. Polleux, T. Vignaud, S. Zanivan, C.C. Friedel, Z. Sun, A. Raducanu, K.E.

Gottschalk, M. Thery, M. Mann, R. Fassler, Beta1- and alphav-class integrins cooperate to regulate myosin II during rigidity sensing of fibronectin-based microenvironments, Nat. Cell Biol. 15 (6) (2013) 625–636.
[29] S. Niland, C. Westerhausen, S.W. Schneider, B. Eckes, M.F. Schneider, J.A. Eble, Biofunctionalization of a generic collagenous triple helix with the alpha2beta1 integrin binding site allows molecular force measurements, Int. J. Biochem. Cell Biol. 43 (5) (2011) 721-31.
[30] F. Kong, A.J. Garcia, A.P. Mould, M.J. Humphries, C. Zhu, Demonstration of catch bonds between an integrin and its ligand, J. Cell Biol. 185 (7) (2009) 1275-84.
[31] G. Jiang, G. Giannone, D.R. Critchley, E. Fukumoto, M.P. Sheetz, Two-piconewton slip bond between fibronectin and the cytoskeleton depends on talin, Nature 424 (6946) (2003) 334-7.
[32] P. Roca-Cusachs, N.C. Gauthier, A. Del Rio, M.P. Sheetz, Clustering of alpha(5)beta(1) integrins determines adhesion strength whereas alpha(v)beta(3) and talin enable mechanotransduction, Proc. Natl. Acad. Sci. U. S. A. 106 (38) (2009) 16245-50.
[33] R.I. Litvinov, V. Barsegov, A.J. Schissler, A.R. Fisher, J.S. Bennett, J.W. Weisel, H. Shuman, Dissociation of bimolecular alphaIIbbeta3-fibrinogen complex under a constant tensile force, Biophys. J. 100 (1) (2011) 165-73.
[34] J.M. de Pereda, E. Ortega, N. Alonso-Garcia, M. Gomez-Hernandez, A. Sonnenberg, Advances and perspectives of the architecture of hemidesmosomes: lessons from structural biology, Cell Adhes. Migr. 3 (4) (2009) 361-4.
[35] K.R. Legate, R. Fassler, Mechanisms that regulate adaptor binding to beta-integrin cytoplasmic tails, J. Cell Sci. 122 (Pt 2) (2009) 187-98.
[36] M. Moser, K.R. Legate, R. Zent, R. Fassler, The tail of integrins, talin, and kindlins, Science 324 (5929) (2009) 895-9.
[37] G.C. Roberts, D.R. Critchley, Structural and biophysical properties of the integrin-associated cytoskeletal protein talin, Biophys. Rev. 1 (2) (2009) 61–69.
[38] K. Bledzka, K. Bialkowska, K. Sossey-Alaoui, J. Vaynberg, E. Pluskota, J. Qin, E.F. Plow, Kindlin-2 directly binds actin and regulates integrin outside-in signaling, J. Cell Biol. 213 (1) (2016) 97–108.
[39] M.D. Schaller, C.A. Otey, J.D. Hildebrand, J.T. Parsons, Focal adhesion kinase and paxillin bind to peptides mimicking beta integrin cytoplasmic domains, J. Cell Biol. 130 (5) (1995) 1181-7.
[40] D.D. Chang, C. Wong, H. Smith, J. Liu, ICAP-1, a novel beta1 integrin cytoplasmic domain-associated protein, binds to a conserved and functionally important NPXY sequence motif of beta1 integrin, J. Cell Biol. 138 (5) (1997) 1149-57.
[41] J.K. Rantala, J. Pouwels, T. Pellinen, S. Veltel, P. Laasola, E. Mattila, C.S. Potter, T. Duffy, J.P. Sundberg, O. Kallioniemi, J.A. Askari, M.J. Humphries, M. Parsons, M. Salmi, J. Ivaska, SHARPIN is an endogenous inhibitor of beta1-integrin activation, Nat. Cell Biol. 13 (11) (2011) 1315-24.
[42] P. Atherton, B. Stutchbury, D.Y. Wang, D. Jethwa, R. Tsang, E. Meiler-Rodriguez, P. Wang, N. Bate, R. Zent, I.L. Barsukov, B.T. Goult, D.R. Critchley, C. Ballestrem, Vinculin controls talin engagement with the actomyosin machinery, Nat. Commun. 6 (2015) 10038.
[43] A. del Rio, R. Perez-Jimenez, R. Liu, P. Roca-Cusachs, J.M. Fernandez, M.P. Sheetz, Stretching single talin rod molecules activates vinculin binding, Science 323 (5914) (2009) 638-41.
[44] K. Austen, P. Ringer, A. Mehlich, A. Chrostek-Grashoff, C. Kluger, C. Klingner, B. Sabass, R. Zent, M. Rief, C. Grashoff, Extracellular rigidity sensing by talin isoform-specific mechanical linkages, Nat. Cell Biol. 17 (12) (2015) 1597-606.
[45] B.M. Sefton, T. Hunter, E.H. Ball, S.J. Singer, Vinculin: a cytoskeletal target of the transforming protein of Rous sarcoma virus, Cell 24 (1) (1981) 165-74.
[46] Z. Zhang, G. Izaguirre, S.Y. Lin, H.Y. Lee, E. Schaefer, B. Haimovich, The phosphorylation of vinculin on tyrosine residues 100 and 1065, mediated by SRC kinases, affects cell spreading, Mol. Biol. Cell 15 (9) (2004) 4234-47.
[47] Y. Sawada, M. Tamada, B.J. Dubin-Thaler, O. Cherniavskaya, R. Sakai, S. Tanaka, M.P. Sheetz, Force sensing by mechanical extension of the Src family kinase substrate p130Cas, Cell 127 (5) (2006) 1015-26.
[48] T.P. Lele, J. Pendse, S. Kumar, M. Salanga, J. Karavitis, D.E. Ingber, Mechanical forces alter zyxin unbinding kinetics within focal adhesions of living cells, J. Cell. Physiol. 207 (1) (2006) 187–194.
[49] Y.X. Wang, E.L. Botvinick, Y.H. Zhao, M.W. Berns, S. Usami, R.Y. Tsien, S. Chien, Visualizing the mechanical activation of Src, Nature 434 (7036) (2005) 1040–1045.
[50] M. Prager-Khoutorsky, A. Lichtenstein, R. Krishnan, K. Rajendran, A. Mayo, Z. Kam, B. Geiger, A.D. Bershadsky, Fibroblast polarization is a matrix-rigidity-dependent process controlled by focal adhesion mechanosensing, Nat. Cell Biol. 13 (12) (2011) 1457-65.
[51] B. Yang, Z.Z. Lieu, H. Wolfenson, F.M. Hameed, A.D. Bershadsky, M.P. Sheetz, Mechanosensing controlled directly by tyrosine kinases, Nano Lett. (2016).
[52] F.J. Sulzmaier, C. Jean, D.D. Schlaepfer, FAK in cancer: mechanistic findings and clinical applications, Nat. Rev. Cancer 14 (9) (2014) 598–610.
[53] J.M. Laakso, J.H. Lewis, H. Shuman, E.M. Ostap, Myosin I can act as a molecular force sensor, Science 321 (5885) (2008) 133-6.
[54] M.J. Greenberg, T. Lin, Y.E. Goldman, H. Shuman, E.M. Ostap, Myosin IC generates power over a range of loads via a new tension-sensing mechanism, Proc. Natl. Acad. Sci. U. S. A. 109 (37) (2012) E2433-40.
[55] K. Hayakawa, H. Tatsumi, M. Sokabe, Actin filaments function as a tension sensor by tension-dependent binding of cofilin to the filament, J. Cell Biol. 195 (5) (2011) 721–727.
[56] A. Hall, Rho GTPases and the actin cytoskeleton, Science 279 (5350) (1998) 509-14.
[57] R. Straussman, L. Even, S. Ravid, Myosin II heavy chain isoforms are phosphorylated in an EGF-dependent manner: involvement of protein kinase C, J. Cell Sci. 114 (Pt 16) (2001) 3047-57.
[58] F. Fauchereau, U. Herbrand, P. Chafey, A. Eberth, A. Koulakoff, M.C. Vinet, M.R. Ahmadian, J. Chelly, P. Billuart, The RhoGAP activity of OPHN1, a new F-actin-binding protein, is negatively controlled by its amino-terminal domain, Mol. Cell. Neurosci. 23 (4) (2003) 574–586.
[59] K. Burridge, E.S. Wittchen, The tension mounts: stress fibers as force-generating mechanotransducers, J. Cell Biol. 200 (1) (2013) 9–19.
[60] T.D. Pollard, J.A. Cooper, Actin, a central player in cell shape and movement, Science 326 (5957) (2009) 1208–1212.
[61] S. Tojkander, G. Gateva, P. Lappalainen, Actin stress fibers — assembly, dynamics and biological roles, J. Cell Sci. 125 (8) (2012) 1855–1864.

Please cite this article as: P. Ringer, et al., Sensing the mechano-chemical properties of the extracellular matrix, Matrix Biol (2017), http://dx.doi.org/10.1016/j.matbio.2017.03.004

[62] B. Hinz, G. Gabbiani, C. Chaponnier, The NH2-terminal peptide of alpha-smooth muscle actin inhibits force generation by the myofibroblast in vitro and in vivo, J. Cell Biol. 157 (4) (2002) 657–663.
[63] M. Vicente-Manzanares, J. Zareno, L. Whitmore, C.K. Choi, A.F. Horwitz, Regulation of protrusion, adhesion dynamics, and polarity by myosins IIA and IIB in migrating cells, J. Cell Biol. 176 (5) (2007) 573-80.
[64] B. Geiger, K.M. Yamada, Molecular architecture and function of matrix adhesions, Cold Spring Harb. Perspect. Biol. 3 (5) (2011).
[65] E. Zamir, M. Katz, Y. Posen, N. Erez, K.M. Yamada, B.Z. Katz, S. Lin, D.C. Lin, A. Bershadsky, Z. Kam, B. Geiger, Dynamics and segregation of cell-matrix adhesions in cultured fibroblasts, Nat. Cell Biol. 2 (4) (2000) 191–196.
[66] C.J. McCleverty, D.C. Lin, R.C. Liddington, Structure of the PTB domain of tensin1 and a model for its recruitment to fibrillar adhesions, Protein Sci. 16 (6) (2007) 1223-9.
[67] E. Cukierman, R. Pankov, D.R. Stevens, K.M. Yamada, Taking cell-matrix adhesions to the third dimension, Science 294 (5547) (2001) 1708–1712.
[68] K. Clark, J.D. Howe, C.E. Pullar, J.A. Green, V.V. Artym, K.M. Yamada, D.R. Critchley, Tensin 2 modulates cell contractility in 3D collagen gels through the RhoGAP DLC1, J. Cell. Biochem. 109 (4) (2010) 808–817.
[69] Z. Sun, H.Y. Tseng, S. Tan, F. Senger, L. Kurzawa, D. Dedden, N. Mizuno, A.A. Wasik, M. Thery, A.R. Dunn, R. Fassler, Kank2 activates talin, reduces force transduction across integrins and induces central adhesion formation, Nat. Cell Biol. 18 (9) (2016) 941-53.
[70] B.P. Bouchet, R.E. Gough, Y.C. Ammon, D. van de Willige, H. Post, G. Jacquemet, A.M. Altelaar, A.J. Heck, B.T. Goult, A. Akhmanova, Talin-KANK1 interaction controls the recruitment of cortical microtubule stabilizing complexes to focal adhesions, elife 5 (2016).
[71] B. van der Vaart, W.E. van Riel, H. Doodhi, J.T. Kevenaar, E.A. Katrukha, L. Gumy, B.P. Bouchet, I. Grigoriev, S.A. Spangler, K.L. Yu, P.S. Wulf, J.C. Wu, G. Lansbergen, E.Y. van Battum, R.J. Pasterkamp, Y. Mimori-Kiyosue, J. Demmers, N. Olieric, I.V. Maly, C.C. Hoogenraad, A. Akhmanovaz, CFEOM1-associated kinesin KIF21A is a cortical microtubule growth inhibitor, Dev. Cell 27 (2) (2013) 145–160.
[72] I. Kaverina, K. Rottner, J.V. Small, Targeting, capture, and stabilization of microtubules at early focal adhesions, J. Cell Biol. 142 (1) (1998) 181–190.
[73] I. Kaverina, O. Krylyshkina, J.V. Small, Microtubule targeting of substrate contacts promotes their relaxation and dissociation, J. Cell Biol. 146 (5) (1999) 1033–1043.
[74] M.J. Paszek, D. Boettiger, V.M. Weaver, D.A. Hammer, Integrin clustering is driven by mechanical resistance from the glycocalyx and the substrate, PLoS Comput. Biol. 5 (12) (2009), e1000604.
[75] M.J. Paszek, C.C. DuFort, O. Rossier, R. Bainer, J.K. Mouw, K. Godula, J.E. Hudak, J.N. Lakins, A.C. Wijekoon, L. Cassereau, M.G. Rubashkin, M.J. Magbanua, K.S. Thorn, M.W. Davidson, H.S. Rugo, J.W. Park, D.A. Hammer, G. Giannone, C.R. Bertozzi, V.M. Weaver, The cancer glycocalyx mechanically primes integrin-mediated growth and survival, Nature 511 (7509) (2014) 319-25.
[76] D. Riveline, E. Zamir, N.Q. Balaban, U.S. Schwarz, T. Ishizaki, S. Narumiya, Z. Kam, B. Geiger, A.D. Bershadsky, Focal contacts as mechanosensors: externally applied local mechanical force induces growth of focal contacts by an mDia1-dependent and ROCK-independent mechanism, J. Cell Biol. 153 (6) (2001) 1175-86.
[77] N.Q. Balaban, U.S. Schwarz, D. Riveline, P. Goichberg, G. Tzur, I. Sabanay, D. Mahalu, S. Safran, A. Bershadsky, L. Addadi, B. Geiger, Force and focal adhesion assembly: a close relationship studied using elastic micropatterned substrates, Nat. Cell Biol. 3 (5) (2001) 466–472.
[78] J.L. Tan, J. Tien, D.M. Pirone, D.S. Gray, K. Bhadriraju, C.S. Chen, Cells lying on a bed of microneedles: an approach to isolate mechanical force, Proc. Natl. Acad. Sci. U. S. A. 100 (4) (2003) 1484–1489.
[79] F. Kong, Z. Li, W.M. Parks, D.W. Dumbauld, A.J. Garcia, A.P. Mould, M.J. Humphries, C. Zhu, Cyclic mechanical reinforcement of integrin-ligand interactions, Mol. Cell 49 (6) (2013) 1060–1068.
[80] H. Delanoe-Ayari, J. Brevier, D. Riveline, Scaling concepts in cell physics: paradigms for cell adhesion, Soft Matter 7 (3) (2011) 824–829.
[81] U.S. Schwarz, T. Erdmann, I.B. Bischofs, Focal adhesions as mechanosensors: the two-spring model, Biosystems 83 (2–3) (2006) 225-32.
[82] A. Nicolas, B. Geiger, S.A. Safran, Cell mechanosensitivity controls the anisotropy of focal adhesions, Proc. Natl. Acad. Sci. U. S. A. 101 (34) (2004) 12520–12525.
[83] C.E. Chan, D.J. Odde, Traction dynamics of filopodia on compliant substrates, Science 322 (5908) (2008) 1687–1691.
[84] S. Munevar, Y.L. Wang, M. Dembo, Distinct roles of frontal and rear cell-substrate adhesions in fibroblast migration, Mol. Biol. Cell 12 (12) (2001) 3947-54.
[85] S.J. Han, Y. Oak, A. Groisman, G. Danuser, Traction microscopy to identify force modulation in subresolution adhesions, Nat. Methods 12 (7) (2015) 653-6.
[86] B.L. Blakely, C.E. Dumelin, B. Trappmann, L.M. McGregor, C.K. Choi, P.C. Anthony, V.K. Duesterberg, B.M. Baker, S.M. Block, D.R. Liu, C.S. Chen, A DNA-based molecular probe for optically reporting cellular traction forces, Nat. Methods 11 (12) (2014) 1229-32.
[87] A. Chopra, M.E. Murray, F.J. Byfield, M.G. Mendez, R. Halleluyan, D.J. Restle, D. Raz-Ben Aroush, P.A. Galie, K. Pogoda, R. Bucki, C. Marcinkiewicz, G.D. Prestwich, T.I. Zarembinski, C.S. Chen, E. Pure, J.Y. Kresh, P.A. Janmey, Augmentation of integrin-mediated mechanotransduction by hyaluronic acid, Biomaterials 35 (1) (2014) 71–82.
[88] I. Patla, T. Volberg, N. Elad, V. Hirschfeld-Warneken, C. Grashoff, R. Fassler, J.P. Spatz, B. Geiger, O. Medalia, Dissecting the molecular architecture of integrin adhesion sites by cryo-electron tomography, Nat. Cell Biol. 12 (9) (2010) 909–915.
[89] S. Hu, Y.H. Tee, A. Kabla, R. Zaidel-Bar, A. Bershadsky, P. Hersen, Structured illumination microscopy reveals focal adhesions are composed of linear subunits, Cytoskeleton (Hoboken) 72 (5) (2015) 235-45.
[90] F. Rechenmacher, S. Neubauer, C. Mas-Moruno, P.M. Dorfner, J. Polleux, J. Guasch, B. Conings, H.G. Boyen, A. Bochen, T.R. Sobahi, R. Burgkart, J.P. Spatz, R. Fassler, H. Kessler, A molecular toolkit for the functionalization of titanium-based biomaterials that selectively control integrin-mediated cell adhesion, Chem. Eur. J. 19 (28) (2013) 9218–9223.
[91] C. Mas-Moruno, R. Fraioli, F. Rechenmacher, S. Neubauer, T.G. Kapp, H. Kessler, alphavbeta3- or alpha5beta1-integrin-selective peptidomimetics for surface coating, Angew. Chem. Int. Ed. Eng. 55 (25) (2016) 7048-67.

Please cite this article as: P. Ringer, et al., Sensing the mechano-chemical properties of the extracellular matrix, Matrix Biol (2017), http://dx.doi.org/10.1016/j.matbio.2017.03.004

[92] M. Shi, V. Pedchenko, B.H. Greer, W.D. Van Horn, S.A. Santoro, C.R. Sanders, B.G. Hudson, B.F. Eichman, R. Zent, A. Pozzi, Enhancing integrin alpha1 inserted (I) domain affinity to ligand potentiates integrin alpha1beta1-mediated down-regulation of collagen synthesis, J. Biol. Chem. 287 (42) (2012) 35139-52.

[93] F. Li, S.D. Redick, H.P. Erickson, V.T. Moy, Force measurements of the alpha5beta1 integrin-fibronectin interaction, Biophys. J. 84 (2 Pt 1) (2003) 1252–1262.

[94] X. Wang, T. Ha, Defining single molecular forces required to activate integrin and notch signaling, Science 340 (6135) (2013) 991-4.

[95] M. Morimatsu, A.H. Mekhdjian, A.S. Adhikari, A.R. Dunn, Molecular tension sensors report forces generated by single integrin molecules in living cells, Nano Lett. 13 (9) (2013) 3985-9.

[96] A.C. Chang, A.H. Mekhdjian, M. Morimatsu, A.K. Denisin, B.L. Pruitt, A.R. Dunn, Single molecule force measurements in living cells reveal a minimally tensioned integrin state, ACS Nano 10 (12) (2016) 10745–10752.

[97] O. Rossier, V. Octeau, J.B. Sibarita, C. Leduc, B. Tessier, D. Nair, V. Gatterdam, O. Destaing, C. Albiges-Rizo, R. Tampe, L. Cognet, D. Choquet, B. Lounis, G. Giannone, Integrins beta1 and beta3 exhibit distinct dynamic nanoscale organizations inside focal adhesions, Nat. Cell Biol. 14 (10) (2012) 1057-67.

[98] S.J. Humphrey, S.B. Azimifar, M. Mann, High-throughput phosphoproteomics reveals in vivo insulin signaling dynamics, Nat. Biotechnol. 33 (9) (2015) 990–995.

[99] S.E. Winograd-Katz, R. Fassler, B. Geiger, K.R. Legate, The integrin adhesome: from genes and proteins to human disease, Nat. Rev. Mol. Cell Biol. 15 (4) (2014) 273–288.

[100] E.R. Horton, A. Byron, J.A. Askari, D.H.J. Ng, A. Millon-Fremillon, J. Robertson, E.J. Koper, N.R. Paul, S. Warwood, D. Knight, J.D. Humphries, M.J. Humphries, Definition of a consensus integrin adhesome and its dynamics during adhesion complex assembly and disassembly, Nat. Cell Biol. 17 (12) (2015) 1577–1587.

[101] M.J. Paszek, C.C. DuFort, M.G. Rubashkin, M.W. Davidson, K.S. Thorn, J.T. Liphardt, V.M. Weaver, Scanning angle interference microscopy reveals cell dynamics at the nanoscale, Nat. Methods 9 (8) (2012) 825-7.

[102] A.L. Cost, P. Ringer, A. Chrostek-Grashoff, C. Grashoff, How to measure molecular forces in cells: a guide to evaluating genetically-encoded FRET-based tension sensors, Cell. Mol. Bioeng. 8 (1) (2015) 96–105.

[103] A. Freikamp, A. Mehlich, C. Klingner, C. Grashoff, Investigating piconewton forces in cells by FRET-based molecular force microscopy, J. Struct. Biol. (2016).

[104] A. Freikamp, A.L. Cost, C. Grashoff, The piconewton force awakens: quantifying mechanics in cells, Trends Cell Biol. (2016).

[105] C. Grashoff, B.D. Hoffman, M.D. Brenner, R. Zhou, M. Parsons, M.T. Yang, M.A. McLean, S.G. Sligar, C.S. Chen, T. Ha, M.A. Schwartz, Measuring mechanical tension across vinculin reveals regulation of focal adhesion dynamics, Nature 466 (7303) (2010) 263-6.

[106] A. Kumar, M.X. Ouyang, K. Van den Dries, E.J. McGhee, K. Tanaka, M.D. Anderson, A. Groisman, B.T. Goult, K.I. Anderson, M.A. Schwartz, Talin tension sensor reveals novel features of focal adhesion force transmission and mechanosensitivity, J. Cell Biol. 213 (3) (2016) 371–383.

[107] A. Juanes-Garcia, J.R. Chapman, R. Aguilar-Cuenca, C. Delgado-Arevalo, J. Hodges, L.A. Whitmore, J. Shabanowitz, D.F. Hunt, A.R. Horwitz, M. Vicente-Manzanares, A regulatory motif in nonmuscle myosin II-B regulates its role in migratory front-back polarity, J. Cell Biol. 209 (1) (2015) 23–32.

[108] A. Ponti, M. Machacek, S.L. Gupton, C.M. Waterman-Storer, G. Danuser, Two distinct actin networks drive the protrusion of migrating cells, Science 305 (5691) (2004) 1782-6.

[109] K. Hu, L. Ji, K.T. Applegate, G. Danuser, C.M. Waterman-Storer, Differential transmission of actin motion within focal adhesions, Science 315 (5808) (2007) 111-5.

[110] K. Xu, H.P. Babcock, X. Zhuang, Dual-objective STORM reveals three-dimensional filament organization in the actin cytoskeleton, Nat. Methods 9 (2) (2012) 185-8.

[111] A. Dubrovsky, S. Sorrentino, J. Harapin, K.T. Sapra, O. Medalia, Developments in cryo-electron tomography for in situ structural analysis, Arch. Biochem. Biophys. 581 (2015) 78–85.

[112] J. Guo, Y. Wang, F. Sachs, F. Meng, Actin stress in cell reprogramming, Proc. Natl. Acad. Sci. U. S. A. 111 (49) (2014) E5252-61.

[113] T. Mitchison, M. Kirschner, Cytoskeletal dynamics and nerve growth, Neuron 1 (9) (1988) 761-72.

[114] S.V. Plotnikov, A.M. Pasapera, B. Sabass, C.M. Waterman, Force fluctuations within focal adhesions mediate ECM-rigidity sensing to guide directed cell migration, Cell 151 (7) (2012) 1513-27.

[115] P.C. Georges, W.J. Miller, D.F. Meaney, E.S. Sawyer, P.A. Janmey, Matrices with compliance comparable to that of brain tissue select neuronal over glial growth in mixed cortical cultures, Biophys. J. 90 (8) (2006) 3012–3018.

[116] B.L. Bangasser, S.S. Rosenfeld, D.J. Odde, Determinants of maximal force transmission in a motor-clutch model of cell traction in a compliant microenvironment, Biophys. J. 105 (3) (2013) 581-92.

[117] A. Elosegui-Artola, E. Bazellieres, M.D. Allen, I. Andreu, R. Oria, R. Sunyer, J.J. Gomm, J.F. Marshall, J.L. Jones, X. Trepat, P. Roca-Cusachs, Rigidity sensing and adaptation through regulation of integrin types, Nat. Mater. 13 (6) (2014) 631-7.

[118] A. Elosegui-Artola, R. Oria, Y. Chen, A. Kosmalska, C. Perez-Gonzalez, N. Castro, C. Zhu, X. Trepat, P. Roca-Cusachs, Mechanical regulation of a molecular clutch defines force transmission and transduction in response to matrix rigidity, Nat. Cell Biol. 18 (5) (2016) 540-8.

[119] F. Lagarrigue, P. Vikas Anekal, H.S. Lee, A.I. Bachir, J.N. Ablack, A.F. Horwitz, M.H. Ginsberg, A RIAM/lamellipodin-talin-integrin complex forms the tip of sticky fingers that guide cell migration, Nat. Commun. 6 (2015) 8492.

[120] Y. Tseng, T.P. Kole, J.S.H. Lee, E. Fedorov, S.C. Alino, B.W. Schafer, D. Wirtz, How actin crosslinking and bundling proteins cooperate to generate an enhanced cell mechanical response, Biochem. Biophys. Res. Commun. 334 (1) (2005) 183–192.

[121] X. Cao, E. Moeendarbary, P. Isermann, P.M. Davidson, X. Wang, M.B. Chen, A.K. Burkart, J. Lammerding, R.D. Kamm, V.B. Shenoy, A Chemomechanical model for nuclear morphology and stresses during cell Transendothelial migration, Biophys. J. 111 (7) (2016) 1541–1552.

Please cite this article as: P. Ringer, et al., Sensing the mechano-chemical properties of the extracellular matrix, Matrix Biol (2017), http://dx.doi.org/10.1016/j.matbio.2017.03.004

Multiplexing molecular tension sensors reveals piconewton force gradient across talin-1

Pia Ringer[1], Andreas Weißl[2], Anna-Lena Cost[1], Andrea Freikamp[1], Benedikt Sabass[3], Alexander Mehlich[2], Marc Tramier[4–6], Matthias Rief[2,7] & Carsten Grashoff[1]

Förster resonance energy transfer (FRET)-based tension sensor modules (TSMs) are available for investigating how distinct proteins bear mechanical forces in cells. Yet, forces in the single piconewton (pN) regime remain difficult to resolve, and tools for multiplexed tension sensing are lacking. Here, we report the generation and calibration of a genetically encoded, FRET-based biosensor called FL-TSM, which is characterized by a near-digital force response and increased sensitivity at 3–5 pN. In addition, we present a method allowing the simultaneous evaluation of coexpressed tension sensor constructs using two-color fluorescence lifetime microscopy. Finally, we introduce a procedure to calculate the fraction of mechanically engaged molecules within cells. Application of these techniques to new talin biosensors reveals an intramolecular tension gradient across talin-1 that is established upon integrin-mediated cell adhesion. The tension gradient is actomyosin- and vinculin-dependent and sensitive to the rigidity of the extracellular environment.

Mechanical forces of just a few pN can regulate the activity of proteins and thereby modulate a wide range of biological processes[1,2]. Forces of about 3–5 pN, for instance, speed proteolytic cleavage of the Notch receptor[3], while the affinity of the actin crosslinking protein filamin to its binding partners increases after application of 2–5 pN[4]. Binding of the cell adhesion protein vinculin to the integrin activator talin-1 is induced by mechanical tension of 2–12 pN[5], and the cadherin–catenin interaction, which is central to intercellular cohesion, strengthens under mechanical loads of about 5 pN[6]. *In vitro*, cytoskeletal motor proteins like myosins generate exactly these magnitudes of force—namely, about 4–5 pN per motor protein[7]. FRET-based tension sensors have been developed to quantify such pN-scale forces, and different molecular designs have been realized to determine forces within cells[8,9] or at the cell surface[10–12].

Genetically encoded probes are ideally suited to measure intracellular forces. They typically comprise two GFP-like fluorophores connected by a mechanosensitive linker peptide that extends in response to mechanical tension[13]. As FRET is distance dependent, forces elongating the linker peptide reduce FRET, which can be quantified microscopically. Our first single-molecule-calibrated TSM used the 40 amino acid (aa)-long flagelliform peptide (F40), which behaves like a molecular spring and gradually elongates when forces between 1–6 pN[8] are applied. To quantify greater forces, we developed a biosensor using the 35-aa-long villin headpiece peptide (HP), which responds to about 6–8 pN[9]; a third biosensor was based upon a stabilized HP peptide (HPst) that displayed maximal sensitivity at 9–11 pN[9]. These TSMs have been applied to study various mechanotransduction processes in cells; notably, the F40-TSM has been extensively used in a range of cell types and model organisms[13–18]. Owing to the gradual FRET response of the F40 module, however, forces below 6 pN have remained difficult to resolve[13,19], and it has been virtually impossible to determine how many molecules of a given population are mechanically engaged. Moreover, methods to analyze distinct force sensor constructs within the same cell have been lacking. We addressed these limitations by developing a novel 3–5-pN-sensitive TSM, establishing a method to evaluate two coexpressed TSMs simultaneously, and introducing a data analysis algorithm to estimate the fraction of mechanically engaged sensor molecules.

RESULTS

Generation and calibration of a 3–5-pN-sensitive tension sensor module

Live-cell tension sensor experiments are typically performed as ensemble measurements that provide an average force value. When TSMs with a spring-like force response are used, it is challenging to determine how much tension individual molecules experience in cells, as the percentage of molecules actively engaged in a given force transduction process is usually unknown[13,19]. To address this problem, we engineered a new TSM through using a ferredoxin-like (FL) linker peptide that was expected to display more digital force response characteristics (**Fig. 1a**)[20]. Indeed,

[1]Group of Molecular Mechanotransduction, Max Planck Institute of Biochemistry, Martinsried, Germany. [2]Physics Department E22, Technical University of Munich, Garching, Germany. [3]ICS-2/IAS-2, Forschungszentrum Jülich, Jülich, Germany. [4]CNRS, UMR 6290, Rennes, France. [5]Institut de Génétique et Développement de Rennes, Université de Rennes, Rennes, France. [6]Microscopy Rennes Imaging Centre, Université de Rennes, Rennes, France. [7]Munich Centre for Integrated Protein Science, Munich, Germany. Correspondence should be addressed to C.G. (cgrasho@biochem.mpg.de).

RECEIVED 12 APRIL; ACCEPTED 18 AUGUST; PUBLISHED ONLINE 18 SEPTEMBER 2017; DOI:10.1038/NMETH.4431

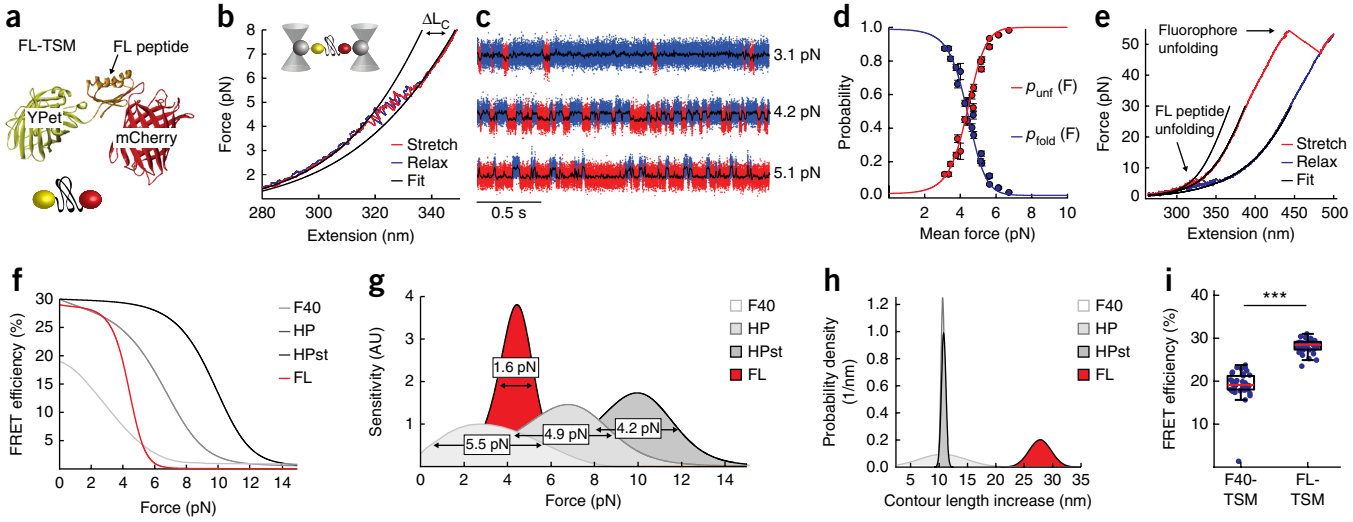

Figure 1 | Calibration of FL-TSM. (**a**) Schematic of FL-TSM. (**b**) Representative example of stretch–relax trace fitted with an extensible worm-like chain model (black line); the overlapping stretch (red) and relax (blue) traces indicate the absence of hysteresis (pulling velocity 10 nm/s). ΔL_C indicates the observed contour length increase. (**c**) Representative passive mode traces at 3.1 pN, 4.2 pN, and 5.1 pN. Folded FL states are colored in blue and unfolded FL states are in red. (**d**) Probability of FL-TSM to be in the folded (blue) or unfolded (red) state at a given force. (**e**) Representative stretch–relax trace covering 1–55 pN (pulling velocity 100 nm/s). Note that fluorophores unfold at much higher forces as compared to the FL peptide. (**f**) FRET–force correlation of FL-TSM (red) compared with previously described TSMs (gray). FL-TSM (red) is characterized by a sharp transition between 3–5 pN. (**g**) Sensitivity–force correlation of single-molecule-calibrated TSMs. FL-TSM (red) displays the sharpest force response as indicated by the full width at half maximum values. (**h**) Histograms of experimentally observed contour length increases ΔL_C. FL-TSM (red) yields an average maximum extension of 27.4 ± 2.8 nm (n = 269 unfolding events from 15 FL-TSM molecules in six independent experiments), while the previously described TSMs (grays) yield a mean contour length gain of about 11 nm. (**i**) Live-cell FLIM analysis of F40-TSM and FL-TSM expressed in the cytoplasm of cells (n = 38 and 33 cells, pooled from three independent experiments; Kolmogorov–Smirnov (KS) test; ***, $P < 0.001$). See Online Methods for definition of box plot elements.

calibration of the purified FL-TSM by single-molecule force spectroscopy revealed that the FL peptide remains in the folded state up to about 3 pN, whereas increasing tension to 5 pN induces a fast transition to the open state; both states were equally populated at about 4 pN. Unfolding was reversible, and FL sensors quickly returned to their original conformation once the mechanical load was reduced to below 3 pN. Furthermore, fluorophores remained stably folded until forces of about 40–55 pN were applied (**Fig. 1b–e**), as has been previously described[9,21].

To allow a direct comparison with F40-TSM, which was originally calibrated in the absence of fluorophores attached to N and C terminals and with a different instrument[8], we purified the full-length F40-TSM and reanalyzed F40-TSM molecules with the dual-trap optical tweezer setup. Consistent with previously published results[8], we did not observe a characteristic unfolding event as shown for the FL-TSM. Instead, the data suggested a gradual extension of the F40 peptide at low-pN force (**Supplementary Fig. 1**). Together, these experiments demonstrate that FL-TSM and F40-TSM display very different force responses.

Converting the force–extension data into FRET–force and sensitivity–force correlations confirmed the unique properties of FL-TSM (see Online Methods and **Supplementary Fig. 2**). The new probe displayed the highest sensitivity of all single-molecule-calibrated, genetically encoded TSMs reported thus far (**Fig. 1f, g**); the force-induced contour length increase was significantly larger for the FL linker than for previously developed sensor peptides, and FL-TSM displayed higher zero-force FRET efficiencies than the F40-based module, which indicated efficient peptide folding in cells (**Fig. 1h,i**). Hence, the novel biosensor should allow more accurate intracellular force measurements in the low-pN force regime.

Generation of new talin biosensors to evaluate tension across the talin rod domain

To test the performance of FL-TSM in living cells, we applied it to talin-1. Talin-1 is an essential cell adhesion protein comprising an N-terminal head domain that binds and activates integrin receptors; the C-terminal talin rod domain is made of thirteen helical bundles, which connect to the actomyosin cytoskeleton by two f-actin binding sites (called ABS2 and ABS3) as well as 11 vinculin binding motifs[22,23]. We had previously inserted the HP-TSM between the talin head and talin rod domains at aa 447 (a construct hereafter called talin-HP-447) and demonstrated that talin molecules experience forces of more than 7 pN during cell adhesion[9]. Yet it remained unclear how tension is distributed across the 190-kDa-long talin rod domain.

Therefore, we generated a set of talin biosensors in which HP- or FL-TSM was inserted at two distinct sites of the talin rod domain—namely, at aa 447 and between the two actin-binding sites at aa 1973. As controls, we fused talin-1 C terminally with the donor fluorophore YPet or either the HP- or FL-TSM, or we internally tagged talin-1 with individual fluorophores (**Fig. 2a** and **Supplementary Fig. 3**). Expression of either of these constructs rescued the adhesion and spreading phenotype of fibroblasts lacking talin-1 and talin-2 ($Tln1^{-/-}Tln2^{-/-}$); and the size of focal adhesions (FAs) was equally restored (**Fig. 2b,c** and **Supplementary Fig. 4**). The subcellular dynamics of talin were similar to those described in previously published results[9]; and internally or C terminally tagged constructs displayed comparable FA turnover rates as determined by fluorescence recovery after photobleaching (FRAP) experiments (**Fig. 2d,e**). Moreover, the fluorescence lifetimes of the integrated fluorophores were unchanged at positions aa 447 and aa 1973 (**Fig. 2f**), and intermolecular FRET at

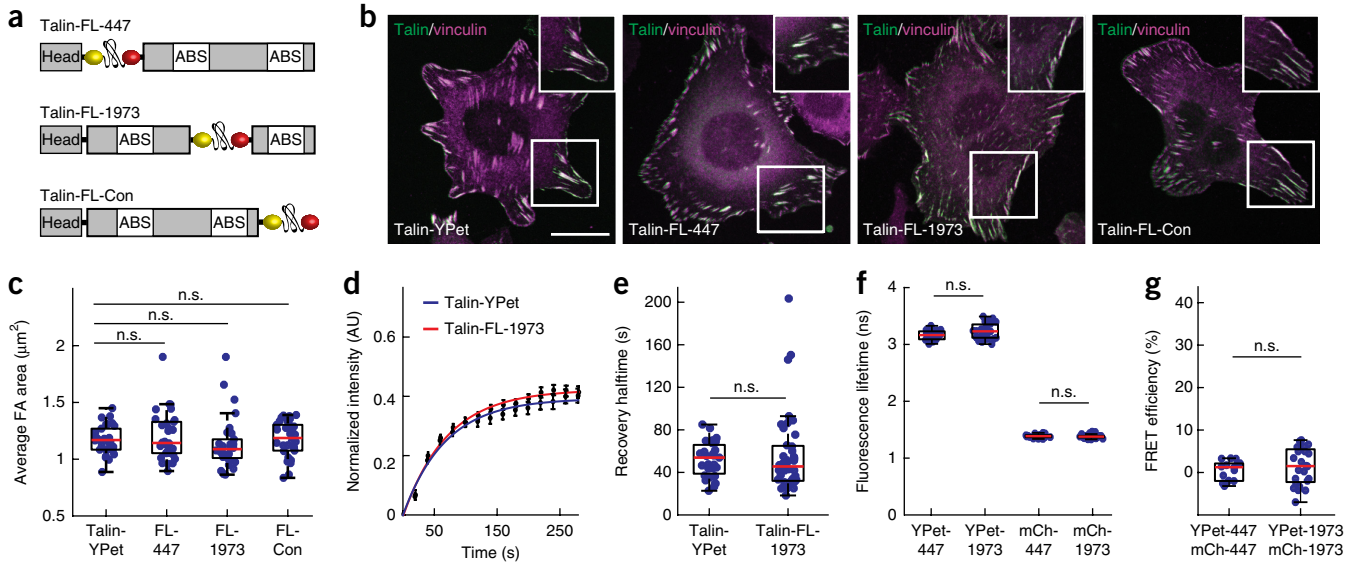

Figure 2 | Evaluation of FL-TSM-based talin tension sensors. (**a**) Schematic illustration of FL-based talin tension sensor constructs. FL-TSM was inserted after aa 447 or after aa 1973; as a control, the FL-TSM was C terminally fused to talin-1. (**b**) Stable expression of talin constructs (green) in $Tln1^{-/-}Tln2^{-/-}$ cells reveals normal subcellular localization to FAs marked by vinculin (magenta); scale bar, 20 µm. (**c**) FA analysis reveals comparable average FA sizes in control and tension-sensor-expressing cells (n = 30, 30, 30, 30 cells, pooled from three independent experiments). (**d**) FRAP experiments in cells expressing talin-YPet (blue) or talin-FL-1973 (red) showing normal talin-1 turnover dynamics in FAs (error bars indicate s.e.m; n = 31 and 40 cells, pooled from six independent experiments). (**e**) Normal fluorescence recovery halftimes in talin-FL-1973 cells as compared to those in talin-YPet expressing cells. (**f**) The fluorescence lifetimes of YPet and mCherry are unaffected by integration into talin-1 at aa 447 or aa 1973 (n = 22, 28, 23, 34 cells, pooled from five independent experiments). (**g**) Intermolecular FRET at position aa 447 and aa 1973 is similarly low (n = 15, 24 cells, pooled from four independent experiments). (**c,e–g**, KS test; n.s., not significant, $P > 0.05$).

aa 1973 was similarly low as for aa 447 (**Fig. 2g**). Together, these results show that TSMs can be inserted into talin-1 at aa 447 and at aa 1973 without disturbing talin function or the fluorophore's photophysical properties.

Talin-1 displays an intramolecular tension gradient during cell adhesion

To determine FRET efficiencies in living cells, we performed fluorescence lifetime imaging microscopy (FLIM) experiments as previously described[9,24] and as illustrated in **Supplementary Figure 5**. Consistent with previous measurements[9], evaluation of the HP-based talin sensor indicated an average mechanical tension of more than 7 pN at aa 447 when cells were seeded on fibronectin (FN)-coated glass slides. As a control, cells were analyzed on poly-L-Lysine (pLL)-coated surfaces, upon which FAs do not form. Remarkably, FRET efficiencies in cells expressing talin-HP-1973 were indistinguishable from pLL control values, and this suggested that the C-terminal part of the talin rod domain does not experience forces higher than 7 pN (**Fig. 3a**). Results of the respective FL-based talin sensors were consistent with high tension at aa 447; however, FRET efficiency values for cells expressing talin-FL-1973 were lower than control levels, which indicated mechanical tension of more than 3 pN at aa 1973 (**Fig. 3b**).

Since F40-TSM should also respond to the low forces observed at aa 1973 (**Fig. 1f,g**), we generated a set of F40-based talin sensors to confirm our observations. Indeed, F40-based measurements yielded similar results, but differences of talin-F40-1973 to control conditions were significantly smaller (**Fig. 3c**). As fluorescence intensities were comparable between all constructs and did not correlate with fluorescence lifetime values (**Supplementary Fig. 6**), the less pronounced differences in F40-based measurements are likely a result of the limited dynamic range of F40-TSM. More importantly, the data did not allow us to estimate how much tension individual talin molecules experience at aa 1973, owing to the gradual force–FRET response characteristics of F40-TSM (**Fig. 1f,g** and **Supplementary Fig. 1**)[8]. By contrast, FL-TSM-based measurements indicated that forces must have surpassed 3 pN to cause a significant decrease in FRET efficiencies (**Fig. 1c–g**).

To validate the FL-TSM-based measurements with an independent FRET method, we performed ratiometric imaging. Consistent with the experiments described above, we observed low FRET indices for cells expressing talin-FL-447 and increased FRET values at aa 1973; again, FRET in cells expressing talin-FL-1973 was lower than control levels (**Fig. 3d,e**).

Together, the data suggested that the talin rod domain experiences a force gradient upon integrin-mediated cell adhesion. These forces exceed 7 pN between talin head and talin rod domains, and they exceed 3 pN between the C-terminal ABSs.

Forces at talin's C-terminal region are sensitive to myosin activity and focal adhesion morphology

Next, we treated talin-FL-sensor-expressing $Tln1^{-/-}Tln2^{-/-}$ cells with the Y-27632 compound, which reduces myosin-II activity. Similar to previously published integrin tension measurements[11], forces at aa 447 were lowered by Y-27632 treatment but did not seem to be entirely lost (**Fig. 4a**), probably because talin molecules within the remaining adhesion structures were still experiencing residual mechanical loads (**Supplementary Fig. 7a**). By contrast, forces at aa 1973 were abolished after addition of Y-27632 (**Fig. 4a**). We confirmed these observations with ratiometric imaging, in which individual Y-27632-treated cells were evaluated over time. Also in these experiments, tension at aa 447 was gradually

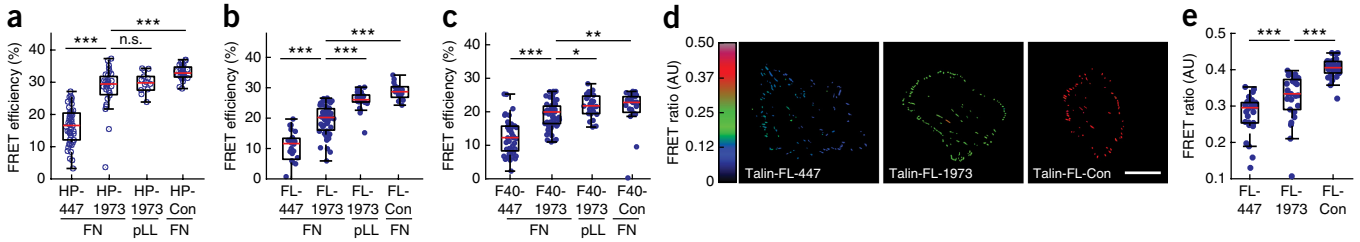

Figure 3 | Evaluating the intramolecular talin tension gradient. (**a**) FRET in talin-HP-1973-expressing cells is similar when cells are analyzed on fibronectin (FN)- and poly-L-Lysine (pLL)-coated glass slides (n = 45, 31, 31, 16 cells, pooled from five independent experiments). Talin-HP-Con cells display marginally higher FRET values on account of slightly increased intermolecular FRET[9]. (**b**) Live-cell FLIM analysis of FL-TSM-based talin sensors reveals significant tension at aa 1973 (n = 24, 59, 25, 17 cells, pooled from two to five independent experiments). (**c**) F40-TSM-based talin constructs confirmed decreased tension at aa 1973, but differences to pLL conditions were smaller (n = 41, 55, 26, 27 cells, pooled from four independent experiments). (**d**) Representative ratiometric FRET images of cells expressing talin-FL-447, talin-FL-1973, and talin-FL-Con; scale bar, 20 µm. (**e**) Mean FA-FRET as determined by ratiometric imaging (n = 26, 26, 26 cells, pooled from four independent experiments). (**a**–**c**,**e**: KS test; ***, $P < 0.001$; **, $P < 0.01$; *, $P < 0.05$; n.s., not significant, $P > 0.05$).

reduced, while forces at aa 1973 were lowered to control levels (**Fig. 4b,c** and **Supplementary Fig. 7b–d**).

As myosin-II activity is often positively correlated with FA size[25], we speculated that talin may experience mechanical tension at aa 1973 predominantly in large, mature FAs that are connected to contractile f-actin bundles. To test this hypothesis, we seeded cells onto two different micropatterned surfaces, upon which cells adapted very distinct morphologies (**Fig. 4d,e** and **Supplementary Fig. 8**). On triangular patterns cells displayed large and elongated FAs, strong peripheral stress fibers, and high myosin-II activity as indicated by myosin light chain phosphorylation (**Fig. 4d**). On disc-shaped micropatterns, cells formed mostly small FAs and displayed few stress fibers and little myosin-II activation (**Fig. 4e**). Consistent with our hypothesis, forces at aa 1973 were low in FAs of cells on round substrates but increased in large FAs of cells on triangular patterns (**Fig. 4f,g** and **Supplementary Fig. 9**).

The talin-1 tension gradient is vinculin dependent and sensitive to extracellular rigidity

We then tested how the presence of talin's binding partner vinculin affects the intramolecular tension gradient by expressing talin-FL-447 and talin-FL-1973 in vinculin-positive ($Vin^{f/f}$) or vinculin-deficient ($Vin^{-/-}$) fibroblasts. As expected, we observed different talin force values at aa 447 and aa 1973 in $Vin^{f/f}$ cells, similar to experiments in reconstituted $Tln1^{-/-}Tln2^{-/-}$ cell lines. By contrast, FRET efficiency differences were virtually absent in $Vin^{-/-}$ cells (**Fig. 4h**) because forces at aa 447 were markedly reduced. Thus, the intramolecular talin tension gradient is vinculin dependent.

Tension at aa 1973 was insensitive to vinculin expression, and this indicated that the low forces observed at the C-terminal region of talin are mediated by ABS3. To provide direct evidence for this, we generated talin-ABS3-deletion constructs and analyzed

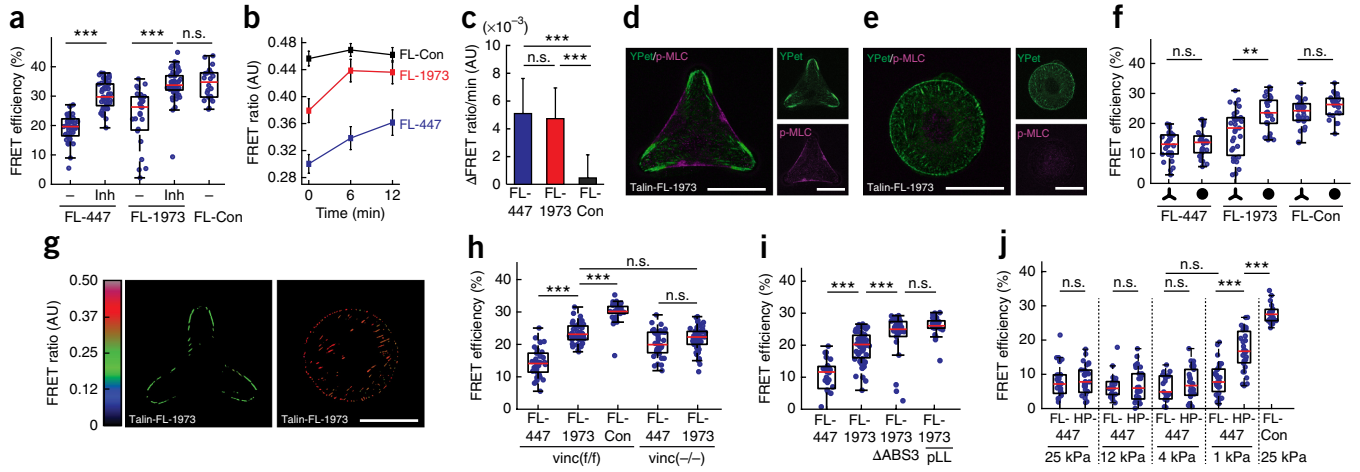

Figure 4 | Regulation of the intramolecular force gradient across talin. (**a**) FRET efficiencies in FAs of cells expressing distinct talin constructs before and after Y-27632 treatment (n = 49, 51, 37, 54, 22 cells, pooled from three independent experiments). (**b**) Mean FRET ratio change after Y-27632 treatment (n = 14, 16, 11 cells, pooled from five experiments). (**c**) Evaluation of FRET ratio change per minute reveals significant increase in FRET after Y-27632 treatment for talin-FL-447 and talin-FL-1973; FRET in talin-FL-Con cells is unaffected. (**d**,**e**) Representative cell seeded on a triangular or disc-shaped micropatterned substrate. Phosphorylated myosin light chain (p-MLC) signal is shown in magenta; the talin signal is displayed in green. (**f**) FA-FRET efficiencies in cells seeded on micropatterned substrates (n = 32, 27, 35, 27, 30, 23 cells, pooled from four experiments). (**g**) Representative FRET ratio image of a talin-FL-1973 cell seeded on a triangular or disc-shaped pattern. (**h**) Live-cell FRET analysis of talin-FL-447 and talin-FL-1973 expressed in $Vinc^{f/f}$ or $Vinc^{-/-}$ fibroblasts (n = 34, 42, 36, 40, 51 cells, pooled from four independent experiments). (**i**) Deletion of ABS3 leads to loss of tension at aa 1973 (talin-FL-1973-ΔABS3 n = 34, pooled from three experiments; other data as in **Fig. 3b**). (**j**) Live-cell FLIM analysis of cells expressing talin-FL-447 and talin-FL-1973 on FN-coated substrates with distinct rigidities (n = 29, 29, 20, 27, 19, 26, 31, 31, 20 cells, pooled from six independent experiments). (**a**, **c**, **f**, **h**–**j** KS test; ***, $P < 0.001$; *, $P < 0.05$; n.s., not significant, $P > 0.05$). Scale bars, 20 µm.

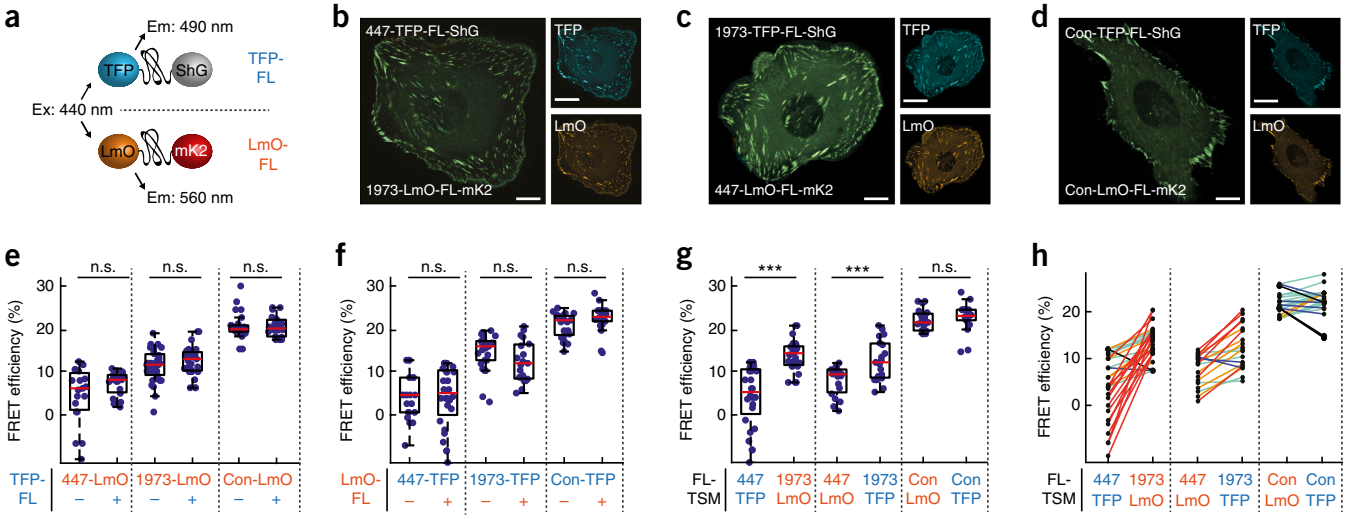

Figure 5 | Tension sensor multiplexing. (**a**) Schematic illustration of two orthogonal TSMs; both constructs are excitable by 440-nm light, but their emission wavelengths can be separated spectrally. (**b**,**c**) Stable coexpression of two orthogonal FL-based talin sensors (talin-FL-447 and talin-FL-1973); the constructs display indistinguishable subcellular localization. (**d**) Stable coexpression of two orthogonal talin control constructs (talin-FL-Con) showing identical subcellular localization. (**e**) Live-cell FLIM analysis of the LmO-FL-based talin sensors in the presence or absence of TFP-FL-based talin sensors (n = 19, 19, 35, 29, 26, 22 cells, pooled from six independent experiments). (**f**) Live-cell FLIM analysis of the TFP-FL-based talin sensors in the presence or absence of the LmO–FL construct (n = 19, 29, 26, 19, 27, 22 cells, pooled from six independent experiments). (**g**) Live-cell, dual-color FLIM confirms the intramolecular tension gradient across talin-1 (n = 29, 19, 22 cells, pooled from six independent experiments). (**h**) Visualization of corresponding FRET efficiency values from individual cells (same data as shown in **g**). Red colors indicate a steep tension differential; black colors indicate its absence. (**e**,**f**, KS test; **g**, paired t-test; ***, $P < 0.001$; n.s., not significant, $P > 0.05$). Scale bars, 20 µm.

them in Tln1$^{-/-}$Tln2$^{-/-}$ cells. As previously observed[26], ABS3-deficient constructs only partially rescued the spreading defect of talin-deficient cells (**Supplementary Fig. 10**), and we focused the analysis on cells that did form FAs. These experiments revealed strongly increased FRET values, which suggested that an intact ABS3 is required for tension at aa 1973 (**Fig. 4i**). Finally, we investigated how talin mechanics are affected by the stiffness of the extracellular substrate. While forces at aa 1973 remained rather constant and comparable to those measured on glass slides, talin-HP-447 experiments revealed reduced tension at N-terminal parts of the rod domain on soft, 1-kPa surfaces (**Fig. 4j** and **Supplementary Fig. 11**).

Together, these experiments demonstrate that the intramolecular tension gradient across talin-1 can be modulated at the N- and C-terminal parts of the talin rod domain. The tension differential is controlled by f-actin binding and myosin activity; it is vinculin dependent, and it is sensitive to the stiffness of the extracellular substrate.

Orthogonal tension sensor module pairs allow tension sensor multiplexing by dual-color FLIM

A limitation of the described experiments was that the two biosensors were analyzed in parallel, but not within the same cell. We therefore generated two orthogonal TSMs, called multiplexing (MPX) TSMs, that could be imaged simultaneously using single-excitation wavelength, dual-color FLIM[27]. For the first MPX-TSM, we used mTFP1 as a donor and the dark quencher ShadowG as an acceptor[27,28]; for the second module, we combined the long Stokes shift (LSS) fluorophore LSSmOrange with mKate2 (refs. 27,29; **Fig. 5a**). Evaluation of the individual fluorophores and MPX-TSMs revealed a narrow fluorescence lifetime distribution of mTFP1 and LSSmOrange and similar, albeit not identical, FRET efficiencies of the respective MPX-TSMs (**Fig. 5** and **Supplementary Fig. 12a**). Coexpression of the corresponding multiplexing talin-FL-447, talin-FL-1973, and control constructs in Tln1$^{-/-}$Tln2$^{-/-}$cells demonstrated normal subcellular localization (**Fig. 5b–d**). Consistent with the experiments above, we observed low FRET values for talin-FL-447 and higher transfer rates for talin-FL-1973 constructs. Notably, results did not depend on the choice of TSM or whether cells expressed just one or both constructs, demonstrating that the MPX-TSMs can indeed be used orthogonally (**Fig. 5e,f** and **Supplementary Fig. 12b**). Simultaneous evaluation by dual-color FLIM confirmed these observations. As two distinct fluorophore pairs were used, differences in FRET efficiency were not identical, but the overall tendencies were consistently reproduced (**Fig. 5g,h**). Of note, some lifetime values were unusually high, and this resulted in negative FRET values, probably a consequence of reduced FRET efficiency in MPX-TSM constructs and the normal spread in the data. The negative FRET efficiencies may also indicate less efficient folding or chromophore maturation in the employed fluorophores; thus, future studies may be directed toward optimizing orthogonal FRET pairs with increased FRET efficiencies and efficient maturation rates. Yet, the observations were consistent with the experiments in which TSMs were analyzed separately (**Figs. 3** and **4**) and so provided direct evidence for an intramolecular force gradient across talin.

Calculating the fraction of mechanically engaged talin molecules using FL-TSM

Given the virtually digital nature of FL-TSM (**Fig. 1**) as well as the observed differences between talin-FL-447 and talin-FL-1973 (**Fig. 3**), the data indicated that only a fraction of FA-localized talin molecules experiences mechanical forces of more than 3 pN at talin's C-terminal region. To estimate this fraction, we

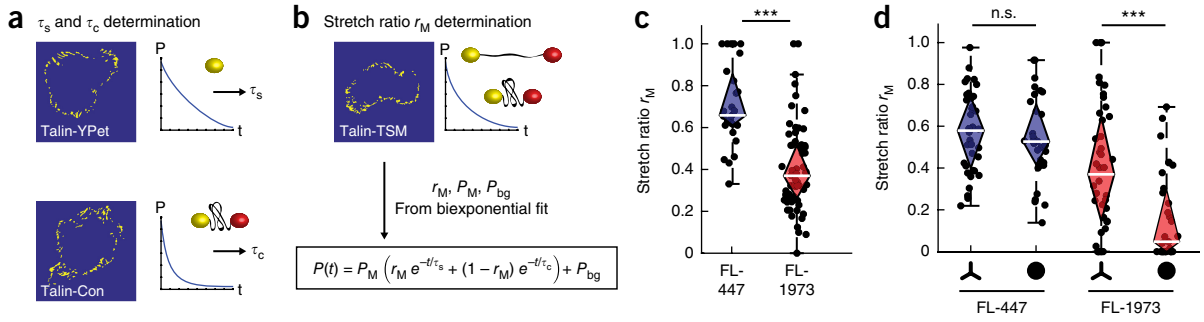

Figure 6 | Estimating the molecular engagement ratio. (**a**) Fluorescence lifetimes of stretched (s) and closed (c) sensor molecules τ_s and τ_c can be experimentally determined from cells expressing talin-YPet and talin-Con. (**b**) The biexponential fit of the photon count $P(t)$ can be performed with τ_s and τ_c and used to calculate the photon count rates of biosensor (P_M) and background (P_{bg}) as well as the molecular stretch ratio r_M. (**c**) Evaluating the molecular engagement ratio using FLIM data from cells expressing talin-FL-447 and talin-FL-1973 (same experiment as in **Fig. 3b**; n = 27, 64 cells, pooled from two to five independent experiments). (**d**) Evaluating the molecular engagement ratio using the FLIM data shown in **Figure 4f** (n = 36, 31, 42, 31 cells, pooled from four independent experiments). (**c**,**d**: Mann–Whitney U test; ***, $P < 0.001$; n.s., not significant, $P > 0.05$).

determined the fluorescence donor lifetime of FL-TSM in the stressed state (corresponding to the donor-only lifetime) and unstressed state (lifetime of talin-Con), and we used these values when fitting a biexponential decay function to the talin-FL-447 and talin-FL-1973 lifetime data (**Fig. 6a,b**). An estimation of the minimum amount of photon counts necessary for statistically reliable calculations indicated that about 10,000 photons are required (**Supplementary Fig. 13**), a number that is surpassed in our experiments. Consistent with the assumption that the FL-based sensors essentially exist in two states (high FRET and no FRET), the data were well described by the biexponential function, as indicated by the Pearson's chi-squared test (talin-FL-447, ~0.43; talin-FL-1973, ~0.46).

Evaluation of FLIM data sets from adherent cells showed that about 70% of talin molecules are exposed to tension at aa 447, while only about 40% of talin molecules experience mechanical loads at aa 1973 (**Fig. 6c**). As expected, evaluation of micropatterning data sets demonstrated that the fraction of molecules bearing tension at aa 1973 is higher in cells on triangular patterns as compared to conditions of low intracellular contractility (**Fig. 6d**). Together, the results imply that cells not only modulate the amount of force per molecule but also adjust the number of talin molecules mechanically engaged through ABS3.

DISCUSSION

This study establishes a powerful method to quantify molecular pN-scale forces within cells. FL-TSM benefits from a sharp force response that allows quantitative interpretation of ensemble measurements in the low-pN force regime at 3–5 pN. In comparison with the widely used F40-based construct[8], FL-TSM exceled because of an improved FRET efficiency at zero-force and enlarged contour length increase under tension, resulting in an increased dynamic range. Most importantly, the near-digital force response characteristic of FL-TSM can be harnessed to estimate the fraction of mechanically engaged molecules from FLIM-based ensemble measurements.

In addition, we established a method to quantify two intracellular tension sensor constructs simultaneously. The tension sensor multiplexing technique can be used to determine pN-scale forces across different domains of individual proteins, but it should be particularly valuable for studying the molecular mechanics of two distinct molecules that may or may not reside in the same subcellular structure.

When applied to talin, these tools revealed an intramolecular tension gradient characterized by comparatively high forces of more than 7 pN at the N-terminal part of the talin rod domain and lower tension at the C-terminal talin region between ABS2 and ABS3. We thus conclude that the previously described force-induced vinculin binding is likely to occur primarily at N-terminal regions of the talin rod domain[30,31], and it will be interesting to study how the described tension differential across talin affects the overall mechanics of cell adhesion. The implementation of a tension gradient into the molecular clutch model of FAs[32,33] or similar theoretical frameworks[34] seems especially important, because the presented data demonstrate that integrin force transduction through talin is regulated on at least two levels. First, talin molecules are exposed to a range of forces that are typically above 7 pN in the N-terminal part of the molecule and lower than 7 pN in C-terminal regions. Second, cells tune how many talin molecules are mechanically engaged. Both modes of regulation are sensitive to vinculin binding, f-actin association, and myosin-II activity; and the recent identification of additional talin interactors suggests additional layers of modulation[35,36].

Altogether, the data show that experimentally addressing molecular mechanisms of force transduction requires a set of calibrated tension sensors to investigate the whole range of forces experienced by molecules in cells as well as advanced data analysis tools to study proteins' engagement ratio. The methods described above should be valuable for these studies and adaptable to a wide range of research questions.

METHODS

Methods, including statements of data availability and any associated accession codes and references, are available in the online version of the paper.

Note: Any Supplementary Information and Source Data files are available in the online version of the paper.

ACKNOWLEDGMENTS

The authors thank R. Fässler (MPI of Biochemistry, Department of Molecular Medicine) for providing talin-deficient cells, C. Schweizer for help with programming, the MPIB core facility for technical support, and the Microscopy Rennes Imaging Centre (MRic), where multiplex FRET experiments were

performed. C.G. is supported by the German Research Council (DFG, GR3399/5-1 and GR3399/6–1), the Collaborative Research Centre SFB863 (B9), and the Max Planck Förderstiftung. M.R. acknowledges support from the German Research Council through the Collaborative Research Centre SFB863 (A2), and M.T. acknowledges funding by the Ligue Régionale Contre le Cancer. A.F. was supported by the Boehringer Ingelheim Fonds.

AUTHOR CONTRIBUTIONS

P.R. generated expression constructs and cell lines, performed experiments, wrote data analysis software, and analyzed data. A.W. performed calibration experiments, data analysis, and theoretical modeling with A.M. under the supervision of M.R. A.-L.C. wrote FLIM analysis software and advanced data analysis algorithms with assistance from B.S. A.F. generated tools and performed initial experiments. M.T. provided multiplexing fluorophores and supervised dual-colour FLIM experiments and data analysis. C.G. purified TSMs, coordinated experiments, and wrote the manuscript with input from all authors.

COMPETING FINANCIAL INTERESTS

The authors declare no competing financial interests.

1. Petridou, N.I., Spiró, Z. & Heisenberg, C.P. Multiscale force sensing in development. *Nat. Cell Biol.* **19**, 581–588 (2017).
2. Vogel, V. & Sheetz, M. Local force and geometry sensing regulate cell functions. *Nat. Rev. Mol. Cell Biol.* **7**, 265–275 (2006).
3. Gordon, W.R. *et al.* Mechanical allostery: evidence for a force requirement in the proteolytic activation of notch. *Dev. Cell* **33**, 729–736 (2015).
4. Rognoni, L., Stigler, J., Pelz, B., Ylänne, J. & Rief, M. Dynamic force sensing of filamin revealed in single-molecule experiments. *Proc. Natl. Acad. Sci. USA* **109**, 19679–19684 (2012).
5. del Rio, A. *et al.* Stretching single talin rod molecules activates vinculin binding. *Science* **323**, 638–641 (2009).
6. Buckley, C.D. *et al.* Cell adhesion. The minimal cadherin-catenin complex binds to actin filaments under force. *Science* **346**, 1254211 (2014).
7. Finer, J.T., Simmons, R.M. & Spudich, J.A. Single myosin molecule mechanics: piconewton forces and nanometre steps. *Nature* **368**, 113–119 (1994).
8. Grashoff, C. *et al.* Measuring mechanical tension across vinculin reveals regulation of focal adhesion dynamics. *Nature* **466**, 263–266 (2010).
9. Austen, K. *et al.* Extracellular rigidity sensing by talin isoform-specific mechanical linkages. *Nat. Cell Biol.* **17**, 1597–1606 (2015).
10. Wang, X. & Ha, T. Defining single molecular forces required to activate integrin and notch signaling. *Science* **340**, 991–994 (2013).
11. Zhang, Y., Ge, C., Zhu, C. & Salaita, K. DNA-based digital tension probes reveal integrin forces during early cell adhesion. *Nat. Commun.* **5**, 5167 (2014).
12. Morimatsu, M., Mekhdjian, A.H., Chang, A.C., Tan, S.J. & Dunn, A.R. Visualizing the interior architecture of focal adhesions with high-resolution traction maps. *Nano Lett.* **15**, 2220–2228 (2015).
13. Freikamp, A., Cost, A.L. & Grashoff, C. The piconewton force awakens: quantifying mechanics in cells. *Trends Cell Biol.* **26**, 838–847 (2016).
14. Borghi, N. *et al.* E-cadherin is under constitutive actomyosin-generated tension that is increased at cell–cell contacts upon externally applied stretch. *Proc. Natl. Acad. Sci. USA* **109**, 12568–12573 (2012).
15. Chang, C.W. & Kumar, S. Vinculin tension distributions of individual stress fibers within cell–matrix adhesions. *J. Cell Sci.* **126**, 3021–3030 (2013).
16. Krieg, M., Dunn, A.R. & Goodman, M.B. Mechanical control of the sense of touch by β-spectrin. *Nat. Cell Biol.* **16**, 224–233 (2014).
17. Paszek, M.J. *et al.* The cancer glycocalyx mechanically primes integrin-mediated growth and survival. *Nature* **511**, 319–325 (2014).
18. Hernández-Varas, P., Berge, U., Lock, J.G. & Strömblad, S. A plastic relationship between vinculin-mediated tension and adhesion complex area defines adhesion size and lifetime. *Nat. Commun.* **6**, 7524 (2015).
19. Sun, Z., Guo, S.S. & Fässler, R. Integrin-mediated mechanotransduction. *J. Cell Biol.* **215**, 445–456 (2016).
20. Fang, J. *et al.* Forced protein unfolding leads to highly elastic and tough protein hydrogels. *Nat. Commun.* **4**, 2974 (2013).
21. Dietz, H. & Rief, M. Exploring the energy landscape of GFP by single-molecule mechanical experiments. *Proc. Natl. Acad. Sci. USA* **101**, 16192–16197 (2004).
22. Critchley, D.R. Biochemical and structural properties of the integrin-associated cytoskeletal protein talin. *Annu. Rev. Biophys.* **38**, 235–254 (2009).
23. Calderwood, D.A., Campbell, I.D. & Critchley, D.R. Talins and kindlins: partners in integrin-mediated adhesion. *Nat. Rev. Mol. Cell Biol.* **14**, 503–517 (2013).
24. Mehlich, A., Austen, K., Ringer, P., Rief, M. & Grashoff, C. Evaluation of molecular tension sensors using single-molecule force spectroscopy and live cell FRET imaging. *Protocol Exchange* http://dx.doi.org/10.1038/protex.2015.095 (2015).
25. Geiger, B., Spatz, J.P. & Bershadsky, A.D. Environmental sensing through focal adhesions. *Nat. Rev. Mol. Cell Biol.* **10**, 21–33 (2009).
26. Atherton, P. *et al.* Vinculin controls talin engagement with the actomyosin machinery. *Nat. Commun.* **6**, 10038 (2015).
27. Demeautis, C. *et al.* Multiplexing PKA and ERK1&2 kinases FRET biosensors in living cells using single excitation wavelength dual colour FLIM. *Sci. Rep.* **7**, 41026 (2017).
28. Murakoshi, H., Shibata, A.C.E., Nakahata, Y. & Nabekura, J. A dark green fluorescent protein as an acceptor for measurement of Förster resonance energy transfer. *Sci. Rep.* **5**, 15334 (2015).
29. Shcherbakova, D.M., Hink, M.A., Joosen, L., Gadella, T.W.J. & Verkhusha, V.V. An orange fluorescent protein with a large Stokes shift for single-excitation multicolor FCCS and FRET imaging. *J. Am. Chem. Soc.* **134**, 7913–7923 (2012).
30. Yao, M. *et al.* The mechanical response of talin. *Nat. Commun.* **7**, 11966 (2016).
31. Haining, A.W.M., von Essen, M., Attwood, S.J., Hytönen, V.P. & Del Río Hernández, A. All subdomains of the talin rod are mechanically vulnerable and may contribute to cellular mechanosensing. *ACS Nano* **10**, 6648–6658 (2016).
32. Chan, C.E. & Odde, D.J. Traction dynamics of filopodia on compliant substrates. *Science* **322**, 1687–1691 (2008).
33. Elosegui-Artola, A. *et al.* Mechanical regulation of a molecular clutch defines force transmission and transduction in response to matrix rigidity. *Nat. Cell Biol.* **18**, 540–548 (2016).
34. Besser, A. & Safran, S.A. Force-induced adsorption and anisotropic growth of focal adhesions. *Biophys. J.* **90**, 3469–3484 (2006).
35. Bouchet, B.P. *et al.* Talin-KANK1 interaction controls the recruitment of cortical microtubule stabilizing complexes to focal adhesions. *eLife* **5**, e18124 (2016).
36. Sun, Z. *et al.* Kank2 activates talin, reduces force transduction across integrins and induces central adhesion formation. *Nat. Cell Biol.* **18**, 941–953 (2016).

ONLINE METHODS

Protocol. A detailed protocol on single-molecule force spectroscopy calibration of FRET-based tension sensors and time-correlated single-photon counting (TCSPC)-FLIM analysis is available in *Protocol Exchange*[24].

Antibodies and reagents. The following antibodies and reagents were used: anti-vinculin (hVIN-1) (V9131, Sigma; IF 1:200), anti-paxillin (610051, BD Transduction L.; IF 1:400), anti-p-MLC (Ser19) (3671, NEB; IF 1:50), anti-mouse IgGAlexa Fluor-405 (A31553; IF 1:400; Thermo Fisher Scientific), Alexa Fluor-647 phalloidin (A22287; IF 1:200; Thermo Fisher Scientific), poly-L Lysine (P4707; Sigma), fibronectin (341631; Calbiochem), puromycin (P8833; Sigma), hygromycin B (H3274; Sigma). Micropatterned substrates (10-011-00-18, 10-002-10-18; CYTOO), softview Easy Coat substrate dishes: 1.0, 4.0, 12 and 25 kPa dishes (Matrigen), Y-27632 (Y0505, Sigma).

Plasmid construction. The cDNA of TSMs as well as talin biosensors was constructed according to our published protocols[37]. Plasmids will be distributed through AddGene (http://www.addgene.org/). Complete plasmid information is available through Genbank using the following accession codes: HP35-TSM (MF685010), F40-TSM (MF685012) and FL-TSM (MF685013).

Generation of FL-TSM. To generate the FL-based TSM, restriction sites were added to the cDNA of YPet (aa 1–228) (5Xho/3′BamHI) and mCherry (5′BamHI/3′NotI) by polymerase chain reaction (PCR), and PCR products were combined in pBluescript SK(+). The cDNA sequence encoding for the FL peptide (MGE FDI RFR TDD DEQ FEK VLK EMN RRA RKD AGT VTY TRD GND FEI RIT GIS EQN RKE LAK EVE RLA KEQ NIT VTY TER GSL E) was synthesized (5′-ATG GGC GAG TTT GAC ATC CGG TTT CGG ACT GAT GAC GAC GAA CAG TTC GAG AAA GTG CTG AAG GAG ATG AAT CGT CGA GCC AGA AAG GAT GCT GGA ACT GTG ACC TAC ACA AGG GAT GGG AAT GAC TTC GAG ATT CGC ATT ACC GGC ATA AGC GAG CAA AAC CGC AAA GAA CTG GCC AAA GAG GTT GAA AGG CTT GCA AAG GAA CAG AAC ATC ACA GTC ACG TAT ACC GAG AGA GGT TCC CTC GAA-3′; Eurofins Genomics) and inserted between the fluorophore cDNAs using 5′BglII/3′BamHI overhangs; this FL-TSM cDNA was then transferred into the pLPCX expression plasmid (Clontech). For single-molecule force spectroscopy calibration, terminal cysteine residues to allow attachment of DNA oligonucleotides and a histidine tag for protein purification were added. mTFP1–ShadowG and LSSmOrange–mKate2 constructs were assembled in pLPCX by standard PCR and Gibson assembly (Gibson Assembly Cloning Kit; New England Biolabs). All sequences were confirmed by DNA sequencing (Eurofins Genomics).

Generation of talin expression constructs. Talin-TSM-447 and control cDNAs were generated according to the previously published strategy[9,37]. To insert the respective TSM at aa 1973 of talin-1 (i.e., talin-TSM-1973 constructs), we generated 5′XhoI/3′NotI restriction sites after aa 1973 using standard PCR and Gibson assembly. cDNAs were assembled in the pLPCX or pLHCX vectors, and the correct sequence of constructs was confirmed by DNA sequencing. C-terminal fusion constructs were cloned by assembling the PCR products of the respective TSM or fluorophores using 3′ClaI/5′NotI restriction sites that were inserted after the cDNA of talin-1.

FL-sensor module expression and purification. For FL-TSM and F40-TSM protein expression, HEK293 cells were transfected by $CaPO_4$-precipitation. After 48 h, cells were detached, resuspended in hypotonic lysis buffer (20 mM Tris, 2 mM $MgCl_2$, pH 7.4), incubated for 20 min on ice, and then lysed with a Dounce homogenizer. Cell lysates were cleared by 10 min centrifugation at 4 °C and purified by metal ion affinity chromatography (His-Trap; GE Healthcare), followed by ion-exchange chromatography (Sephadex; GE Healthcare). Purified samples were then concentrated to about 20 µM by membrane ultrafiltration (Vivaspin; GE Healthcare) and stored at −80 °C in phosphate buffered saline (PBS; pH 6.7) supplemented with 0.2 mM Tris-2-carboxyethylphosphine (TCEP) to avoid oligomerization via terminal cysteines.

Assembling protein–DNA conjugates. To attach DNA handles to the purified FL-TSM, lyophilized maleimide-modified single-stranded (ss) DNA oligonucleotides were dissolved in PBS (pH 6.7) and incubated with the purified protein for 1 h at room temperature (RT). Unreacted components were removed using metal ion affinity chromatography (His-Trap, GE Healthcare) and size-exclusion chromatography (Superdex 200; GE Healthcare). Next, 185 nm long, double stranded (ds) DNA handles (λ-DNA; NEB) carrying a biotin or a digoxigenin modification and a complementary ss overhang were hybridized with the protein–DNA chimera. The sample was then prepared by incubating streptavidin-coated 1 µm sized silica beads (Bangs Laboratories) with the protein–DNA chimeras for 5 min in PBS (pH 7.4). Functionalized antidigoxigenin silica beads were added subsequently; glucose oxidase and catalase were used as an oxygen scavenger system. Finally, one of each bead species was caught in the two traps and moved in close proximity to allow tether formation. Then the protein was unfolded and refolded in stretch–relax cycles by periodically changing the trap distance with constant velocity. For equilibrium measurements, traps held at constant distance and bead positions were recorded during unfolding and refolding.

Single-molecule force spectroscopy calibration. Single-molecule force spectroscopy measurements were performed on a custom-built, dual-trap optical tweezers setup with back focal plane detection as described before[24,38]. In short, excitation light of a diode pumped Nd:YVO_4 laser (Spectra Physics) was split into two beams by a polarizing beam splitter. A piezo mirror stage (Mad City Labs) was used to laterally displace one beam in the sample plane. A second polarizing beam splitter was installed to combine and focus both beams onto the sample plane by a microscope objective (63×/1.20 W Corr, C-Apochromat; Zeiss). To monitor bead displacement, the forward-scattered light was collected by an identical objective, and the back focal plane was imaged by quadrant photo diodes (QP154-Q-HVSD, First Sensor). The calibration of trap stiffness and detector sensitivity was performed as described earlier[39]; the signals were detected at 150 kHz and averaged to 30 kHz before storage. To improve resolution, analysis was performed on the difference of the two signals as described[40].

doi:10.1038/nmeth.4431

Calibration data analysis. Singe-molecule data analysis followed the procedures described before[9,24]. To extract the mechanical properties of the dsDNA handles, an extensible worm-like chain model (eWLC)[41] was fit to the measured force–extension data according to equation (1)

$$F_{\mathrm{eWLC}}(x_{\mathrm{DNA}}, L_{\mathrm{DNA}}, p_{\mathrm{DNA}}, K) = \frac{k_B T}{p_{DNA}}\left[\frac{1}{4\left(1-\frac{x_{\mathrm{DNA}}}{L_{\mathrm{DNA}}}+\frac{F_{\mathrm{WLC}}}{K}\right)^2}+\frac{x_{\mathrm{DNA}}}{L_{\mathrm{DNA}}}-\frac{F_{\mathrm{WLC}}}{K}-\frac{1}{4}\right] \quad (1)$$

where x_{DNA} is the measured extension of the DNA tether; and L_{DNA}, p_{DNA}, and K are fit parameters that correspond to the contour length, the persistence length and the stretch modulus of the dsDNA handles. The temperature inside the measurement chamber was assumed to be T = 303 K. In our experiments, the average fit persistence length was 16.3 nm, the stretch modulus between 150–300 pN, and the averaged fit contour length 362.6 nm, values consistent with the expected length of 370 nm of the two dsDNA handles. For extracting the mechanical response parameters of the protein, a basic worm-like chain model was fitted in series with the eWLC to the data according to equation (2):

$$F_{\mathrm{WLC}}(x_p, L_p, p_p) = \frac{k_B T}{p_p}\left[\frac{1}{4\left(1-\frac{x_p}{L_p}\right)^2}+\frac{x_p}{L_p}-\frac{1}{4}\right] \quad (2)$$

where x_p is the measured protein extension, and L_p is the fitted protein contour length gain. The experimentally determined contour length gain was 27.4 ± 2.6 nm, which is in agreement with previously published data[20].

With the assumption that the dsDNA handles are at equilibrium with the unfolded protein, the acting forces can be set equal: $F_{\mathrm{eWLC}} = F_{\mathrm{WLC}} = F$. Thus, the total extension of the tether can be expressed according to equation (3):

$$x_{\mathrm{tether}}(F) = x_{\mathrm{DNA}}(F) + x_p(F)\cdot P_{\mathrm{unf}}(F) \quad (3)$$

$x_{\mathrm{DNA}}(F)$ and $x_p(F)$ being the extension of DNA handles and protein, and $P_{\mathrm{unf}}(F)$ being the unfolding probability. Inversion yields the force–extension correlation for the entire tether.

In the low-pN force regime, optical traps can be assumed to have a harmonic potential and follow the Hookean law according to

$$F(d) = k_{\mathrm{eff}}\cdot\langle x_{\mathrm{B}}\rangle \quad (4)$$

where

$$k_{\mathrm{eff}} = \left(\frac{1}{k_1}+\frac{1}{k_2}\right)^{-1}$$

is the effective trap stiffness, and $x_B = x_{B1} + x_{B2}$ the displacement of the two beads from the respective trap centers. The extension of the tethered construct x_{tether} can be calculated by subtracting the sum of bead displacement $x_{B1} + x_{B2}$ and twice the bead diameter R from the distance of the trap centers d

$$x_{\mathrm{tether}} = d - (2R + x_{B1} + x_{B2}) \quad (5)$$

The mean displacement can be expressed as

$$\langle x_B\rangle = \int_{-\infty}^{+\infty} dx_B x_B \cdot p(x_B) \quad (6)$$

where $p(x_B)$ is the Boltzmann probability distribution

$$p(x_B) = \frac{1}{Z}\cdot\exp\left(-\frac{H(x_B)}{k_B T}\right) \quad (7)$$

with the canonical partition function

$$Z = \int_{-\infty}^{+\infty} dx_B \exp\left(-\frac{H(x_B)}{k_B T}\right)$$

and the Hamiltonian

$$H(x,i) = (1-i)\cdot\Delta G^0 + \frac{1}{2}k_{\mathrm{eff}}x^2 + \int_0^{d-x} dx_{\mathrm{tether}} F_{\mathrm{tether}}(i\cdot L_p, x_{\mathrm{tether}} \quad (8)$$

with i representing the number of unfolded subunits, and F_{tether} being the inversion of equation (3). As FL-TSM is a two-state folder, $i \in \{0,1\}$, the force–distance relation given by equation (4) is hence described by

$$F(d) = \frac{k_{\mathrm{eff}}}{\int_{-\infty}^{+\infty} dx \sum_{i=0}^{1}\exp\left(\frac{H(x,i)}{k_B T}\right)}\cdot\int_{-\infty}^{+\infty} dx\, x\cdot\sum_{i=0}^{1}\exp\left(\frac{H(x,i)}{k_B T}\right) \quad (9)$$

The force–distance relation (equation (9)) depends only on the Hamiltonian $H(x,i)$ (equation (8)). Thus, the free parameters are x_{tether}, which is a directly measured quantity; L_p, which is obtained by fitting constant velocity traces according to equation (2); and the folding free energy ΔG^0.

Free energy calculation from constant distance measurements. In contrast to our previous study[9], ΔG^0 was determined from passive, constant distance measurements. In this mode, the trap distance is kept constant, and iterative unfolding and refolding events are observed over time. A hidden Markov (HM) analysis was performed on the raw data as described before[42] to assign a state to each recorded data point. The time trajectories were coarse grained in 100 bins to facilitate numerical calculations. To initialize the HM analysis, emission probabilities, which reflect the deflection distribution of each state, were retrieved from Gaussian fits to a histogram of the respective time trajectory.

The force-dependent folding and unfolding probabilities $P_{\mathrm{fold}}(F)$ and $P_{\mathrm{unf}}(F)$ (**Fig. 1d** and **Supplementary Fig. 2b**) and thus the relative amount of time of the FL-TSM spent in the folded and unfolded states were sampled by recording traces at different trap distances (**Fig. 1c**). The total energy in the system G_i (F_i) at a given force F_i in state i is described by equation (10):

$$G_i(F_i) = G_i^0 + G_i^{\mathrm{device}} = G_i^0 + G_i^{\mathrm{bead}}(F_i) + G_i^{\mathrm{DNA}}(F_i) + G_i^p(F_i) \quad (10)$$

where G_i^0 is the free energy of the protein in state i;

$$G_i^{\text{bead}}(F_i)=\frac{1}{2}x_B(F_i)\bullet F_i$$

the energy stored in bead deflection x_B. G_i^{DNA} and G_i^p correspond to the energy stored in the stretched DNA and polypeptide chain. The free energy difference between two states i and j is given by

$$\Delta G_{ij}\left(F_i,F_j\right)=\Delta G_{ij}^0+\Delta G_{ij}^{\text{device}}\left(F_i,F_j\right) \quad (11)$$

The free energy difference of the protein states ΔG_{ij}^0 was obtained by performing a global fit to the force-dependent probabilities according to equation (12):

$$P_i(F)=\frac{1}{1+\sum_{i\neq j}\exp\left(-\frac{\Delta G_{ij}^0}{k_BT}+\frac{\Delta G_{ij}^{\text{device}}\left(F,F_j\right)}{k_BT}\right)} \quad (12)$$

The obtained free energy difference ΔG_0 for FL-TSM was 4.3 ± 1 k_BT.

Calculating the FRET efficiency-force correlation. The FRET–force correlation, depicted in **Figure 1f**, can be calculated by

$$E_{\text{FRET}}(F)=E_{\text{FRET}}\left(x_p^{\text{fold}}\right)\cdot P_{\text{fold}}(F)+E_{\text{FRET}}\left(x_{\text{p}}^{\text{unf}}(F)\right)\cdot P_{\text{unf}}(F) \quad (13)$$

$E_{\text{FRET}}\left(x_p^{\text{fold}}\right)$ corresponds to the FRET efficiency when the sensor protein is still folded (**Supplementary Fig. 2a,c**). This FRET efficiency was about 29% in our live-cell experiments (**Fig. 1i**), which corresponds to a fluorophore separation distance of approximately 6.7 nm.

Calculating the tension sensor model sensitivity. The sensitivity of the TSMs is defined as the absolute slopes of the FRET–force relation (equation (13)). Obtained sensitivity curves were multiplied with a normalization constant, which sets the maximum of the first reported TSM, F40-TSM, equal to one. The full width at half maximum of each curve serves as a measure of the digital nature of the sensor (**Fig. 1g**).

Single-molecule measurements with the F40-TSM. For calibration of F40-TSM, single-molecule force experiments were conducted as with FL-TSM, meaning DNA handles were attached to N and C termini, and stretch–relax traces were recorded. As expected, no distinct unfolding event could be observed, owing to the nano-spring-like properties of the F40 peptide[8] (**Supplementary Fig. 1a,b**). Therefore, at the end of each experiment, the construct was stretched to 40–55 pN to unfold the fluorophores and to ensure that a functional F40-TSM construct had been trapped (**Supplementary Fig. 1a**). The additional length gain arising from stretching the F40 peptide can be measured indirectly. The contour length of the entire tether of the F40-TSM calibration construct (i.e., the F40-TSM protein plus the DNA handles) was compared to the contour length of the entire tether of the folded FL-TSM calibration construct (**Supplementary Fig. 1b**). The observed differences correspond to the extension of the F40 peptide, and a Gaussian fit of these data yielded a mean contour length increase of 10.6 ± 5.9 nm for F40-TSM (**Supplementary Fig. 1c**). Of note, this type of measurement yields a much broader probability density histogram when compared to direct contour length measurement (as done for FL-TSM, HP35st-TSM, and HP35-TSM). However, previously published force-FRET-efficiency data[8] were reproduced well with the model described above and the experimentally determined F40-TSM contour length of about 10.6 nm (data not shown). Thus, a conversion of the force–FRET correlation, which matches the zero-force FRET efficiency of theYPet–mCherry construct used here, could be calculated.

Cell culture conditions and expression of FRET constructs. All cell lines (i.e., Tln1$^{-/-}$Tln2$^{-/-}$cells, Vin$^{f/f}$ cells, Vin$^{-/-}$ cells, and HEK293 cells) were cultured in high-glucose DMEM-GlutaMAX medium (Thermo Fisher Scientific) supplemented with 10% fetal bovine serum (FBS; Thermo Fisher Scientific) and 1% penicillin/streptomycin (P/S; Thermo Fisher Scientific). For live-cell imaging, DMEM without phenol red containing 4.5 mg/ml glucose, 25 mM HEPES, 2 mM glutamine (Thermo Fisher Scientific) supplemented with 10% FBS and 1% P/S was used. Stable cell lines were established by using the phoenix cell transfection system. Ecotropic, retroviral particles were produced according to established protocols[37], and target cells were infected in the presence of 5 µg/ml polybrene. After five infection cycles, cells were selected with puromycin or hygromycin depending on the expression vector used. For transient expression, cells were transduced with Lipofectamine 2000 (Invitrogen).

Immunostaining and isolation of focal-adhesion-specific signal. For immunostaining and FA analysis, cells were seeded on no. 1.5 glass slides (Menzel) coated with 10 µg/ml FN. Cells were allowed to spread overnight (O/N), then they were fixed with 4% paraformaldehyde (PFA) for 10 min at RT and washed in PBS (pH 7.4). Immunostainings were performed using standard protocols and antibody concentrations indicated above. Samples were then washed in PBS, mounted in Prolong Gold antifade mountant (Thermo Fisher Scientific) and stored at 4 °C. Images were acquired using a LSM780 confocal scanning microscope (Zeiss) equipped with a 100× oil objective (Plan-APOCHROMAT, NA = 1.46). For determining the FA area, fluorescence images were imported into MATLAB (Mathworks), and regions of interest (ROI) were manually drawn around individual cells. Using a custom-written MATLAB program, the FA signal was extracted by convoluting the image (Gaussian structure element; width, 25; height, 2) and applying a top-hat filtering step (disk, SE; radius, 7 pixels) as described before[43]. For FA analysis, the area of each FA mask was used to calculate the mean FA size per cell.

Ratiometric Förster resonance energy transfer. Ratiometric FRET analysis of living cells was performed on a Leica SP8 confocal laser scanning microscope equipped with a 63× water objective (HCX PL APO, NA = 1.2); cells were excited at 514 nm, and intensities of donor (522–550 nm) and acceptor (600–700 nm) emission were recorded simultaneously. To isolate FA-specific signals, the MATLAB program described above was employed. As before, the FA signal was extracted by convoluting the image and applying a top-hat filtering step; the resulting FA masks were used

doi:10.1038/nmeth.4431

to calculate a mean FA intensity of donor and acceptor signal. Ratiometric FRET values were then calculated by mean intensity acceptor/donor division as described[9].

ROCK inhibitor (Y-27632) experiments. Cells were allowed to spread on FN-coated glass coverslips O/N. For FLIM analysis, Y-27632 (final concentration, 1 μM) was added to the medium, and lifetime images were recorded after 12 min of incubation. Effects of ROCK inhibition were analyzed by acquiring an initial FRET ratio image, then adding Y-27632 (1 μM) and acquiring FRET ratio images after 6 min and 12 min. The FA signal was extracted, using the MATLAB algorithm described above, followed by a two-class Otsu thresholding, which was necessary to extract the comparably weak FA signal that is characteristic for ROCK-inhibited cells. The mean acceptor values were only used if they were 1.3 times larger than the manually determined average background signal.

Fluorescence recovery after photobleaching. For the characterization of turnover rates of talin-YPet and talin-FL-1973, we performed FRAP experiments with cells seeded on Y-shaped FN-coated micropatterned substrates (CYTOO)[9]. Briefly, using a Leica SP8 confocal laser scanning microscope equipped with a 63× water objective (HCX PL APO, NA = 1.2) cells were excited at 514 nm with a laser power of 5% to record two prebleach images every 10 s. After photobleaching of a selected FA with 100% laser power for 1 s, postbleach images were acquired every 20 s for a period of 280 s. The fluorescence emission was recorded between 530–570 nm. For data analysis, the ImageJ plugin 'FRAP profiler' was used to extract raw fluorescence recovery curves, which were then normalized to the minimal and maximal intensity using MATLAB. The mean as well as the s.e.m. of the normalized data was calculated and plotted against time after photobleaching. To determine the fluorescence recovery, we fitted the data assuming a reaction-dominated model as described[44] using data with a fitting quality of $R^2 \geq 0.98$. Mobile fraction (A) and half-time of recovery ($\tau_{1/2}$) values were extracted and plotted individually.

Time-correlated single-photon-counting fluorescence lifetime microscopy. Live-cell TCSPC-FLIM experiments were performed on a confocal laser scanning microscope (Leica TCS SP5 X). The instrument was equipped with a pulsed white light laser (WLL, 80 MHz repetition rate; NKT Photonics), a FLIM X16 TCSPC detector (LaVision Biotech), and a 63× water objective (HCX PL APO CS, NA = 1.2); a bandpass filter 545/30 (AHF Analysentechnik; Chroma) was used to block photons emitted by the acceptor fluorophore. Images were acquired with a scanning velocity of 400 Hz, a spatial resolution of 512 × 512 pixels, and resulting image field coverage of 123.02 × 123.02 μm^2. For each experimental condition, 15–20 cells were recorded, and this procedure was repeated on 2–5 individual days. Custom-written MATLAB programs based on previously published software[9] were used for the subsequent data analysis. As illustrated in **Supplementary Figure 5**, an ROI was manually drawn around the cell of interest, and the FA signal was extracted by multi-Otsu thresholding with three intensity classes. Next, a histogram of photon arrival times of the donor fluorophore was fitted by a monoexponential decay function, and if the fit quality was sufficiently high ($R^2 > 0.98$) the data were used to calculate the fluorescence lifetime of the donor in the absence or presence of the acceptor fluorophore. FRET efficiency E was calculated according to equation (14), where τ_D is the mean donor only lifetime, and τ_{DA} is the lifetime of the donor in presence of an acceptor fluorophore.

$$E = 1 - \frac{\tau_{DA}}{\tau_D} \quad (14)$$

Thus, the described procedure provides the average FRET efficiency of all FAs from one individual cell; this value is displayed as one data point in the respective box plots. As the experiments typically used more than 30 cells, the data are based upon a couple of hundred to thousands of individual FAs.

Live-cell fluorescence lifetime imaging microscopy. To determine live-cell FRET efficiencies of talin constructs, live-cell dishes (81158; ibidi) were coated with either FN (10 μg/ml) or poly-L-Lysine (pLL, 0.1% (w/v)). For FN experiments, cells were seeded O/N; for the pLL control, cells were seeded for 5 min. To investigate the dependence of talin tension on substrate stiffness, cells were seeded on softview dishes (coated with 10 μg/ml FN), and fluorescence lifetime measurements were performed using a 40× long-distance water objective (APO 40× /1.10W CORR C S2). Intermolecular FRET was determined by fluorescence lifetime measurements in Tln1$^{-/-}$/Tln2$^{-/-}$ cells coexpressing either talin-YPet-447 and talin-mCherry-447 or talin-YPet-1973 and talin-mCherry-1973. Fluorescence lifetime measurements of mCherry-tagged constructs were performed using an excitation wavelength of 586 nm.

Single excitation wavelength dual-color TCSPC-FLIM. Live-cell dual-color TCSPC-FLIM experiments were performed using a Leica SP8 confocal laser scanning microscope equipped with a 440 nm pulsed diode laser (40 MHz repetition rate), a 63× immersion oil objective (HCPL APO CS2, NA = 1.4) and the PicoHarp 300 TCSPC module (PicoQuant). Cells were seeded on FN-coated Lab-Tek Chamber Slides (ThermoFisher Scientific) and allowed to spread O/N. Images of living cells were acquired with a laser intensity of 10 μW, a scanning velocity of 400 Hz, a spatial resolution of 512 × 512 pixels, and a resulting image field coverage of 92.26 × 92.26 μm^2 per channel; the emitted fluorescence was split into two channels at 467–499 nm and 525–565 nm. Photons in the first channel were detected by a single-photon-counting detector module (PDM; Micro Photon Devices); photons in the second channel were detected by a red-sensitive single-photon avalanche diode (TauSPAD; PicoQuant). For data analysis, the SymphoTime software (PicoQuant) was employed; an ROI was set for each cell manually, and the fluorescence lifetime values in each channel were determined by fitting a monoexponential decay curve to the respective histogram of photon arrival times. FRET efficiencies were calculated according to equation (14).

Algorithm to calculate molecular stretch ratio. To estimate the amount of mechanically engaged sensor molecules from TCSPC-FLIM data, we assumed that the observed histogram of photon arrival times comprises two underlying fluorescence lifetimes: the fluorescence lifetime of FL-TSM in the closed (c) and in the stretched (s) state, which correspond to the folded and unfolded conformation of the FL peptide. Under this assumption, the

experimentally determined fluorescence lifetime decays can be described by a biexponential function

$$P(t) = A_s e^{-\frac{t}{\tau_s}} + A_c e^{-\frac{t}{\tau_c}} + P_{bg} \quad (15)$$

where A_s and A_c are initial photon count rates from stretched molecules with lifetime τ_s and closed molecules with lifetime τ_c; P_{bg} is the background photon count rate. We note that, for long observation times, the photon count for molecules in the stretched and non-stretched state $N_{s,c}$ is approximated by

$$N_{s,c} \approx \int_0^\infty A_{s,c} e^{-\frac{t}{\tau_{s,c}}} dt = A_{s,c}\tau_{s,c} \quad (16)$$

where the indices reference to either stretched (s) or closed (c) states. Thus, equation (15) can be rewritten as

$$P(t) = \frac{N_s}{\tau_s} e^{-\frac{t}{\tau_s}} + \frac{N_c}{\tau_c} e^{-\frac{t}{\tau_c}} + P_{bg} \quad (17)$$

Under the assumption that the total sensor photon count N is the sum of photons from the stretched N_s and closed N_c sensor molecules, the relative amount of photons in the stretched state r_N is defined by

$$r_N = \frac{N_s}{N} \quad (18)$$

and equation (17) can be rewritten as

$$P(t) = N\left(\frac{r_N}{\tau_s} e^{-\frac{t}{\tau_s}} + \frac{1-r_N}{\tau_c} e^{-\frac{t}{\tau_c}}\right) + P_{bg} \quad (19)$$

As FRET reduces the amount of photons emitted by the donor fluorophore, the relative amount of photons r_N is not equivalent to the relative amount of molecules r_M. Here, we use the approximation that the number of molecules $M_{s,c}$ is proportional to the number of photons and inversely related to the fluorescence lifetime[45]

$$M_{s,c} \propto \frac{N_{s,c}}{\tau_{s,c}} \quad (20)$$

which allows reformulation of equation (19). The molecular stretch ratio is then described by equation (21), as shown in **Figure 6b**.

$$r_M = \frac{M_s}{M} = \frac{r_N\tau_c}{r_N\tau_c + (1-r_N)\tau_s} \quad (21)$$

Thus, equation (19) can be rewritten as

$$P(t) = \frac{N}{r_M\tau_s + (1-r_M)\tau_c}\left(r_M e^{-\frac{t}{\tau_s}} + (1-r_M)e^{-\frac{t}{\tau_c}}\right) + P_{bg} = P_M\left(r_M e^{-\frac{t}{\tau_s}} + (1-r_M)e^{-\frac{t}{\tau_c}}\right) + P_{bg} \quad (22)$$

Calculation of molecular stretch ratio. The biexponential model in equation (15) has five free parameters, two of which can be experimentally determined to increase the fit robustness. The lifetime of the non-stretched, closed FL-TSM (τ_c) can be extracted from control experiments in which FL-TSM is C terminally attached to the protein of interest. Given the large contour length increase of FL-TSM under force, the fluorescence lifetime of the stretched sensor (τ_s) is equal to the lifetime of YPet, which can also be measured (**Fig. 6a**).

Data fits were performed using the maximum likelihood function $L_{poisson}$ to account for the underlying statistics of TCSPC-FLIM measurements. The photon counts in each time bin i of the width Δt are Poisson distributed, and the assumption that their mean value $n_i \approx \sim P(t_i)\Delta t$ is a good approximation when Δt is considerably shorter than the fluorescence lifetimes ($\Delta t << \tau_{s,c}$) Thus, we used equation (23):

$$L_{Poisson}(n;m) = \prod_i \frac{e^{-n_i} n_i^{m_i}}{m_i!}, \quad (23)$$

where m_i is the experimentally measured photon count per time bin. The application of the maximum likelihood function as a point estimator was performed by solving the negative logarithm of equation (23) with the built-in MATLAB function 'FMINSEARCH'. To determine the relative amount of photons emitted from stretched molecules $r_N \in [0,1]$, boundaries for r_N were implemented by using the transformation $r_N = (1 - \sin\rho)/2$ and fitting ρ[46].

Estimation of the minimally required photon number. To a priori estimate the lower bound for the total number of photons N_t required for the determination of stretch ratio r_M, we assume that the experimental data are described by the biexponential model. The probability p_i that a photon is detected in bin i is then given by

$$p_i = (1-b)\left[r_M \frac{\left(e^{\frac{\Delta t}{\tau_s}} - 1\right)e^{-\frac{t_i}{\tau_s}}}{1 - e^{-\frac{t_i}{\tau_s}}} + (1-r_M)\frac{\left(e^{\frac{\Delta t}{\tau_c}} - 1\right)e^{-\frac{t_i}{\tau_c}}}{1 - e^{-\frac{t_i}{\tau_c}}}\right] + \frac{b}{N_t} \quad (24)$$

where b is the relative amount of background photons, Δt the bin width, and $\tau_{s,c}$ the lifetimes of stretched or closed sensor. Assuming that the Cramér–Rao inequality for unbiased estimators holds, the variance σ^2 is bounded by

$$\sigma_{pg}^2 \geq \frac{I_{pq}^{-1}}{N_t},$$

where

$$I_{pq} = \sum_i \frac{1}{p_i}\left(\frac{dp_i}{dx_p}\right)\left(\frac{dp_i}{dx_q}\right)$$

In this way, the minimum number of photons can be calculated for a given target variance σ^{*2}. Based on these calculations, photon count histograms were used if at least 10,000 photons were collected. Note that in these cases, the raw data for fitting monoexponential or biexponential models were identical.

Statistical analysis. Error bars indicate the s.e.m. if not indicated otherwise. Bar plots display the mean value and the s.d. as error bars. Normal distribution of FRAP data was confirmed by the Lillifors test. For statistical evaluation of FLIM data, a two-sided

doi:10.1038/nmeth.4431

Kolmogorov–Smirnov test with a default significance level of $\alpha = 0.05$ (two-sided) was used; the thereby calculated statistical significance was given by a P value. Additional testing was performed with a paired t-test (significance level of $\alpha = 0.05$, two-sided) and the two-sided Mann–Whitney U test ($\alpha = 0.05$), as indicated. The following nomenclature was used in all figures: ***, $P < 0.001$; **, $P < 0.01$; *, $P < 0.05$; not significant, n.s., $P > 0.05$. Box plots were generated using the MATLAB function 'boxplot()', indicating the median (indicated by red line), the 25th and the 75th percentiles, as well as whiskers that reach out to 1.5 interquartile range (IQR) corresponding to 2.7 s.d. (σ) for normally distributed data. Detailed information on the statistics of each data set can be found in **Supplementary Table 1**; and additional background information on sample size and data exclusion is provided in the **Life Sciences Reporting Summary**.

Computational codes. Mechanical fits for the force spectroscopy analysis were performed using previously published custom-written code[42]; the analysis software code runs on IGOR Pro 6.31, 64-bit. Software for FA-FRAP and TCSPC-FLIM analyses was published before[9] and can be used in MATLAB. Computational codes are available upon request.

Data availability statement. The authors confirm that all relevant data are included in this published article (and its supplementary information files). Additional data that support the findings of this study are available upon request. Accession codes: HP35-TSM (MF685010), F40-TSM (MF685012) and FL-TSM (MF685013).

37. Austen, K., Kluger, C., Freikamp, A., Chrostek-Grashoff, A. & Grashoff, C. Generation and analysis of biosensors to measure mechanical forces within cells. *Methods Mol. Biol.* **1066**, 169–184 (2013).
38. von Hansen, Y., Mehlich, A., Pelz, B., Rief, M. & Netz, R.R. Auto- and cross-power spectral analysis of dual trap optical tweezer experiments using Bayesian inference. *Rev. Sci. Instrum.* **83**, 095116 (2012).
39. Tolić-Nørrelykke, S.F. *et al.* Calibration of optical tweezers with positional detection in the back focal plane. *Rev. Sci. Instrum.* **77**, 103101 (2006).
40. Moffitt, J.R., Chemla, Y.R., Izhaky, D. & Bustamante, C. Differential detection of dual traps improves the spatial resolution of optical tweezers. *Proc. Natl. Acad. Sci. USA* **103**, 9006–9011 (2006).
41. Wang, M.D., Yin, H., Landick, R., Gelles, J. & Block, S.M. Stretching DNA with optical tweezers. *Biophys. J.* **72**, 1335–1346 (1997).
42. Stigler, J., Ziegler, F., Gieseke, A., Gebhardt, J.C. & Rief, M. The complex folding network of single calmodulin molecules. *Science* **334**, 512–516 (2011).
43. Würflinger, T., Gamper, I., Aach, T. & Sechi, A.S. Automated segmentation and tracking for large-scale analysis of focal adhesion dynamics. *J. Microsc.* **241**, 37–53 (2011).
44. Sprague, B.L. & McNally, J.G. FRAP analysis of binding: proper and fitting. *Trends Cell Biol.* **15**, 84–91 (2005).
45. Verveer, P.J., Squire, A. & Bastiaens, P.I. Global analysis of fluorescence lifetime imaging microscopy data. *Biophys. J.* **78**, 2127–2137 (2000).
46. James, F. *Statistical Methods in Experimental Physics* 2nd edn. (World Scientific Publishing Co., 2006).